STRUCTURE-BASED DRUG DESIGN OF

11β-HYDROXYSTEROID DEHYDROGENASE

TYPE 1 INHIBITORS

Jillian E. Adie

Thesis Presented for the Degree of Doctor of Philosophy

The University of Edinburgh

2009

Abstract

The enzyme 11β-Hydroxysteroid Dehydrogenase 1 (11β-HSD1) catalyses the intracellular biosynthesis of the active glucocorticoid cortisol. Tissue specific dysregulation of the enzyme has been implicated in the development of metabolic syndrome and other associated diseases. Experiments with transgenic mice and prototype inhibitors show that inhibition of 11β-HSD1 in visceral adipose tissue and liver leads to a resistance of diet-induced hyperglycemia and a favourable lipid and lipoprotein profile as compared to controls. 11β-HSD1 inhibition has thus been proposed as an effective strategy to decrease intracellular glucocorticoid levels without affecting circulating glucocorticoid levels that are essential for stress responses. The clinical development of selective and potent drugs has therefore become a priority. In this research, a process of virtual screening employing the novel algorithm UFSRAT (Ultra Fast Shape Recognition with Atom Types) was used to discover compounds which had specific physicochemical and spatial atomic parameters deemed essential for inhibition of 11β-HSD1. The top scoring compounds were assayed for inhibitory activity against recombinant human and mouse enzyme, using a fluorescence spectroscopy approach. In addition, HEK-293 cell based assays with either human, mouse or rat enzymes were carried out using a scintillation proximity assay (SPA). The most potent compound competitively inhibited human 11β-HSD1 with a Ki_{app} value of 51 nM. Recombinant mouse and human enzyme were expressed, purified and characterised and used in a series of ligand binding assays. Further to this, an X-ray crystal structure of mouse 11β-HSD1 in complex with a tight binding inhibitor – carbenoxolone was solved.

Declaration

The work presented in this thesis is the original work of the author, unless referenced to other sources. This thesis has been composed by the author and has not been submitted in whole or part for any other degree.

Jillian Elizabeth Adie

Acknowledgements

Firstly, I would like to thank Professor Malcolm Walkinshaw for all his gracious support and guidance during my PhD studies.

Secondly a big thank-you to Dr. Scott Webster (QMRI, University of Edinburgh), our main collaborator, for providing experimental equipment, cell lines, DNA and expertise; and Dr. Steven Shave for his collaborative and exciting work with UFSRAT.

This work was also made possible with help from Dr. Martin Wear, Dr. Iain McNae and Ms. Sandra Bruce, and I thank them for their ready technical help, explanations and assistance.

Thanks also to Dr. Hugh Morgan, Dr. Matt Nowicki, Dr. Conny Ludwig, Ms. Aileen Grieg and Dr. Kok-Lian Ho for their ideas, support and assistance; and all members of the Walkinshaw Team on Swann Level 3, especially Dr. Laura Campbell.

Lastly I would like to thank my wonderful family for their never ending support; also Roland and Laura for being amazing.

Abbreviations

AMP	Adenosine MonoPhosphate
ATP	Adenosine TriPhosphate
BBB	Blood Brain Barrier
CBX	Carbenoxolone
CMC	Critical Micelle Concentration
CNS	Central Nervous System
11-DHC	11-Dehydrocorticosterone
DNA	Deoxyribonucleic Acid
EDULISS	EDinburgh University LIgand Selection System
FPLC	Fast Protein Liquid Chromatography
GA	Glycyrrhetinic Acid
GALF	Glycyrrhetinic Acid Like Factor
GE	Glycyrrhizin (also known as Glycyrrhizic Acid)
GR	Glucocorticoid Receptor
H6PD	Hexose -6- Phosphate Dehydrogenase
HBA	Hydrogen Bond Acceptor
HBD	Hydrogen Bond Donor
HEK-293	Human Embryonic Kidney cells 293
HPLC	High Performance Liquid Chromatography
IC_{50}	Half maximal (50%) inhibitory concentration
IMAC	Immobilised Metal Affinity Chromatography
K_{cat}	Catalytic Constant (sec^{-1})
Ki_{app}	Apparent Dissociation Constant of an inhibitor
K_i	Dissocitaion Constant of an inhibitor
K_m	Michaelis Constant (i.e. substrate concentration at ½ V_{max})
LIDAEUS	Ligand Discovery at Edinburgh UniverSity
LogP	Water / Octanol Partition Co-efficient
MALDI-TOF	Matrix Assisted Laser Desorption Ionisation- Time Of Flight
MLogP	Moriguchi Water / Octanol Partition Co-efficient
MR	Mineralocorticoid Receptor
mRNA	messenger Ribonucleic Acid
MW	Molecular Weight
NADP(H)	Nicotinamide Adenine Dinucleotide Phosphate
NAD(H)	Nicotinamide Adenine Dinucleotide
PDB	Protein Data Bank
PTM	Post Translational Modification
QSAR	Quantitative Structure Activity Relationship
SAR	Structure Activity Relationship
SDR	Short-Chain Dehydrogenases / Reductases
SDS-PAGE	Sodium-Dodecyl-Sulfate Polyacrylamide Gel Electrophoresis
SPA	Scintillation Proximity Assay
UFSRAT	Ultra-Fast Shape Recognition with Atom Types
V_{max}	Maximal Enzyme Velocity
VS	Virtual Screening

TABLE OF CONTENTS

CHAPTER 2: EXPRESSION AND PURIFICATION OF 11β-HSD1

CHAPTER 3: BIOCHEMICAL CHARACTERISATION OF 11β-HSD1

CHAPTER 4: DESIGN AND SELECTION OF INHIBITORS FOR INHIBITION OF 11-β HSD1 ACTIVITY

CHAPTER 1:

11-β HYDROXYSTEROID DEHYDROGENASE TYPE 1

1. INTRODUCTION

Glucocorticoids are an important class of steroid hormones essential to life. They play a large role in glucose homeostasis, maintenance of blood pressure and most importantly, regulation of stress and inflammatory responses (Tomlinson et al. 2004). The major active glucocorticoid found in higher organisms is cortisol with the inactive form known as cortisone.

The enzyme 11β-Hydroxysteroid Dehydrogenase type 1 (11β-HSD1, E.C. 1.1.1.146) interconverts the steroid hormone cortisone to cortisol in humans, or dehydrocorticosterone and corticosterone in rodents, birds and amphibians. It is a co-factor dependent, bidirectional enzyme that is thought to act primarily as a reductase *in vivo* (i.e. cortisone → cortisol with the concurrent oxidation of NADPH to NADP) (Bujalska et al. 1997). However, the bidirectionality is heavily influenced by the surrounding cellular milieu. The basic reaction is shown below, in figure 1.1.

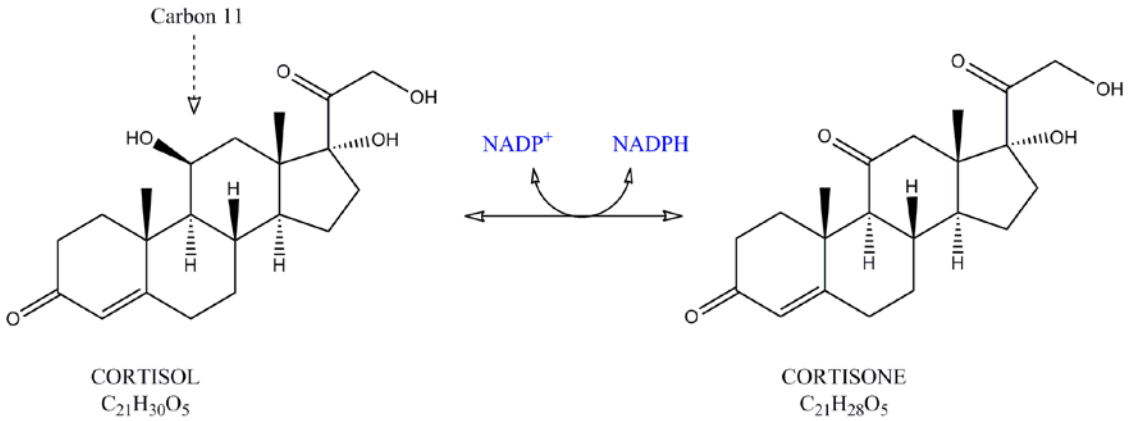

Figure 1.1: Reaction catalysed by 11β-HSD1: the dehydrogenase reaction is the forward reaction (the reductase reaction is the reverse) where the substrate cortisol is oxidised by 11β-HSD1 and thus transfers one proton and a pair of electrons to an acceptor; the co-factor $NADP^+$.

The enzyme is expressed and active in skeletal muscle, white adipose tissue and the liver. It follows then that the principal role of 11β-HSD1 is to regulate cortisol levels in these key tissues; this regulation prevents cortisol binding to the intrinsically non-selective mineralocorticoid receptor (MR), allowing binding to its endogenous glucocorticoid receptor (GR).

Functionally, the enzyme 11β-HSD1 may be divided into several important regions. This is depicted below in figure 1.2. At the N-terminus is found the transmembrane domain, allowing the enzyme to attach itself to the lumen of the endoplasmic reticulum (ER) consisting of residues 1 – 23 in humans. Adjacent to this is the dinucleotide binding domain, characterized by a Rossman fold (co-factor binding domain in figure 1.2). This is followed by a cluster of catalytic residues which constitute the active site. Finally, the C-terminal domain, which plays a key role in dimerisation of the enzyme.

Each of these regions are discussed in further detail in this chapter. Structurally, it is composed of 11 α-helices, 7 β-sheets and is 34 KDa in size.

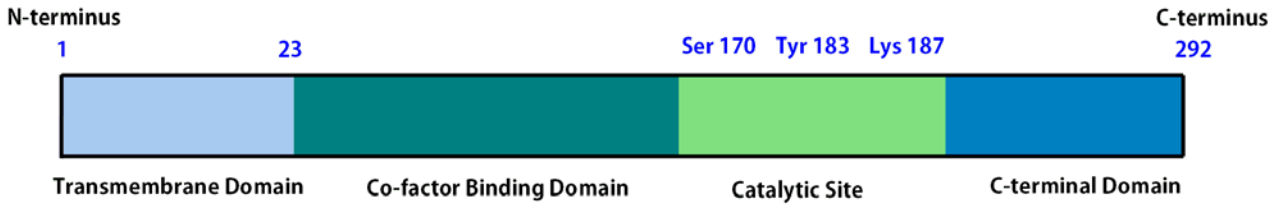

Figure 1.2: The functional regions of 11β-HSD1: (from left to right) the transmembrane domain (residues 1 – 23), the nucleotide binding domain, the catalytic site (showing the catalytic triad of residues) and the C-terminal domain which plays an important role in oligomerisation of the enzyme.

1.1 Steroid Hormones

There are five classes of steroid hormones, the precursor for all of which is cholesterol. Briefly, these five classes are: Glucocortocoids (e.g. cortisone), mineralocorticoids (e.g. aldosterone) and the sex steroids – the androgens, oestrogens and progestins. These are depicted below in figure 1.3. Synthesis and secretion of the glucocorticoids and mineralocorticoids occurs from the adrenal cortex, from where they are transported humorally to their target sites. As the steroids are hydrophobic in nature they must be transported in complex with a plasma protein such as transcortin, which acts as a carrier.

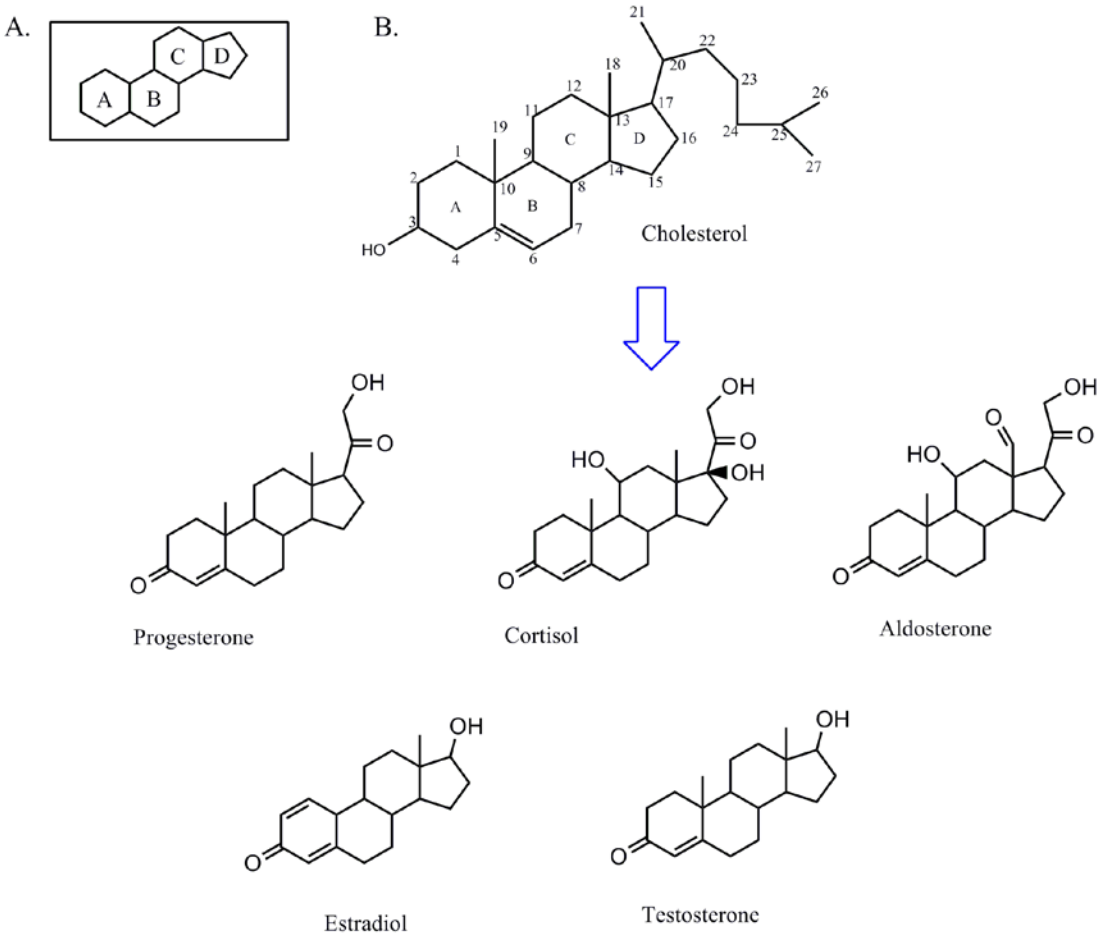

Figure 1.3: A: the basic structure of steroids: cyclopentanoperhydrophenanthrene, showing the ring nomenclature. B: the molecular structures of: the steroid precursor cholesterol, progesterone (a progestin, C-21), cortisol (a glucocorticoid, C-21), aldosterone (mineralocorticoid, C-21), testosterone (an androgen, C-19) and estradiol (an estrogen, C-18).

There is diurnal variation in the plasma concentration of endogenous glucocorticoids with the levels higher in the morning (~450 nmol/L) and lower (~110 nmol/L) in the evening (Rang et al. 2005).

The steroids are not stored *in vivo*, but are produced as required; self-regulated by a negative feedback loop. This is part of the hypothalamic-pituitary-adrenal axis (HPA); the system that regulates glucocorticoid plasma levels in the body.

1.2 Two Isoforms of 11β-HSD

There are two isozymes of 11β-HSD in human; types 1 and 2 (Rusvai, Naray-Fejes-Toth 1993) which despite nearly identical enzymatic actions share a low homology; a sequence identity of 14 % (Stewart, Krozowski 1999). This can be seen below in the sequence alignment in figure 1.5. There are also several splice variants that have been identified in numerous species (known as 11β-HSD1 A-C; not shown below).

Structurally, the enzymes differ significantly, with the type 2 isoform having 3 membrane insertions as opposed to one for isoform 1. This is depicted in figure 1.4, in an image taken from Odermatt et al, 2006.

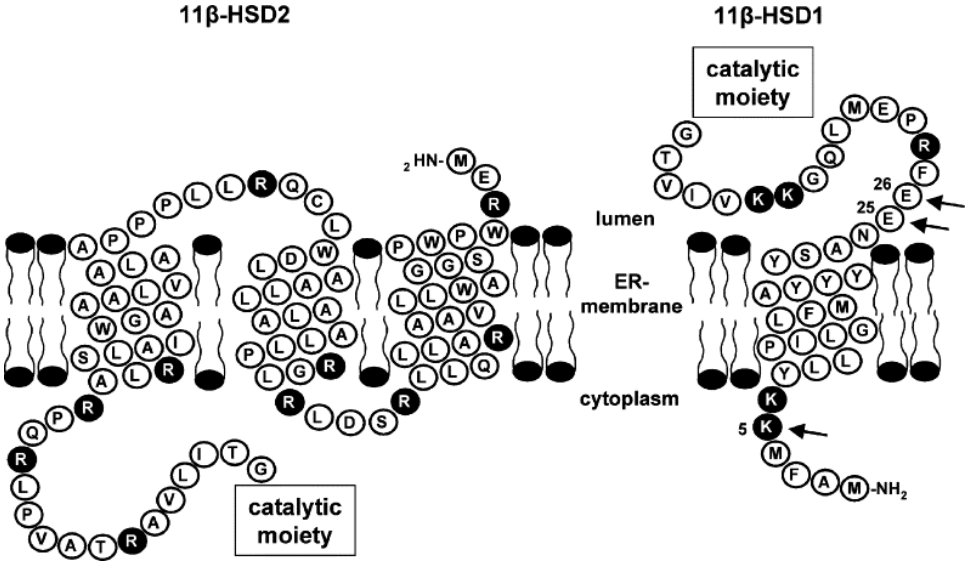

Figure 1.4: circle model of the N-terminal membrane anchor sequences of 11β-HSD2 (left) and 11β-HSD1 (right). The amino acids are indicated in single letter code, with positively charged residues in white on black background. The residues Lys 5 and Glu 25, Glu 26 determine the lumenal orientation of 11β-HSD1, and are indicated by arrows.

Figure 1.5: A multiple amino acid sequence alignment of the human 11β-HSD type 1 and 11β-HSD type 2 (denoted HSD1 and HSD2 respectively in the alignment below). The colours represent amino acids of similar properties:

Residue:	Colour:	Property:
AVFPMILW	RED	Small (small+ hydrophobic (incl.aromatic -Y))
DE	BLUE	Acidic
RK	MAGENTA	Basic
STYHCNGQ	GREEN	Hydroxyl + Amine + Basic - Q
Others	GREY	

```
HSD1            ------------------------------------------MAFMKKYLLP---ILGL 14
HSD2            MERWPWPSGGAWLLVAARALLQLLRSDLRLGRPLLAALALLAALDWLCQRLLPPPAALAV 60
                                                          : :: : ***    *.:

HSD1            FMAYYYYSANEEFRPEMLQGKK--VIVTGASKGIGREMAYHLAKMGAHVVVTARSKETLQ 72
HSD2            LAAAGWIALSRLARPQRLPVATRAVLITGCDSGFGKETAKKLDSMGFTVLATVLELNSPG 120
                : *  : : ..  **: *   .  *::**...*:*:* * :* .**  *:.*. . ::

HSD1            KVVS-HCLELGAASAHYIAGTMEDMTFAEQFVAQAGKLMGGLDMLILNHITNTSLNLFHD 131
HSD2            AIELRTCCSPRLRLLQMDLTKPGDISRVLEFTKAHTTSTGLWGLVNNAGHNEVVADAELS 180
                 :    * .      :    .  *:: . :*.    .  *  .::     .:.  :   .

HSD1            DIHHVRKSMEVNFLSYVVLTVAALPMLKQSNGSIVVVSSLAGKVAYPMVAAYSASKFALD 191
HSD2            PVATFRSCMEVNFFGALELTKGLLPLLRSSRGRIVTVGSPAGDMPYPCLGAYGTSKAAVA 240
                 :  .*..*****:. : ** . **:*:.*.* **.*.* **.:.** :.**.:** *:

HSD1            GFFSSIRKEYSVSRVNVSIT----------------------LCVLGLIDTETAMKAVSGI 230
HSD2            LLMDTFSCELLPWGVKVSIIQPGCFKTESVRNVGQWEKRKQLLLANLPQELLQAYGKDYI 300
                 ::.::  *     *:***                        * : .* :      . . *

HSD1            VHMQAAPKEECALEIIKGG-----------ALRQEEVYYDSS-----LWTTLLIRNPCRK 274
HSD2            EHLHGQFLHSLRLAMSDLTPVVDAITDALLAARPRRRYYPGQGLGLMYFIHYYLPEGLRR 360
                 *::.   ..  * : .             * * .. ** ..      :    : :  *:

HSD1            ILEFLYSTSYNMDRFINK-------------------------- 292
HSD2            RFLQAFFISHCLPRALQPGQPGTTPPQDAAQDPNLSPGPSPAVAR 405
                 :   :  *: : * ::
```

Legend of characters used on the bottom row:

*** indicates identical residues,**

: indicates semi-conserved residues in accordance with the colour chart described above,

. indicates no conservation. The sequence alignment was performed using ClustalW (http://www.ebi.ac.uk/Tools/clustalw2/index.html).

The two isozymes are different gene products and differ in their regulation and tissue distribution. Isoform 1 is highly expressed in many glucocorticoid target tissues, such as liver, adipose tissue, skeletal muscle and macrophages. Isoform 2 is located in kidney, colon, placenta and inflamed tissue. This is summarised in table 1.2.

The major difference between the two isozymes aside from their amino acid sequences is the cellular location of their catalytic domain. The type 1 enzyme is found in the lumen of the endoplasmic reticulum, anchored by an N-terminal transmembrane domain, however the type 2 isoform faces into the cytosolic space. This is potentially one reason behind the differing catalytic predispositions of the two enzymes and co-factor recruitment; 11β-HSD1 takes NADPH as a co-factor for reduction of cortisone whereas 11β-HSD2 will utilise NAD for the reaction of dehydrogenating cortisol.

Table 1.2: A summary of the main characteristics of the two human 11β-HSD isoforms, adapted from Sandeep and Walker, 2001.

	Isoform 1	**Isoform 2**
Enzyme Characteristics	Reductase; NADPH as co-factor Faces the ER lumen; N-terminus inserted into membrane;	Dehydrogenase; NADH as co-factor; Faces the ER cytoplasm; 3 membrane spanning domains;
Sites Synthesised	Liver, adipose tissue, brain, lung, pituitary, gonads, skeletal muscle, vascular smooth muscle, macrophages	Kidney, colon, salivary glands, sweat glands, placenta, vascular endothelium, inflamed tissue
Molecular Biology	▪ 34 KDa ▪ 292 amino acids ▪ Chromosome 1 ▪ >20 kb cDNA ▪ 6 exons	▪ 44 KDa ▪ 405 amino acids ▪ Chromosome 16 ▪ 5.3 kb cDNA ▪ 5 exons

The type 2 isoform is not thought to be highly regulated and is seemingly a constitutive enzyme (Sandeep, Walker 2001). In contrast, the type 1 isoform of 11β-HSD is tightly regulated by several complex factors including glucocorticoids, sex steroids, growth hormones, cytokines and stress (Seckl, Walker 2001;Stewart, Krozowski 1999).

The current paradigm states that 11β-HSD1 is responsible for providing and regulating the levels of active glucocorticoid, i.e. cortisol, in GR-abundant tissue (Arampatzis et al. 2005;Atanasov, Odermatt 2007;Odermatt et al. 2006). On the other hand, the primary role of 11β-HSD2 is to oxidise free cortisol to produce inactive cortisone, preventing it interacting with the MR and thus the enzyme is located in MR rich tissues (Albiston et al. 1994).

1.3 Protein family: The Short Chain Dehydrogenases/ Reductases

The enzyme 11β-HSD types 1 and 2 are members of the Short-chain Dehydrogenases/ Reductases (SDR) family of proteins. This family of enzymes is known to be NADP(H) or NAD(H) dependent oxidoreductases (defined as an enzyme which will catalyse the transfer of electrons from one molecule – the reductant - to another – the oxidant) and convert secondary alcohols to ketones (and vice versa). They generally possess two binding domains – one for the co-factor and another for substrate. The overall sequence similarity is typically 10 – 30 %, but all members share a high degree of secondary structure conservation (Benyajati et al. 1981). The active site cavities for all enzymes in the SDR family are unique which is in accordance with the wide range of substrate specificities observed.

Overall, little sequence similarity is found within members of the SDR protein family, with the exception of the Rossman fold and two conserved motifs which are detailed in the following sections.

1.4 The Rossmann Fold

The Rossmann fold is a structural motif of β-sheets interconnected by α-helices first observed by Rossmann (Rao, Rossmann 1973). It is an arrangement that forms a cleft for nucleotide co-factors to bind and has a unique topology.

In 11β-HSD1, this is represented by a central seven-stranded parallel β-sheet, sandwiched between three alpha helices on either side. The seven beta strands (named β-A to β-G) twist by 90° and it is the first six of these (β-A to β-F) that comprise the principal end of the Rossmann fold. The carboxyl ends of the β-strands β-A, β-B and β-C along with the α-helices α –2 and α-3 (figure 1.6B) bind the AMP portion of NADP. The remaining structural components (β-D, β-E, β-F and α–5 and α-6/7) bind the nicotinamide moiety of the dinucleotide co-factor. The strands of the β-sheet are ordered 3-2-1-4-5-6.

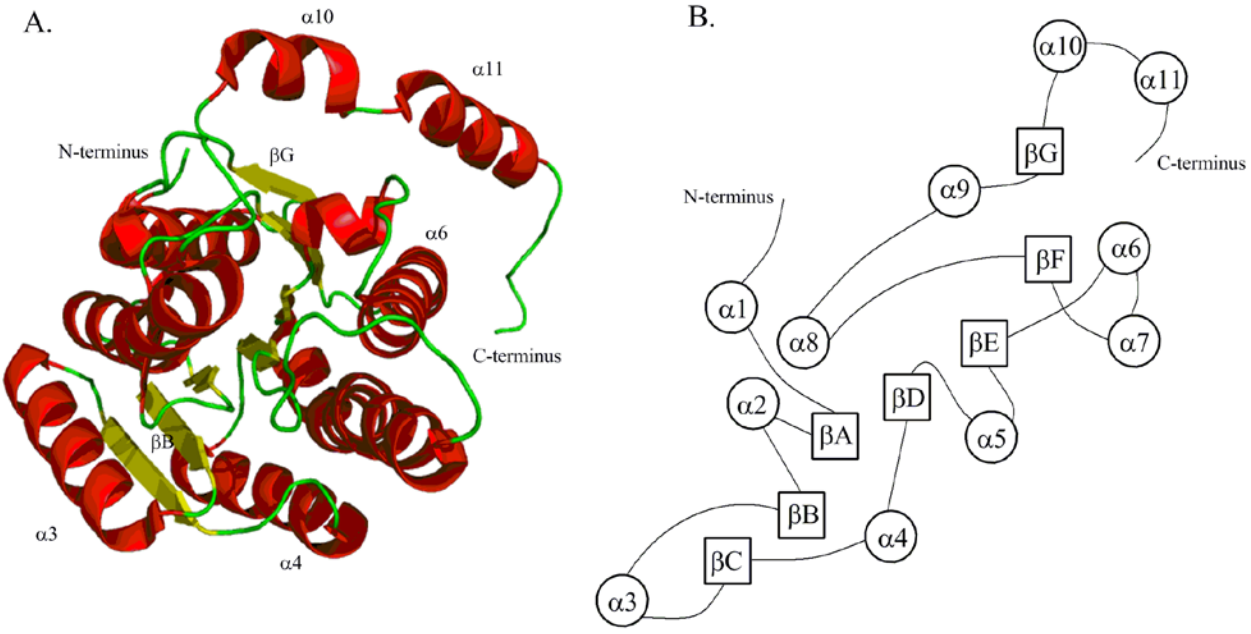

Figure 1.6: (A) A 3-dimensional representation of 11β-HSD1 from PDB entry 3CH6 showing the α-helices in red and the β-sheets in yellow. The N- and C- termini are labeled as are several of the structural components. The Rossmann fold consists of 6 of the 7 β-strands and 4 of the 11 α-helices. (B) 2-dimensional representation is shown in a simpler format with each component labeled.

This is also depicted in figure 1.7A and B.

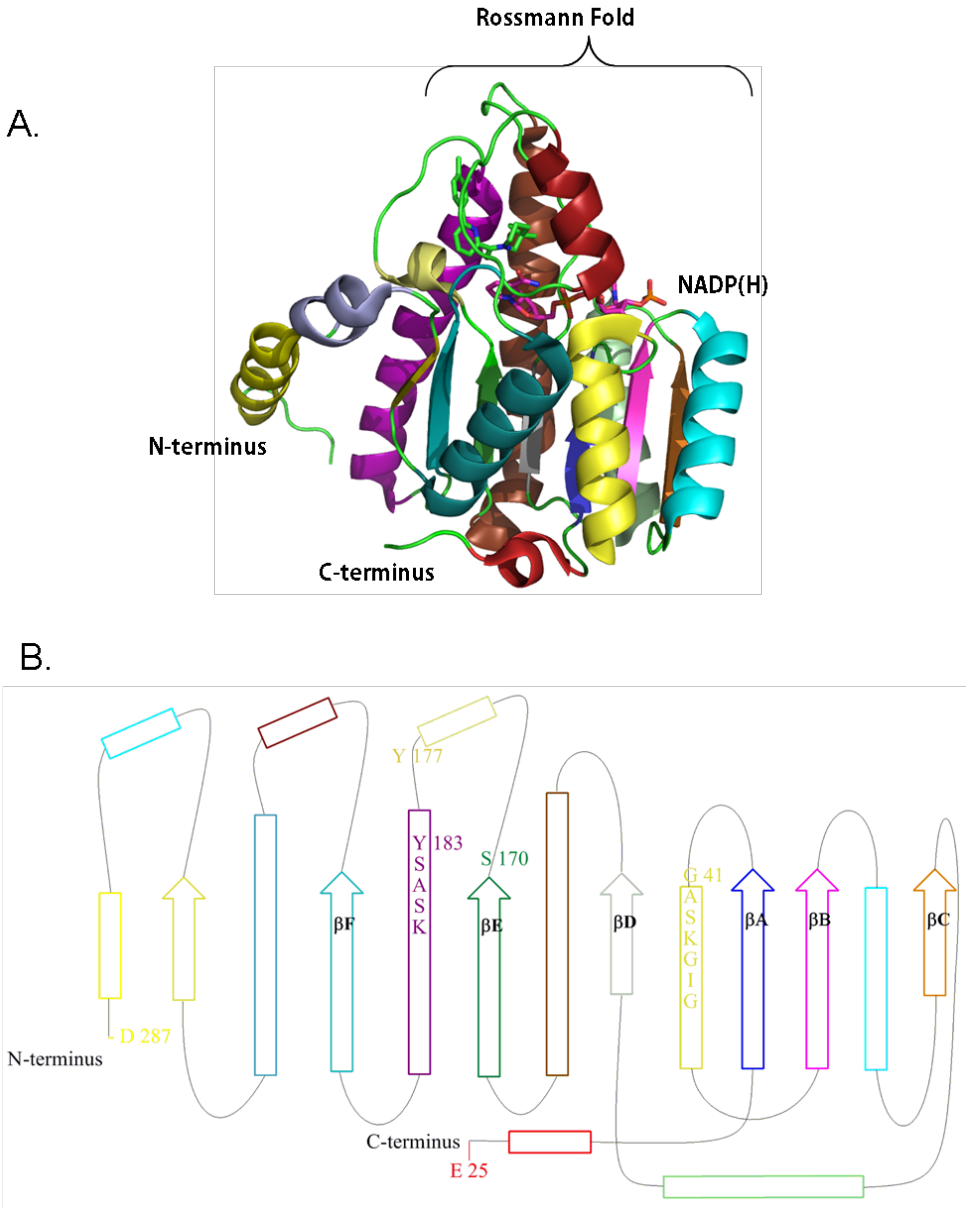

Figure 1.7: (A) A recent crystal structure of a human 11β-HSD1 monomer, showing the Rossman fold and the orientation of NADPH in the protein. The beta-sheets and alpha-helices are colour-coded to correspond to figure 1.4B. This particular structure is 3CH6 (Wang et al. 2008) deposited in the PDB in 2008 by Bristol-Myers Squibb and shown with a novel pyridine inhibitor (stick format, green) and co-factor NADPH (stick format, purple). The monomer is shown here is a double mutant (L262R, F278E). (B): A two dimensional representation of the enzyme 11β-HSD1 showing the beta-sheets labeled βA to βF, which form part of the Rossmann fold. Noted in the figure are residues involved in binding the co-factor and substrate (Ser 170 and Tyr 183); and the two sequence motifs (which start at Gly 41 and Tyr 183) and the start and finish residues (Glu 24 and Asp 287 respectively).

All dehydrogenases of known structure utilise NAD(H) or NADP(H) as co-factors and almost all have a similar dinucleotide binding domain formed by the Rossmann fold prompting speculation as to the evolutionary convergence or divergence of these enzymes (Creighton 1984). Inhibitors exist which competitively inhibit dinucleotide binding to the Rossmann fold; in clinical use is Gossypol (Vander Jagt et al. 2000) which is a polyphenol compound derived from the *Gossypium* cotton plant and was initially developed as a male anti-fertility agent.

The enzyme 11β-HSD1 confers a specificity for NADP(H) and not NAD(H) through an electrostatic interaction between the guanidine moiety of an arginine residue at position 66 and the ribose 2'-phosphate of NADP(H) (Hosfield et al. 2005). As may be expected, this arginine residue is not seen in the NAD(H)-dependent type 2 isoform. Turn-over of cortisol to cortisone and vice versa will occur in the presence of NAD(H) (Bush et al. 1968) however at a much reduced rate.

1.5 Overall Structure and Functionally Important Regions of 11β-HSD1

In addition to displaying the typical SDR architecture of a Rossman fold, 11β-HSD1 possesses two conserved motifs which are also observed within SDR families. Of the two conserved sequences, one is located within the N-terminal nucleotide binding domain (section 1.5.1) and the other within the catalytic site (section 1.5.2).

1.5.1 SDR Conserved Sequences: The Dinucleotide Binding P-Loop

The first SDR-typical motif is the phosphate binding loop – a P-Loop; the primary structure of which typically consists of a glycine-rich loop proceeded by a Lys, Ser or Thr residue (Saraste et al. 1990). In 11β-HSD1 this conserved sequence is located in the N-terminal nucleotide binding domain between the β-sheet 'β-A', and the α-helix 'α-2' (figure 1.6B). This P-loop directly contacts the ribose sugar and pyrophosphate (Hosfield et al. 2005). It consists of the sequence motif: Gly-X-X-X-Gly-X-Gly (X = any residue, but typically 'Gly-Ala-Ser-Lys-Gly-Ile-Gly') which confers specificity to NADPH, but with only Ser 43 and Ile 46 making any polar interactions, as illustrated in figure 1.8.

1.5.2 SDR Conserved Sequences: The Catalytic Triad of Residues

In the central active site the amino acid sequence Tyr-X-X-X-Lys (Tyr 183, Lys 187) is often combined with a conserved serine (Ser 170). These three residues orient the substrate, catalyse the proton transfer to and from reaction intermediates (Hosfield et al. 2005) and are thought of as the 'catalytic triad' when found as Ser-Tyr-Lys.

The Tyr 183 residue forms hydrogen bonds with the cortisone keto-group at position C-11 (figure 1.10). The conserved lysine (Lys 187) residue forms hydrogen bonds with the nicotinamide ribose hydroxyls from NADP(H) and also lowers the pKa of the neighbouring tyrosine hydroxyl group through electrostatic interactions. This lowered pKa of Tyr 183 (which is ~ 9.7 in model peptides but may range from 9 to 12 in proteins) promotes proton transfer to the reactive keto-oxygen of bound cortisone. In addition to this, a hydride is donated from NADPH, and the reduced glucocorticoid is produced; cortisol (Filling et al. 2002;Hosfield et al. 2005). The catalytic residues are arranged in a suitable assembly for carrying out a similar mechanism in cortisol oxidation. These are pictured in figure 1.8, in a diagram depicting overall co-factor binding. Substrate binding is shown in figure 1.10.

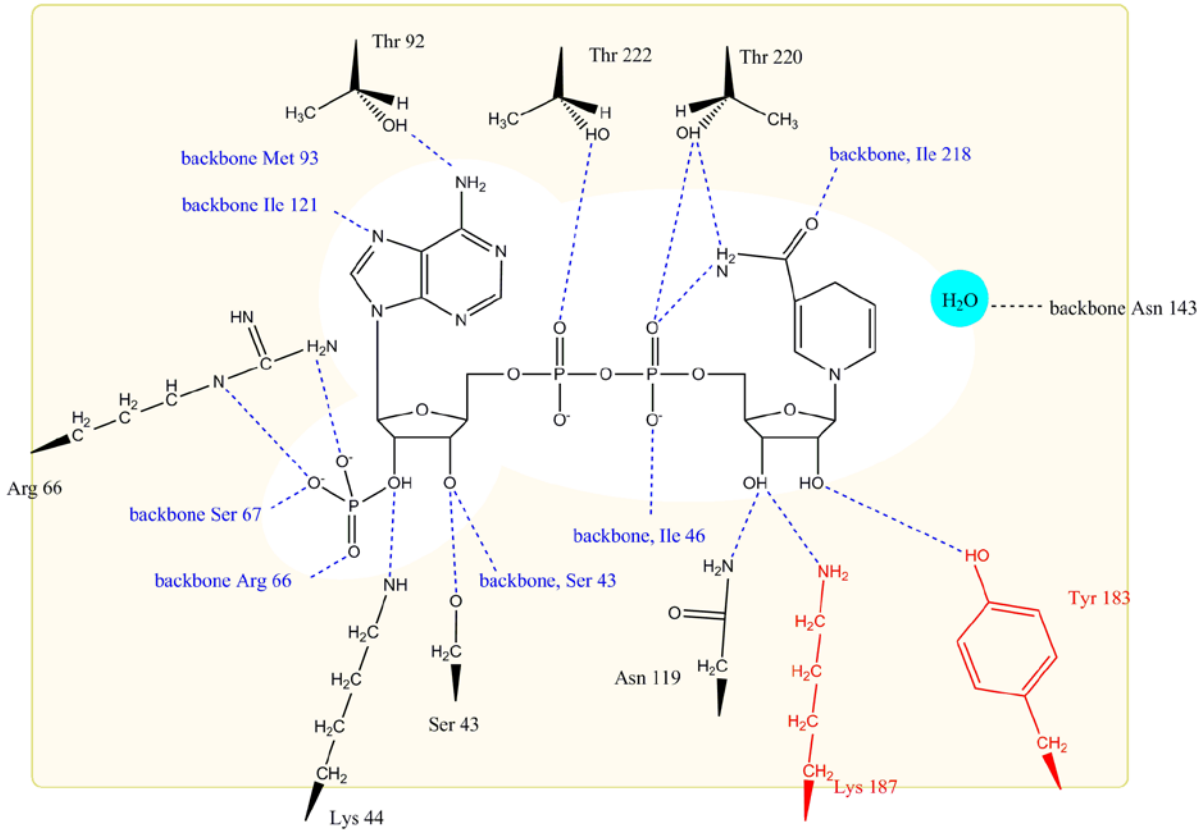

Figure 1.8: A 1-dimensional, simplified diagram showing the polar interactions involved in binding NADPH. Importantly, Tyr 183 and Lys 187 interact with the nicotinamide ribose hydroxyl groups as described. These residues are highlighted in red. This crucial interaction facilitates electron transfer. Also important are residues Ser 67 and Arg 66 which confer the specificity for NADPH over NADH. Co-factor binding also entails stacking interactions with Arg 66 on one face of the purine ring and His 120 on the opposite face (not shown).

Also pictured in figure 1.8 is an SDR conserved water molecule, ligated to the carbonyl backbone of Asn 143. This water plays a role in the proton relay system with bulk solvent when re-protonating Tyr 183.

1.5.3 Binding in the Catalytic Site: Additional Residues Involved

The catalytic triad and other residues involved in substrate binding are shown in figure 1.9.

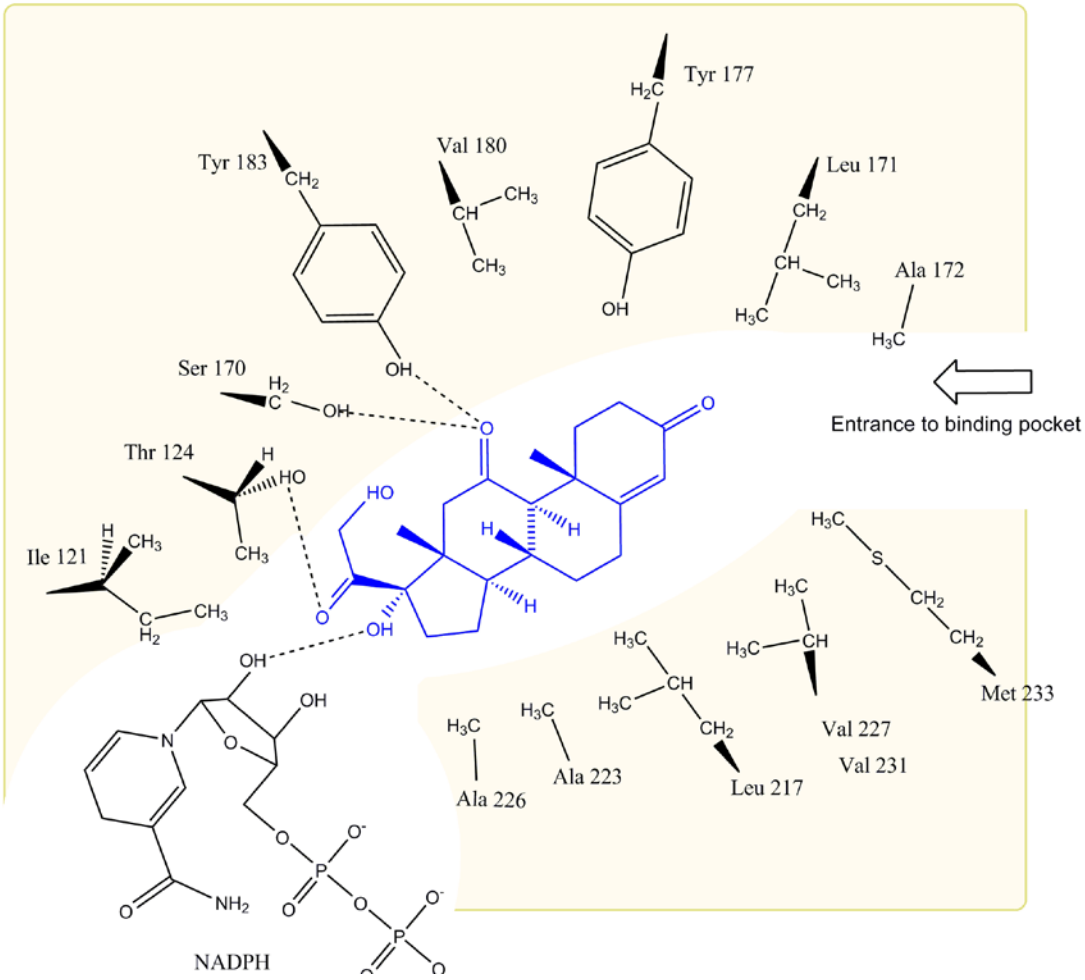

Figure 1.9: Diagram showing the principal residues in the human 11β-HSD1 active site involved in binding substrate and ligands. On the steroid beta-face (bold bonds) are Ile 121, Thr 124, Ser 170, Val 171, Ala 172, Tyr 177, Val 180 and Tyr 183. On the alpha-face (dashed bonds) are Lei 217, Ala 223, Ala 226, Val 227, Val 231 and Met 233. Two of the catalytic residues – Ser 170 and Tyr 183 - interact with the substrate cortisone (shown in blue). There are also interactions between the ribose hydroxyl and the hydroxyl at the 17 position of the steroid.

The substrate binding pocket and the co-factor binding site are situated closely enough to allow stabilising interactions between co-factor - primarily the nicotinamide of NADPH - and substrate. This is illustrated in figure 1.10A. The presence and proximity of NADPH is essential for catalysis of the substrate; it is

necessary as an electron acceptor for the dehydrogenase reaction and an electron donor in the reductase reaction. The short distance between the NADP(H) nicotinamide ring and the substrate allows for π-stacking between ring structures, further enhancing stabilisation. The interactions between substrate and the catalytic site are principally hydrophobic; indeed the substrate binding site is a hydrophobic tunnel as shown in figure 1.10B. The hydrophobic tunnel connects to the co-factor binding site; NADP(H) enters the tunnel from the opposite end to the substrate.

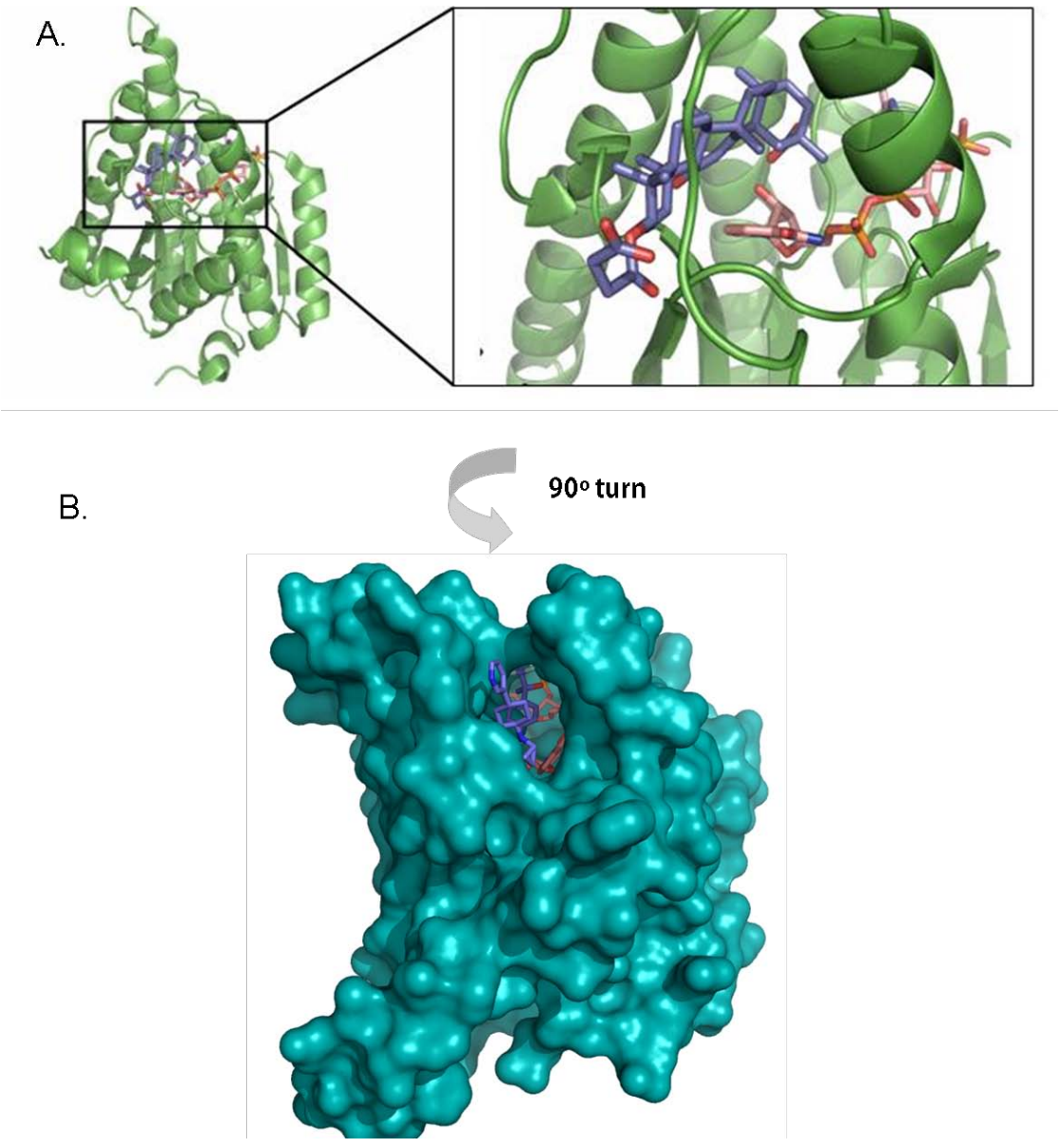

Figure 1.10 (A) Cartoon representation of crystal structure of human 11β-HSD1 (PDB accession 2BEL). One subunit is shown, NADPH is pink and carbenoxolone blue. (B) 3D3E monomer, NADPH (pink, only just seen) and benzamide inhibitor (blue). A surface has been applied to the structure to allow a clearer envisagement of the tunnel.

Figure 1.11 shows the interactions of bound substrate as seen from the opening of the catalytic pocket.

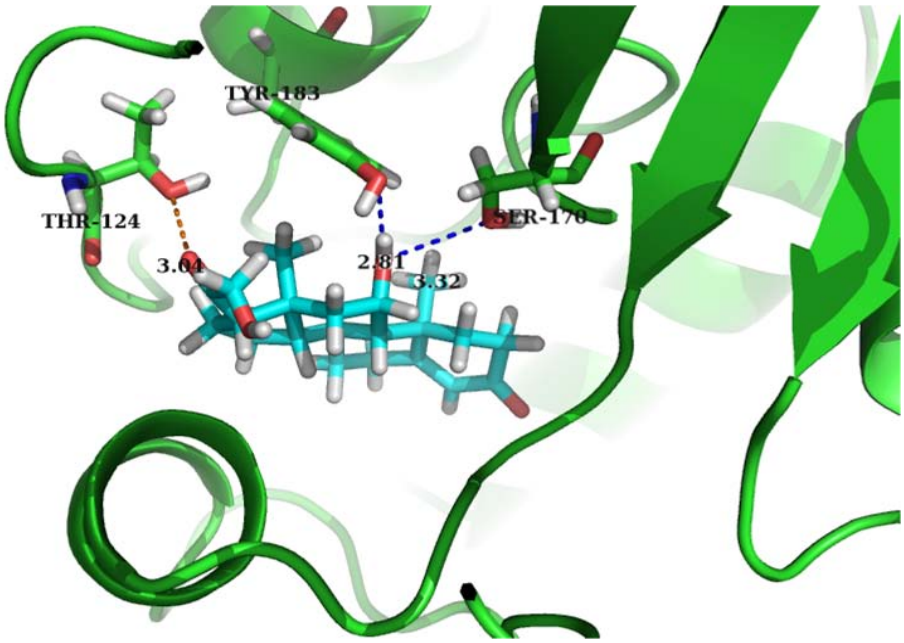

Figure 1.11: A 3-dimensional model of cortisol binding in the human active site, taken from crystal structure 1XU7 (Hosfield et al. 2005) prepared with Pymol. The hydrogen atoms are shown in white.

The residue Tyr 177 was also thought to play a role in substrate binding through polar interactions (shown in figure 1.9 and 1.11) however a recent mutagenesis study with Y 177 (to either Y177Q or Y177A) suggested that it did not participate in hydrogen bonding but instead in hydrophobic interactions with the substrates cortisone and cortisol (Kim et al. 2006). An exchange to phenylalanine (Y177F) did not significantly alter the K_m of 11β-HSD1 for cortisone; both Y 177 and F 177 have a K_m of ~600 nM (Kim et al. 2006). These mutations resulted in increased K_m values for cortisone: from ~ 600 nM to ~ 4.5 μM and ~ 8.3 μM respectively. As the mutations Y177Q or Y177A would effectively remove the hydrophobic character at this position, the increase in K_m values supports the hypothesis that Tyr 177 is more likely to be involved in substrate binding through its hydrophobic side chain as opposed to hydrogen bonding. Interestingly, the mutation of Y 177 to a glutamine or alanine residue altered the affinity of 11β-HSD1 for selected inhibitors, such as glycyrrhetinic acid ($C_{30}H_{46}O_4$, GA), substantially increasing the IC_{50} from ~ 55 nM (wild-type) to ~ 425 nM (Y177Q) and 275 nM (Y177A) (Kim et al. 2006).

Interestingly, the residue Tyr 280 (a serine residue in mouse 11β-HSD1) which is found in the C-terminal domain, is thought to play a role in the selectivity of the enzyme toward ligands (Kim et al. 2007) but its direct involvement in inhibitor binding is dependent on the overall structure of the inhibitor. For example, it is not essential in carbenoxolone binding (as seen in the crystal structure 2BEL (Hale et al. 2008)) although it is a vital point of interaction with another non-selective 11β-HSD1 inhibitor glychyrrhitinic acid (GA) as determined by a mutagenesis study, where the mutation of Y280 to A280 or F280 caused drastic changes in the IC_{50} of GA (Kim et al. 2007).

1.6 Species Variation in the Catalytic Site

There are several important differences between the rodent and human catalytic residues, as would be expected for enzymes with slightly different substrates (figure 1.12).

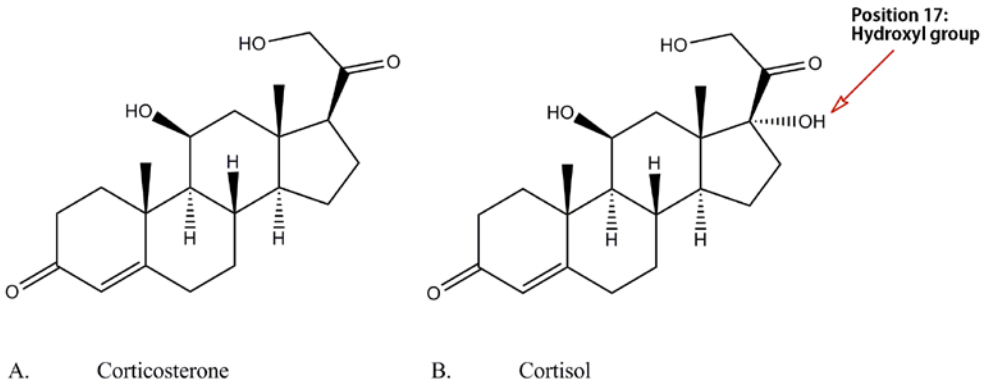

Figure 1.12: (A) corticosterone, the active glucocorticoid in rodents, birds and amphibians. B: Cortisol, the active glucocorticoid in higher organisms. Both are reduced by 11β-HSD1 to yield 11-dehydrocorticosterone (from compound A) and cortisone (from B). The only difference between the two compounds is the presence of a hydroxyl group at position 17 in the cortisol and cortisone, as indicated by the red arrow.

The single difference between the rodent and human substrate is the additional hydroxyl group found at position 17 of the steroid molecule in humans. Position 17 of the steroid molecule is anticipated at to bind deep within the catalytic site, close to NADP(H).

The most important difference between the rodent and human active site residues is the replacement of tyrosine (Y 177) in human to glutamine (Q 177) in rodents. This is shown in figure 1.13. Interestingly, mutations of Q 177 to alanine or glutamate do not affect the affinity of the human 11β-HSD1 enzyme for the rodent substrate: 11-dehydrocorticosterone (11-DHC) the reduced form of figure 1.12A (Kim et al. 2006).

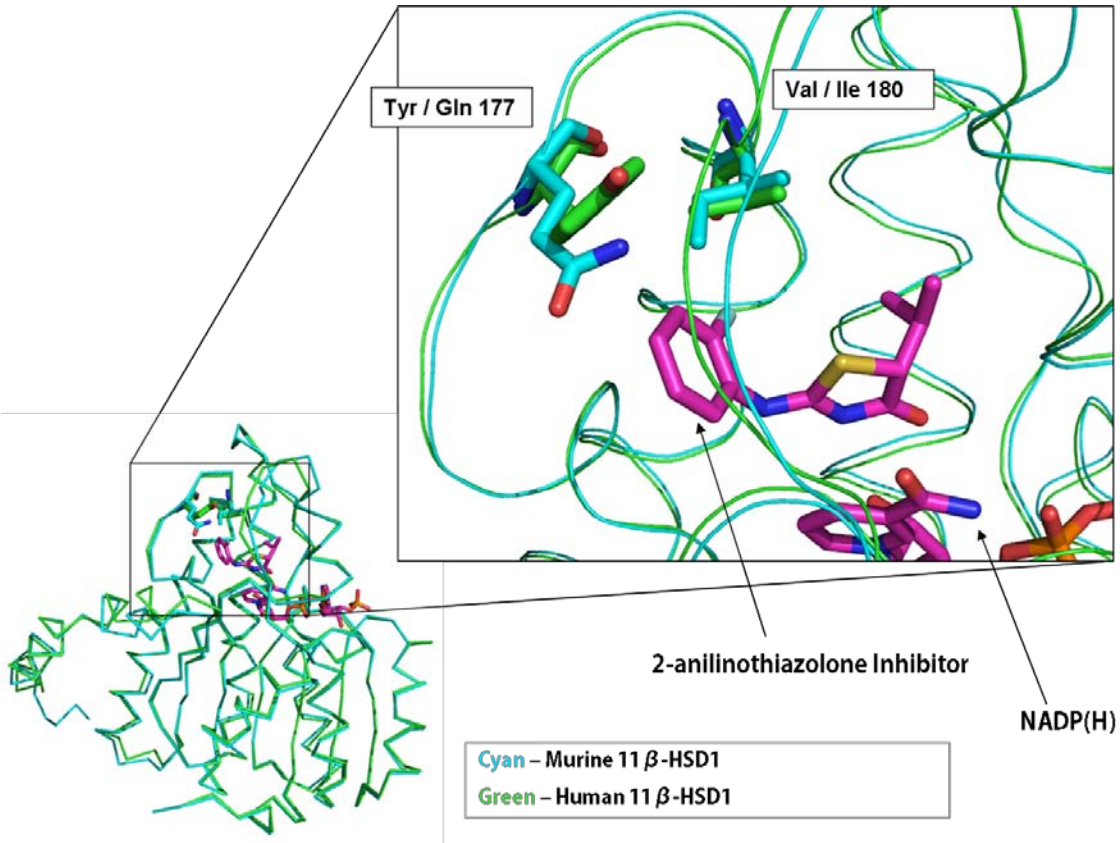

Figure 1.13: Overlay of human and mouse 11β-HSD1 monomers from 1Y5M (mouse, in blue ribbon) and 2RBE (human, in green ribbon). Overall, the structures are strikingly similar. A close-up of the active site of this overlay reveals a 2-anilinothiazolone inhibitor (shown in pink) NADPH can be seen to the bottom right.

There exist 17 crystallographic structures of 11β-HSD1 currently in the protein data bank (PDB). These are summarised in table 6.1, and discussed in chapter 6.

1.7 Bidirectionality of 11β -HSD1

In vivo, the catalytic domain of 11β-HSD1 faces the lumen of the endoplasmic reticulum. This surrounding oxidising environment allows the enzyme to function primarily as a reductase (Odermatt et al. 1999;Ozols 1995) and provides a degree of hydrophobic active site sheltering. It also allows for the hydrophobic substrate, the inactive cortisone, to freely diffuse across the membrane and into the catalytic site (Odermatt et al. 2006) although the mechanisms behind steroid entry into target cells remains poorly understood.

Although the enzyme is reported to favour the reductase reaction *in vivo*, it has been observed during this research and previously that this activity is reduced after cell lysis (Lakshmi, Monder 1988) which may be an effect of local *in vitro* conditions. As the reaction has a relatively low free enthalpy change, the enzyme activity greatly depends on the [NADPH]/[$NADP^+$] ratio in the ER lumen (Atanasov et al. 2004). Furthermore, an excess of approximately 10-fold NADPH is required to induce the functioning of 11β-HSD1 as a reductase. There is a significant increase in the activity starting at a 9 [NADPH]: 1 [$NADP^+$] ratio (Dzyakanchuk et al. 2009).

In addition to the local environment conditions, current research has pointed towards the presence of a second enzyme; hexose-6-phosphate dehydrogenase (Hewitt et al. 2005) as a prime determinant of 11β-HSD1 activity. Hexose-6-phosphate dehydrogenase (H6PD) is an enzyme which catalyses the first two steps of the pentose phosphate pathway. It regenerates reduced NADPH in the lumen of the endoplasmic reticulum, supplying its neighbouring enzyme - 11β-HSD1 – with a constant replenishment of reductase co-factor. Certainly, this has proven to be the case in intact culture cells (HEK293 cells) as the co-expression of H6PD stimulated reductase activity 5-fold and decreased the dehydrogenase activity six-fold, as compared to controls without co-expression of H6PD (Atanasov et al. 2004).

1.8 Alternate Roles of 11β -HSD1

There are secondary, additional roles that 11β-HSD1 has *in vivo*, which are not fully understood or documented. Evidence exists for a role for 11β-HSD1 in the detoxification of several non-steroidal carbonyl compounds; the enzyme reduces

these compounds to their corresponding hydroxyl derivatives (Maser, Oppermann 1997). This is in addition to detected 11β-HSD1 activity reducing neurosteroids 7-keto-, 7-α-hydroxy- and 7-β-hydroxy-dehydroepiandrosterone, DHEA (Nashev et al. 2007). The non-steroidal carbonyl compounds reduced by 11β-HSD1 include a tobacco derivative; nitrosamine 4-methylnitrosamino-1-(3-pyridyl)-1-butanone (NNK) (Maser 1998;Maser et al. 2003) the most potent carcinogenic agent in cigarette smoke (Maser et al. 2006) as well as a new anticancer drug oracin (Wsol et al. 2004). The structures of both xenobiotics are shown in figure 1.14.

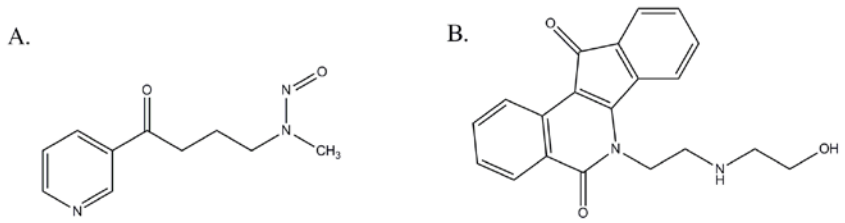

Figure 1.14 Structure of non-steroidal substrates of 11β-HSD1 (A) NKK (B) Oracin. Illustration prepared with Chemdraw 11.0.

This xenobiotic carbonyl compound-reducing activity is typical of many hydroxysteroid dehydrogenase enzymes from the SDR family and from the aldo-keto reductase family of enzymes. There is evidence to suggest that it is a bidirectional activity which is heavily influenced by hexose-6-phosphate dehydrogenase (H6PD) (Nashev et al. 2007) as with endogenous substrate.

1.8 Oligomerisation State of 11β-HSD1

The active form of 11β-HSD1 has been shown to be homodimeric and tetrameric in solution, initially evidenced through gel filtration chromatography (Kim et al. 2007) in addition to the more definitive crystal structures of the enzyme (table 6.1).

The overall organisation and topology of the homodimer as seen in figure 1.15B, is very similar to other Short-Chain Dehydrogenase / Reductase (SDR) family member species and consists of the C-terminal helix of one monomer and the C-terminal helix of the other to face each other in an anti-parallel manner. Each C-terminal helix will face its dimer partners' substrate binding pocket, and several residues act as a 'cap' structure over the substrate pocket. The interactions are hydrophobic and involve residues located on helices α-4 and α-5 (nomenclature from figure 1.3). Residues Arg 273, Lys 274 and Glu 277 on the C-terminal helix from one monomer interact with core residues on its dimer partner: Asp 191, Arg 198, Lys 199, Glu 254 and Glu 255. These interactions anchor the macromolecules together. The total buried surface area of the dimer interface is large at around 5129 Å (Zhang et al. 2005).

The C-terminal tail of 11β-HSD1 is relatively flexible, approximately 15 amino acids in length, and is not always well resolved in crystal structure refinements.

Tetramer formation involves pairs of C-termini in anti-parallel directions, generating a central four helix bundle of the C-terminal helices and a localization of active sites (figure 1.15D). Mutagenesis studies have shown that in the absence of the C-terminal (an 11β-HSD1 mutant lacking the last 28 amino acids), the enzyme cannot form a tetramer (Hosfield et al. 2005) verifying that this domain mediates tetramer assembly.

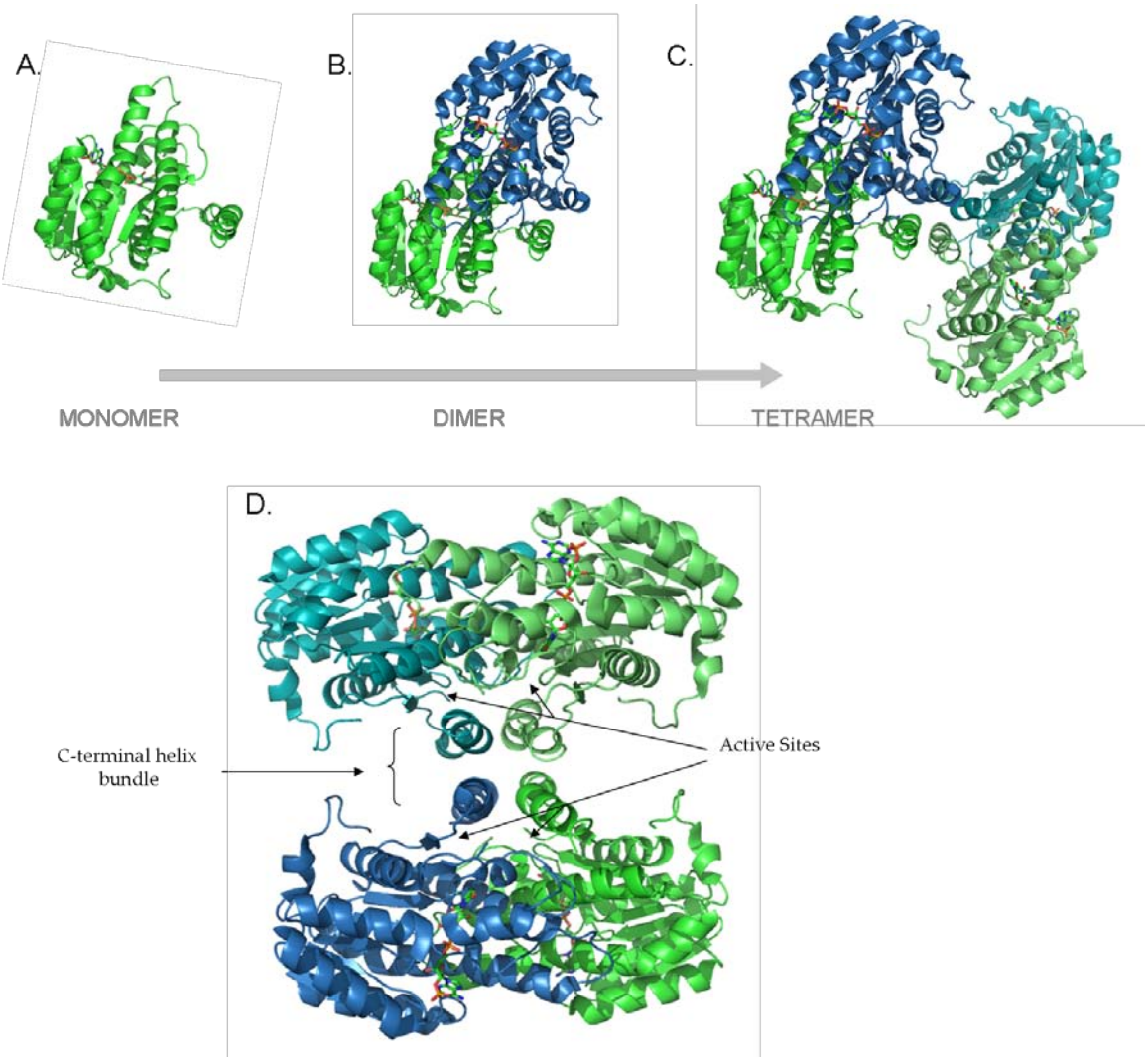

Figure 1.15: Oligomeric structures of 11β-HSD1: (A) monomer subunit (green) (B) Homodimer: the monomer from 1.14A in the same position (green) and a second monomer (blue) pictured. NADP(H) is visible in stick format. (C) Homo-tetramer: as 1.14B but with their tetrameric partners (pale green and teal). NADP(H) is visible in the Rossmann fold, in stick format. (D) Re-orientation of the tetramer showing the central four helix bundle of C-terminal helices and the positions of all four active sites. Pictures from the crystal structure 3D3E, prepared using Pymol.

1.9 Post-Translational Modifications of 11β-HSD1

The local cellular microenvironment of 11β-HSD1 has a knock-on effect not only on the bidirectionality of the enzyme but also its topology and post-translational modifications (PTMs). The lumen of the ER is an oxidising environment and therefore may facilitate formation of intra-chain sulphide bonds (Ozols 1995) particularly between Cys 77 and Cys 212.

Other PTMs of 11β-HSD1 include glycosylation, initially thought to affect the activity of the enzyme. More recent mutagenesis research indicates that glycosylation is important for preventing aggregation of the protein and stabilisation, but does not affect the activity or protein folding (Blum et al. 2000). Glycosylation sites include Asn 123, Asn 162, and Asn 207 (Arampatzis et al, 2005) for the human enzyme, however Asn 123 is located in a variable region of the enzyme and so is exchanged for Gln (in rat and mouse variants) and Tyr (in hamster and guinea-pig variants).

1.10 Pre-receptor Regulation of Glucocorticoid Activity

Glucocorticoids act through binding to the glucocorticoid receptor (GR), a nuclear hormone receptor which causes the transactivation or transrepression of numerous genes. These genes are involved in processes such as immune and stress responses, maturation and differentiation of cells, and the regulation of bone, carbohydrate, amino acid and lipid metabolism (Barnes 2005). Indeed, cortisol is one of the strongest known endogenous suppressors of the immune system but plays a modulatory role during inflammation and infection. The effects of cortisol are modulated by two mediators; (a) the glucocorticoid receptor and (b) the local tissue concentration of cortisol which is regulated by the 'pre-receptor metabolism' activity carried out by 11β-HSD1 and 11β–HSD2 (Classen-Houben et al. 2009).

Excessive glucocorticoid activity results in "Cushing's Syndrome", a disease with phenotypical characteristics such as high blood pressure, osteoporosis, abdominal obesity and a higher cardiovascular mortality risk. While Cushing's syndrome is rare, it does exemplify the pathological effects associated with imbalances in circulating cortisol levels.

Although the exact role of 11β-HSD1 in metabolic disease still remains to be fully elucidated, it is clear that it exerts an effect on the local glucocorticoid receptor activation; after all it has the role of metabolising cortisol in significant metabolic physiological locations, such as adipose tissue and liver.

1.10.1 Metabolic Syndrome

The metabolic syndrome can be broadly defined as a collective of medical disorders that includes type 2 diabetes, high blood pressure, central obesity, low HDL (high density lipoprotein) cholesterol, elevated triglycerides and uric acid levels and non-alcoholic fatty liver disease (NAFLD). Each of these symptoms alone can cause a higher risk of cardiovascular disease, but when combined increase the risk even further. The symptoms of metabolic syndrome are not always consistently defined but it is estimated that over 20 % of the U.S.A population currently live with the condition and its prevalence is strongly and unfailingly age-dependent (Eckel et al. 2005). This is summarized in figure 1.16.

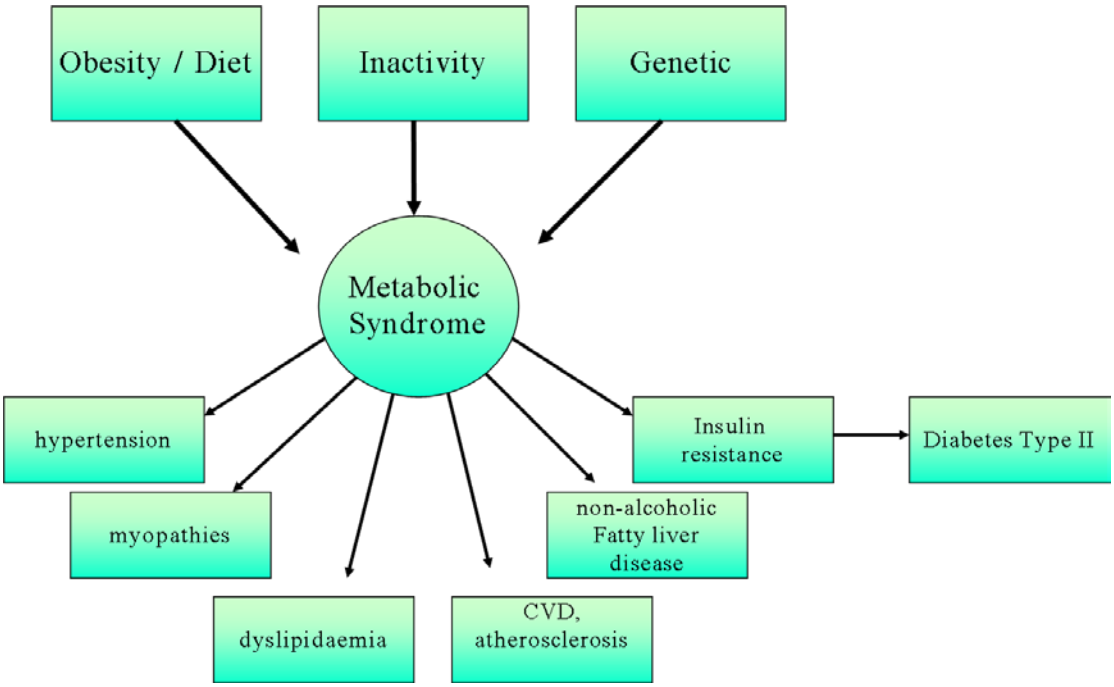

Figure 1.16: Flow chart indicating the risk factors for metabolic syndrome, and the disorders that this syndrome envelops.

The majority of current research focuses on the role of 11β-HSD1 inhibitors as a prophylactic treatment for complications associated with the metabolic syndrome; primarily in the prevention or reduction of obesity and type 2 diabetes. Disease models for obesity or insulin resistance are readily available and well-developed. For example, genetically obese Zucker rats are homozygous for the fatty (*fa)* allele which results in leptin receptor defects and leads to hyperphagia and obesity. Koletsky rats are obese and hypertensive, and Wistar Ottawa Karlsburg W rats are a new strain which exhibit many metabolic syndrome characteristics (Aleixandre de Artinano, Miguel 2009).

1.10.2 11β-HSD1 and Type 2 Diabetes

One potential therapeutic area for 11β-HSD1 is type 2 diabetes and its precursor: insulin resistance. Currently the 6th leading cause of death in the U.S.A, it has been estimated that by 2010, diabetes will exceed both heart disease and cancer as the leading cause of death through complications. Type 2 diabetes is closely associated with obesity and is characterised by an initial phase of progressive insulin resistance followed by the ensuing β–cell exhaustion (β–cells are the insulin producing pancreatic islet cells). This results in an unusually high blood glucose level through a lack of blood glucose control usually regulated by insulin.

A key feature in insulin resistance and the subsequent development of type 2 diabetes is postulated to be abnormal hepatic 11β-HSD1 reductase activity. Glucocorticoids are involved in the transcriptional control of several genes involved in the regulation of hepatic glucose production, such as the gene encoding PEPCK – an enzyme which catalyses the rate limiting step in gluconeogenesis. An excess of glucocorticoids may thus result in glucose intolerance and insulin resistance. It follows that inhibition of 11β-HSD1 would decrease the level of cortisol available, thus decreasing excessive hepatic glucose production in hyperglycemia and so potentially type 2 diabetes. Indeed, this hypothesis has been tested in several mouse models of type 2 diabetes which were given a small, non-steroidal selective inhibitor of 11β-HSD1 known as "BVT.2733" over a period of seven days (Alberts et al. 2003). BVT.2733 (synthesised by Biovitrum, Sweden) derives from the

arylsulfonamidothiazole class of inhibitors and is shown in figure 1.21. The results of this study showed a significant reduction in blood glucose and serum insulin levels in mice treated with BVT.2733 compared to mice treated with a placebo. The drug also improved insulin sensitivity, supporting the notion of 11β-HSD1 as a target for the treatment of type 2 diabetes.

It is noteworthy however, that administration of carbenoxolone - a non-selective 11β-HSD inhibitor - was found not to improve insulin sensitivity or glucose tolerance in lean or obese Zucker rats (Livingstone, Walker 2003). This was due to the liver-specific nature of carbenoxolone, which did not penetrate adipose layers and so did not inhibit adipose 11β-HSD1. Thus, a successful 11β-HSD1-inhibiting treatment for type 2 diabetes would require improved pharmacokinetic parameters.

1.10.3 11β-HSD1 and Obesity

Obesity is a condition which affects up to 300 million individuals globally according to World Health Organisation (WHO) statistics from 2003. A third of the U.S.A population was declared obese in 2004 (WHO) using criteria based on the number of individuals with a body mass index (BMI) of over 30 kg / m^2. Problems can then stem not only from the associative chronic diseases (as shown in figure 1.16) but also with financial drain on health care resources.

Overall there is a well-documented increase in 11β-HSD1 reductase activity (and thus cortisol) in visceral adipose tissue in obese patients and rodent models (Livingstone et al. 2000;Mericq et al. 2009;Rask et al. 2002;Wake et al. 2003) and reports of increased urinary free cortisol metabolite excretion (Livingstone et al. 2000;Andrew et al. 1998;Wajchenberg 2000;Marin et al. 1992) however the circulating cortisol levels remain constant. This increase in 11β-HSD1 activity (through an increase in enzyme expression) is thought to be regulated by glucocorticoids and insulin (Bujalska et al. 1997). When reproduced in transgenic mouse models overexpressing 11β-HSD1, the phenotypic results mimic those seen in patients with idiopathic obesity; the transgenic mice are found to have visceral obesity, hyperglycemia, hypertension, hyperlipidaemia, hyperphagia (and thus an increased sensitivity to weight gain) and insulin-resistant diabetes (Kotelevtsev et al. 1997).

When fed a high fat diet (45% fat) the transgenic mice were found to be approximately 16% heavier in weight than non-transgenic mice on the same diet (Masuzaki et al. 2001). When 11β-HSD1 is over-expressed in the liver only, mice show a mild insulin resistance, dyslipidaemia, hypertension and fatty liver.

Furthermore, cortisol is required for adipocyte differentiation (Liu et al. 2007) and accordingly is found in adipose tissue *in vivo*. Interestingly, there is an increase in the expression of H6PD during preadipocyte differentiation to adipocytes (Odermatt et al. 2006) suggesting a high local requirement for NADPH, potentially for the purpose of funding 11β-HSD1 with co-factor to enable cortisone reduction.

These studies show that there is clearly a role for 11β-HSD1 in obesity and insulin resistance. This raises more specific questions about the possible effects of 11β-HSD1 inhibition and whether the enzyme would make an effective drug target. This has been studied; in rodent obesity models, removing glucocorticoids will tend to reverse obesity and its metabolic abnormalities. In addition, mice given a daily administration of carbenoxolone - a non-selective 11β-HSD inhibitor – show a reverse in the effects of high-fat diet induced obesity and insulin resistance (Nuotio-Antar et al. 2007;Taylor et al. 2008) with no change in feeding habits.

By far the best example of the potential of 11β-HSD1 inhibition is observed in 11β-HSD1 knock-out mice which show improved glucose tolerance, reduced weight gain, reduced visceral fat accumulation (with chronic high-fat feeding) and a 'diabetes-resistant' phenotype (Kotelevtsev et al. 1997). This is summarised in figure 1.17.

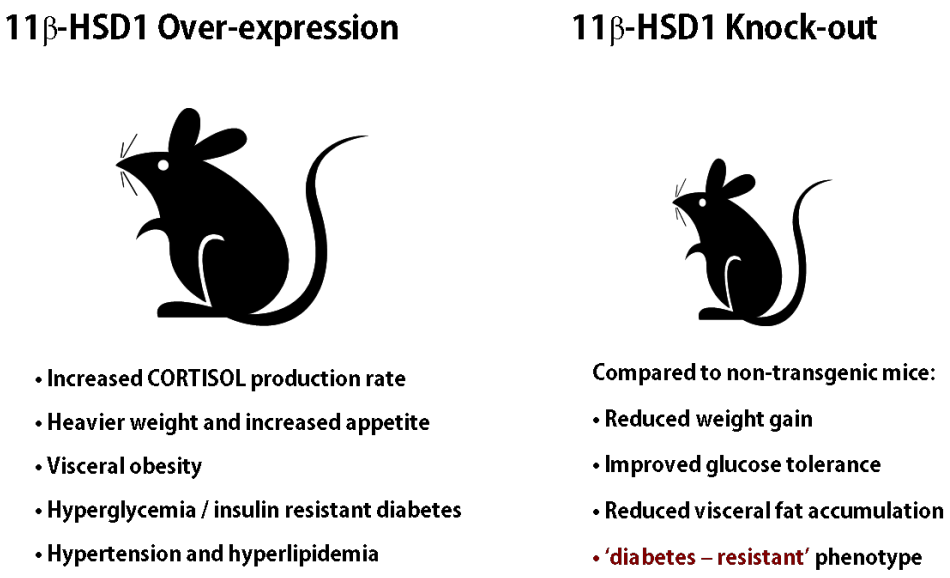

Figure 1.17: Cartoon mouse models illustrating the effects of excess 11β-HSD1 (on left, in a transgenic mouse model over-expressing 11β-HSD1 in visceral adipose tissue) and the absence of 11β-HSD1 (mouse on right, an 11β-HSD1 knock-out mouse).

Selective inhibition of 11β-HSD1 has therefore been proposed as a novel drug target for treatment of disorders associated with cortisol excess such as obesity, insulin resistance and type 2 diabetes with additional benefits in dyslipidaemia and hypertension.

Also, 11β-HSD1 inhibitors have been postulated to have a beneficial effect on cognitive impairment and other associated conditions.

1.11 11β-HSD1 and Cognitive Function

The role of 11β-HSD1 is less well documented for cognitive function compared to metabolic syndrome. Importantly, a rare polymorphism in the gene encoding 11β-HSD1 (*HSD11B1*) has recently been linked with increased risk of developing Alzheimer's disease; rs846911-C/A (Deary et al. 2006;de Quervain et al. 2004). Several other polymorphisms of the *HSD11B1* gene have been identified; interestingly some are associated with a cardiometabolic phenotype.

In addition to metabolic tissue, 11β-HSD1 mRNA has been localized to the human hippocampus, frontal cortex and cerebellum (Sandeep et al. 2004). Elevated cortisol levels in elderly humans and rodents correlate with hippocampus-dependent

memory impairments (Yau et al. 2007) and chronic glucocorticoid excess can have detrimental effects in the brain. These deleterious effects include psychosis, depression, neuroendocrine dysfunction, structural deterioration and cognitive impairment (Seckl, Walker 2004).

In the hippocampus specifically, an excess of glucocorticoids can potentiate excitatory neurotransmission, which has a knock-on effect on other electrophysiological brain functions such as long-term potentiation (LTP) – the process underlying memory formation and learning (McEwen et al. 1999). Indeed, mild cognitive impairment has been linked in the past with variations in glucocorticoid exposure (Lupien et al. 1998). Studies on rats with controlled low glucocorticoid levels throughout life (i.e. through neonatal handling or an adrenalectomy) show attenuation of certain deficits associated with ageing, such as hippocampal atrophy and cognitive decline, when compared to controls (Landfield et al, 1981, Meaney et al, 1988).

Human parallels have been carried out in small scale clinical trials. It has been observed that administration of carbenoxolone to healthy elderly men (55 – 75 years of age) or to elderly men with type 2 diabetes showed improved verbal fluency and verbal memory, respectively (Sandeep et al. 2004). When combined with the - albeit rare - polymorphism, an apparent role for 11β-HSD1 in cognitive decline and other age related mental deterioration emerges. However, the underlying biological complexities, intricacies and mechanisms involved in cognitive function and dysfunction mean that further detailed research is required in this area. A further challenge would be the design of CNS specific 11β-HSD1 inhibitors.

1.12 11β-HSD1 is a Pre-receptor Drug Target

It is apparent from the published evidence that it is the effects of excess cortisol in specific tissues which cause varying degrees of the metabolic syndrome. Therefore the objective in investigating treatments for these interventions is to target and antagonise receptors and enzymes involved in the production of cortisol, for example, certain key adrenal steroidogenic enzymes and the GR. Indeed there are clinically available GR antagonists (e.g. dexamethasone) and drugs which inhibit key enzymes involved in adrenal steroidogenesis (e.g. ketoconazole). The caveats of cortisol antagonism through these methods are the systemic side effects, particularly in times of physiological stress when an increase in glucocorticoids is necessary to elicit correct immune response but also interference with the negative feedback loop. Therefore a clear advantage of targeting 11β-HSD1 lies in the natural tissue selectivity presented by the enzyme, which has a high expression in white adipose tissue and the liver, allowing circumvention of the majority of systemic side effects. It is also a well defined and characterised protein with good quality structural data available and much documented evidence as to the benefits of its inhibition. The enzyme 11β-HSD1 is therefore an attractive therapeutic venture as a means of controlling local tissue concentrations of cortisol: a pre-receptor target.

1.13 Inhibitors of 11β-HSD1: Clinical and Preclinical

1.13.1 Selectivity

The selectivity of new inhibitors is of supreme importance to prevent any side effects associated with the ligand binding non-selectively to 11β–HSD2 or indeed other hydroxysteroid dehydrogenase enzymes such as 17β-HSD.

The isoform 11β–HSD2 will preferentially produce the inactive glucocorticoid in specific tissues in order to prevent the activation of the mineralocorticoid receptor (MR) by active glucocorticoid. Mineralocorticoid receptor activation by cortisol is, for unknown reasons, preferential to activation by its endogenous ligand – aldosterone (structure shown in figure 1.3). Inhibition of 11β–HSD2 would lead to an over-activated MR resulting in hypokalemia (potassium deficiency) and hypernatremia (elevated sodium levels) which would lead to hypertension.

Binding of inhibitors to alternative hydroxysteroid dehydrogenase enzymes would interfere with the sex steroid metabolism, for example, 17β-HSD inhibition would affect local estrogen metabolism. Therefore selectivity is the ultimate criteria in the development of new inhibitors for 11β -HSD1.

1.13.2 Endogenous Inhibitors of 11β-HSD1

Several endogenous substances have been reported to display inhibition of either isoform of 11β-HSD. Coined 'Glycyrrhetinic Acid-Like Factors' (GALFs)(Morris et al. 1992) they are endogenous substances initially detected in urine known to non-selectively inhibit 11β-HSD1. Further investigation is required to fully elucidate the mechanism and regulation of these substances, some of which are derivatives of cortisol and corticosterone. Those which inhibit 11β-HSD1 and 11β-HSD2 dehydrogenase are 3α-5α-tetrahydrocorticosterone, a derivative 3α-5α-tetrahydro-11β-hydroxyprogesterone, and 3α-5α-tetrahydro-11β-hydroxytestosterone. The compounds found to preferentially inhibit 11β-HSD1 reductase are 11-keto-3α-5α-tetrahydro-derivatives (Latif et al. 2005;Morris et al. 2007).

1.13.3 Clinically Available Inhibitors: Carbenoxolone

Currently there is one clinically available inhibitor for 11β -HSD1: carbenoxolone. It is a steroidal compound with an extended acidic chain on the A ring (figure 1.17). This extension protrudes from the mouth of the active site when bound, the remainder of the molecule is held in position by Leu 217, Ser 170 and Tyr 183 (the last two form part of the catalytic triad). In addition, polar interactions occur between the nicotinamide ring nitrogens and the carboxyl group of the 5th ring (figure 1.18).

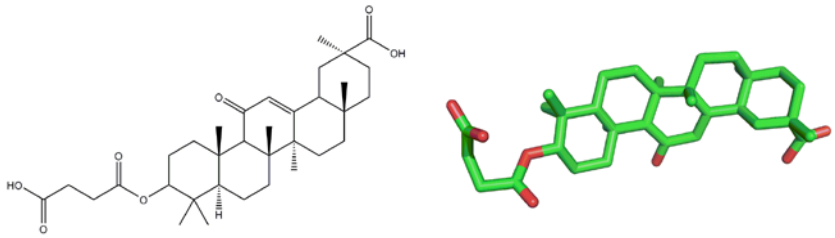

Figure 1.18: The 2-D and 3-D molecular structure of carbenoxolone, a clinically used inhibitor of 11β-HSD1 and 11β–HSD2, derived from the natural compound glycyrrhizin (GA). Figure prepared with Pymol.

There are also several major hydrophobic interactions and π-stacking keeping the carbenoxolone bound, resulting in a K_i of 20 nM. Inhibitor binding is shown in figure 1.19.

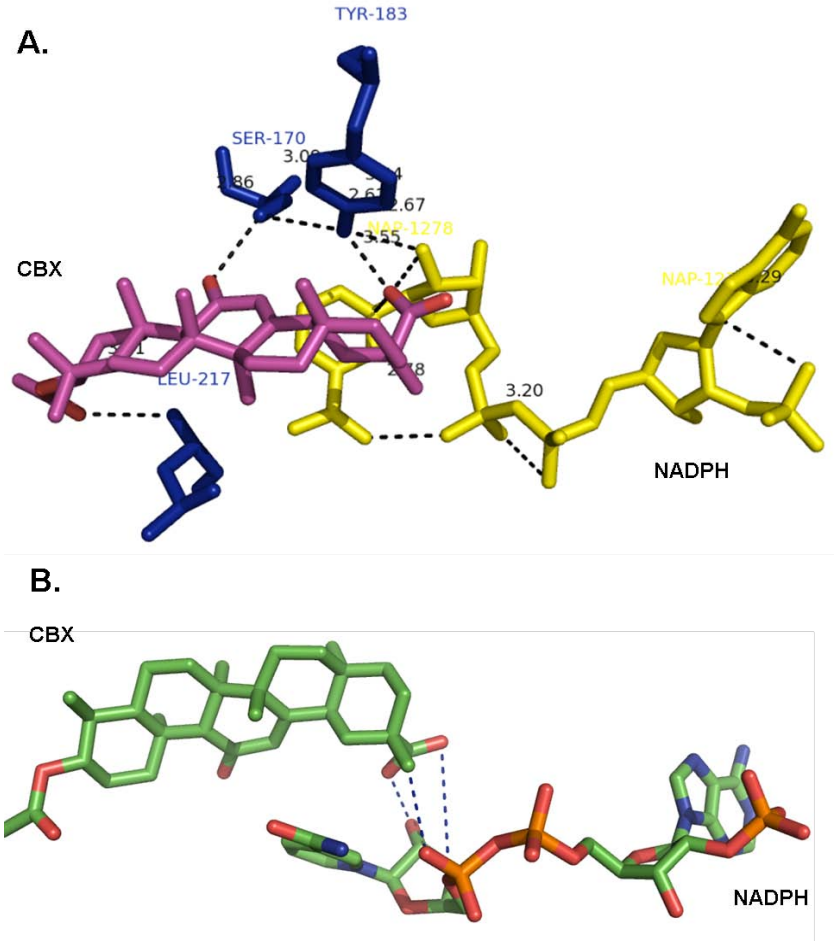

Figure 1.19: Carbenoxolone binding. (A) 3-D model of carbenoxolone (magenta) binding in the active site of the enzyme (blue), showing the 3 main interactions with Leu 217, Ser 170 and Tyr 183 and co-factor (yellow). (B) Simplified model of the interactions between carbenoxolone and co-factor NADP(H). Prepared with Pymol.

Crucially, carbenoxolone is a non-selective compound and inhibits both 11β-HSD1 and 11β–HSD2. Clinically it has been in use for almost 50 years, and is prescribed as a treatment for gastric ulcers in combination with other drugs to supplement the subsequently decreased potassium levels brought about by over-stimulation of the mineralocorticoid receptor. Carbenoxolone displays a liver-specific inhibition of 11β-HSD1, observed in both obese Zucker rats (Livingstone, Walker 2003) and humans with type 2 diabetes (Andrews et al. 2003). This has been postulated to be a pharmacokinetic challenge rather than one relating to experimental design or non-selective inhibition of other pathways.

Interestingly, carbenoxolone is a derivative of the natural product glycyrrhizin (GE) – a compound derived from liquorice root *Glycyrrhizia glabra*. Other derivatives from

this source have been harvested and analysed successfully for 11β-HSD1 selective inhibition such as 18α-glycyrrhetinic acid (18α-GA) and 18β-glycyrrhetinic acid (18β-GA) (Classen-Houben et al. 2009) which are discussed later in the text.

Pertinently, carbenoxolone appears to be several-fold more effective in inhibiting the mouse, rat and human enzymes as compared to dog, hamster and guinea-pig enzymes (Arampatzis et al, 2005) highlighting important cross species differences between the active sites of 11β-HSD1.

1.14 Preclinical Inhibitors: A Brief Introduction

In the interest of this project, the pre-clinical inhibitors covered in this section will be only those which have a corresponding 11β-HSD1 published crystal structure complex. This allows a detailed and more accurate analysis of the binding mechanistics for each inhibitor compound, expounding the available data for a rational drug design project such as this. Thus, it is by no means an exhaustive list of all current pre-clinical inhibitors, simply those that are most relevant. The compounds cited are summarised in table 1.5 at the end of this section for clarity.

Despite the enzyme being effectively characterised in the 1960s, it is only recently that patents have been filed for compounds inhibiting 11β-HSD1. In 2001 the first patent was claimed, and there has been a swift growth in the number of patents claimed since 2004. It is estimated that there are over 60 patents currently filed (Webster, Pallin 2007). As of 2007, there were three compounds in clinical development: INCB-13739, AMG-221, and PF-915275, with many more in pre-clinical stages. All of the compounds in clinical development are reportedly targeting type 2 diabetes rather than any other element of the metabolic syndrome, as it has the most validated research.

Numerous other pharmaceutical companies have filed for patents; a recent report documented over 14 individual pharmaceutical companies filing for patent applications for 11β-HSD1 inhibiting compounds, with many filing more than one patent. The principal players were Incyte and Biovitrum (these compounds were subsequently sold to Amgen in 2003) (Norman 2007).

1.14.1 Liquorice Root Derivatives

Although these compounds do not share a co-crystal structure, liquorice root derivatives such as glycyrrhizin (GE), 18β-glycyrrhetinic acid (18β-GA, shown in figure 1.20A) and subsequent derivatives - such as carbenoxolone (CBX) – are known potent inhibitors of 11β-HSD1. This has led to a dynamic search for the development of more active and selective natural-product derived inhibitors for 11β-HSD1.

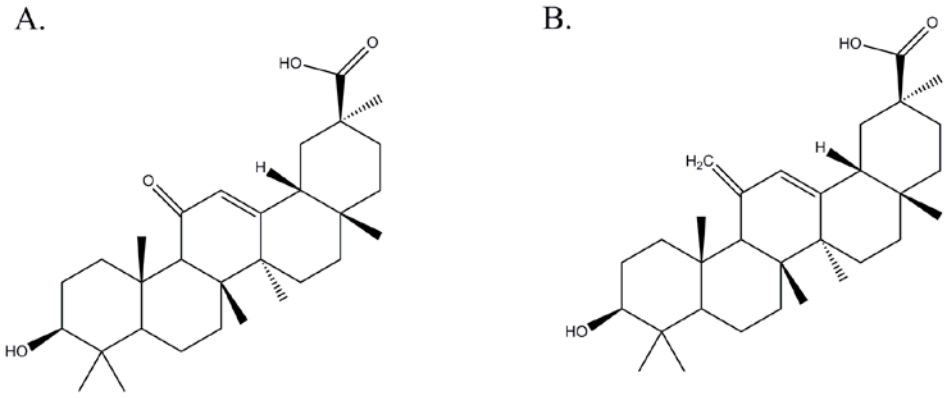

Figure 1.20: (A) Chemical structure of 18β-glycerrhetinic acid (18β-GA) (B) The chemical structure of the 11-exo-methylene derivative of 18β-GA demonstrating the importance of the hydrogen acceptor suitability of the 11-position (Su et al. 2007).

The compound 18β-GA is a potent, non-selective inhibitor of 11β-HSD with an IC_{50} value in the nano-molar range (Buhler et al. 1991;Monder et al. 1989). Although non-selective, it has been trialled clinically, and 18β-GA has even reportedly been shown to reduce subcutaneous thigh fat after topical application (Armanini et al. 2005). Furthermore, several 18β-GA derivatives have been discovered to be selective 11β-HSD1 inhibitors (Su et al. 2007) as shown by inhibition assays using homogenous time resolved fluorescence (HTRF) on human liver microsome fractions. Modifications made to the parent compound at positions 11 and 30 (see figure 1.3 for carbon numbering in steroids) conferred selectivity against the rat enzyme. These assays also confirmed the importance of a hydrogen bond acceptor group at position 11 by demonstrating the loss of potency of the compound when a methylene group is substituted, as shown in figure 1.20B.

Further development is currently underway with compounds similar to 18β-GA (Classen-Houben et al. 2009) however concerns regarding the cell membrane permeability of this class of compounds have been raised.

1.14.2 β-keto Sulfone Inhibitors

The β-keto sulfones are a class of selective inhibitors developed by Wyeth with a ketone moiety which mimics the ketone group in cortisone, as shown in figure 1.21.

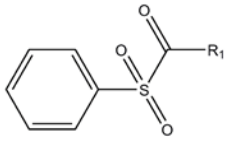

Figure 1.21: Skeleton structure of β-keto sulfone class of inhibitors. The highest potency is found when R^1 = 3-MeO-Ph.

However the β-keto sulfone series hold a drawback: the potential for 11β-HSD1 to turn-over this compound, producing potentially ineffective hydroxyl sulfones (Xiang et al. 2005, Xiang et al. 2007). Similar in nanomolar IC_{50} potency are the arylsulfonamidothiazole and arylsulfonamidooxazole compounds shown in figure 1.22, apparently circumventing the metabolic challenges faced by the β-keto sulfone class by the addition of an amido substituent from the central sulfur atom.

1.14.3 Sulfonamides

The sulfonamide moiety is an important central scaffold for inhibitors of 11β-HSD1, as it provides a hydrogen bond acceptor group which then interacts with Tyr 183 and Ser 170 of the catalytic triad. Understandably then, this scaffold has been repeatedly seen in reports of potent inhibitors, typically unearthed using pharmacophore models of existing potent inhibitors and also through structure based drug design (Barf et al. 2002;Yang et al. 2009). Indeed this scaffold can be seen in INCB-13739 (Incyte) which is one of the three 11β-HSD1 inhibitors currently undergoing clinical trials. The compound INCB-13739 has been reported to markedly enhance hepatic and peripheral insulin sensitivity in a trial of 30 patients with type 2 diabetes (Hawkins M et al. 2008). It was also a feature of BVT 3498 (Biovitrum) which entered clinical trials in 2003 but was a phase II failure.

Currently in development by Amgen (Tu et al. 2008) are a class of sulfonamides reported to be selective nanomolar inhibitors. The original skeleton structure of this series is shown in figure 1.22A, with the most potent drug in this class (figure 1.22B)

which has been co-crystallised with the human enzyme. The class of inhibitors consisted of the sulfonamide core, with additional substitutions on and off the benzamide ring. The addition of a long chain with one additional hydrogen acceptor and one hydrogen donor group (1.22B) was found to very slightly enhance binding to the human enzyme, from an IC_{50} of 2.1 nM to 1.2 nM.

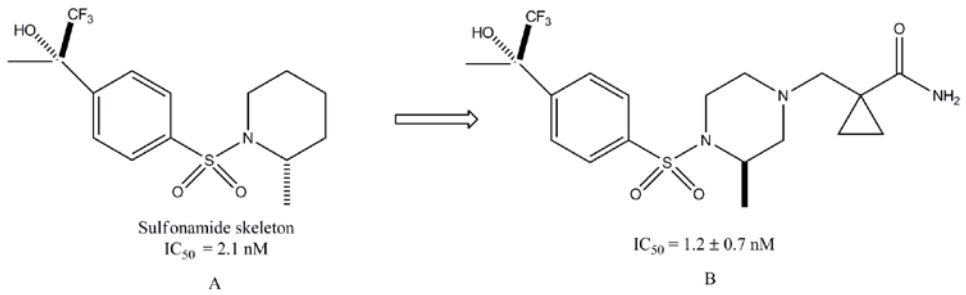

Figure 1.22: (A) the chemical structure of sulfonamide skeleton (B) the most potent compound in the sulfonamide series.

The sulfonamide compound B (figure 1.22B) binds in a competitive manner in the active site as demonstrated by scintillation proximity assays (described in chapter 5) using recombinant full-length human enzyme, with an approximate K_i of 1 nM for the reductase reaction. A crystal structure of a tetrameric 11β-HSD1 in complex with the highly potent sulfonamide compound B was subsequently deposited in 2008 (PDB accession 3D4N (Tu et al. 2008)) and demonstrates inhibitor binding in the catalytic site, reproduced simplistically in figure 1.23A. It is interesting to note that despite predictions of interaction with the catalytic triad, there are no direct contacts between the central sulfonyl group and these residues, simply a hydrogen bond between the backbone of Ala 172 and the oxygen from the sulfonyl group.

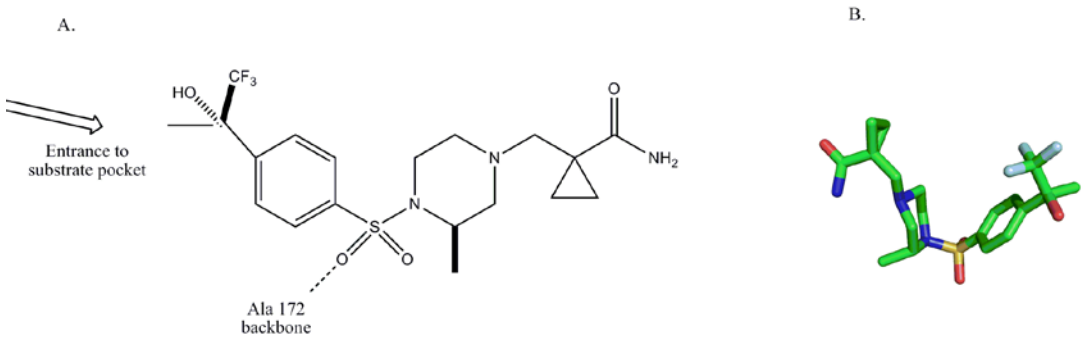

Figure 1.23: (A) Depiction of sulfonamide inhibitor binding in the active site of 11β-HSD1. (B) 3-D model of the molecule.

The 3-dimensional structure of the molecule (1.23B) shows it exists and binds in a V-shape. When bound the cyclopropane carboxamide group points toward the exterior of the protein (and the C-terminal dimer interface of the adjoining dimer).

Other sulfonamide scaffolds in development by Biovitrum (Barf et al. 2002) are the arylsulfonamides. These were discovered through a high-through put screen of the in-house compound database then a lead optimisation process.

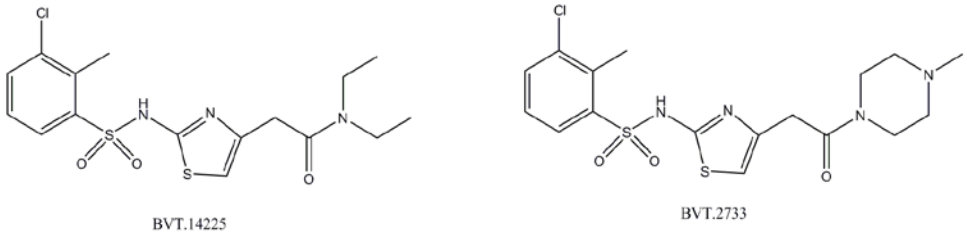

Figure 1.24: Chemical structure of two arylsulfonamide compounds; BVT 14255 (left), and BVT 2733 (right), Biovitrum.

These compounds showed a good metabolic profile and were selective for 11β-HSD1. However, they were not as potent as the competitor compounds, with IC_{50} values of 52 nM and 3341 nM for BVT 14225 and BVT 2733 respectively.

With regards to this project, the relevance of these inhibitors is the different affinity in human and mouse recombinant 11β-HSD1. As seen in figure 1.24, the single difference between the two compounds is the nature of the substitution – one diethylamide and the other N-methylpiperazinamide. The bulky piperazinamide (BVT 2733) is not tolerated well in the human enzyme, thus reducing the affinity of binding for human enzyme. In mouse enzyme assays this bulky group appears to enhance binding affinity, giving an IC_{50} of 96 nM (compared to a human assay IC_{50} 3.3 nM). A smaller, more flexible substituent in BVT 14255 produces better binding in human (IC_{50} 52 nM) compared to mouse (IC_{50} 284 nM). The authors suggest that it is this solvent-facing end of the molecule which can dictate the extent of inhibition in either mouse or human enzyme.

1.14.4 Benzamides

An additional series of inhibitors developed by Amgen stemmed from the core sulfonamide structure BVT 14225 (figure 1.24) replacing the sulfonyl group with an amide defining the benzamide class (figure 1.25, Julian et al. 2008).

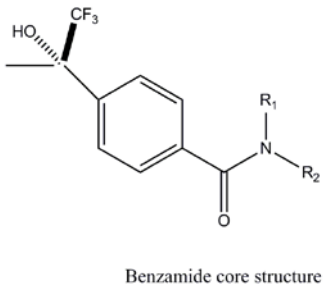

Benzamide core structure

Figure 1.25: Chemical structure of core benzamide compound.

One of the principal aims of employing this new class of inhibitors was to attain a drug with an improved metabolic profile, therefore substitutions made at R_1 and R_2 were initially based not only on potency but also on metabolic stability in cultured rat and human liver microsomes. Improved *in vitro* human metabolic stability was explored when R_1 = *N*-cyclopropyl, which, when combined with R_2 = a trans-aryl, hetero-aryl or alkyl group demonstrated a set of three corresponding compounds with the most promising *in vitro* and *in vivo* pharmacokinetic profiles. In particular, the substitution of R_1 = N-cyclopropyl and R_2 = hetero-aryl displayed an IC_{50} of 1.4 nM with recombinant human enzyme as determined by scintillation proximity assay (SPA). This compound is seen in a complex with the enzyme in PDB deposition 3D3E (Julian et al. 2008) and is observed to bind in a V-shape with the pyridine ring toward the exterior and the trifluoromethyl tertiary alcohol buried within the active site in close proximity to the co-factor. This can be seen in figure 1.26B.

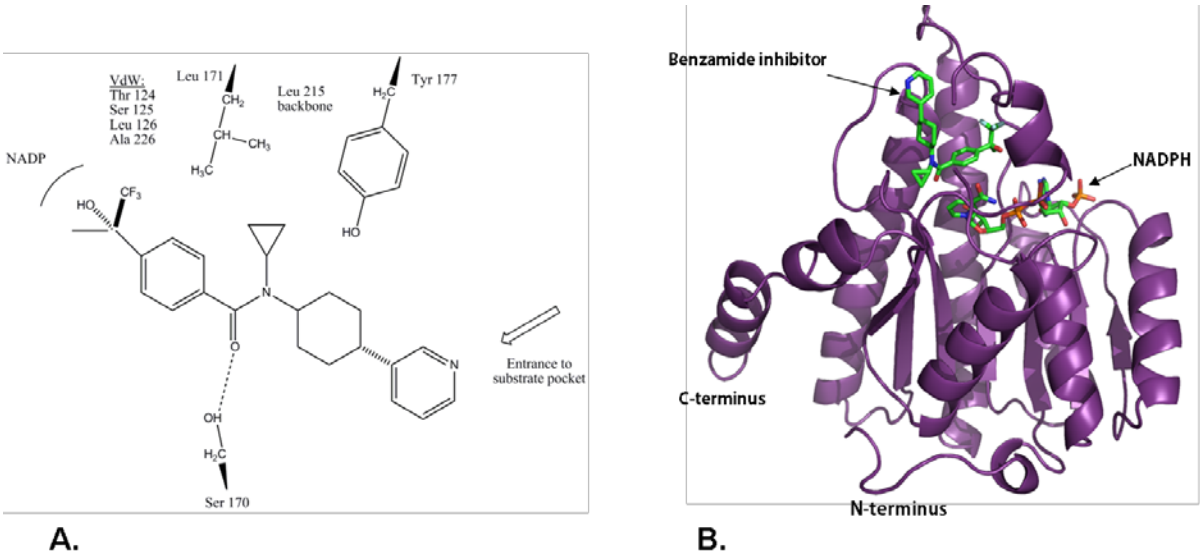

Figure 1.26: The most promising compound from the benzamide series, (A) A 2-D drawing of the benzamide ligand binding. (B) Benzamide compound bound to enzyme (one 3D3E monomer shown in purple). The ligand can be seen on the left hand side forming a V-shape, with the piperazine ring facing out of the binding pocket. The trifluoromethyl tertiary alcohol is buried into the pocket in close proximity to co-factor which can also be seen on the right hand side. Illustration prepared with Pymol.

1.14.5 Triazoles

The triazole class of 11β-HSD1 inhibitors have been developed by Amgen (Tu et al. 2008) with a subsequent X-ray crystallography structure deposited in the PDB in May 2008 (3D5Q). The triazole compound shown in figure 1.27 is the most potent, with a mixed inhibition profile.

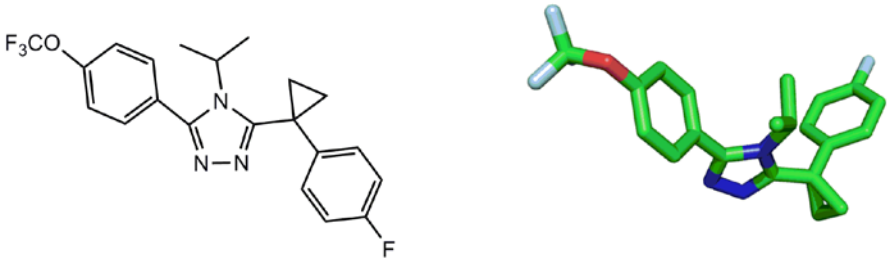

Figure 1.27: Chemical structure of Amgen triazole compound seen in the co-crystal structure 3D5Q. On the right hand side is a 3-D model of the molecule, to demonstrate the V-shape formed. This illustration prepared with Pymol.

The calculated IC_{50} value for this selective compound is 1.6 ± 0.5 nM for the reductase reaction, as determined by SPA in full-length recombinant 11β-HSD1. The compound binds to 11β-HSD1 in an L-shape through two members of the catalytic triad, Tyr 183 and Ser 170 acting as hydrogen bond donors to the nitrogen atoms in the triazole ring. Several Van der Waals interactions between the fluoro-phenyl group, buried into the active site, exist between the phenyl ring and Thr 124, Leu 126; and the fluoride atom and Ser 125, Leu 126. The presence and bulk of this compound forces not only Ser 170 to rotate 180° but also Tyr 177 to arc away from its usual position at the mouth of the enzyme due to the presence of the trifluoromethyoxy phenyl group. This is demonstrated in a 1-dimensional format in figure 1.28A and a close up of the active site from 3D5Q in figure 1.28B.

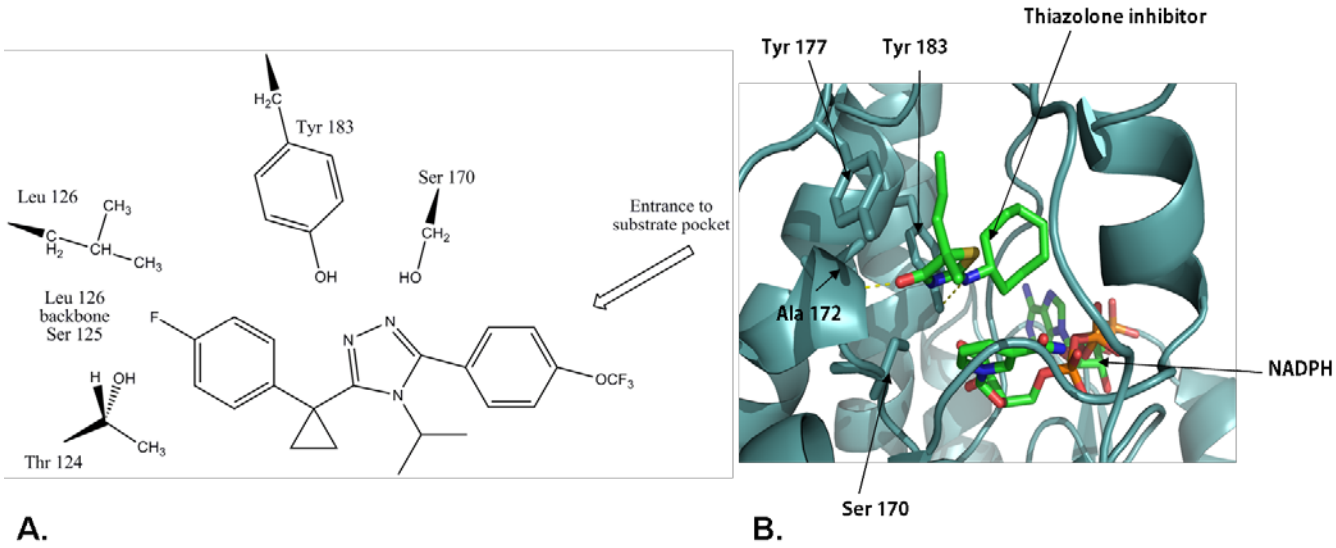

Figure 1.28: (A) Residues involved in Amgen triazole inhibitor binding (B) enzyme complexed with triazole compound.

1.14.6 Adamantanes

Abbott (Sorensen et al. 2006) developed a series of adamantane amide inhibitors which were reportedly long-acting, dually potent (against human and mouse), with good metabolic profiles.

The adamantane scaffold is shown in figure 1.29, with three of the highest potency compounds, labeled 2-4. Due to the lipophilicity of the steroid binding site of 11β-HSD1, potential inhibitors must have several hydrophobic features, but also

maintain a good metabolic stability. To this end, the addition of polar groups at either end of the inhibitor molecule may improve metabolic stability but may equally reduce permeability.

A year later a new series of adamantyl inhibitors emerged from Abbott (Sorensen et al. 2007) with a sulfone group off the adamantane (figure 1.29, compound 5). This appeared to help resolve issues with metabolic stability and consequently a crystal structure of human 11β-HSD1 in complex with an adamantane sulfone compound (compound 6 in figure 1.29) emerged (PDB 2ILT). From this structure it is possible to observe that the adamantyl sulfones bind in a manner similar to the sulfones; that is to say that the central carbonyl group acts as a hydrogen bond acceptor from Tyr 183 and Ser 170 in the catalytic site. This particular compound (compound 6 in figure 1.29) was also found to strongly inhibit liver, fat and brain 11β-HSD1 and was a long-acting inhibitor.

In addition to these adamantane containing compounds are a series of adamantyl amides developed at the University of Edinburgh (Webster et al. 2007), one of which is depicted in figure 1.29, compound 7. Replacement of the adamantyl moiety with smaller substituents resulted in a decrease in potency suggesting the importance of a bulky, lipophilic group. Also noted was that the addition of larger phenyl or benzyl groups from the piperazine structure resulted in a loss of potency. Keeping this substituent small and relatively hydrophobic increased potency (in compound 7 it is an ethyl). Potentially it is this region of the molecule which is in close contact with the co-factor deep within the pocket where space and hydrophobicity is at a premium.

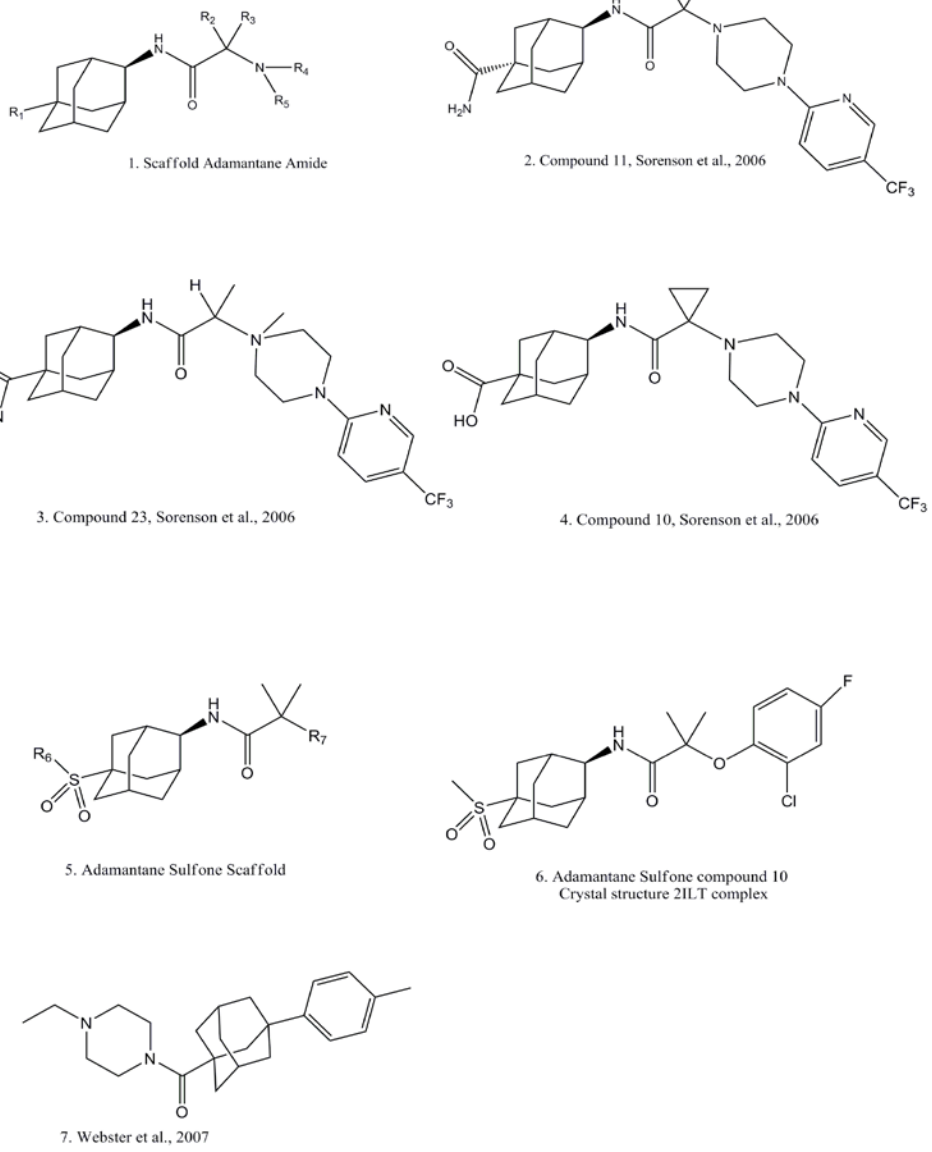

Figure 1.29: Overview of adamantane inhibitors. (1) is the adamantane scaffold molecule, compounds (2), (3) and (4) (Sorensen et al. 2006) are the most potent variations of the scaffold molecule with differing substituents. Compounds (2) and (3) were potent against human and mouse enzyme but (4) was less potent. For compounds (2), (3) and (4) the human K_i values were: 8 nM, 9 nM and 7 nM respectively. For mouse 11β-HSD1, the K_i values are: 15 nM, 5 nM and 500 nM respectively. In human 11β-HSD1 expressing HEK-293 based assays, the IC_{50} values are 22 nM, 45 nM and 45 nM, respectively. Compounds (5) and (6) (Sorensen et al. 2007) are adamantyl sulfones, (5) is the scaffold of this series, (6) is one of the more potent inhibitors from this series (K_i 7 nM with human recombinant protein, 4 nM with mouse recombinant enzyme and an IC_{50} of 98 nM in HEK-293 cells over-expressing human 11β-HSD1). (7) (Webster et al. 2007) shows an IC_{50} of 82 nM for human enzyme.

Further to this, Merck-Serono have used the adamantine series of inhibitors as lead compounds and by using a structure activity relationship (SAR) methodology have designed structurally divergent inhibitors currently in pre-clinical development (Roche et al. 2009).

1.14.7 Thiazolones

Another class of compounds in complex with a published crystal structure of 11β-HSD1 are the thiazolones. The 2-anilinothiazolones are a novel class of inhibitors designed in a collaborative effort by Amgen and Biovitrum (Yuan et al. 2007). These compounds were designed using a systematic structure-activity relationship (SAR) based approach. The compound shown in complex in the published crystal structure 2RBE is shown in figure 1.30.

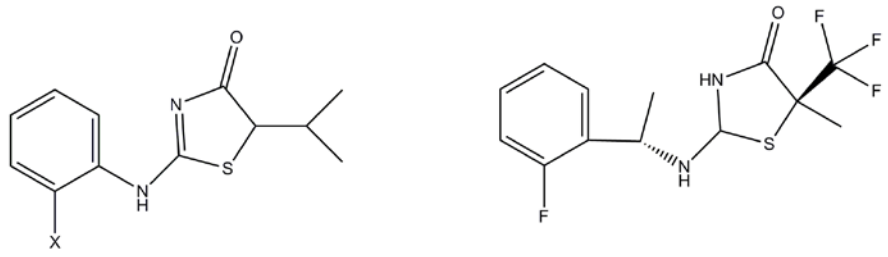

A. 2-anilinothiazolone scaffold
X = F is the inhibitor in the published crystal structure 2RBE
Yuan et al., 2007

B. Structure of inhibitor in 3BZU
Hale et al., 2007

Figure 1.30: A: 2-anilinothiazolone scaffold from (Yuan et al. 2007), B: thiazolone inhibitor in complex with human 11β-HSD1 in 3BZU.

A SAR approach was taken in the design of these compounds initially replacing the isopropyl group with lipophilic substituents, followed by systematic replacement of the aryl group with various heteroaromatic groups. The most potent substitution at this point was isoquinolinyl which gave a K_i of 32 nM (compared to 110 nM for an aryl group). However, this substituent was thought to affect membrane permeability of the compound as the cell-based IC_{50} value was significantly higher.

Subsequently the C-5 substituent was varied ('X' in figure 1.30A). The most potent substituent at this location was a fluorine or a chlorine atom, which gave a K_i of 17 nM and 7.2 nM respectively and it is the 2-fluoro structure that is seen in 2RBE. This binds in a manner similar to the sulfones; there are interactions of the imine-like and endocyclic nitrogens with Ser 170 and Tyr 183 of the catalytic triad. In addition the

Tyr 177 phenyl ring and the thiazolone core are both perpendicularly planar allowing for π-stacking interactions.

Another 11β-HSD1 inhibiting compound which has a co-crystal structure published with the enzyme (3BYZ) is (5S)-2-(cyclooctylamino)-5-methyl-5-propyl- 1,3-thiazol-4(5H)-one, a member of a thiazolone class of compounds from Amgen/Biovitrum (Johansson et al. 2008). This particular compound (figure 1.31A) has a K_i of 28 ± 9 nM in human enzyme assays. Binding is shown in figure 1.31C.

This set of ligands was a continuation from the previous set, the anilinothiazolones; where the same scaffold structure is maintained and compounds were assessed via their SAR and correspondingly optimised. It is surprising then, to discover that this compound binds differently to that observed in 2RBE and 3BYZ with the fluorophenylthiazolone compounds (shown in figure 1.30A and B).

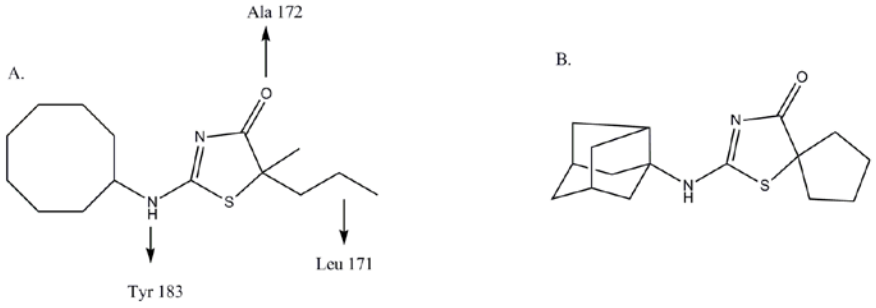

Figure 1.31 (A) (5S)-2-(cyclooctylamino)-5-methyl-5-propyl-1,3-thiazol-4(5H)-one: the ligand present in 3BYZ. (B) Further optimisation yielded this ligand.

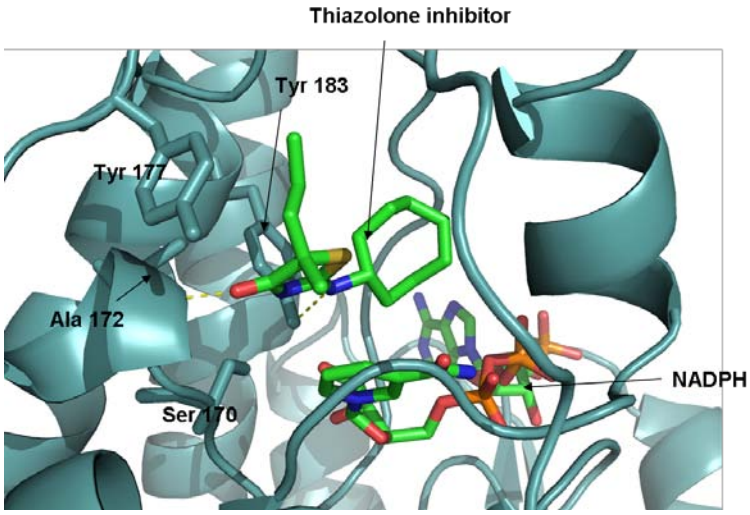

Figure 1.31 (C) An illustration of the binding site from 3BYZ.

The main differences in binding are a direct interaction between the carbonyl of the thiazolone group with the backbone NH proton of Ala 172, in 3BYZ, whereas in 2RBE there is an indirect interaction: the backbone NH proton of Ala 172 interacts instead with Ser 170, and the OH proton of the Ser 170 then forms an interaction with the exocyclic nitrogen lone pair on the inhibitor. The varying tautomeric states of both ligands (from 3BYZ and 2RBE) allow for different interactions in the binding site. This applies also to the Tyr 177 residue near the mouth of the binding pocket; the phenyl ring of this residue π-stacks with the planar thiazolone ring of the inhibitor in 2RBE. However in 3BYZ this does not occur: the Tyr 177 swings away from the inhibitor and subsequently the neighbouring residue Leu 171 forms contacts with the propyl moiety from the thiazolone ring (Johansson et al. 2008;Yuan et al. 2007).

Following the publication of 3BYZ, further SAR carried out yielded a far more potent inhibitor shown in figure 1.31B, which has a 5-membered ring replacing the propyl chain at position 5 of the thiazolone and a noradamantyl function replacing the cyclo-octyl ring. This added bulkiness on the left hand side of the molecule (this is the part of the molecule which is buried into the hydrophobic pocket), appears to enhance potency in human enzyme as observed with the adamantine series. The potency is increased to yield a K_i of 3 ± 1 nM in human enzyme assays and displays excellent selectivity and pharmacokinetic data, despite a much lower potency in the mouse enzyme.

1.14.8 Arylsulfonylpiperazines

In 2008, Amgen put forward another series of inhibitors: the arylsulfonyl piperazines, as potent and selective inhibitors of 11β-HSD1 (Sun et al. 2008;Sun et al. 2009) and in addition published the co-crystal structures (PDB accession 3CZR and 3D4N). Previous 11β-HSD1 inhibitor series' from Amgen have also included compounds with a central sulfonyl group, which was found to be important for 11β-HSD1 inhibition. This was determined using a SAR approach and varying each moiety systematically. This is demonstrated in figure 1.32A which is the chemical

structure of the most potent inhibitor from this series and is the compound seen in the crystal structure 3CZR (Sun et al. 2008).

Indeed, the development of these inhibitors is an exquisite example of employing SAR to significantly improve the potency and pharmacokinetic properties of a compound. Initially the sulfonyl group was replaced with urea, amides or methylene groups, finding the original sulfonyl compounds to be most potent. Subsequently, the sulfonyl aryl group was varied and investigated (figure 1.32A, area 2) followed by substitutions and replacements at the pyridyl ring (figure 1.32A, part 3 and 4), substitutions from this and finally the piperazine ring (figure 1.32A, part 5). However the most potent compound from this series (shown in figure 1.32, A and B) displayed a poor oral bioavailability in rodents and was water-insoluble. Further SAR was carried out (Sun et al. 2009) to yield the structure shown in figure 1.32C and D.

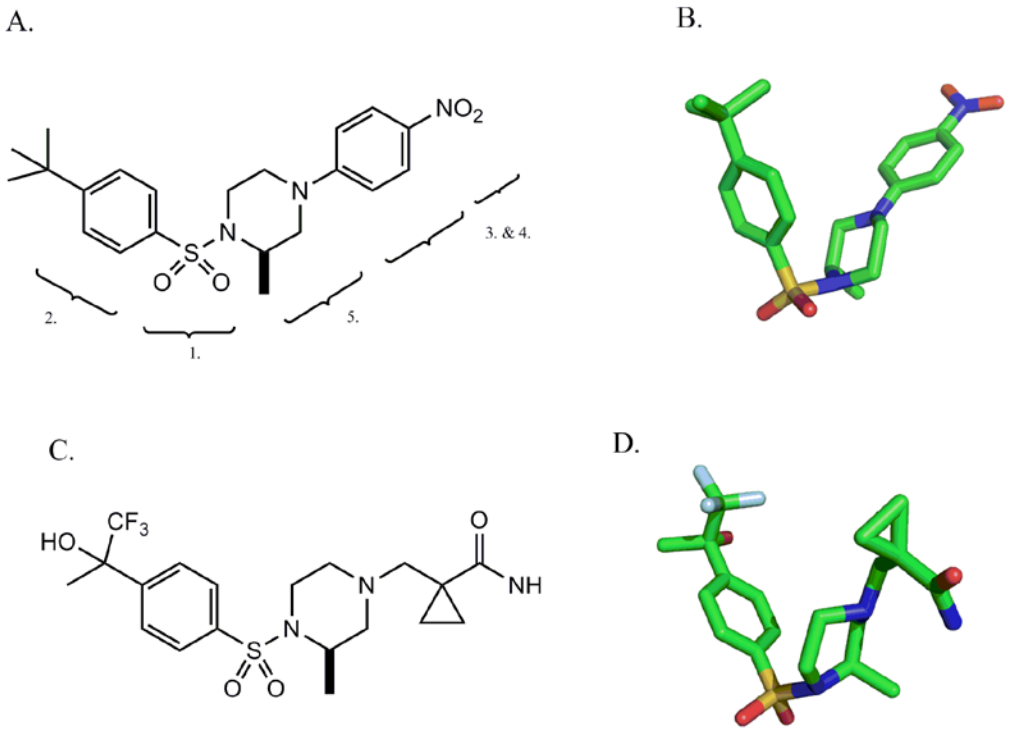

Figure 1.32: Overview of the arylsulfonylpiperazines. (A) and (B) Chemical structure of the most potent compound from the arylsulfonylpiperazine series, the 3-D model structure shows that it forms a V-shape similar to previous 11β-HSD1 inhibitor series'. (C) and (D) Further SAR yielded a compound with higher potency which co-crystallised with human 11β-HSD1.

The tert-butylphenyl group of the initial compound (1.32A: on the left hand side of the molecule) is located in close proximity to the co-factor and the backbone of Ala 172. The hydroxyl of Ser 170 forms a polar contact with the sulfonyl group oxygen atoms. The second compound (figure 1.32C) was found to bind to the enzyme in the same manner but exhibited improved kinetics: the IC_{50} of A was 10 nM, of B was 0.7 nM in recombinant human enzyme SPA. In HEK293 cells overexpressing 11β-HSD1, the IC_{50} values were: for B = 14 nM, A = 247 nM.

1.14.9 Pyridine Amides

This class of compounds were developed by Bristol-Myers Squibb (Wang et al. 2008) and have a co-crystal structure which was deposited in March 2008 (3CH6). A SAR approach concluded that meta-substituted regio-isomers showed higher potency than para-substituted analogues on the central pyridine ring. Lipophilic substituents such as 3,3-dimethylpiperidyl amide enhanced potency. In addition, linear isomers tended to exhibit weaker potency as compared to V-shaped molecules.

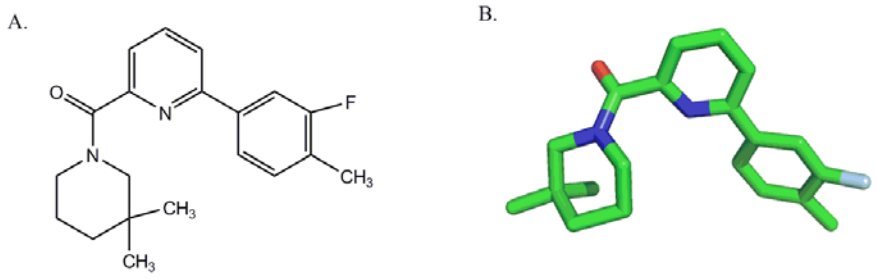

Figure 1.33: Chemical structure of the most potent compound from the pyridine amide series, in a 2-dimensional drawing (A, left) and a three-dimensional model (B, right).

The compound observed in the X-ray crystal structure 3CH6 is shown in figure 1.33, and forms polar interactions with Ser 170 and Tyr 183; while the dimethylpiperidyl substituent is buried further into the binding pocket; the central pyridine core forms contacts with Tyr 177. In SPA this compound exhibited one of the highest potencies with an IC_{50} of 0.1 nM.

1.15 An 11β-HSD1 Inhibitor Summary

There are currently several classes of 11β-HSD1 inhibitors under investigation, many with nanomolar inhibition kinetics and reasonable metabolic profiles. These investigations allow for a SAR analysis across many different compound classes, allowing for the improvement of existing inhibitors and an excellent starting point and comparison in the development of new inhibitors; as in the case of this PhD project. The major classes of 11β-HSD1 inhibitors which are relevant to this project have been tabulated for comparison in table 1.5.

Inhibitor binding is mediated by a group of 8 to 10 amino acids in the active site; the residues involved differ depending on the structural features of the 11β-HSD1 inhibiting compounds. An overview and further analysis of each inhibitor class binding is shown in figure 1.34.

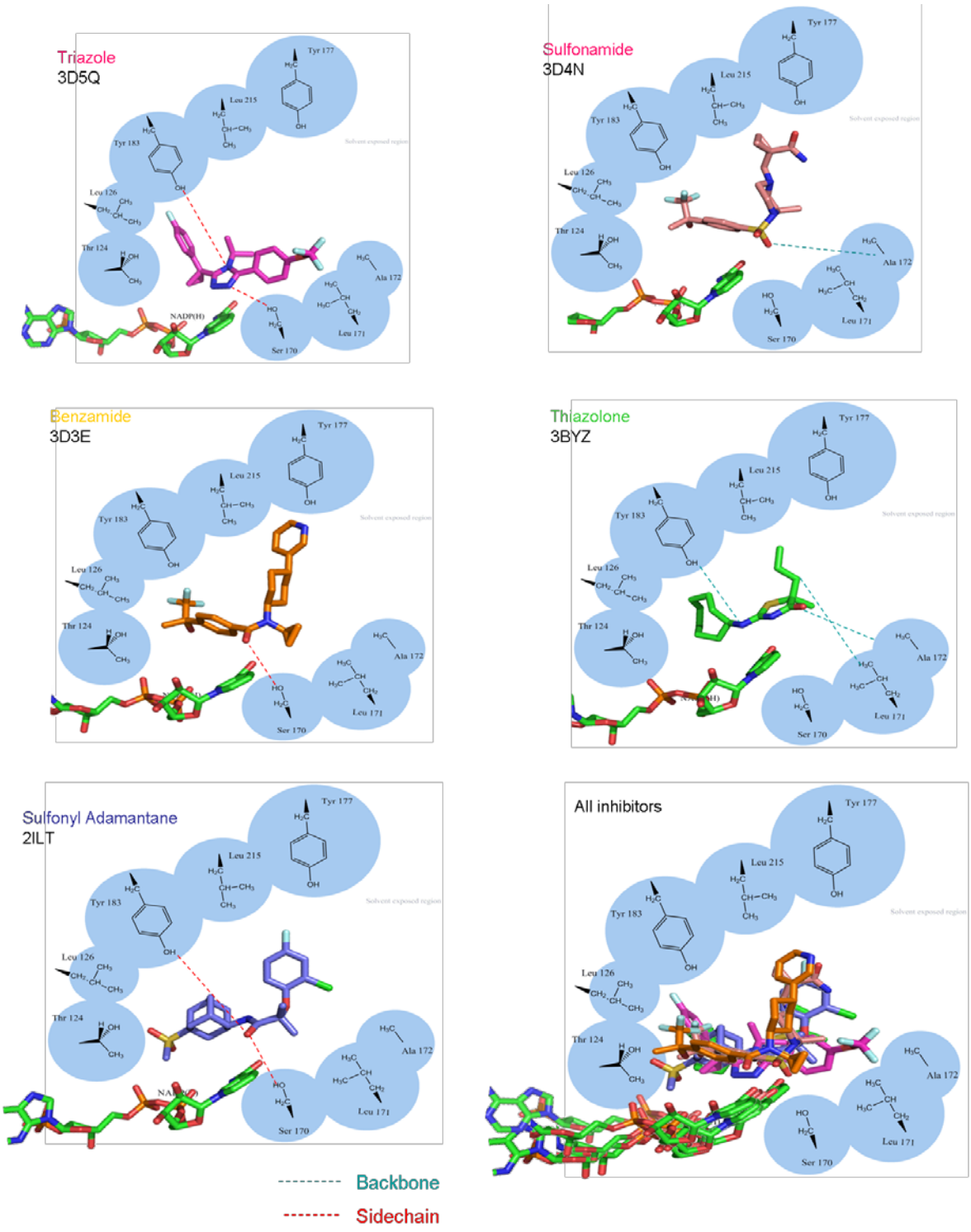

Figure 1.34: Illustration of the active site of 11β-HSD1 (each residue shown in blue) and five important classes of inhibitors superimposed in the binding site. These are identified by their differing colours and are labeled. The compounds shown are those which exhibited the highest potency of their compound class in 11β-HSD1 inhibition assays and are discussed in the text. Final image is a superimposition of all 5 inhibitors onto the 11β-HSD1 active site. NADPH is shown at the bottom, in green, distances are not to scale.

An additional analysis of the 11β-HSD1 binding pocket was carried out by examining existing ligand orientation and position in crystal structures and superimposing them (figures 1.34 (final image) and 1.35).

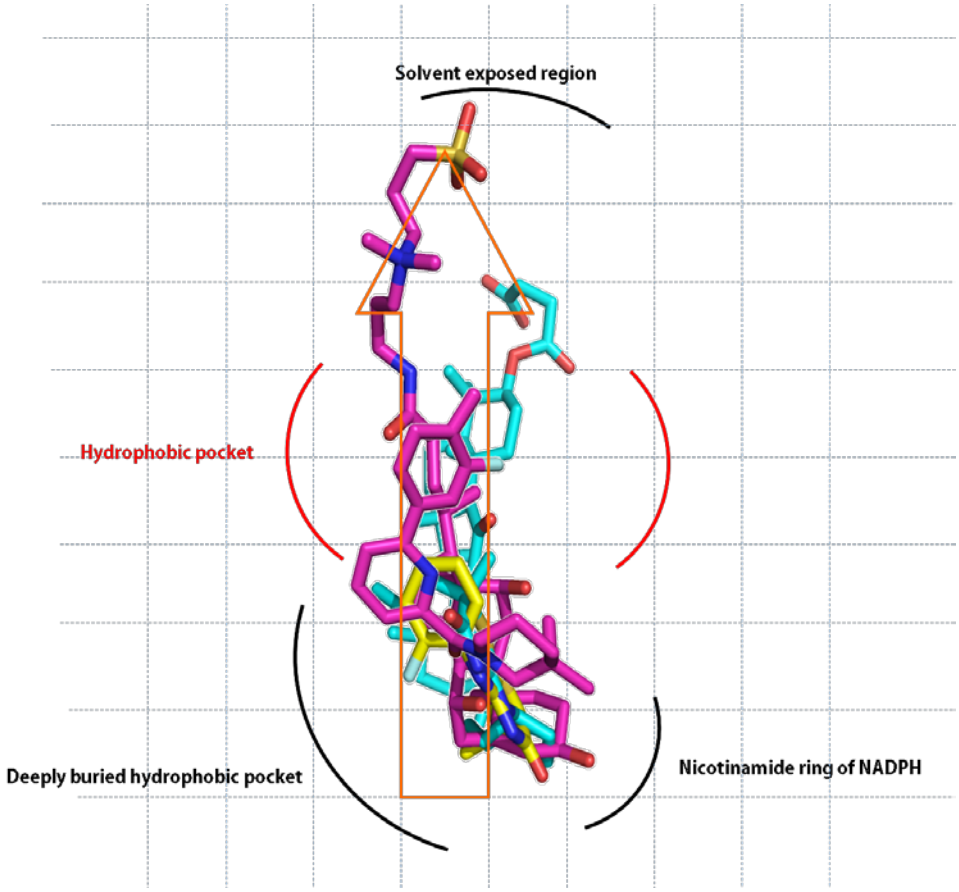

Figure 1.35: Superimposition of various ligands from crystal structures 2BEL (carbenoxolone, blue), 2RBE (2-anilinothiazolone, magenta), 3BYZ (a thiazolone, yellow), and 2IRW (adamantyl ether, blue), 3CH6 (pyridine amide, pink). Superimposing the ligands in this manner allows an insight into the regions of the binding pocket and the potential substituents which will interact with them. Illustration adapted from (Lee et al. 2008). The orange arrow points toward the entrance of the pocket.

The majority of potent inhibitors appear to have a slight V-shape enabling a better fit in the active site. It can be seen from figure 1.35 that there are 4 parts to be taken into consideration when designing potential ligands for this active site. These are:

- A solvent exposed region at the opening of the binding site. Importantly, a tyrosine residue (Tyr 177) situated at the entrance often interacts

hydrophobically with extended molecules - the phenyl ring has been observed to π-stack with the thiazolone in the co-crystal structure 2RBE (Yuan et al. 2007).

- A region for co-factor interaction; the close proximity of the nicotinamide ring allows for hydrophobic interactions between the ligand and co-factor as observed with carbenoxolone (figure 1.18).
- A buried hydrophobic pocket, divided into two sections: a deeply buried hydrophobic pocket and a second section closer to the entrance of the pocket. A hydrophobic group would be necessary here as seen with the sulfone adamantyl class of inhibitors.

This simple analysis of the binding site allows predictions for the types of atoms or in fact substituents necessary in specific positions for potential inhibitors. It suggests that an ideal potential inhibitor molecule would have to be overall hydrophobic with a lipophilic group located near the buried hydrophobic pocket and an aromatic group with a hydrogen acceptor substituent located close to the nicotinamide ring of the NADPH to allow interactions.

Further analysis of the residues involved in binding show that a central hydrogen acceptor is crucial for tight binding following interactions with Ser 170 and Tyr 183 as depicted in figure 1.34. This is seen with the majority of inhibitors currently in development.

Several of the inhibitors covered in this chapter will be used as 'template' or query molecules to discover novel inhibitors of 11β-HSD1 as discussed in chapter 4.

Compound Class	Structure	K_i / IC_{50}	PDB Code	Comment
Carbenoxolone	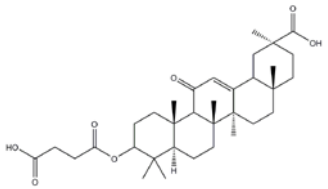	K_i 20 nM	2BEL	Non-selective, potent, competitive inhibition;
Sulfonamide	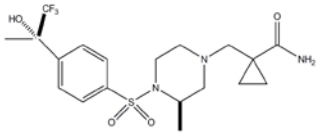	IC_{50} 1.2 nM	3D4N	Selective and potent competitive inhibition; Interaction with sulfonyl oxygen and Ala 172 backbone;
Benzamide	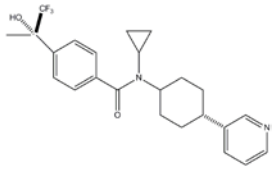	IC_{50} 1.4 nM	3D3E, 3FRJ, 3FCO	Selective, potent and metabolically stable, competitive inhibition; Interaction of central benzamide oxygen and Ser 170;
Triazole	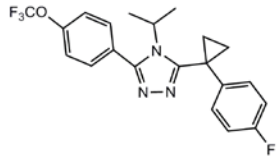	IC_{50} 1.6 nM	3D5Q	Selective, potent, mixed inhibition; Tyr 183 and Ser 170 act as hydrogen bond donors to the nitrogen atoms in the triazole ring;
Adamantane	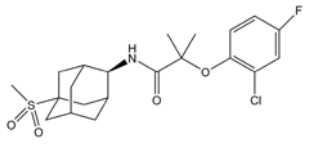	K_i 7 nM	2ILT, 2IRW	Selective, potent, competitive inhibition; Highlights the importance of a bulky, lipophilic group in compound; central carbonyl interacts with Ser 170, Tyr 183;

Compound Class	Structure	K_i / IC_{50}	PDB Code	Comment
Thiazolone	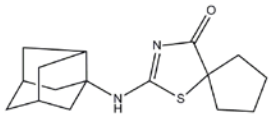	K_i 7.2 nM	2RBE, 3BZU, 3BYZ, 3EY4	Potent, selective, competitive inhibition; Binding similar to sulfonamide class; binding enhanced with the addition of a bulkier substituent;
Arylsulfonyl Piperazine	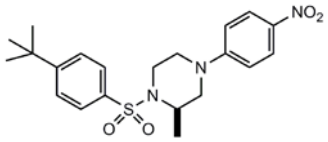	IC_{50} 0.7 nM	3CZR	Potent, selective; initial difficulties with solubility; binding similar to the sulfonyl class of inhibitors;
Pyridine Amide	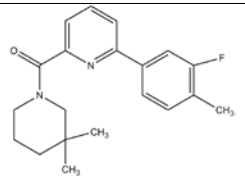	IC_{50} 0.1 nM	3CH6	Potent, selective; V-shape enhances potency as does lipophilicity and position (meta > para) of substituents from central pyridine;

Table 1.5: A summary of 11β-HSD1 inhibitors currently in development and with a co-crystal structure in the PDB.

CHAPTER 2
EXPRESSION AND PURIFICATION OF 11β–HYDROXYSTEROID DEHYDROGENASE TYPE I

2.1 Expression

2.1.1 DNA and Cloning of Mouse, Rat and Human 11β-HSD1

The human cDNA of 11β-HSD1was first isolated and cloned in 1991 (Tannin et al 1991) from a human testis cDNA library, using hybridization with the previously isolated rat cDNA (Agarwal et al 1989b). The mouse variant followed soon after (Oppermann et al 1995; Rajan et al 1995) along with several new 11β-HSD1 constructs engineered with and without tags for expression and purification of the enzyme (Odermatt et al 1999).

The DNA plasmids used in this instance for human and murine 11β-HSD1 were kindly provided by Dr. Scott Webster from the Endocrinology Unit at the University of Edinburgh. In both cases, a truncated 11β-HSD1 gene had been cloned into the bacterial expression vector pET-28b. The pET system (Novagen) has been developed for the cloning and expression of recombinant proteins in *Escherichia coli* (*E. coli*), under the transcriptional control of the T7 promoter. The expression vector pET-28b encodes a hexa-histidine tag upstream of the inserted gene, resulting in an N-terminal His-tag when the protein is expressed. The inclusion of a His-tag on the C-terminus has shown to affect solubility and activity of the enzyme (Walker et al 2001). The His-tag is linked to the 11β-HSD1 gene through a short peptide sequence of 9 residues, 6 of which encode the thrombin cleavage site (underlined):

Ser Ser Gly <u>Leu Val Pro Arg Gly Ser</u>

This expression vector has been employed previously to successfully express the catalytic domain of human 11β-HSD1 (Walker et al 2001b).

The final construct and sequences used are shown in figures 2.1A and B; the methods for cloning and cell transformation are described in Chapter 7 (Materials and Methods).

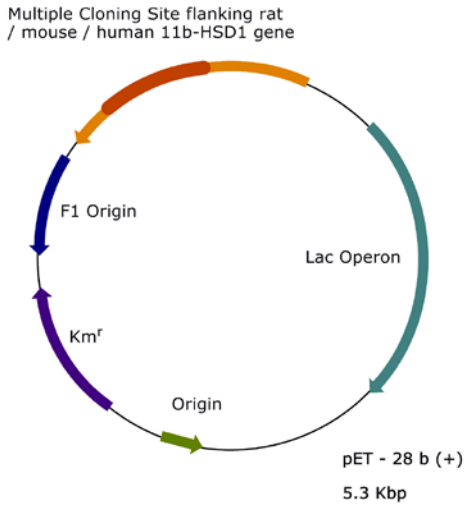

Figure 2.1(A) Simplified vector map of pET28-b depicting the location of the 11β-HSD1 gene, the lac operon, Km^r (kanamycin resistance gene), the F1 origin, and the pBR322 origin of replication. The T7 promoter and terminator are located within the multiple cloning site.

Figure 2.1(B) Alignment of the amino acid sequences of human, mouse and rat 11β-HSD1. The sequence commences with the hexa-His tag (green) with linker sequence. The first 23 (or 19 in rat) residues from the N-termini (orange) were truncated so the sequence starts with 'NEE…' (black). Alignment prepared using the ClustalW server.

The 11β-HSD1 gene has been deliberately truncated so that the first 23 amino acids are deleted, in both the human and mouse gene (19 in the rat variant) as seen in figure 2.1B. This region of the protein has a high percentage of hydrophobic

residues which are used to anchor the protein into the membrane *in vivo*. Removing these residues results in a more soluble protein product, as described previously (Kim et al 2006b) with no adverse effects on activity.

The rat DNA was synthesized and optimized by Codon Devices, a biotechnology company which specializes in construction of synthetic (and *E. coli* codon-optimised) cDNA clones. Biased codon usage can result in a lower rate of mammalian protein production in *E. coli* cells. Optimising the codons used can overcome this problem - now more cost-effectively than before - without the need for rare codon tRNAs in specific cell lines (e.g. the *E. coli* Rosetta™ strain) or targeted mutagenesis to remove rare codons (Burgess-Brown et al 2008).

The synthesized rat DNA product was supplied in a pUC19 plasmid, which was subsequently exchanged for pET-28b as this has been successfully used to express the mouse enzyme (materials and methods are in chapter 7). The plasmids are depicted in figure 2.2.

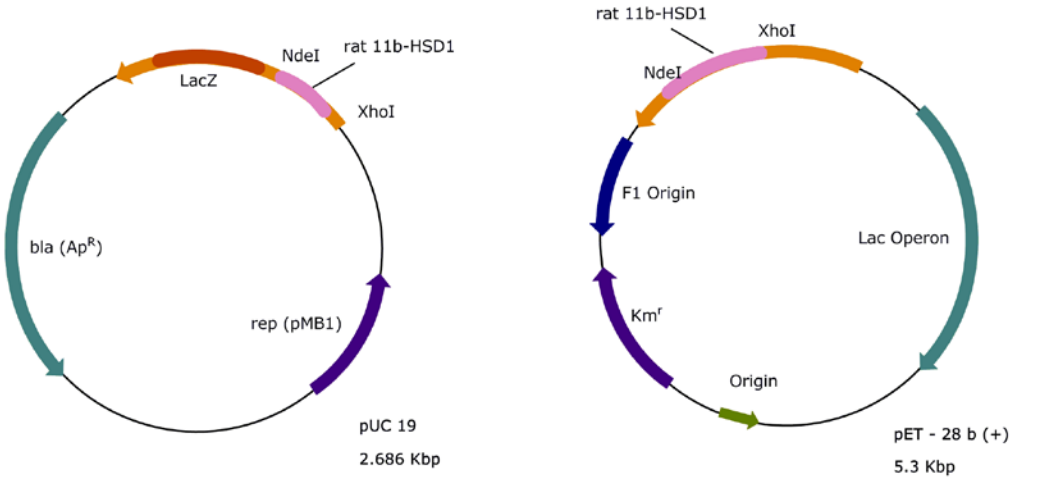

A. pUC19 vector containing the rat 11b-HSD1 gene

B. pET28-b vector containing the rat 11b-HSD1 gene, flanked by the multiple cloning site

Figure 2.2 (A) Expression plasmid pUC-19 (Fermentas) and position of the rat 11β-HSD1 gene (Codon Devices). (B) Expression plasmid pET28-b (Novagen) showing position of the rat 11β-HSD1 gene. Picture prepared with ChemDraw 11.0.

2.1.2 Three Species of 11β-HSD1: Human, Mouse and Rat

The significance of selecting mouse and rat 11β-HSD1 genes to express in addition to the human enzyme gene was three-fold:

1. to complement the novel inhibitor studies carried out on the human enzyme;
2. to draw conclusions from the variation in ligand binding between the species through analysis of amino acid differences, enabling a more detailed structure activity analysis to be developed;
3. to pre-empt problems in pre-clinical development with rodent models.

The three forms of 11β-HSD1 all share a high amino acid sequence identity as detailed in table 2.1.

Table 2.1: The isoelectric point (pI), the molecular weight, the number of residues and similarity to each species homolog and the number of published crystal structures are shown. These values were calculated by Protparam, an online protein parameter predictor (http://www.expasy.ch/tools/protparam.html).

	Rat	Mouse	Human
Predicted pI (native form)	8.36	9.16	8.71
Predicted pI (Δ1-19 / 23 truncated)	7.88	8.35	8.3
Predicted weight (native form)	31883 Da	37396.6 Da	32400.9 Da
Predicted weight (Δ1-19 / 23 truncated)	29633.4 Da	29591.5 Da	29620.5 Da
Number of residues (native form)	288 a.a	292 a.a	292 a.a
Number of residues (Δ1-19 / 23 truncated)	269 a.a	269 a.a	269 a.a
Sequence homology to human	76%	78%	-
Sequence homology to mouse	87%	-	-
Crystal Structures	0	2	11

The most significant differences between the three forms of 11β-HSD1 lie in five distinct areas, as previously described by Arampatzis (Arampatzis et al 2005) and are apparent from an amino acid sequence alignment of all three full-length

sequences. These are shown in figure 2.3, labelled I - V. Of the five variable regions (in order of N-terminus toward C-terminus); the first is a site of potential glycosylation; the second and most important is a highly conserved tyrosine residue at position 177, which is replaced with glutamine in rodent forms. The third is downstream of the catalytic site and involves several residues (human: Tyr 201, Ser 202). The fourth and fifth regions (the fifth region having the highest level of changeability) exist in the C-terminal region but do not include the residues involved in dimerisation (Arampatzis, Kadereit, Schuster, Balazs, Schweizer, Frey, Langer, and Odermatt 2005; Hult et al 2006c).

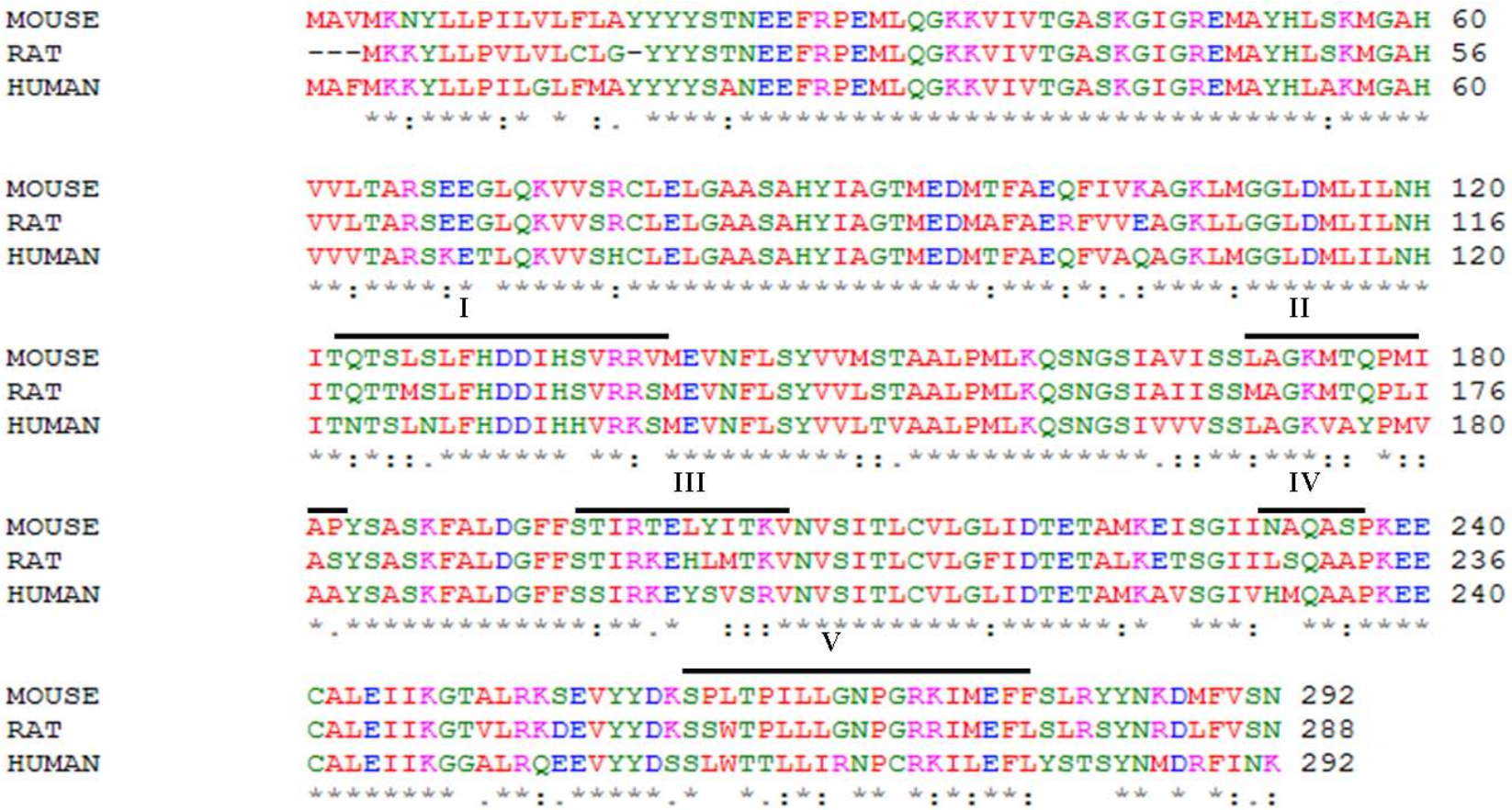
MOUSE MAVMKNYLLPILVLFLAYYYYSTNEEFRPEMLQGKKVIVTGASKGIGREMAYHLSKMGAH 60
RAT ---MKKYLLPVLVLCLG-YYYSTNEEFRPEMLQGKKVIVTGASKGIGREMAYHLSKMGAH 56
HUMAN MAFMKKYLLPILGLFMAYYYYSANEEFRPEMLQGKKVIVTGASKGIGREMAYHLAKMGAH 60
MOUSE VVLTARSEEGLQKVVSRCLELGAASAHYIAGTMEDMTFAEQFIVKAGKLMGGLDMLILNH 120
RAT VVLTARSEEGLQKVVSRCLELGAASAHYIAGTMEDMAFAERFVVEAGKLLGGLDMLILNH 116
HUMAN VVVTARSKETLQKVVSHCLELGAASAHYIAGTMEDMTFAEQFVAQAGKLMGGLDMLILNH 120
I
II
MOUSE ITQTSLSLFHDDIHSVRRVMEVNFLSYVVMSTAALPMLKQSNGSIAVISSLAGKMTQPMI 180
RAT ITQTTMSLFHDDIHSVRRSMEVNFLSYVVLSTAALPMLKQSNGSIAIISSMAGKMTQPLI 176
HUMAN ITNTSLNLFHDDIHHVRKSMEVNFLSYVVLTVAALPMLKQSNGSIVVVSSLAGKVAYPMV 180
III
IV
MOUSE APYSASKFALDGFFSTIRTELYITKVNVSITLCVLGLIDTETAMKEISGIINAQASPKEE 240
RAT ASYSASKFALDGFFSTIRKEHLMTKVNVSITLCVLGFIDTETALKETSGIILSQAAPKEE 236
HUMAN AAYSASKFALDGFFSSIRKEYSVSRVNVSITLCVLGLIDTETAMKAVSGIVHMQAAPKEE 240
V
MOUSE CALEIIKGTALRKSEVYYDKSPLTPILLGNPGRKIMEFFSLRYYNKDMFVSN 292
RAT CALEIIKGTVLRKDEVYYDKSSWTPLLLGNPGRRIMEFLSLRSYNRDLFVSN 288
HUMAN CALEIIKGGALRQEEVYYDSSLWTTLLIRNPCRKILEFLYSTSYNMDRFINK 292

Figure 2.3: A multiple amino acid sequence alignment of sequences from human, mouse and rat 11β-HSD1. Overlaid are the five distinct regions of the enzyme as described by Arampatzis et al., 2005 (regions labelled I –V). The colours represent amino acids of similar properties, as shown in the legend.

Residue	Colour	Property
A, V, F, P, M, I, L, W	Red	Small + hydrophobic (incl. aromatic Y)
D, E	Blue	Acidic
R, K	Magenta	Basic
S, T, Y, H, C, N, G, Q	Green	Hydroxyl + amine + basic -Q
Others	Grey	

Legend of characters used on the bottom row:

*** indicates identical residues,**

: indicates semi-conserved residues in accordance with the colour chart described above,

. indicates no conservation. The sequence alignment was performed using ClustalW (http://www.ebi.ac.uk/Tools/clustalw2/index.html).

2.2 Aims of 11β-HSD1 Expression

The main objectives of the expression protocol were to produce a large quantity of each of human, mouse and rat enzyme, which must be soluble and active. This was to be produced from a bacterial expression system as opposed to previous more frequently employed mammalian and yeast expression systems.

To optimise conditions of the expression, small scale expression trials were systematically carried out, in addition to testing co-expression with bacterial chaperone proteins to promote correct folding of the enzyme.

Furthermore, the 11β-HSD1 enzyme produced must also be of a sufficient activity for use in enzyme assays and biophysical characterisation, an effort that has been rarely achieved in prokaryotic expression systems. A successful bacterial expression system would allow for a large quantity of protein to be expressed, necessary for subsequent crystallographic trials of 11β-HSD1.

2.3 Expression System for 11β -HSD1

Previous studies with 11β-HSD1 have employed many different cell types for the expression of 11β-HSD1. These have typically included mammalian cell lines such as; Human Embryonic Kidney (HEK293) (Arampatzis, Kadereit, Schuster, Balazs, Schweizer, Frey, Langer, and Odermatt 2005), Chinese Hamster Ovary (CHO cells) (Agarwal et al 1989c), and Rat hepatic cells (2S-FAZA) (Voice et al 1996). In addition to these, yeast (*Pichia pastoris*) has proven to be a successful expression system (Hult et al 1998; Hult et al 2001a; Nobel et al 2002a) but fewer have successfully employed bacterial expression systems until more recently. This was predominantly due to the low yield of soluble protein expressed which would be principally found as multimeric aggregates or insoluble and packed into inclusion bodies, regardless of the N-terminal truncation (Blum et al 2000b; Elleby et al 2004a).

There are many advantages to utilizing a bacterial system for expression of recombinant proteins such as: potentially high expression of protein; simplicity; the cost-effectiveness; and the speed of production. However this expression system also poses several caveats - for example a lack of certain post-translational modifications – which can ultimately lead to the formation of inclusion bodies and protease-mediated degradation of the protein expressed.

2.3.1 Full-Length 11β-HSD1 Expression

The majority of 11β-HSD1 constructs that have been successfully expressed have been truncated versions, notably N-terminal truncations (Elleby et al 2004b; Walker et al 2001c) and occasionally C-terminal. The expression of full-length 11β-HSD1 with retained enzymatic activity is notoriously difficult but not impossible as demonstrated in more recent years by Hult et al. and Nobel et al. - both research groups based in Sweden (Hult et al 2001b; Nobel et al 2002b). In each case the enzyme was expressed in the yeast strain *Pichia pastoris*.

In 2006 during the period of this research, 11β-HSD1 (residues 24 – 292) expression was achieved in *E. coli* cells (Kim et al 2006a) by Amgen Inc., and a further publication emerged (Castro et al 2007c) the following year from Pfizer, also

expressing human 11β-HSD1 (residues 24 – 292) in *E. coli* BL21(DE3) cells. Experimental reproduction of the brief methods detailed in the published articles (which made no mention of any specialised methods to aid expression such as co-expression of chaperones or supplements to the media) resulted in the enzyme being detected in inclusion bodies, in the insoluble fraction, of the lysed cell pellets. This indicated that further experimental adjustments were to be made, for example the co-expression of GroEL and GroES (the bacterial chaperone proteins) alongside 11β-HSD1 as demonstrated previously (Elleby et al 2004c). Consequently, co-expression was explored and is discussed in section 2.4.

2.4 Co-Expression of Chaperonins with 11β-HSD1 to Improve Yield

Initial expression protocols of 11β-HSD1 in *E. coli* resulted in the majority of the enzyme being present in the insoluble fraction of the bacterial cell pellet in inclusion bodies. Frequently, this is a result of the misfolding or lack of folding of nascent polypeptides in the cell, which are subsequently sequestered into inclusion bodies in the cell.

Subsequent experimental work attempting to solubilise and potentially refold the enzyme was avoided in order to prevent possible loss of enzyme activity, following previous research (Blum et al 2000a). Instead, the molecular chaperones GroEL and GroES were simultaneously co-overexpressed with all species' 11β-HSD1 enzyme in *E. coli* (Elleby et al 2004d). This enabled soluble protein to be expressed and purified however, it emerged that a large part of the protein preparation remained in complex with the chaperone proteins once extracted from the cells and purified.

2.4.1 Background to Chaperonins

Molecular chaperones are ubiquitous proteins, identified in the majority of micro-organism and cellular components to date. Their major role is to enable proteins to form the correct tertiary structure and oligomeric form whilst preventing aggregation and without themselves forming part of the structure in doing so. Many of the molecular chaperones are heat-shock proteins – proteins which are

constitutively expressed at a level of 1 – 2% of the total cell protein when unstressed and more abundantly so upon induction with temperature (an increase to 12 % at 46 °C) (Thomas and Baneyx 1996). GroEL and its co-chaperonin GroES are the heat-shock proteins of the bacteria *E. coli*, and are the archetypal members of this family of protein folding engines. They are oligomeric proteins of 58 KDa and 11 KDa in size, respectively. GroEL is organised into a double stack of heptameric rings, forming a molecular cylinder, GroES forms a single heptameric ring, and caps the end of the cylinder structure formed by GroEL (Lin and Rye 2006b). This means that when fully formed, the massive chaperonin macromolecule is composed of 14 GroEL monomers and 7 GroES monomers, with a weight of 889 KDa (Shimamura et al 2003). Crystal structure analysis of the GroEL tetradecamer (Braig et al 1994) and the full GroEL/ES (ADP) macromolecule (Xu et al 1997) have greatly advanced the understanding of the protein folding mechanism. A general overview of their mechanism of action is shown in figure 2.3.

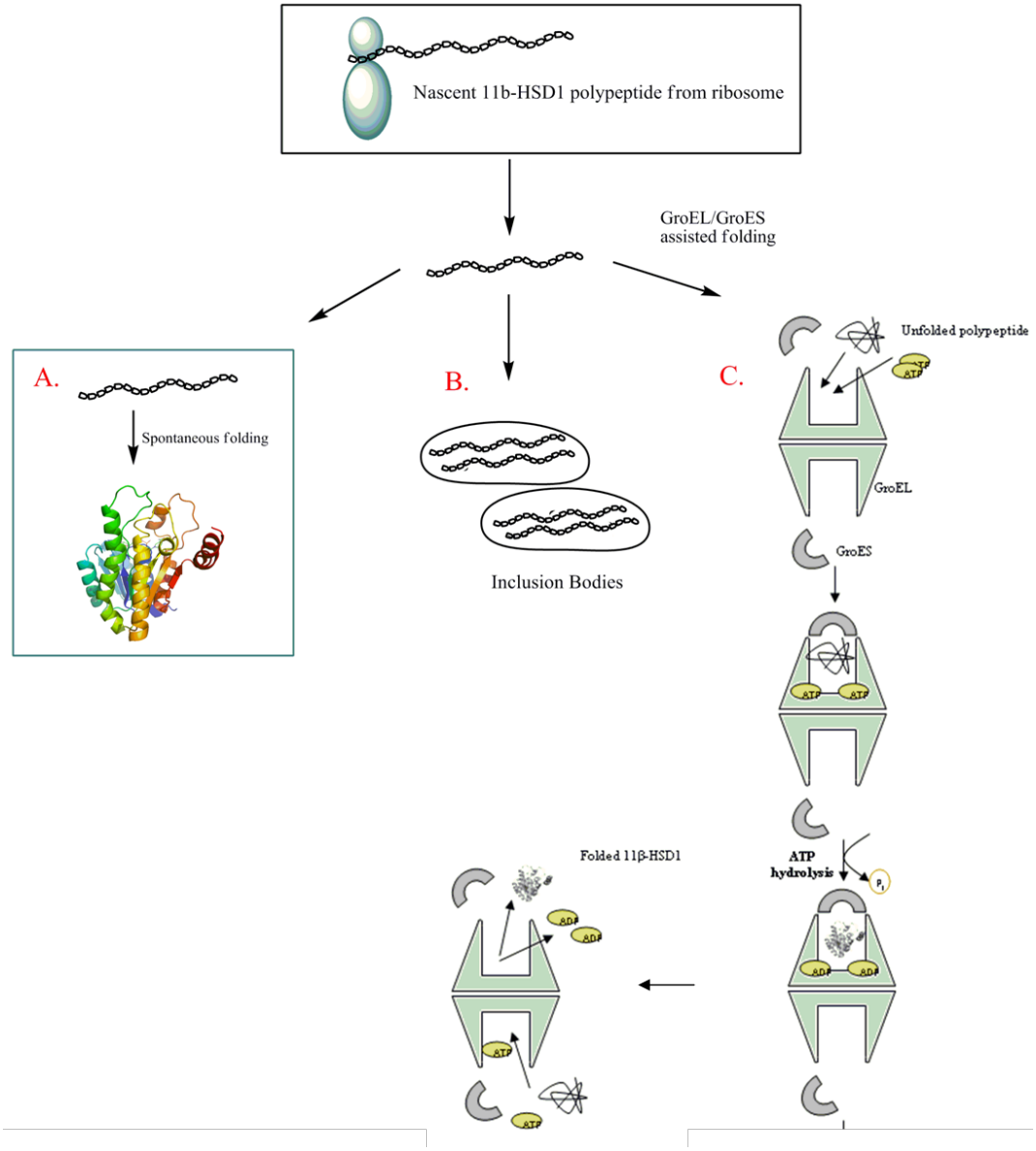

Figure 2.3: Diagram demonstrating the usefulness of concomitant expression of GroEL/ES with 11β-HSD1. (A) Spontaneous folding of the nascent polypeptide chain occurs at an extremely low level for 11β-HSD1 with the remaining expressed protein deposited into inclusion bodies in the bacterial cells (B). The presence of chaperones assists folding of the nascent polypeptide chain, as shown in (C) (adapted from (Lin and Rye 2006a)).

The presence and overexpression of both GroEL and GroES is required in order to enable proper folding of nascent 11β-HSD1 polypeptides in an ATP-dependent manner. They are expressed from one polycistronic expression vector pGro7 (Takara, Japan, figure 2.4). The chaperone plasmid, pGro7, contains an origin of

replication derived from pACYC and a chloramphenicol resistance gene. The chaperonin genes are located downstream of the araB promoter with expression induced by L-arabinose.

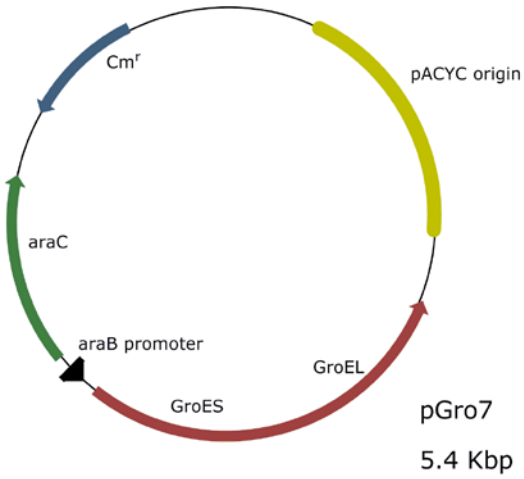

Fig. 2.4: Simplified vector map of pGro7 – a commercially available chaperone plasmid encoding GroEL and GroES – illustrating the location of Cm^r (chloramphenicol resistance gene), pACYC origin of replication, and the arabinose operon.

Temporal control of over-expression of the chaperone proteins and of 11β-HSD1 is paramount; it is necessary that the chaperones GroEL and GroES are already present in the cells and able to receive nascent 11β-HSD1 polypeptides from the ribosome. Accordingly, pGro7 is induced prior to the plasmid encoding 11β-HSD1. It is significant for compatibility that both expression vectors (pGro7, figure 2.4, and pET28-b, figure 2.1) utilize different promoters (and thus inducers) and different antibiotic resistance genes for selectivity.

2.4.2 The Glucose Effect

Glucose and sucrose are added to the culture media concomitantly with the L-arabinose inducer. These additional sugars act indirectly as a lac promoter repressor (Grossman et al 1998) by enabling the bacteria to utilize glucose as a carbon source, which strongly and negatively influences the cyclic adenosine monophosphate (cAMP) levels in the cell. A reduction in the intracellular levels of cAMP will result in a more tightly controlled expression system; this is because cAMP stimulates the lac promoter. This characteristic is known as the 'glucose

effect' and is present in several *E. coli* operons (Robert Novy and Barbara Morris 2001).

2.4.3 Unraveling 11β-HSD1– GroEL Complexes

In order to separate the 11β-HSD1 - GroEL complex, two main approaches were taken in an attempt to bypass this phenomenon:

1. Varying expression conditions in an attempt to optimize yield and solubility of free enzyme
2. Supplementing the culture media, lysis buffer and / or purification buffers with various ligands

These methods are discussed more fully in the following sections in this chapter.

2.4.4 Media Culture Additives to Enhance 11β-HSD1 Expression

The addition of ligands to the culture media has been used successfully with 11β-HSD1 by Oppermann et al., who published their results in 2008 detailing the supplementation of the culture media prior to protein induction with the clinically used 11β-HSD1 inhibitor carbenoxolone (Hozjan et al 2008a), figure 2.4.

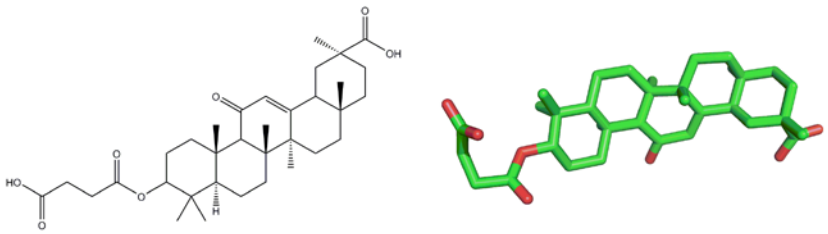

Figure 2.4: (A) 2-D carbenoxolone, (B) carbenoxolone in a 3-dimensional format.

Prior to this the only known additive to culture media which improved 11β-HSD1 yield was BVT.4584 (Biovitrum, Stockholm, Sweden), an arylsulfonamidothiazole inhibitor (Elleby et al 2004e) which increased the protein solubility and stability and increased yield approximately 50-fold. Addition of a tightly binding compound such as carbenoxolone is thought to enhance stability and encourage the dissociation of 11β-HSD1 from the chaperone proteins. This is demonstrated in figure 2.5.

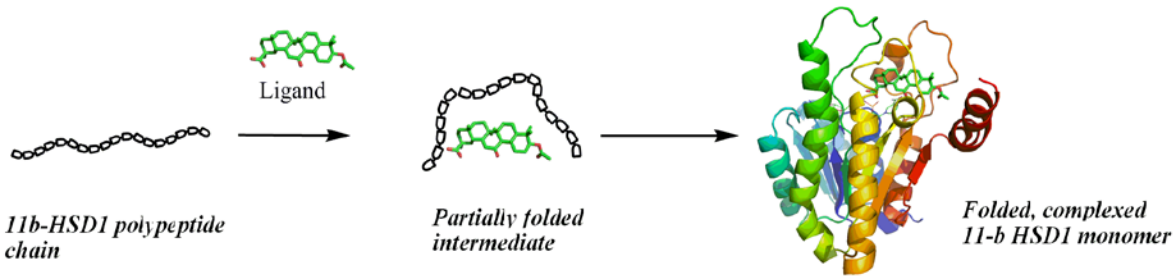

Figure 2.5: The polypeptide chain from the ribosome may be encouraged to fold by the presence of tight binding ligands in the surrounding environment. Pictured here is carbenoxolone, which binds to the active site of the enzyme with a K_i of 20 nM.

Following the success of these examples, the same was attempted in this research. The supplements tried were either endogenous ligands or known binders of the enzyme, or compounds with published evidence of previously enhancing expression yield of difficult-to-express proteins, for example ethanol (Barroso et al 2003b).

2.5 Results

2.5.1 Expression Trials of Human, Mouse and Rat 11β-HSD1

Determination of the optimal expression conditions through expression trials was carried out in an attempt to improve soluble protein yield. Small-scale screening and optimization of protein expression is a valuable method for determining subsequent high-yield experimental procedures as it reduces the cost and time of each expression trial and therefore allows for more conditions to be assessed simultaneously (Berrow et al 2006). It can also prove to be a useful indicator of the amount of soluble protein that may be produced on a larger scale.

There were several main 11β-HSD1 expression conditions that could be varied for the expression trials. These are tabulated for clarity, in tables 2.3, 2.4, and 2.5, alongside the results.

Trials were carried out systematically for all three species, initially by only varying one condition per trial. Controls were carried out alongside the expression trials and were identical in set-up to the experimental expression trial flasks in all conditions, but 11β-HSD1 expression was not induced. A 'favourable' condition was defined as one which caused the greatest increase in 11β-HSD1 protein expression, determined by running an aliquot from each trial sample and a control on an SDS-PAGE gel followed by analysis. Conditions for cell harvesting and lysis were standardised with all samples and the same volume of material was loaded each time onto the SDS-PAGE gels to correct for errors of variability. The materials and methods used are in chapter 7.

Table 2.3: Expression conditions varied for human, mouse and rat 11β-HSD1. The small scale expression trials were carried out systematically by adjusting one of the following conditions per expression trial alongside appropriate controls.

Expression Condition	Variation
***E. coli* Cell Strain:**	BL21(DE3), BL21, C41, C43
Culture Media:	LB, 2xYT, Terrific Broth
Concentration of IPTG for induction of 11β-HSD1:	0.25mM, 0.5mM, 1mM, 2mM, 5mM final concentration
Incubation Temperature:	Cells were consistently grown to an optical density of A_{600} 0.6 at 37°C. At this point (prior to induction) the temperature was changed to: 10°C, 20°C, 25°C, 30°C, or 37°C.
Incubation Period:	The period of incubation after induction was varied from 3 hours up to a period of 20 hours.

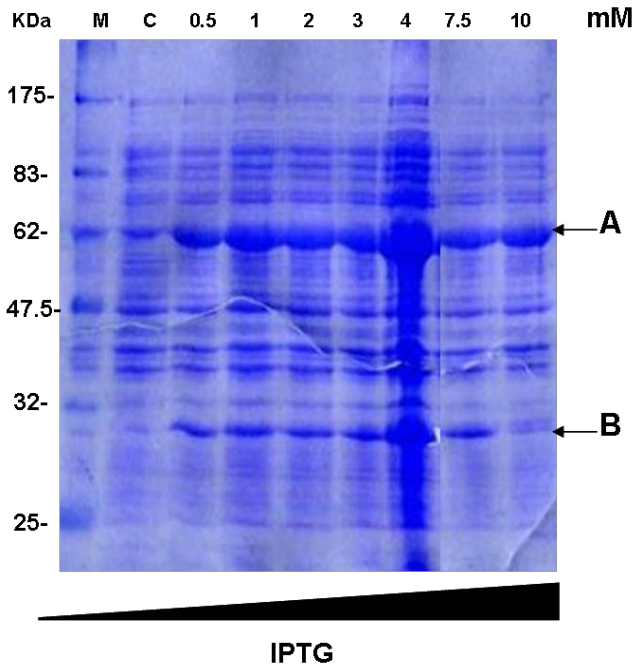

Figure 2.6: 12 % SDS-PAGE showing the effects of increasing IPTG on the expression of human 11β-HSD1. IPTG increases in final concentration from left to right. The level of 11β-HSD1 appears to be stable with increasing IPTG and decreases past 7.5 mM.
(A) is the band corresponding to GroEL (58 KDa), (B) is 11β-HSD1 (30 KDa). An error in the lane corresponding to 4 mM IPTG has occurred as is smeary and appears overloaded, so is not taken into account in this instance. The molecular weight marker (NEB) is shown in lane 'M'.

Table 2.4: Expression conditions varied for the concomitant expression of GroEL and GroES. The chaperone proteins were induced one hour prior to 11β-HSD1 protein expression induction and were consistently expressed alongside 11β-HSD1 in the following trials.

Expression Condition	Variation
Concentration of L-arabinose for induction of GroEL and GroES	**Manufacturer recommendation:** 0.05 %. **Varied:** 0.01 %, 0.05 %, 0.1 %, 0.2 %, 0.5 %, 1 %, and 5 % final v/v L-arabinose.
Concentration of sucrose and glucose	**Manufacturer recommendation:** 1 % of each. **Varied:** 0.25 %, 0.5 %, 0.75 % 1 %, 2 % final v/v glucose and sucrose, either; - added concomitantly with L-arabinose. - added to culture media at start of cell growth.

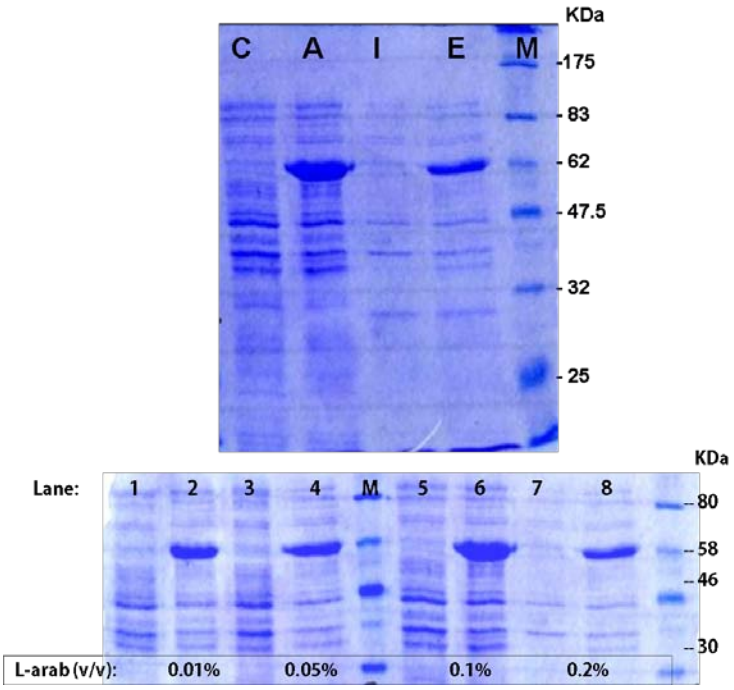

Figure 2.7 (top gel): Mouse 11β-HSD1 initial expression trials, showing:

C = non-induced control,

A = L-arabinose added so GroEL/ES expression only (the band at ~62 KDa is GroEL)

I = IPTG added so only 11β-HSD1 expression (no GroEL/ES induction),

E = L-arabinose and IPTG added, expression of all proteins observed,

M=molecular weight marker, pre-stained broad range, New England Biolabs (NEB).

Figure 2.8 (bottom gel): GroEL/ES expression trials with increasing L-arabinose concentrations (lanes 2, 4, 7 & 9: 0.01 %, 0.05 %, 0.1 %, 0.2 % final v/v L-arabinose, respectively) and corresponding controls (lanes 1, 3, 6 & 8). Lanes 'M' and 9 are pre-stained broad range molecular weight markers (New England Biolabs).

Table 2.5: Media culture was supplemented with various compounds detailed below. Concentrations were determined by calculating a five- or ten-fold increase of the reported binding affinity for the enzyme.

Expression Condition	Variation
Additives:	▪ 100 μM cortisol ▪ 100 μM cortisone ▪ 100 μM corticosterone (for murine 11β-HSD1) ▪ 1 mM NADP/NADPH ▪ 50 μM / 100 μM / 200 μM Carbenoxolone ▪ ethanol (All were added concomitantly with L-arabinose)

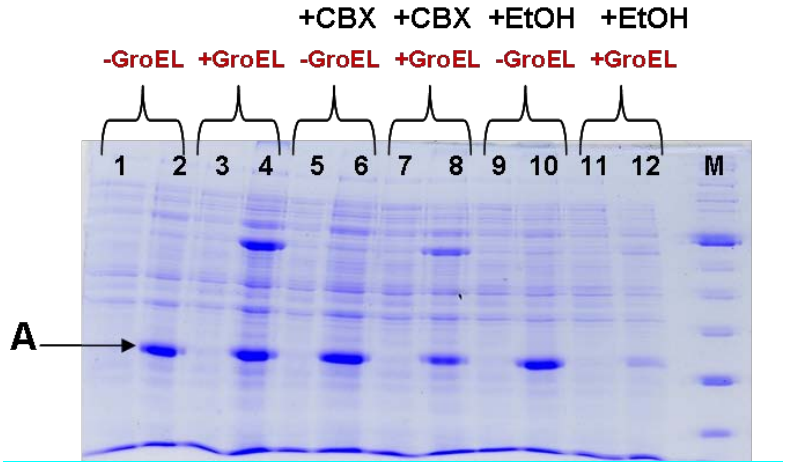

Figure 2.9: 10 % SDS-PAGE gel showing the effects of additives to the culture media during expression of mouse 11β-HSD1 (human 11β-HSD1 in figure 2.10). Un-induced samples are run beside induced samples. The letter 'A' refers to the 11β-HSD1 band at 30 KDa. Corresponding un-induced samples are seen in lanes 2, 4, 6, 8, 10 & 12.

Lane 1 of the SDS-PAGE gel in figure 2.9 has no additives but does have chaperones and very weak expression of mouse 11β-HSD1 (labeled 'A') is observed under these conditions. Lane 3 has no chaperones and no additives and only a low level of expression is observed. Lane 5 shows addition of 100 μM carbenoxolone ('+CBX') to the culture and chaperones are present; this shows the highest level of protein expression. Lane 7 shows a sample with no chaperones and

addition of 100 μM carbenoxolone, with a low level of 11β-HSD1 expression. Lane 9 shows the expression with chaperones and the addition of 3 % ethanol (EtOH) prior to expression, with only weak expression seen. Lane 11 shows addition of 3 % ethanol, no chaperones, and a small amount of 11β-HSD1 expression is observed. Therefore, the optimum conditions are presence of chaperone proteins and the addition of 100 μM (final concentration) carbenoxolone to the culture media.

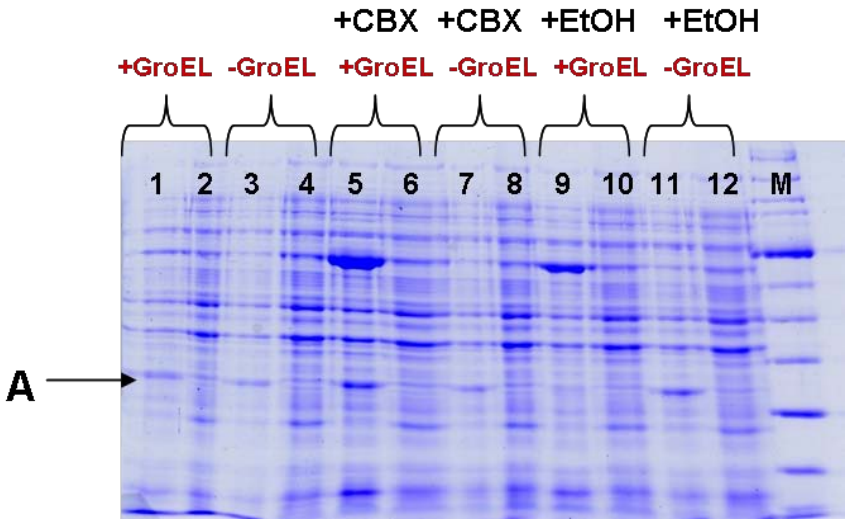

Figure 2.10: 10 % SDS-PAGE gel showing the effects of additives on the expression of human 11β-HSD1. Lanes 2, 4, 6, 8, 10 & 12 are corresponding un-induced lanes. The letter 'A' refers to the gel band corresponding to human 11β-HSD1 at 30 KDa.

In lane 1 of the SDS-PAGE gel in figure 2.10 a faint band (labeled 'A') is visible which corresponds to 11β-HSD1; this sample had chaperone induction but no additives. This faint band is absent in lane 3, where there are no co-expressed chaperones and no additives. In lane 5 there is addition of 100 μM carbenoxolone and chaperones and the highest level of expression is observed with a stronger band at approximately 30 KDa ('A'). The presence of carbenoxolone also appears to increase the level of GroEL observed on the SDS-PAGE. This may be due to the fact that the bacterial chaperones are constantly in use when there are higher 11β-HSD1 expression levels as they facilitate the folding of the enzyme. In situations where there is a lower level of 11β-HSD1 expression, less GroEL/GroES is needed and redundant chaperone protein may be discarded by the bacterial cells.

Lane 7 shows no chaperones (a band often observed at ~ 60 KDa) but the addition of 100 μM carbenoxolone and has a faint band at ~ 30 KDa. Lane 9 shows chaperones and 3 % ethanol, with a faint band for 11β-HSD1, and lane 11 shows 3 % ethanol with no chaperones, which surprisingly appears to have a higher level of expression than with chaperones. The presence of ethanol also has a positive effect on the level of GroEL present. Ethanol is commonly used to increase recombinant protein expression in bacteria through the induction of bacterial heat shock proteins from the bacterial genome, in this case ethanol simply increases the amount of GroEL/ES present (Barroso et al 2003a). As with the mouse variant, the optimum expression conditions are the presence of 100 μM (final concentration) carbenoxolone and chaperones. The final yield of protein is shown in table 2.6.

Table 2.6: Average yield of protein in milligrams per 1 litre of media culture, with and without carbenoxolone (CBX) added to the culture. Mouse enzyme: approximately 80-fold increase in protein yield observed. Human 11β-HSD1: 3.4 fold increase. Protein concentration estimated from densitometric analysis in SDS-PAGE after one-step purification.

Species 11β HSD1	Average yield/ L with GroEL/ES	Average yield/ L with GroEL/ES and CBX
Mouse	250 μg	20 mg
Human	5 mg	18 mg
Rat	Insoluble	500 μg (estimated)

2.5.2 Optimal Expression Conditions for 11β-HSD1

For the expression of human and mouse 11β-HSD1, it was found that the optimum yield of protein was obtained with the following conditions;

1. Co-expression with GroEL and GroES in *E. coli*. BL21(DE3) cell strain
2. High-cell-density fermentors were used
3. The temperature was kept stable at 37°C until the induction of chaperonins (at A_{600} 0.6) and then reduced to 20°C for the following 16h incubation

4. Chaperone induction with (final concentration) 1 % v/v glucose, 1 % v/v sucrose and 0.05 % v/v L-arabinose. After 1 hour, IPTG (final 1 mM concentration) was added to initiate the production of 11β-HSD1.
5. The media culture was supplemented with 100 μM carbenoxolone, a known inhibitor of 11β-HSD1.

2.6 Rat 11β-HSD1: Little Soluble Expression

The rat (*Rattus norvegicus*) variant of 11β-HSD1 did not yield any significant amount of soluble protein. Expression trials were identical to those carried out for the human and mouse enzyme (section 2.5.1).

In contrast to the human and mouse 11β-HSD1 variants, the rat enzyme remained insoluble, present in inclusion bodies. This is shown in figure 2.11; an SDS-PAGE gel of the bacterial cell pellet (insoluble fraction) in lane 3, and the soluble fraction in lane 2. It can be observed that all of the protein (labeled 'A') is present in the insoluble fraction.

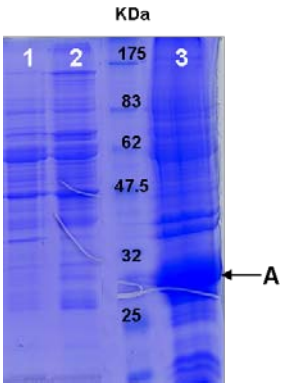

Figure 2.11: 12 % SDS-PAGE gel showing the soluble and insoluble fractions of the bacterial cell cultures. Lane 1 shows the un-induced control, this is the whole cell fraction (soluble and insoluble fractions) run. Lane 2 shows the soluble fraction of the bacterial culture overexpressing GroEL/ES and rat 11β-HSD1. Lane 3 shows the insoluble fraction of the same bacterial cell culture. The soluble and insoluble fractions are prepared by centrifugation post-lysis. The letter 'A' points to the band corresponding to rat 11β-HSD1 at 29 KDa.

For expression trials with rat 11β-HSD1, 100 μM carbenoxolone was added to the expression cultures. This resulted in a small amount of rat 11β-HSD1 being

observed in the soluble fraction, which is shown on the SDS-PAGE gel in figure 2.12. The soluble protein was purified with IMAC (section 2.8) and run on a 12 % SDS-PAGE gel.

A low level of enzyme activity could be detected in these fractions; the specific activity was 3.64 μM $min^{-1}mg^{-1}$ enzyme (with corticosterone), approximately 3-fold lower than the average value for human enzyme under the same conditions (with cortisol) and considerably higher than the only currently published data which is for albino Wistar rat liver preparation, of 0.14 nM $min^{-1}mg^{-1}$ (Bush et al 1968). This value cannot be directly compared to specific activity obtained in this research, but is useful simply as guidance; the strain, origin and assays differ.

It can be seen in figure 2.12 that there is a significantly higher percentage of GroEL/ES present (labeled 'B') than rat 11β-HSD1 (labeled 'A'). It is speculated that these two proteins are in complex; it was not possible to separate them with subsequent purification steps. Further attempts were made to separate the two proteins through the addition of ATP (and $MgCl_2$), $NADP^+$, additional carbenoxolone or corticosterone to the buffers, to stimulate the release of 11β-HSD1 from the GroEL complex. Despite being demonstrated previously with D-glyceraldehyde-3-phosphate dehydrogenase (GAPDH) (Zhang et al 2001), these additions failed to stimulate the release of rat 11β-HSD1.

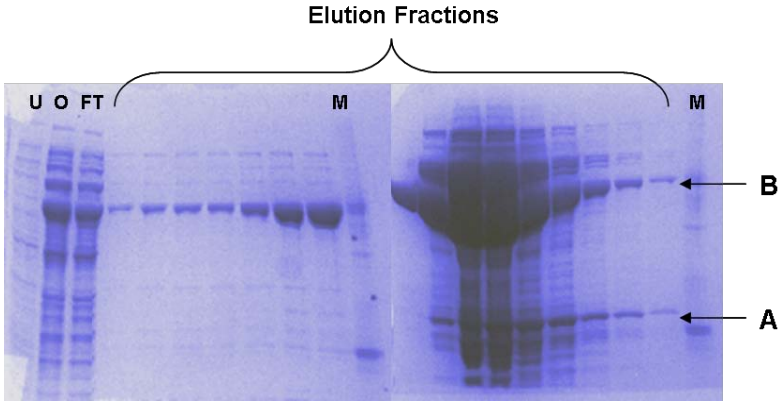

Figure 2.12: A 10 % SDS-PAGE gel of rat 11β-HSD1 stained with Coomassie gel stain. U: uninduced control. O: original sample (the lysate prior to purification). FT: flow through from the IMAC column. Remaining lanes are elution fractions from the IMAC column. M: marker lanes. From left to right the concentration of imidazole increases to elute 11β-HSD1 from the column. A: rat 11β-HSD1 band (29 KDa), B: GroEL (60 KDa).

Attempts at denaturation of the protein present in inclusion bodies with a strongly denaturing solution (methods in chapter 7) were carried out, followed by IMAC purification. This was to denature rat 11β-HSD1 which would dissociate it from any putative GroEL/ES complexes and then purify the enzyme, followed by re-solubilisation.

Previously, expression of the rat enzyme has been possible in cultured CHO cells (Agarwal et al 1989d) where the enzyme was assayed *in situ* (avoiding cell lysis or extraction), in the yeast strain *Pichia Pastoris* (Nobel et al 2002c) from which it was purified, but most significantly *E. coli* (Elleby et al 2004f). Despite these efforts, the rat enzyme has as yet, little or no characterisation published and no crystal structure.

2.6.1 Rat 11β-HSD1: An Isoleucine Deletion

During this research, the rat enzyme remained insoluble or in complex with chaperone proteins. This was due to a deletion of one residue in the sequence, discovered at a later date. The faulty sequence was taken from Uniprot in 2006 and used to generate a synthetic cDNA encoding the rat enzyme. The incorrect sequence was originally deposited in 1989 (Agarwal et al 1989e) from a rat liver preparation, and was missing Ile 242 (in addition, Glu 235 is exchanged for Gln). The original sequence, which was taken from Uniprot, had the accession code AAA40886, and has now been amended. It is thought to have been originally deposited by Agarwal et al. in the 1990s from a sequence of a cDNA clone isolated from rat liver in 1989 (Agarwal et al 1989a). The deletion of an isoleucine at position 242 putatively affects the structural integrity of the enzyme, preventing the majority of it from folding correctly despite the presence of GroEL/ES, yielding an insoluble protein. A predicted three-dimensional structure of the rat enzyme is shown in figure 2.13, constructed using a similar, existing mouse X-ray structure (PDB: 1Y5R) and an online tertiary structure prediction tool, 3D-Jigsaw. The missing residue is highlighted to demonstrate the position and possible intermolecular interactions of Ile 242. This residue is located in helix 7 (for helix numbering see figure 1.6B) which is partially involved in binding the nicotinamide

moiety of the co-factor, although Ile 242 is not known to make any interactions out with the protein.

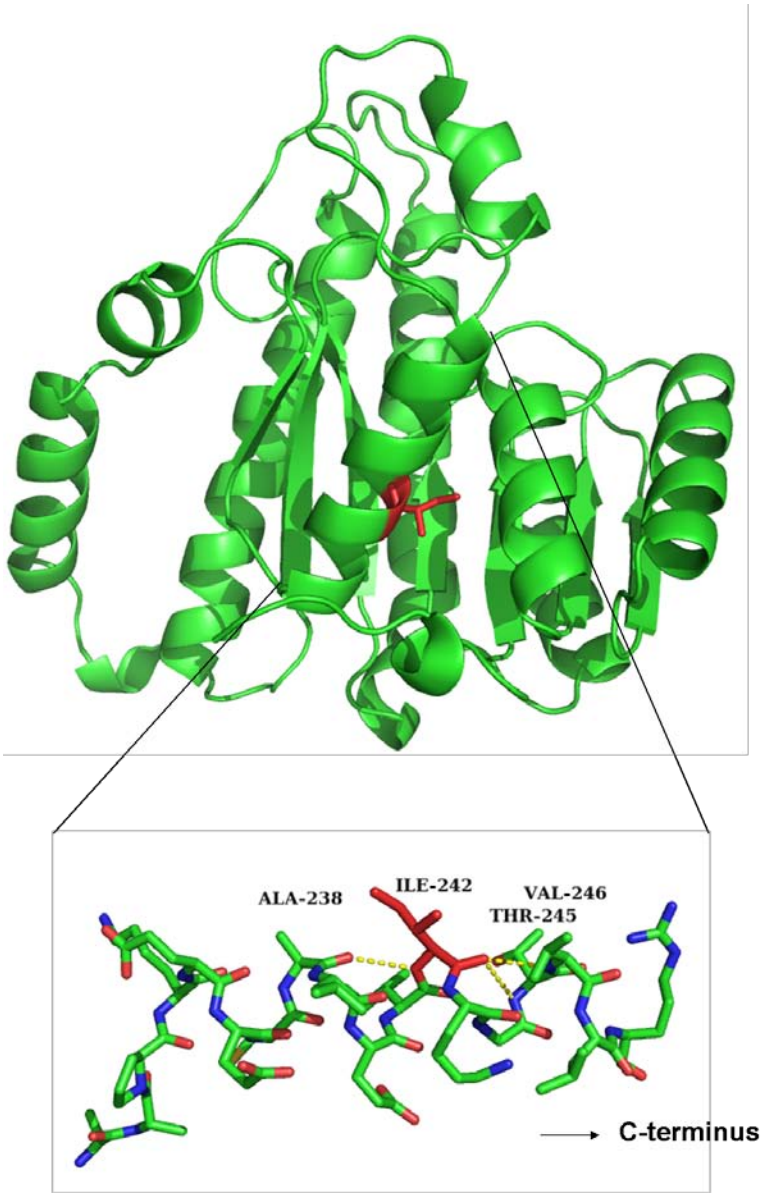

Figure 2.13: Model structure of rat 11β-HSD1 prepared using 3D-Jigsaw and Pymol. Highlighted in red is Ile 242, positioned on helix 7. The backbone of Ile 242 forms a polar interaction with the backbone of alanine 237 (Ile 241 amine to Ala 237 carbonyl) as expected to enable the typical α-helical structure. In addition, interactions are seen with threonine 244 (Ile 242 carbonyl to Thr 244 amine) and valine 245 (Ile 242 carbonyl to Val 245 amine).

As can be seen from figure 2.13, Ile 242 forms several stabilising polar interactions. Isoleucine 242 is a hydrophobic residue and is seen to point inward in figure 2.13, and a disruption of this sequence may affect the overall amphiphilicity of the helix;

that is, one side of the helix is hydrophobic, the other is hydrophilic. This can be seen from the helical wheel representations (Schiffer and Edmundson 1967) in figure 2.14.

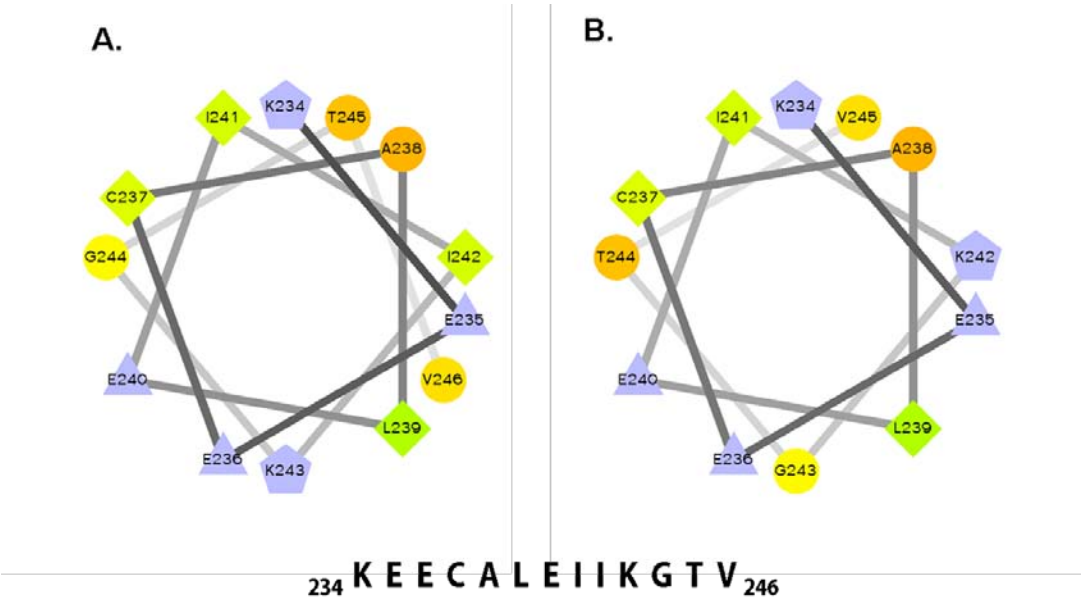

Figure 2.14: 'Helical wheel' drawn from the residues on helix 7. It can be seen that the lower face is charged and the upper face is hydrophobic. The perimeter of the wheel corresponds to the backbone and the coloured boxes represent the amino acids. The hydrophilic residues are circles, hydrophobic are diamonds. Negatively charged residues are triangles and positively charged amino acids are pentagons. Additionally, highly hydrophobic residues are green (with the intensity of colour decreasing proportionally with decreasing hydrophobicity) and red corresponds to hydrophilic residues. Charged residues are light blue. (A) is the wild type helix 7; (B) is the mutant helix 7. The sequence of the helix is shown below. Image created with wheel.pl v 1.3 (Armstrong 2004).

Figure 2.14 shows that the amphiphilicity of the helix is slightly disturbed by the loss of Ile 242, which could have a knock-on effect of disrupting the protein folding resulting in an insoluble rat protein. Previous mutagenesis studies on T4 lysozyme have demonstrated that 55 % of all mutations are tolerated by a general protein structure and do not affect folding or function. Overall, substitutions of surface residues are less likely to have an effect compared to solvent inaccessible residue substitutions or those in active site positions. A much smaller fraction, 16 % are

deleterious, that is, completely abolish protein integrity, which is postulated to have happened in this case.

2.7 Expression of 11β-HSD1: Conclusion

Previous research (Shafqat et al 2003; Walker et al 2001d) has demonstrated expression of an N-terminally truncated 11β-HSD1 in *E. coli* at low levels in the soluble cell fraction. More recently, expression of human 11β-HSD1 in *E. coli* has been shown to be improved by the addition of 11β-HSD1 inhibitors or cortisol (Elleby et al 2004g; Hozjan et al 2008b). In this research a higher level of soluble and active protein was expressed and consequently purified.

This was achieved by using a series of expression trials which indicated the optimal conditions for expression. Several expression conditions are detailed in the literature, such as a lower incubation temperature (Elleby et al 2004h; Walker et al 2001e) and co-expression of GroEL/ES (Lamark et al 2001; Lee et al 2002) although the particular combination of conditions used in this research is novel.

For the human and mouse 11β-HSD1 it was determined that a co-expression with chaperone proteins and the addition of a tight binding inhibitor increased the final yield of the protein by approximately 80-fold. In addition, a bacterial fermentor was utilised to allow the cell cultures to reach a higher cell density under tightly controlled conditions. This increased the yield, as expected, and was consequently employed through out protein production.

The addition of an 11β-HSD1 inhibitor to the culture media has both positive and negative implications. Significantly, carbenoxolone acts to stabilize the enzyme by binding to its active site (approximate K_i 20 nM). This increases the human enzyme yield over 3-fold, as seen in table 2.6. However, the subsequent and necessary removal of carbenoxolone entails a host of lengthy experimental trials and procedures in order to be able to test the activity of 100 % of the newly expressed and purified protein preparation. This is a challenge that has not been covered in literature, despite similar addition of inhibitor.

Ultimately in the case of inhibitor supplements, the benefits outweigh the disadvantages, and thus several methods to displace the majority of the

carbenoxolone were determined. These are detailed at the end of the purification section in this chapter.

2.8 Purification of 11β-HSD1

Difficulties purifying this membrane-integrated enzyme arise due to its *in vivo* dependency on the local phospholipid environment for the stabilization of its three-dimensional architecture. As an alternative *in vitro* measure, the presence of detergents during the lysis and purification process have promoted this stability and enabled a more fruitful procedure.

There is also the intricacy of preserving the enzyme activity during the processes of lysis and purification that must be taken into consideration. This activity loss is not necessarily dependent on any one purification method, as it has also been observed in native enzyme purified from liver, for example (Agarwal et al 1990; Lakshmi and Monder 1988b).

The presence of an N-terminal His-tag on the final 11β-HSD1 protein product was purposefully engineered to enable an effective first purification step of immobilized metal affinity chromatography (IMAC). This applied to both mouse and human enzyme and has been demonstrated previously in literature (Castro et al 2007b; Elleby et al 2004i; Hult et al 2006b; Nobel et al 2002d; Shafqat, Elleby, Svensson, Shafqat, Jornvall, Abrahmsen, and Oppermann 2003; Walker et al 2001f). Often, a second purification step was required for the human but not the mouse enzyme, in which case anion exchange was employed. This was followed by a final polishing step of gel filtration. Out of several purification methods that were tried and tested, it was these 3 chromatographic methods that were selected and optimised to produce the highest yield of pure enzyme.

2.9 Aims of 11β-HSD1 Purification

The aims of the purification step were to produce highly purified 11β-HSD1 that demonstrated both dehydrogenase and reductase activity. The enzyme activity was assayed using a simple fluorescence technique and compared with current literature evaluations. Purified enzyme was required in sufficient amounts to allow

preparation of the enzyme for crystallographic trials (i.e. milligram quantities) as well as in activity assays and inhibitor assays.

2.10 Purification Methods

2.10.1 First Step Purification of 11β-HSD1: IMAC (Immobilized Metal Affinity Chromatography)

In IMAC, the histidine affinity for chelated transition metals is exploited for purification purposes through immobilization of Ni^{2+} on a solid sepharose matrix, over which flows the cell lysate (liquid phase). Ideally, the His-tagged protein will bind to the solid matrix through polar contacts whilst other proteins present in the lysate will instead pass over the solid matrix and through the column. This purification method was chosen for several reasons;

1. Alternative first step methods using a dye-affinity purification (AffyGel Blue) using the co-factor binding site yielded inactive enzyme in the dehydrogenase direction, also seen in literature (Lakshmi and Monder 1988a)
2. IMAC is established as an effective and high-yielding purification procedure as the first step for either the full-length or truncated variants which produce an active enzyme (Castro et al 2007a; Elleby et al 2004j; Hult et al 2006a; Nobel et al 2002e; Shafqat, Elleby, Svensson, Shafqat, Jornvall, Abrahmsen, and Oppermann 2003; Walker et al 2001g).
3. IMAC detergent tolerance – the presence of which is vital for the effectual purification of active 11β-HSD1.

Both Ni^{2+} and Co^{2+} based resins were employed. The cobalt core has a higher selectivity for the hexa-histidine tag compared to a resin with a reactive Ni^{2+} core. This is due to spatial restrictions around the cobalt centre, meaning that only adjacent histidine residues may bind simultaneously. These spatial requirements are not present with a Ni^{2+} core and so it may instead bind histidines present in the protein sequence. The protocol used is described in detail in Chapter 7 (Materials and Methods).

2.10.2 11β-HSD1 Elution Profile from IMAC

Imidazole was used to elute the protein from the column as opposed to a pH elution as fewer bacterial contaminants were eluted alongside the protein with this method. The elution was a gradually increasing gradient of imidazole over the column, which involved an initial wash step with a low concentration of imidazole (30 mM). The elution of protein was detected by UV sensors at 280 nm, but also 340 nm which gives an indication of NADPH present. The first elution peak corresponds to the chaperones GroEL/GroES and other bacterial contaminants (section 1 in figure 2.15(a)). The imidazole gradient is held at 30 – 50 mM until their elution is complete. The second UV peak, at a higher imidazole concentration (70 - 100 mM) corresponds to 11β-HSD1 (section 2, figure 2.15(a)).

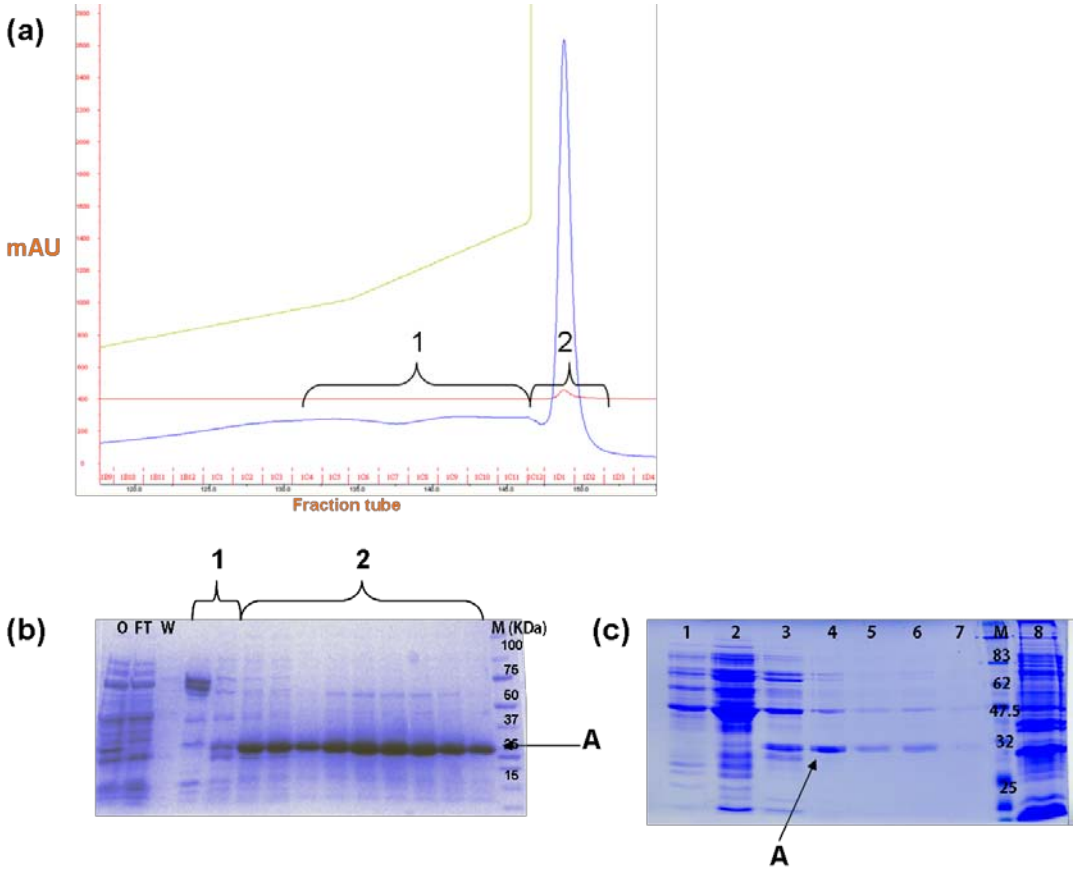

Figure 2.15: (a) A UV trace of the eluates from an IMAC column of human 11β-HSD1. The fraction tube numbers are listed along the bottom of the trace and were 1 ml each. Section '1' of the elution trace is the chaperone proteins eluting from the column. This corresponds to the same section of the SDS-PAGE gel in (b). Section '2' is human 11β-HSD1 elution, with a section on the SDS-PAGE gel below accordingly. This particular protein preparation gave 9 mg of pure protein from a 500 ml culture of bacteria, and had a specific activity of 4.16 μM min^{-1} mg^{-1}. (b) This 12 % SDS-PAGE gel is coupled with the UV trace above (a). Section 1 is predominantly chaperones co-expressed with the enzyme. Only two fractions have been shown on this gel. Section 2 correlates with the elution of the enzyme (enzyme band labeled 'A').

(c) 12 % SDS-PAGE showing the mouse 11β-HSD1 fractions after IMAC (talon). Lane 1 & 2 are the flow-through from the column. Lanes 3, 4, 5, 6 & 7 are the elution fractions after a wash step with 20 mM imidazole. M is the marker lane, a broad range molecular weight marker from NEB. Lane 8 is the crude lysate which was loaded onto the column. The letter 'A' corresponds to the gel band of mouse 11β-HSD1 (30 KDa).

2.10.3 Second Step Purification of 11β-HSD1: Anion Exchange Chromatography

The enzyme was either dialysed overnight or passed over a desalting column to rid the high salt concentration prior to loading onto an anion exchange column. The protein was eluted from the anion exchange column with a NaCl gradient and after elution the relevant fractions were analysed by SDS-PAGE (figure 2.16), assessed for dehydrogenase activity and pooled (details in chapter 7).

Anion exchange was selected over cation exchange; the enzyme has a relatively high pI of 8.3. At lower pH (i.e a pH lower than 5.5) this enzyme is unstable and precipitates out of solution irreversibly, making it unsuitable for cation exchange.

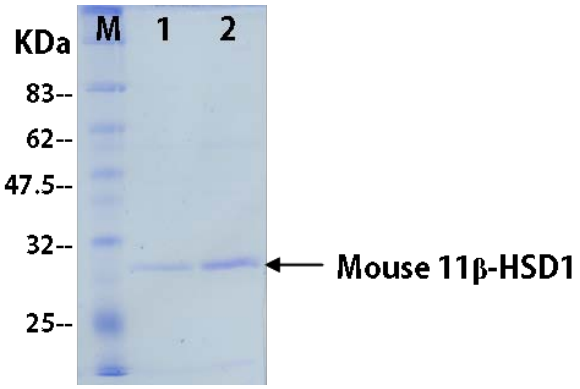

Figure 2.16: 12 % SDS-PAGE of mouse 11β-HSD1 after the second purification step of anion exchange. Lanes 1 and 2 are the same mouse sample loaded at different time points during a concentration step.

2.10.4 Third Step Purification of 11β-HSD1: Gel Filtration Chromatography

The purpose of the gel filtration step is to separate the different oligomeric states and aggregated portion of the protein sample. This is necessary for subsequent characterization; the sample must be pure and homogenous to enable crystallisation to occur.

For this step, a Superdex 200 10/30 column was used. This apparatus has a column volume of 24 ml and a molecular weight range of 10 – 600 KDa. The initial run of human 11β-HSD1 showed that there were approximately two species of 11β-HSD1 present in the sample. These were determined to be a dimeric (64 KDa) and a tetrameric (124 KDa) species and the UV elution peaks for each species appeared to

overlap quite significantly. Further experimentation and details of the methods are covered in chapters 3 and 7 respectively.

2.11 11β-HSD1 Requires Detergent during Purification and Storage

The absence of detergent during the cell lysis and purification processes results in a reduced final yield that is relatively inactive (Elleby et al 2004k). It is therefore a necessary additive for stabilising non-polar regions of the protein and enabling a higher yield. It is also possible to remove the detergent steadily during the last purification steps.

Detergents are amphipathic molecules which consist of both a polar and a hydrophobic group. It is the hydrophobic group in the detergent molecule which comes into close contact with a surface exposed hydrophobic region of the protein which increases the stability of the macromolecule in aqueous solution. It is also this hydrophilic head group which classifies the type of detergent as non-ionic, zwitterionic or anionic.

Various detergents were screened for their ability to promote stability during purification and prevent aggregation of 11β-HSD1. These were Triton X-100, Thesit, and CHAPS (3-((3-cholamidopropyl) dimethylammonium)-1-propanesulfonate). Thesit is a non-ionic detergent that has the typical structure of a hydrophilic polyethylene glycol tail attached to a hydrophobic hydrocarbon head. Triton X-100 is also a mild, non-denaturing non-ionic detergent with hydrophobic hydroalkane chains attached to a longer hydrophilic polyethylene glycol chain. In contrast, CHAPS is a zwitterionic detergent with a steroid-like structure. The three structures are depicted below in figure 2.17.

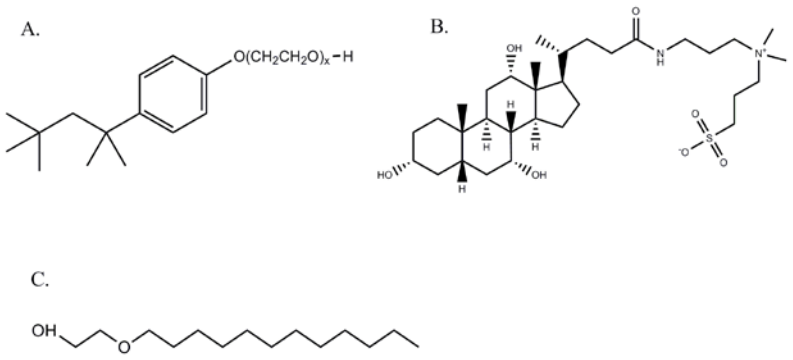

Figure 2.17: A: Triton X-100 (pubchem ID 560774), x = 9.5, B: CHAPS (pubchem ID 107670), C: Thesit (pubchem ID 24750), diagram prepared with Chemdraw 11.0.

The concentrations of detergents used were below their critical micelle concentration (CMC): the concentration at which the detergent will spontaneously form micellular clusters in aqueous solution. Whereas lipids will spontaneously associate to form multi-lamellar (mono or bi-layers) structures in water, detergents will form micelles. These are organized, spherical structures composed of several detergent molecules with their aliphatic chains oriented toward the interior of the micelle and the polar heads facing the solvent.

Thesit emerged as the optimum detergent for use in the purification steps, as it was found to be easier to remove during the final steps of purification.

2.12 Removal of Carbenoxolone from 11β-HSD1 Preparations

Several approaches were considered for the removal of carbenoxolone from the protein preparation. The many wash steps carried out during the purification procedure certainly aided in removing some of the inhibitor, evidenced through an apparent increase in enzyme specific activity, although a precise quantification of this is difficult. Figure 2.18 depicts the three principal methods approached for removal.

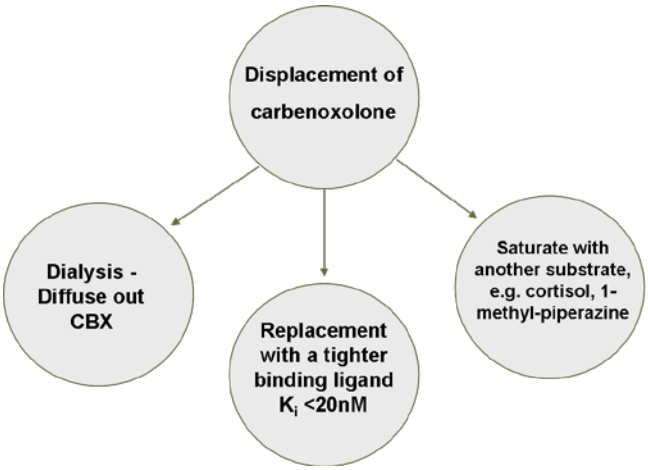

Figure 2.18: Flow chart showing the methods attempted for removal of carbenoxolone. At this point, several wash steps had been undertaken to remove as much as possible during purification. The three methods are dialysis, displacement and saturation.

The principal caveat associated with a dialysis approach is time scale. Based on the Law of Mass Action;

$$E + C \underset{k_{off}}{\overset{k_{on}}{\rightleftharpoons}} EC$$

The rate of a chemical reaction is proportional to the product of the concentration of the reactants; that is to say the ligand carbenoxolone, C, binds to the enzyme, E, with an association rate constant k_{ON} (with units M^{-1} $time^{-1}$) to form EC: the enzyme–carbenoxolone complex. Only one carbenoxolone ligand can bind to the enzyme macromolecule, forming a complex that is stable for a time but eventually dissociates with a dissociation rate constant k_{OFF} (units $time^{-1}$). As there are no catalytic processes involved, the total concentrations of carbenoxolone and enzyme are constant:

$$E + EC = E_{TOT} \quad \text{and} \quad C + EC = C_{TOT}$$

This means that the total concentration of ligand C_{TOT} is simply an addition of the free carbenoxolone (unbound) and bound ligand, and the same applies to the total enzyme concentration. However, this equation assumes there is no ligand depletion; the aim of the dialysis procedure is to provide a diffusion gradient to

encourage diffusion of free carbenoxolone across the dialysis membrane which the enzyme cannot cross. This reduces the levels of free carbenoxolone present in the dialysis bag. After an elapsed time, the dialysis buffer is exchanged for fresh buffer, thereby reducing the amount of carbenoxolone available to bind to the enzyme and a new cycle begins of dissociation and diffusion of the bound carbenoxolone molecules.

Estimating the K_{ON} to be roughly 10 $M^{-1}s^{-1}$ - a relatively average value for protein and ligands - and bearing in mind the nanomolar K_d of carbenoxolone, we may estimate a K_{OFF} in the region of 0.0001 s^{-1}. In practice, the mechanistics of this method were much slower than this estimation. This is due to the hydrophobic interactions between carbenoxolone and 11β-HSD1 which result in a K_{OFF} potentially up to 10 times smaller.

However, dialysis remains the most efficient method for carbenoxolone removal. The other options, displacement and saturation were ineffective; with regards to displacement, there were difficulties with sourcing another inhibitor which would have a smaller K_i than carbenoxolone and the subsequent consequences of this during assays. In future expression trials, the novel inhibitors assayed in this research could be used in place of carbenoxolone. This would facilitate further co-crystallisation trials of the enzyme and novel inhibitor; it would circumvent the potentially destructive process of crystal soaking (into a solution of inhibitor) and by virtue of having a lower K_i than carbenoxolone it would also be easier to remove. In the absence of another suitable inhibitor, saturation of the binding site with another competing ligand would theoretically physically block free carbenoxolone from binding the enzyme. This was carried out with 1-methyl-piperazine and cortisol, with no increase in activity in assays carried out afterward (1-methyl-piperazine: 0.044 μM $sec^{-1}mg^{-1}$ before and after). The specific activity is a good indication of free enzyme (that is: enzyme which is not bound to carbenoxolone).

To encourage dissociation of the inhibitor during dialysis, constant stirring is applied to the solution and also the buffers were varied according to pH, salt

concentration and presence of detergent or glycerol. The effect of varying buffers was insignificant as monitored by enzyme specific activity.

A method for estimating the concentration of active sites ([E]) was used - an active site titration using carbenoxolone - which enabled further enzyme activity studies to be carried out (details are in chapter 3 and 7).

2.13 Confirmation of protein identity

Matrix Assisted Laser Desorption Ionisation–Time of Flight Mass Spectrometry (MALDI-TOF) was used to determine the exact molecular weight of the protein preparation (figure 2.19). In addition, a trypsin digest of the protein preparation was carried out to confirm the identity of the protein. Both methods confirmed that the purified protein was 11β-HSD1, with a molecular weight of 31924.54 g / mol. This molecular weight is slightly higher than the computationally predicted molecular weight (table 2.7). It is postulated that this is due to the presence of triton X-100 or carbenoxolone on corresponding sites in the enzyme. The full-length spectra for human and mouse are shown here (figures 2.19 and 2.20 respectively). A tryptic digest of rat 11β-HSD1 is shown in chapter 8 (appendix).

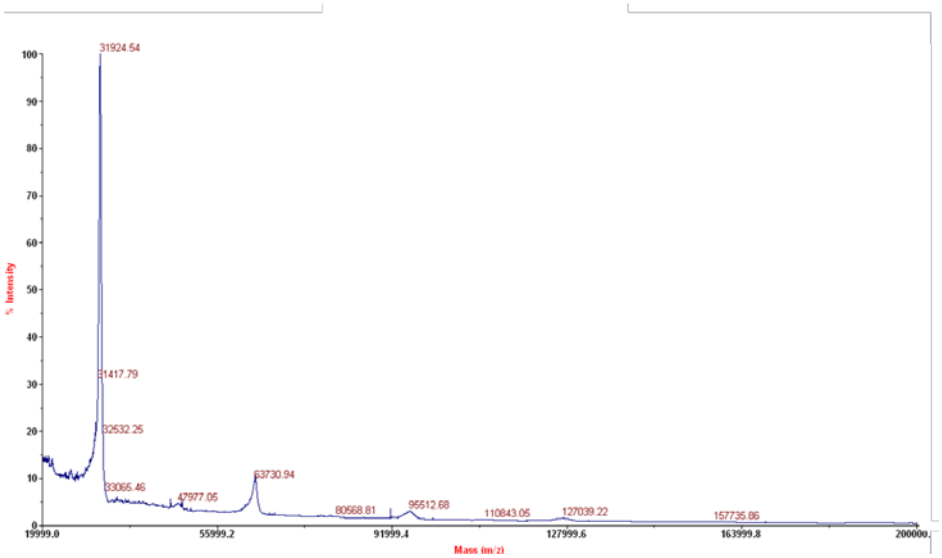

Figure 2.19: A spectrum from MALDI-TOF of human 11β-HSD1, showing a clean spectra with the major peak at 31924 Da which is a monomer species and a second smaller peak at 63730.94 Da which corresponds to a homodimer of 11β-HSD1.

	M.W:	Corresponds to:
MALDI-TOF Peak (human):	31924 Da	Human enzyme + triton X-100 or CBX
Predicted 11β-HSD 1 M.W (human):	31248 Da	-
MALDI-TOF Peak (mouse):	31718 Da	Mouse enzyme + triton X-100 or CBX
Predicted 11β-HSD 1 M.W (mouse):	31255 Da	-
Carbenoxolone (CBX) M.W:	614.72	-
NADPH M.W:	834.33	-
Triton X-100 approximate M.W:	625	-

Table 2.7: Summary of molecular weights of NADPH, carbenoxolone, Triton X-100 and human and mouse 11β-HSD1 from MALDI-TOF (this particular enzyme preparation contained triton X-100)

The molecular weights of the human and murine enzymes from the MALDI-TOF spectra reflect the presence of either co-factor, detergent or carbenoxolone in addition to a smaller molecular weight adjunct, such as an oxidative post translational modification. The exact reason for the discrepancy is unknown.

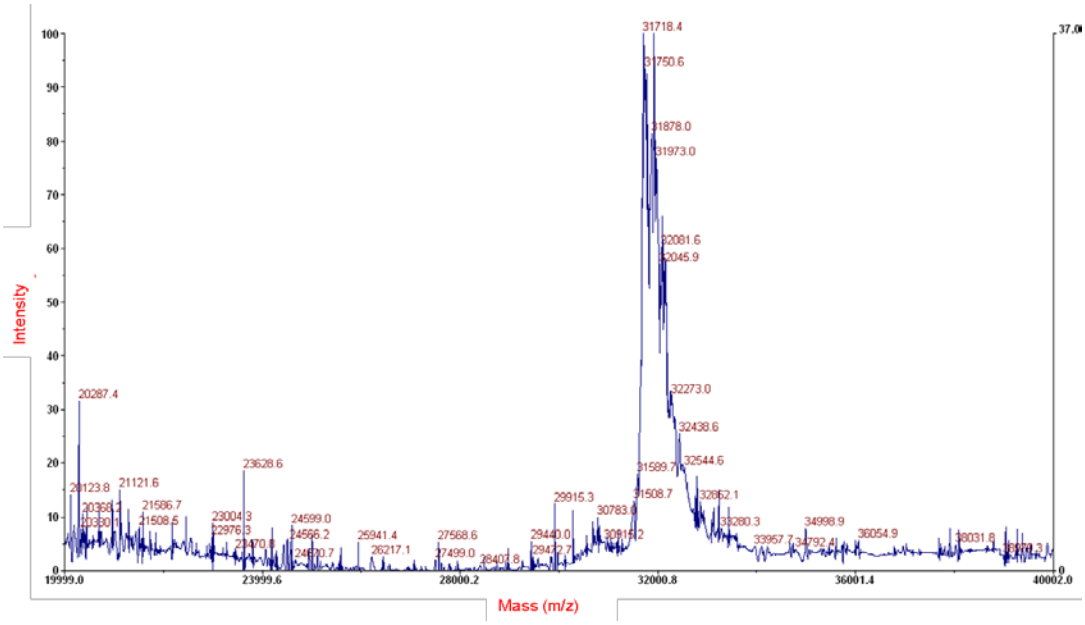

Figure 2.20: A spectrum from MALDI-TOF of mouse 11β-HSD1, showing a spectrum with the major, monomeric peak at 31718 Da.

2.14 Conclusion

An effective purification procedure was determined for human and mouse 11β-HSD1, which yields a protein sample that is stable for up to a week at 4°C and is 95 % pure as determined by densitometric analysis of the SDS-PAGE gel.

Due to the addition of carbenoxolone during expression, the final protein preparation is partially in complex with this tight binding inhibitor. To determine the quantity of carbenoxolone present, active site titration was carried out, which is covered in detail in chapter 3. Methods to dissociate the carbenoxolone from the enzyme were investigated and dialysis was determined as the most effective method. Future work would focus on complete removal of the carbenoxolone from the protein preparation. This could be carried out by attempting to add a tight-binding novel inhibitor (chapter 5) to the expression cultures in place of CBX. Alternatively, the use of commercially available, hydrophobic beads used to remove detergent and other hydrophobic compounds may be used (e.g. BioBeads, BioRad, CA. USA) as have been previously employed with success in the removal of CHAPS (Arnold and Linke 2008; Hall and VandenBerg 1989).

As a membrane-integrated glycoprotein, 11β-HSD1 is a challenging protein to express and purify. Recent evidence suggests that 11β-HSD1 does not require the

post-translational N-linked saccharides to carry out its physiological function (Blum et al 2000c). This is a double-edged sword; it means that it can be expressed in prokaryotic expression systems more easily; however it also results in the exposure of hydrophobic spots which would have previously been linked to saccharides. These hydrophobic spots may putatively interact with the membrane, and increase the yield of insoluble or aggregating enzyme.

Rat 11β-HSD1 proved to be extremely challenging to express and repeated experiments concluded that the problem was due to an incorrect sequence rather than in expression conditions, as variation of several factors made very little difference to the yield of rat 11β-HSD1.

In summary, the expression of high yields of an active and soluble human and mouse enzyme was achieved. Optimization of expression conditions culminated in the combination of co-expression with chaperone proteins and the addition of a supplementary ligand to the culture media, with low temperatures during induction and use of a fermentor. The cell products were subsequently lysed and the 11β-HSD1 was purified in two steps, in the presence of detergents, to apparent homogeneity and 95 % purity.

CHAPTER 3

BIOPHYSICAL CHARACTERISATION OF 11β–HYDROXYSTEROID DEHYDROGENASE TYPE I

3.1 Introduction

Many facets of 11β-HSD1 biochemistry are well-characterised, for example mutagenesis studies have pinpointed essential residues for function (White et al 1997) glycosylation sites (Arampatzis et al 2005; Blum et al 2000), kinetic studies of comparative species (Shafqat et al 2003) and of course several structural studies and X-ray crystal structures (Julian et al 2008, Patel et al 2007, Sorenson et al 2007, Zhang et al 2005). X-ray crystallography has provided definitive evidence of 11β-HSD1 as a tetramer in the crystal unit, as a dimer of dimers. There are several techniques which may be used to estimate the oligomerisation state of the enzyme in solution and also in which state it is active. Using gel filtration and Dynamic Light Scattering (DLS) in the present research, it has been possible to determine these characteristics.

Finally this chapter will provide details of simple kinetic characterization for the mouse and human recombinant enzyme using fluorescence as an assay technique.

3.2 Gel Filtration Analysis

Gel filtration is a high resolution chromatography technique for separating proteins by size. A Superdex 200 10/30 chromatography column was used which has a column volume of 24 ml and has a molecular weight range of 10 – 600 KDa. Superdex is composed of cross linked agarose and dextran and the particulate beads have an average size of 13 μm. It had been previously calibrated with high and low molecular weight gel filtration calibration kits (Amersham Biosciences), carried out in the same buffer and according to the suppliers instructions. This is shown in chapter 8 (Appendix). Each experimental run was carried out with 200 μl of a concentrated sample of human 11β-HSD1 (typically at 35 - 38 mg/ml) with a simple buffer for equilibration and elution (50 mM Tris pH 8.3, 20 mM NaCl, 0.01 % Thesit v/v). The initial run of human 11β-HSD1 showed that there were approximately two species present in the sample, shown in figure 3.1. These were determined to be a dimeric (64 KDa) and a tetrameric (124 KDa) species, although the UV elution peaks for each species appeared to overlap quite significantly.

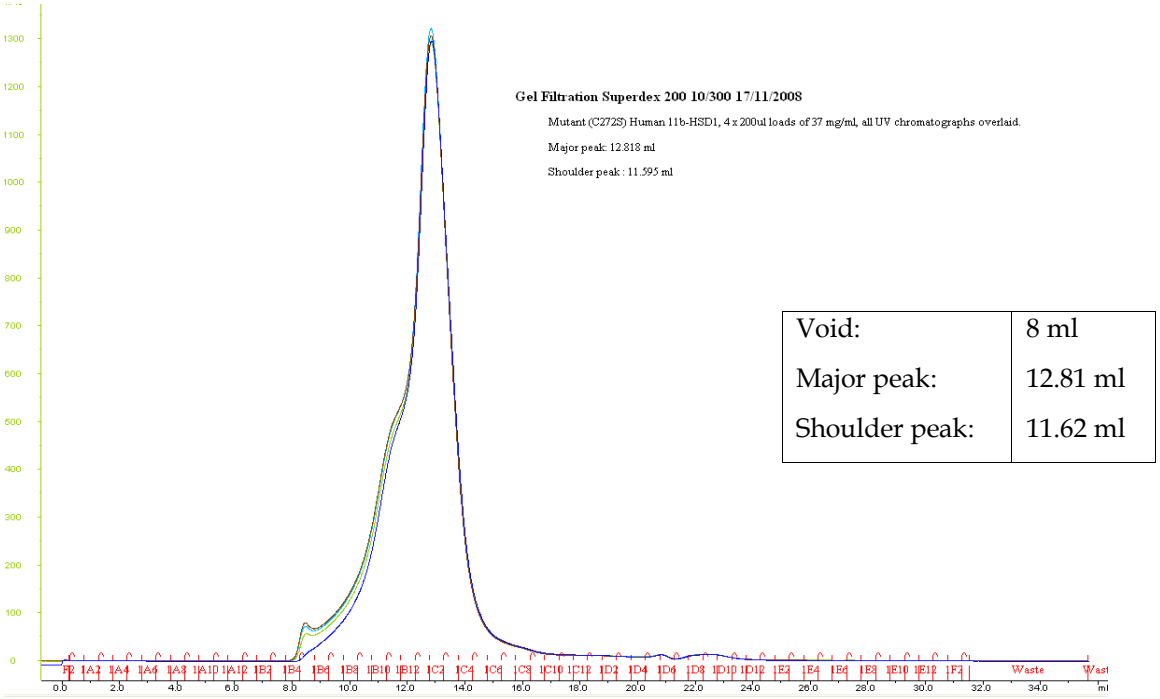

Figure 3.1: Chromatogram of gel filtration column elution (Superdex 200 10/30). Along the abscissa are the fraction tube labels in red, and the volume in millilitres in black. On the ordinate can be seen the UV absorbance units (mAU). Four runs were carried out which are overlaid in various colours.

The apparent molecular weight of each protein species was determined from a calibration curve where the elution volumes of the standard proteins were plotted against the logarithm of their respective molecular weights (chapter 8).

The non-globular three-dimensional shape of 11β-HSD1 purports that the classic method of determining the protein molecular weights from the calibration curve and diffusion co-efficient (K_{AV}) will not generate accurate results. In practice, using this technique generates weights for the two peaks of 11β-HSD1 of 190 KDa for the major peak, and 340 KDa for the shoulder peak: much higher values than should be expected. This is because this method does not cater for discrepancies such as non-globular proteins.

3.2.1 The Effects of Protein Shape on Gel Filtration: 11β-HSD1 is Ellipsoid

Further analysis taking into account the rather ellipsoid shape of the human 11β-HSD1 dimer and tetramer involved basic calculations of the hydrodynamic radius of each oligomeric species. This is shown below, in figure 3.2.

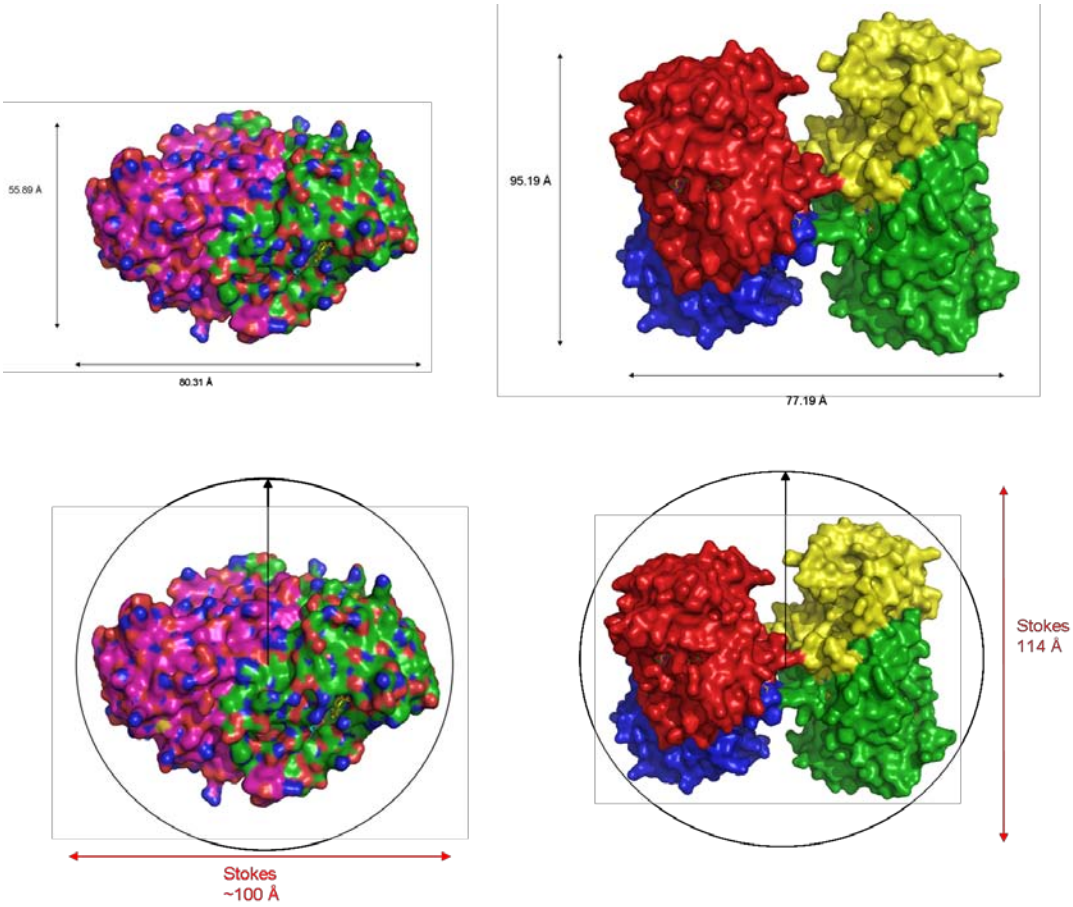

Figure 3.2: Measurements of the length and width of the human 11β-HSD1 dimer (left) and tetramer (right) taken at the longest and widest parts respectively. Overall the dimer has an ellipsoid shape and has an axial radius of 1.4. For this analysis, two crystal structures of human 11β-HSD1 were chosen as models. These were 2IRW (Patel et al 2007) for the dimer, and 1XU7 (Hosfield et al 2005) as the tetramer. For the hydrodynamic radius, the measurements were taken as shown in the lower part of the diagram. The values shown in red are the diameters.

The calibration allowed for a plot of √(-Log K_{AV}) *versus* the Stokes radius to be carried out for each of the calibration proteins. Knowing the diffusion co-efficient and the calculated stokes radius of 11β-HSD1, it was possible to approximate the apparent oligomeric species of the 11β-HSD1 elution peak in question by extrapolating from the plot of the calibration proteins (√ -Log K_{AV}) *vs* Stokes radius. The results are tabulated below for clarity, in table 3.1.

	V_e	K_{AV}	**Calculated** Stokes radius (see appendix) from plot	**Measured** Stokes radius (see fig 2.16)	Correlates to
Major peak	12.83 ml	0.301	48.8 Å	~ 50 Å	DIMER
Shoulder peak	11.69 ml	0.23	57.8 Å	57 Å	TETRAMER

Table 3.1: Calculated molecular weights of the two peaks from gel filtration. The molecular weight is estimated through analysis of the Stokes radii of a set of calibration proteins and the protein of interest and extrapolated.

The major peak corresponds to a Stokes radius of 48.8 Å, which is approximately the length of the tetramer illustrated in figure 3.2 above. The shoulder peak corresponded to a Stokes radius of 57.8 Å, suggesting it is dimeric 11β-HSD1. These results are in accordance with current literature and all published crystal structures (Elleby et al 2004, Hosfield et al 2005, Maser et al 2002).

An overlap observed between two peaks is indicative of either: rapid interchange between two heterologous species in solution, or a result of low resolution from the chromatography column used.

At higher concentrations of 11β-HSD1, it may be that there is an interchange between dimer and tetramer occurring as a result of an increased probability of one 11β-HSD1 dimer encountering another and forming a tetramer. By decreasing the concentration of the sample, this probability is also decreased and therefore promotes a better distinction of the dimer and tetramer peaks. Experiments carried out with a reduced concentration of 11β-HSD1 yielded a similar overlap between the peaks, suggesting no concentration-dependence of the overlap which in turn indicated that no rapid interchange between dimer and tetramer was occurring. As an alternative explanation, it is suggested that as a sample diffuses down a column, the molecules may also diffuse *across* the column; axial diffusion. It is this horizontal diffusion by 11β-HSD1 that may create the overlap in the peaks, and may be fixed by using a higher-resolution column, i.e. one which has a longer column length but smaller diameter. This was tested using a Superdex 200 PC 3.2/30 column, which gives a higher resolution; it has the same length as the Superdex 200 10/30 (that is; 30 cm) but

a smaller radius (3.2 mm) and thus column volume. This chromatogram is shown in figure 3.3.

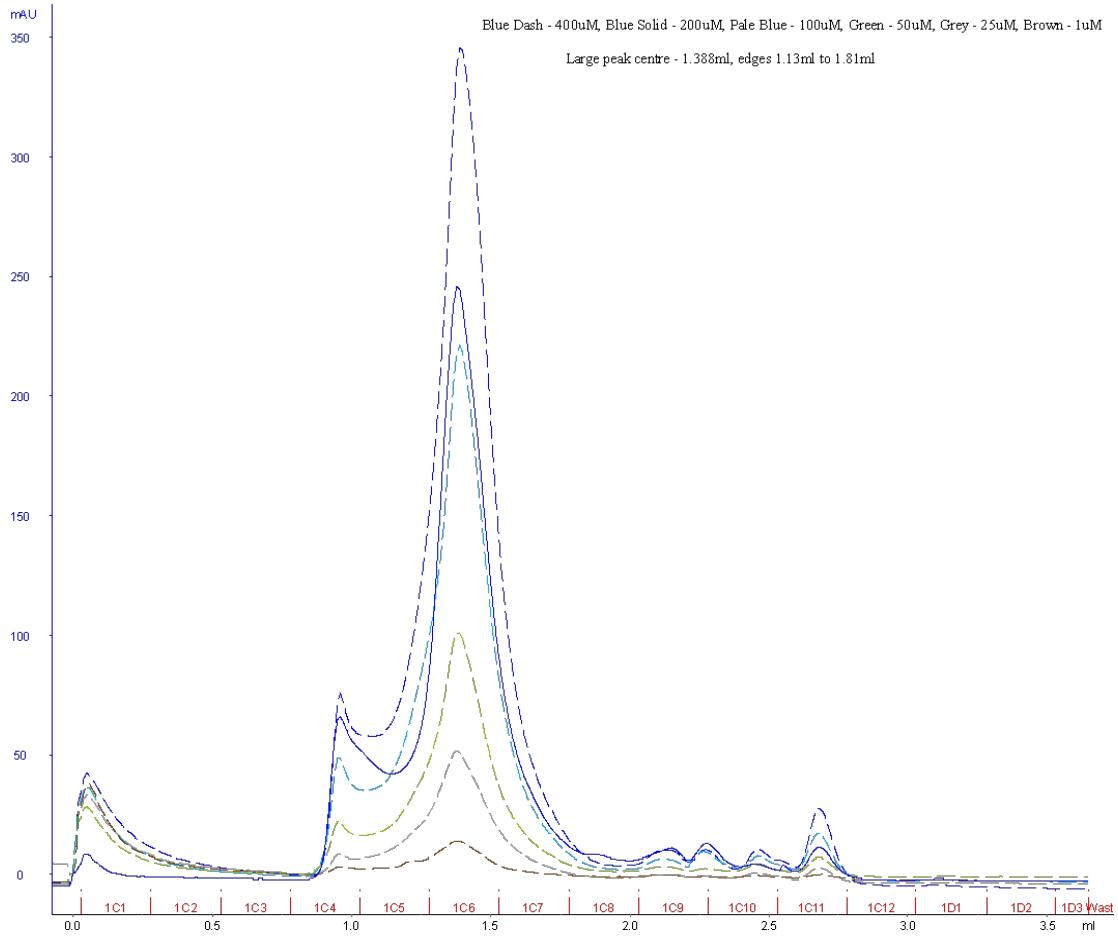

Figure 3.3: A UV trace of elution from the gel filtration column Superdex 200 PC 3.2/30. Six runs were carried out which are overlaid in various colours. Each run consisted of the same volume but different concentration of human 11β-HSD1; 400 µM (blue dash), 200 µM (blue solid), 100 µM (pale blue), 50 µM (green), 25 µM (grey), 1 µM (brown).

As can be seen from figure 3.3, the overlap between the two species' peaks remains, although it is significantly reduced due to the higher resolving power of the Superdex 3.2/30 rather than a decrease in protein concentration.

This suggests that there is no concentration-dependent interchange, but also that increasing the resolution power of the chromatography column has a beneficial effect on separation of the two heterologous species. Previous studies with non-reducing gels show several bands in each lane corresponding to various oligomeric states of the recombinant enzyme (Walker et al 2001), and human liver extracted-11β-HSD1 indicated that there was a combination of oligomers present (Ozols 1995). Therefore,

this apparent heterogeneity is potentially not a result of bacterial expression of recombinant protein but is encountered with various preparations of 11β-HSD1.

In addition to using gel filtration to determine the oligomeric states of human 11β-HSD1, this technique was used to determine whether increasing the concentration of carbenoxolone or thesit detergent would improve the folded: unfolded form ratio or the oligomeric distribution of the enzyme, respectively. This was carried out for human 11β-HSD1, expressed with chaperonins but without the addition of carbenoxolone. To this end, a sample of 30 μM human 11β-HSD1 was applied to a Superdex 200 (10/300 GL) chromatography column with increasing concentrations of carbenoxolone (1-100 μM final concentration) as well as a blank containing ethanol, however this did not have an effect on the amount of folded enzyme, nor on the oligomeric forms. In addition, increasing the concentration of the detergent thesit from 0 – 0.5 % (ranging above and below the CMC) did not affect the oligomeric states of 11β-HSD1, as may be seen in figure 3.4. Detergents may be successfully employed to prevent aggregation and improve solubility of hydrophobic proteins. Consequently, a sample containing no detergent (dark blue trace in figure 3.4) might be expected to have a larger void volume as 11β-HSD1 may aggregate forming high molecular weight clusters. This is not observed, suggesting that the presence of carbenoxolone in the active site and residual thesit molecules from the purification process are sufficient to stabilize 11β-HSD1 in solution and prevent aggregation.

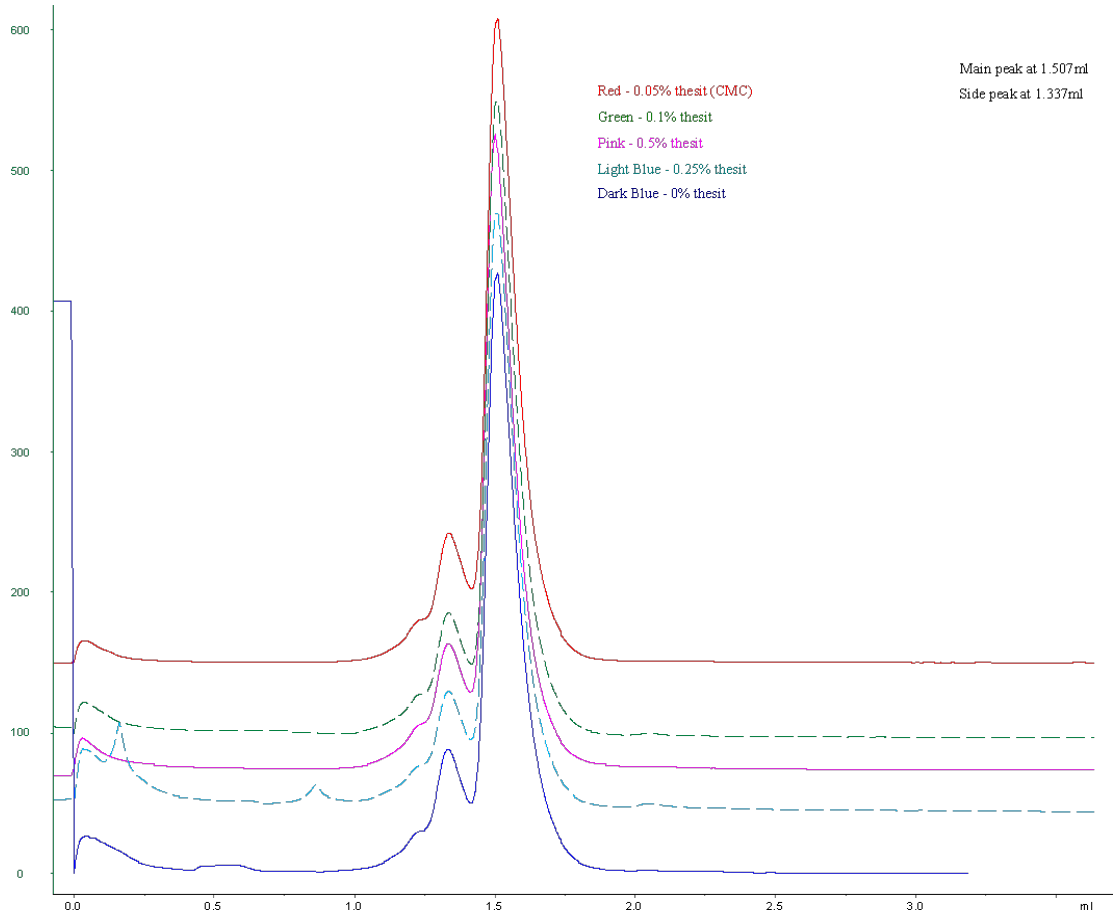

Figure 3.4: A UV trace of elution from the gel filtration column Superdex 200 PC 3.2/30. Five runs were carried out which are overlaid in various colours. Each run consisted of the same volume but different concentration of the non-ionic detergent thesit (and 100 µM of human 11β-HSD 1); 0.05 % (red), 0.1 % (green), 0.5 % (magenta), 0.25 % (pale blue), a 0 % control (dark blue).

3.3 Dynamic Light Scattering

Dynamic Light Scattering (DLS) was used to identify the monodispersity of the mouse enzyme prior to crystallization and the oligomeric state in solution. Experiments were carried out with increasing concentration of enzyme to observe concentration effects on oligomerisation, and also with increasing concentration of a non-ionic detergent, triton X-100.

Enzyme concentration ranged from 0.02 mg/ml to 1 mg/ml with little variation in the oligomerisation state of the enzyme, analogous to studies carried out with gel filtration using the non-ionic detergent thesit (section 3.1). Samples were analysed at

room temperature using a Wyatt DynaPro DLS instrument. A radius of ~14 nm was observed (table 3.2), which correlates to a tetramer assembly of mouse 11β-HSD1, at each concentration tested. The oligomerisation state was determined through comparison of measurements taken of the mouse crystal structure 1Y5R (Zhang et al 2005a) (figure 3.5). Overall, a 50-fold increase in 11β-HSD1 concentration did not have any effect on the oligomerisation state of the protein or on the level of aggregation.

Table 3.2: Effects on enzyme radius with varying concentrations of mouse 11β-HSD1, determined by DLS. Mean radius (nm) is calculated for each concentration with standard deviation (nm). The percentage mass aggregate is the percentage of the sample calculated to be aggregated.

Concentration of enzyme	Mean radius (nm)	Standard deviation (nm)	Percentage aggregates (%)
0.02 mg/ml	13.02	3.78	22.1
0.1 mg/ml	14.49	3.37	28.3
1 mg/ml	13.59	3.66	15.9
0.05 mg/ml + Cortisone + NADPH	7.98	5.31	1.2

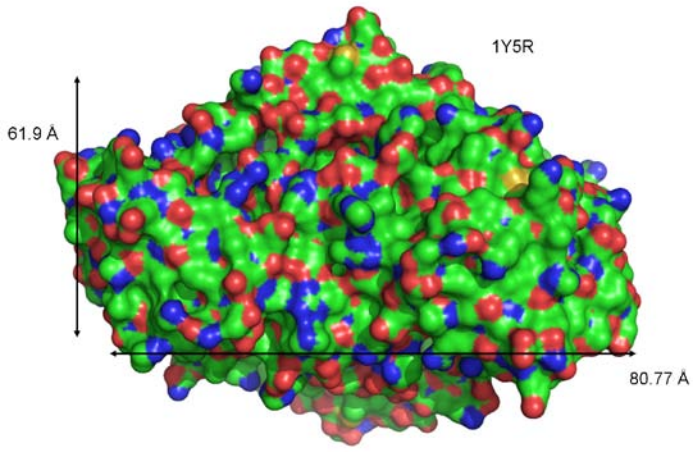

Figure 3.5: A surface representation of 1Y5R, mouse 11β-HSD1, shown as a dimer. Measurements are shown on the diagram, with a lengthwise diameter of ~81 Å and ~62 Å.

However, the addition of cortisone and co-factor resulted in formation of a dimer with a mean radius of ~ 8 nm. The switch from a tetramer to a dimer upon addition of activity-inducing components (substrate and co-factor) suggests that the mouse enzyme may be active in its dimeric form, but is able to create and break a tetrameric assembly when required.

Additional experiments with increasing triton X-100 concentration were carried out in identical conditions, with the exception that purified, active mouse 11β-HSD1 (1.6 μM) was incubated for approximately 2 hours at 4°C in assay buffer (50 mM Tris pH 8.0, 50 mM NaCl) with varying concentrations of the non-ionic detergent Triton X-100. The concentrations varied above and below the critical micelle concentration (CMC) of the detergent (which is 0.015 % / 0.26 mM). The degree of polydispersity was not calculated for samples containing detergent due to the scattering characteristics of triton X-100. In the absence of detergents, it was calculated using either the mono-modal or the bi-modal assumption within the instrumentation software and the four samples were all found to be polydisperse.

Increasing the detergent concentration resulted in a decrease in the mean radius detected by DLS. The data are shown in table 3.3.

Table 3.3: Overview of mouse 11β-HSD1 radius (nm) as determined by DLS, with increasing triton X-100 concentration. The mean radius (nm) of the highest percentage peak is shown, with standard deviation (in nm) and the calculated percentage of aggregates present in the sample.

Triton X-100 concentration, % v/v	Mean Radius (nm)	Standard Deviation (nm)	Percentage aggregates (%)
0.001 %	7.7	4.4	0.8
0.005 %	7.3	4.5	0.6
0.01 %	7.7	5.0	0.9
0.05 %	4.5	5.1	0.1
0.075 %	4.2	0.9	0.8
0.1 %	4.2	0.9	1.6

The data showed a distinct switch from tetramer (below the CMC) to dimer (above the CMC). This is depicted in figure 3.6.

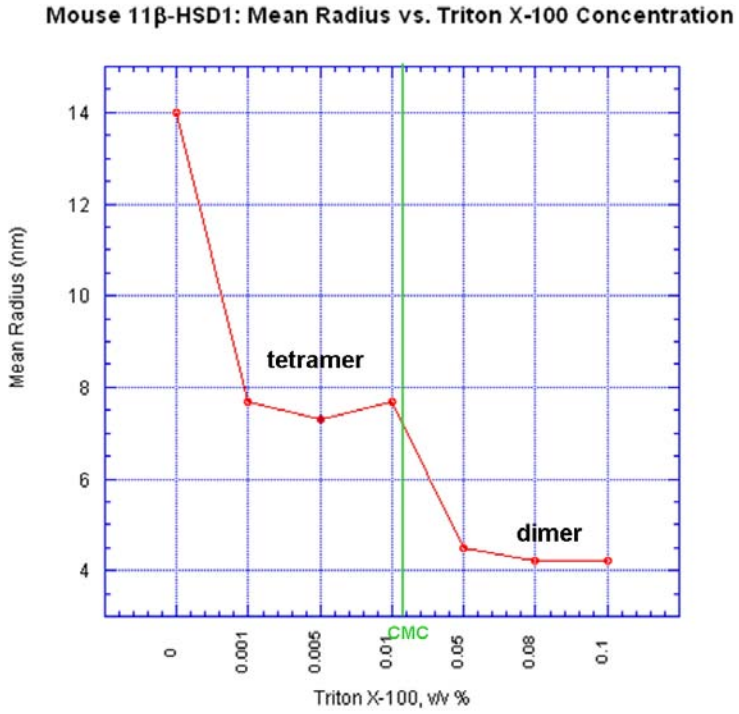

Figure 3.6: Variation of mouse 11β-HSD1 radius with increasing triton X-100. The radius decreases with increasing detergent concentration. The green line depicts the CMC of triton X-100 (0.015 % v/v). A radius of ~ 4 nm corresponds to a dimer, and 8 nm indicates a tetramer assembly as indicated on the graph.

Interestingly, in the absence of triton X-100, the mean radius is ~ 13 – 14 nm (table 3.2), which is twice as large as it is in the presence of 0.001 – 0.01 % triton X-100 at ~ 7 nm (table 3.3). This may well be a result of triton X-100 stabilising the protein in aqueous solution by binding to hydrophobic patches on the surface of the mouse protein, preventing small scale aggregation (which would have a radius ~14 nm, as observed in the absence of triton X-100). It has been noted previously that in the absence of detergent, 11β-HSD1 forms large multimers in solution (Elleby et al 2004). This is in contrast to results obtained with the detergent thesit in gel filtration experiments which did not have a significant effect on the oligomeric state of human 11β-HSD1. This is accounted for by the presence of carbenoxolone in the human enzyme, which is not present in the mouse 11β-HSD1 preparation. Significantly, the

addition of co-factor and cortisone also shows a calculated radius of ~ 8 nm, akin to triton X-100 incubated samples.

In 2005, Hosfield carried out static light scattering experiments with 11β-HSD1 and observed monodisperse masses of about 139 KDa (Hosfield et al 2005): a tetrameric assembly of 11β-HSD1. The results presented here show that in the absence of detergent the enzyme forms large, multimeric aggregates in agreement with previous literature. In addition, 11β-HSD1 appears dimeric above the CMC due to the stabilising effects of the detergent micelles, and tetrameric (or a higher assembly) below the CMC.

3.4 Fluorescence Assay

Background

Fluorescence assays simplistically involve the molecular absorption of light energy at one wavelength and its re-emission at a longer wavelength. The light is absorbed by molecules in approximately 10^{-15} seconds, causing electrons to become excited to a higher electronic state. After approximately 10^{-8} seconds the electrons return to the ground state, emitting energy. Some of this excess energy may be lost through molecular collisions but that which is not can be detected as emission of light energy.

All molecules absorb light, however only a relatively low number of species emit light, more often rigid conjugated polyaromatic hydrocarbons or heterocycles.

It is only the light emitted from the electronically excited singlet state that is known as fluorescence.

In terms of quantitation, enzymatic dehydrogenase reactions can exploit the light-absorbing properties of NADP at 340 nm, which is not exhibited by NADPH. Similarly, the reduced form is capable of fluorescent emission at 458 nm when excited at 340 nm, whereas the oxidised form is not. In this manner, the rate of the enzymatic reaction can be followed as the increase in fluorescence (i.e. the rate of formation of NADPH) emitted over time. The intensifying fluorescence corresponds to an increase in the concentration of NADPH present in the reaction cuvette (or 96-well plate), equivalent to the increase in cortisone concentration, as the reaction has a co-factor to product stoichiometry of 1:1 (figure 3.7A).

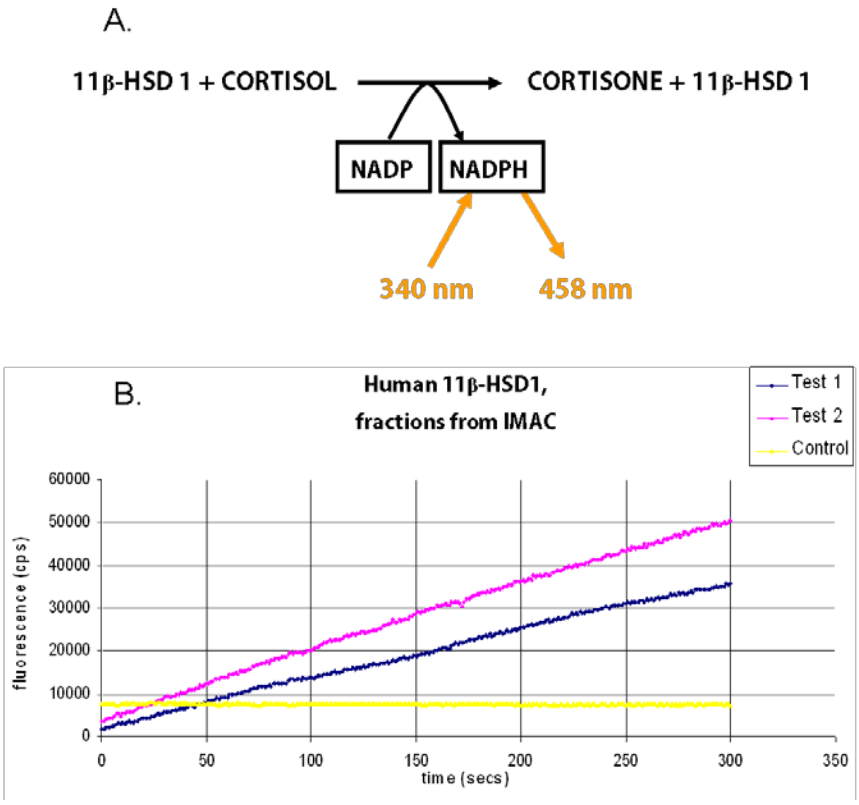

Figure 3.7: (A) Summary of the enzyme reaction resulting in the formation of the fluorescent product NADPH, with excitation and emission wavelengths. (B) Representation of the dehydrogenase reaction raw fluorescence data from two human 11β-HSD1 fractions post-purification (in magenta and blue, control is yellow). The x-axis shows the time scale of the reaction, the y-axis shows the counts per second (CPS) of fluorescence. This is subsequently converted into a quantity of NADPH using calibration charts.

The sensitivity of fluorescence is dependent on the fluorophore and the instrument employed. The response of the fluorophore is dependent on its molar absorption and the quantum yield. The fluorescence quantum yield (Q) is defined as the ratio of the number of fluorescence photons emitted (F) to the number of photons absorbed (A), i.e. the probability that a compound will fluoresce:

$$Q = \frac{F}{A} \qquad \text{Eqn 3.4}$$

The sensitivity of a fluorometer is expressed as the ratio of the signal of a standard sample to the noise level (SNR).

Fluorescence assays were used for the determination of all kinetic data in the dehydrogenase direction. For data pertaining to the reductase direction, SPA was employed (chapter 4). Emission data were obtained with a Molecular Devices SpectraMax M5 Multimode plate reader instrument, with a 340 ± 9 nm bandpass exciter and a 458 ± 15 nm band-pass emitter. Fluorescence has been used previously for determining kinetic data for 11β-HSD1 (Hosfield et al 2005, Hult et al 2006).

Optimisation of fluorescence conditions was determined through a gradual increase in the concentration of 11β-HSD1, with fixed NADP (final 500 μM) and cortisol (final 100 μM) concentrations. It was found that 30-40 μg of enzyme (1 – 1.3 nM) per dehydrogenase reaction would allow for no more than 20 % of substrate conversion, and so measurements were carried out in the linear range of product formation *versus* reaction time and enzyme concentration. This is consistent (Hult et al 2006, Shafqat et al 2003) or is lower than literature values (these are: 5 nM (Castro et al 2007e); 50 nM (Hosfield et al 2005); and 100 nM (Kim et al 2006)).

3.5 Kinetics

Several recent studies have demonstrated the importance of incubating the enzyme with co-factor NADP(H) prior to addition of the steroid or substrate in assays. This is based on evidence of an ordered sequential mechanism, whereby NADP(H) binds first to the enzyme (Castro et al 2007, Monder et al 1991, Sahni-Arya et al 2007). This suggests that binding of the co-factor first allows for a conformation more adept at binding steroids. Certainly, the interactions observed between co-factor and substrate and / or ligands serve to enhance binding (chapter 1). This has also been observed with 11β-HSD2 (Niu and Yang 2002).

In addition, several additives to the assay reaction may increase the activity of 11β-HSD1, as demonstrated by Castro et al., with the addition of various lipids to the reaction. In particular, phosphatidyl serine had a positive effect on both rabbit and human variants of 11β-HSD1 (Castro et al 2007). In a similar manner, in this research the addition of triton X-100 not only facilitated purification, but altered the oligomerisation state (figure 3.6) and also increased the activity of the mouse enzyme, as discussed below.

3.5.1 Effects of Experimental Conditions on Enzyme Activity

The presence of a detergent was found to increase the rate of reaction, as demonstrated in figure 3.8. The detergent tested was triton X-100, a commonly used non-ionic detergent.

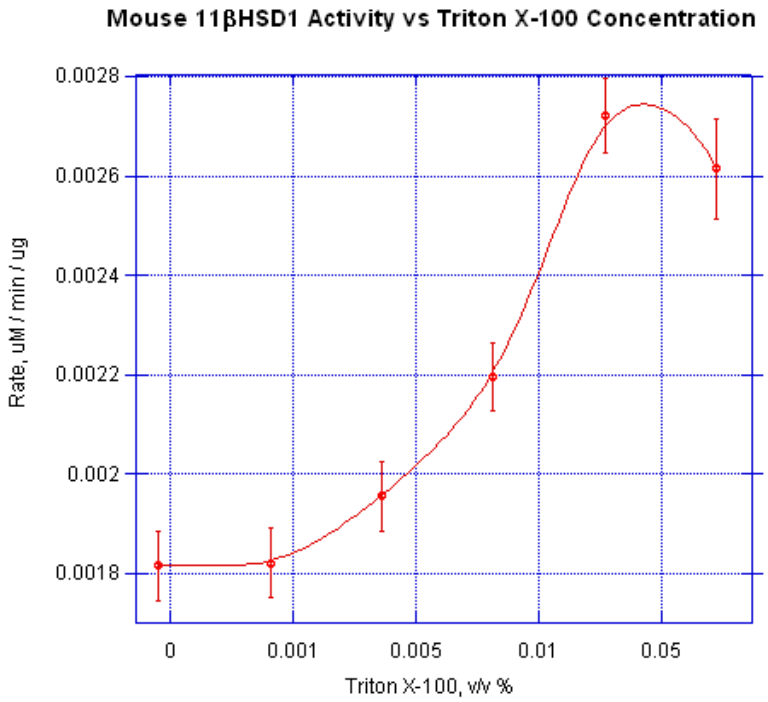

Figure 3.8: Plot showing the rate (V_o) versus the percentage (v/v) of triton X-100 added. As can be clearly seen from the plot, there is an upward trend with additional triton X-100. Standard deviation shown calculated using the 'n-1' method where n=3.

The presence of 0.07 % v/v detergent in the assay buffer increased the rate of reaction (V_o) 1.47-fold. This significant increase has been mirrored in previous studies with the addition of various phospholipids to the assay buffer (Castro et al 2007).

It is postulated that this increase in rate is a direct result from the stability incurred by the presence of hydrophobic additives in the buffer. However, there are more rational and structural-based hypotheses; firstly, *in vivo*, the C-terminal helices of the dimeric enzyme form a non-polar 'plateau' which is in contact with the non-polar region of the membrane. Hydrophobic steroids can then more easily enter the active site of the enzyme, as this arrangement *in vivo* effectively 'funnels' the ligand in. Transferring this to an *in vitro* setting, it is plausible that the presence of a

hydrophobic compound, such as Triton X-100 (above its CMC) or phosphatidyl-serine, may exert a similar effect by similar means. Secondly, research with DLS (from section 3.2) demonstrated that an increased triton X-100 concentration will yield 11β-HSD1 macromolecules with a lower radius i.e. dimers rather than tetramers, as compared to samples with a lower concentration of triton X-100. As the enzyme is thought to be active as a dimer, the increase in triton X-100 may therefore increase the amount of dimeric, active enzyme. A correlation between the enzyme activity and radius is depicted in figure 3.9.

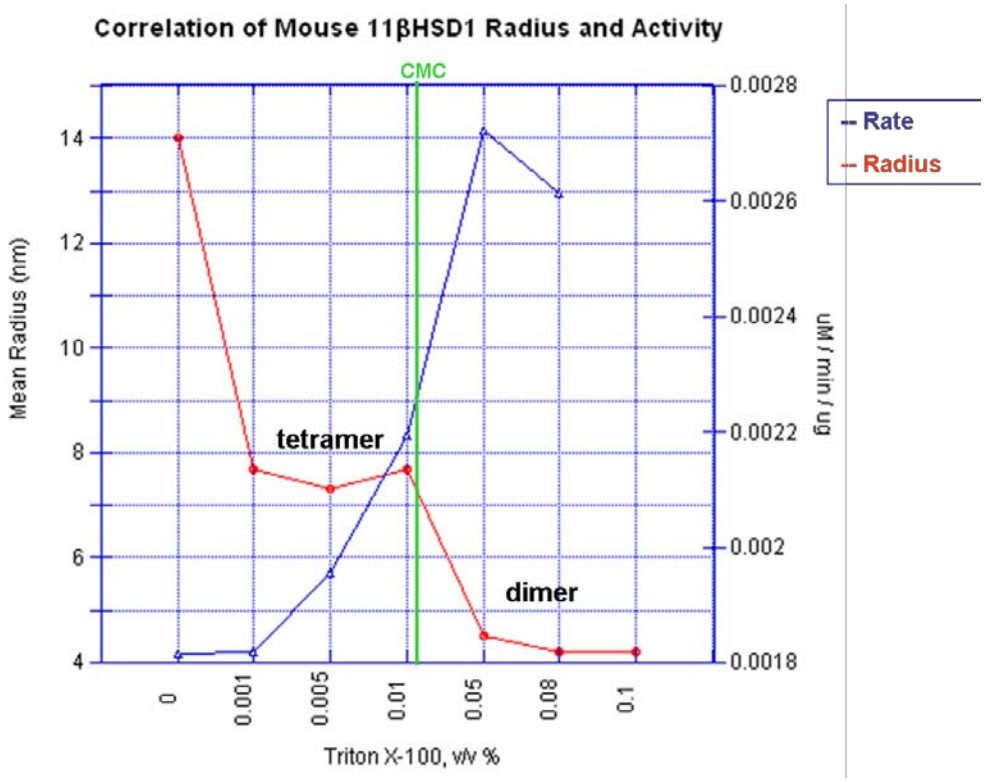

Figure 3.9: Correlation between the mouse 11β-HSD1 radius with increasing triton X-100 and rate of reaction (in μM min^{-1} $μg^{-1}$). DLS experiments were carried out in 50 mM Tris pH 8.0, 50 mM NaCl. Kinetic assays were carried out in 50 mM Tris pH 7.7, 50 mM NaCl,

With increasing triton X-100 concentration, an increase in enzyme activity is observed which reflects the stabilising effects of the detergent, and a switch from the tetramer to the dimer form of the enzyme. The detergent mimics the role of phospholipids *in vivo* by forming micelles which act as artificial membrane structures. This shift in oligomerisation state and increase in activity occurs around

the CMC point of the detergent, which is not an exact boundary but rather a broad transition. The absence of detergent results in enzyme aggregation and a loss of activity. This enhancement of enzyme activity by detergent has also been observed in other membrane-associated enzymes (Kronenburga and de Bont 2001).

Further experiments observing the effects of increasing ethanol or DMSO (dimethylsulfoxide) on activity were carried out (data not shown). A roughly proportional relationship was determined between increasing DMSO and human 11β-HSD1 activity, at low concentrations of DMSO ([specific activity]/ (%DMSO) = 2). A similar trend was seen with ethanol, although the increase in activity was less ([specific activity]/ (% EtOH) = 1.2). Potentially these solvents are having an effect on the substrate rather than the enzyme, facilitating solubilisation of the hydrophobic cortisol, enabling a higher concentration to reach the enzyme.

3.5.2 Enzyme Kinetics

The apparent K_m (K_m^{app}) for 11β-HSD1 may be determined from a standard Michaelis-Menton plot (equation 3.0); the data for the human enzyme is shown in figure 3.10.

$$V = \frac{(V_{max} \times [Substrate])}{(K_m + [Substrate])} \qquad \text{Eqn 3.0}$$

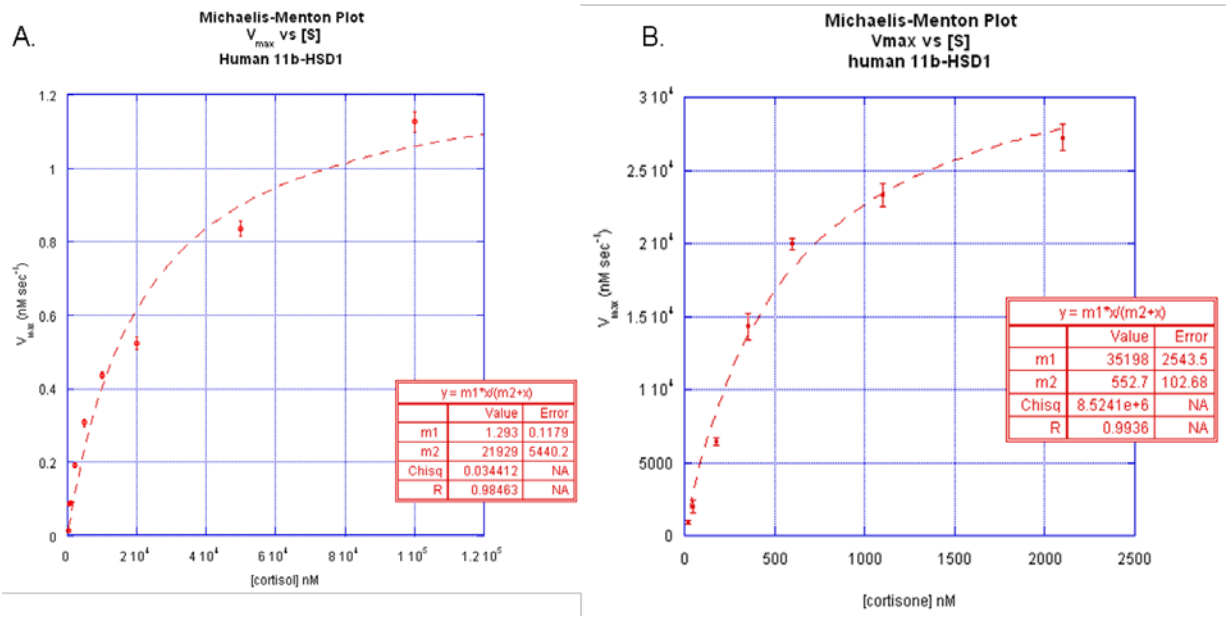

Figure 3.10: A: Michaelis-Menton plot of 11β-HSD 1, dehydrogenase reaction. The K_m^{app} was determining by measuring the rates of conversion of cortisol to cortisone, at a fixed concentration of 1 μM enzyme and NADP. This gives a K_m^{app} of 21.9 μM. B: A Michaelis-Menton plot of the reductase reaction, with cortisone. The K_i^{app} is 0.5 μM.

The mouse enzyme has a lower affinity for cortisol than the human enzyme (the mouse K_m^{app} value is 48 μM ± 8.9, data not shown) as expected; cortisol is not the endogenous substrate; crucial differences between the active sites (Y 177 exchanged for Q 177, chapter 1) which edge the mouse enzyme toward a higher affinity for corticosterone, which has a hydroxyl group at position 17. The values obtained are in general agreement with previous studies (Castro et al 2007, Hult et al 1998, Nobel et al 2002, Shafqat et al 2003). Published kinetic data for 11β-HSD1 can be ambiguous; there can be a roughly a 100-fold variation in K_m values due to the wide variety of expression systems and vectors used. The kinetic data are summarised in table 3.4.

Table 3.4: Summary of averaged kinetic data. Data were determined using a fluorescence assay which monitors the NADPH concentration. All assays were carried out under identical conditions as detailed in materials and methods. The $[E]_t$ was determined using AST and applying equation 3.1.

	Human 11βHSD1	Human 11βHSD1 (C272S)	Mouse 11βHSD1	Rat 11βHSD1
K_m^{app} cortisol	21.9 ± 5.4 μM	20.6 ± 3.2 μM	48 ± 8.9 μM	/
K_m^{app} cortisone	0.55 ± 0.1 μM	1 ± 0.8 μM	/	/
Specific Activity ($\mu M\ min^{-1}mg^{-1}$)	2.82	1.98	2.08	0.4 / (0.9 in lysates)
$[E]_t$	6.2 %	5.8 %	/	/

The K_m^{app} for cortisone (reductase) was lower than the K_m^{app} for cortisol (dehydrogenase reaction) in accordance with previous studies (Shafqat et al 2003) in addition, the V_{max} for cortisol is higher. The kinetic data obtained in this research complements previous studies with tissue-derived or full-length enzyme, demonstrating that recombinant, N-terminally truncated human 11β-HSD1 is viable for use in activity and inhibitor assays, and also structural studies.

In the majority of 11β-HSD1 kinetic studies, homogenated material is used which generally show lower apparent K_m values for cortisone (low micromolar range) whereas higher K_m values are reported for recombinant homogenates or purified samples. This is due to intracellular co-factor availability and the predominance of the reductase reaction *in vivo*, with enzymes exhibiting little dehydrogenase activity. Difficulties arise as values derived from recombinant, purified material may not be consistent with circulating glucocorticoid levels (which are in the nanomolar concentration range). This may be putatively explained with two rationalisations; firstly that the intact intracellular environment primes the enzyme for the reduction of cortisone, by the presence of excess NADPH and possibly substrate, and secondly a hypothesis put forward by Shafqat (Shafqat et al 2003) is that the purified recombinant enzyme is partially inactivated during cell lysis and purification. To

determine the degree of inactive enzyme, active site titration is carried out using a tight binding or irreversible inhibitor.

This technique is extremely useful in this research, due to the necessary addition of carbenoxolone to the culture media to ensure free, folded enzyme. This leads to many active sites of the enzyme being occupied with carbenoxolone, the quantification of which is important for subsequent activity assays.

3.6 Active Site Titration

Active site titration (AST) is a technique based on the partial inactivation of an enzyme preparation with a known quantity of inhibitor, followed by the measurement of residual catalytic activity. The applicability of AST for 11β-HSD1 has been demonstrated previously (Elleby et al 2004, Shafqat et al 2003). The procedure is repeated with increasing amounts of inhibitor (over a range of 1 – 10 μM) until total inactivation is observed, the data is subsequently fitted by non-linear regression to equation 3.1. The amount of inhibitor required for complete inactivation corresponds to the molar equivalent number of active sites.

$$\frac{v_i}{v_o} = (1 - ((E + I + K_i^{app}) - ((E + I + K_i^{app})^2 - (4 \times E \times K_i^{app}))^{\frac{1}{2}}) \times (2 \times E)^{-1}) \quad \textbf{Eqn 3.1}$$

Where: v_i is the observed velocity in the presence of inhibitor, v_o is the uninhibited velocity, [E] is the active enzyme concentration, K_i^{app} is the apparent inhibition constant, I is the concentration of inhibitor. The concentration of active sites was measured for each new protein preparation, with background controls, and a plot of V_i / V_o versus Log[inhibitor] prepared (figure 3.11).

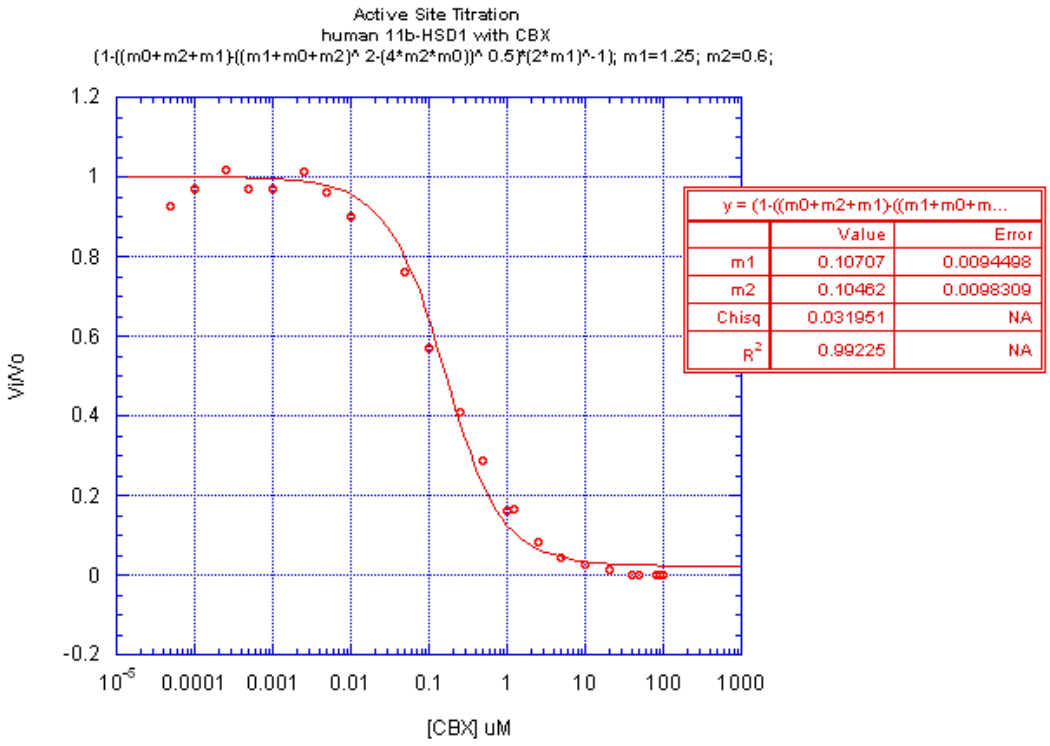

Figure 3.11: Active site titration of human 11β-HSD1, fractional velocities vs. Log [inhibitor]. Fractional velocities (V_i / V_o) of purified material were determined in the presence of increasing concentrations of carbenoxolone. Data was fitted to the equation 3.1, as defined originally by (Morrison 1969). Graph prepared using Kaleidagraph v4.0 (Synergy Software). In the adjoining table, 'm1' corresponds to [E].

Previously, ~ 40 – 50 % (Shafqat et al 2003) and ~20 % (Elleby et al 2004a) of total enzyme preparations were determined to be active using this method with the ligand BVT 24829. In both cases, the protocol for expression and purification are nearly identical (and similar to this research) hence such differences in active site percentages are unexpected but exemplify the possible variation in the quality of protein produced. Nevertheless, this does support the notion of a destabilization of the enzyme during lysis or purification procedures (Monder et al 1991, Nobel et al 2002) and thus a lower value than those published is expected in this research, due to the presence of carbenoxolone. From figure 3.11, [E] is calculated to be 107.07 nM (when taking K_i^{app} to be 20 nM, Webster et al.) indicating that 6.2 % of the enzyme active sites are available and functional in the purified material, a value similar in all other AST assays carried out in this research. This method also allowed monitoring of the levels of carbenoxolone after further dialysis or buffer exchange steps.

AST proved to be a useful tool for removing ambiguity which may surround the nature of the purified enzyme; i.e. that a preparation retaining 25 % of the initial activity may infact be all in the form with 25 % native activity (due to a decrease in V_{max} or increase in K_m) or alternatively 75 % inactive enzyme. Thus, a clear distinction can be made between these two states. It is thought that inactive enzyme may be a reason for higher K_m values obtained from purified samples, as compared to tissue-derived homogenates (Shafqat et al 2003).

CHAPTER 4:

DESIGN AND SELECTION OF COMPOUNDS FOR INHIBITION OF 11β-HSD1 ACTIVITY

4.1 Introduction

'*The most fruitful basis for the discovery of a new drug is to start with an old drug'.*
Sir James Black, the 1988 Nobel Prize winner in Physiology & Medicine.

There is currently a great deal of research and development in pursuing potent and 11β-HSD1-selective small molecule inhibitors by the pharmaceutical industry and academia alike.

In silico methods are now widely used in the early stages of drug design and development (Ekins et al. 2007). A computational approach can include data mining, databases and compound libraries, molecular similarity searches, pharmacophore building and searching, homology modeling, and quantitative structure activity relationships (QSAR). Conveniently, these techniques provide a list of novel molecules which are not only predicted to have an affinity for the particular target, but which have suitable 'drug-like' physicochemical properties and may also have predicted reasonable absorption, distribution, metabolism, excretion and toxicity (ADMET) parameters (Ekins et al. 2007;Lipinski et al. 2001).

Virtual screening is a high throughput method of screening a large compound library for suitable candidate compounds (Ekins et al. 2007). These compounds are subsequently scored and ranked according to one or a consensus of multiple scoring functions. It is a knowledge driven approach, ergo requires input: structural information in the form of either the target site or existing ligands for the target (Ekins et al. 2007).

The principal approaches employed in more recent years to identify novel lead compounds for the inhibition of 11β-HSD1 inevitably employ the high-throughput virtual screening of a small molecule library followed by the identification of hits,

laboratory analysis and subsequent refinement of the candidate compounds to try and increase potency. The vast majority of small molecule 11β-HSD1 inhibitors currently being developed target the active site of the enzyme, as this site will impart the greatest possible selectivity with maximum inhibitory action. This 'linear' process of identification of novel ligands has been extensively employed by Amgen Inc. and Abbott, using in-house compound libraries with a good deal of success (Julian et al. 2008;Rohde et al. 2007;Sorensen et al. 2007).

An overall flow diagram of the process used in this research is shown in figure 4.1.

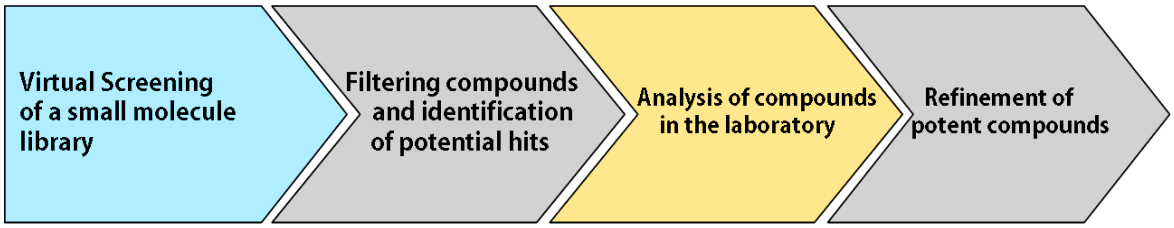

Figure 4.1: Overall linear process of identifying novel ligands.

This approach involves the assignation of molecular descriptors to existing ligands followed by virtual screening for similar compounds. These molecular descriptors may be defined as; *'the end result of an experimental or mathematical procedure transforming chemical information into a useful number'* (Roberto Todeschini and Viviana Consonni 2002). Descriptors vary from method to method, and may be pharmacophoric features of the existing compound (Cheeseright et al. 2006;Schuster et al. 2006) or structural (Ballester, Richards 2007). This method of drug discovery relies heavily on the current scientific paradigm that similar compounds will have similar biological activities.

Accordingly, this approach was employed in this part of the project to develop potent and selective inhibitors of 11β-HSD1 activity. A discussion of the method applied in this project is discussed here alongside the results; the evaluation of the compounds selected is discussed in chapter 5.

4.2 Aims

The aims were to better understand the interactions necessary for an inhibitor to bind to the active site of 11β-HSD1 and ultimately to use this information to fuel the *in silico* drug discovery and selection of novel compounds for the inhibition of 11β-HSD1. This involved an analysis of existing inhibitors, their interactions with the enzyme and co-crystal structures where available. A specialised novel algorithm known as 'Ultra Fast Shape Recognition with Atom Types' (UFSRAT, section 4.4) was used to identify and calculate several specific descriptors on these existing 11β-HSD1 inhibitors, referred to as 'query molecules'. Similar descriptor characteristics were then screened for through millions of molecules (i.e. 'candidate molecules') in the chemical library 'EDULISS' (EDinburgh University LIgand Selection System, section 4.3). The programs UFSRAT and EDULISS were developed at the University of Edinburgh (Taylor et al. 2008) and were employed to identify potential compounds with similar functional and structural properties to the query molecules. This initially produced a large amount of data, which was subsequently filtered and sorted to result in a short-list of available, soluble, small molecules which could potentially inhibit 11β-HSD1. A more detailed perspective of the procedure carried out in this research is shown in figure 4.2.

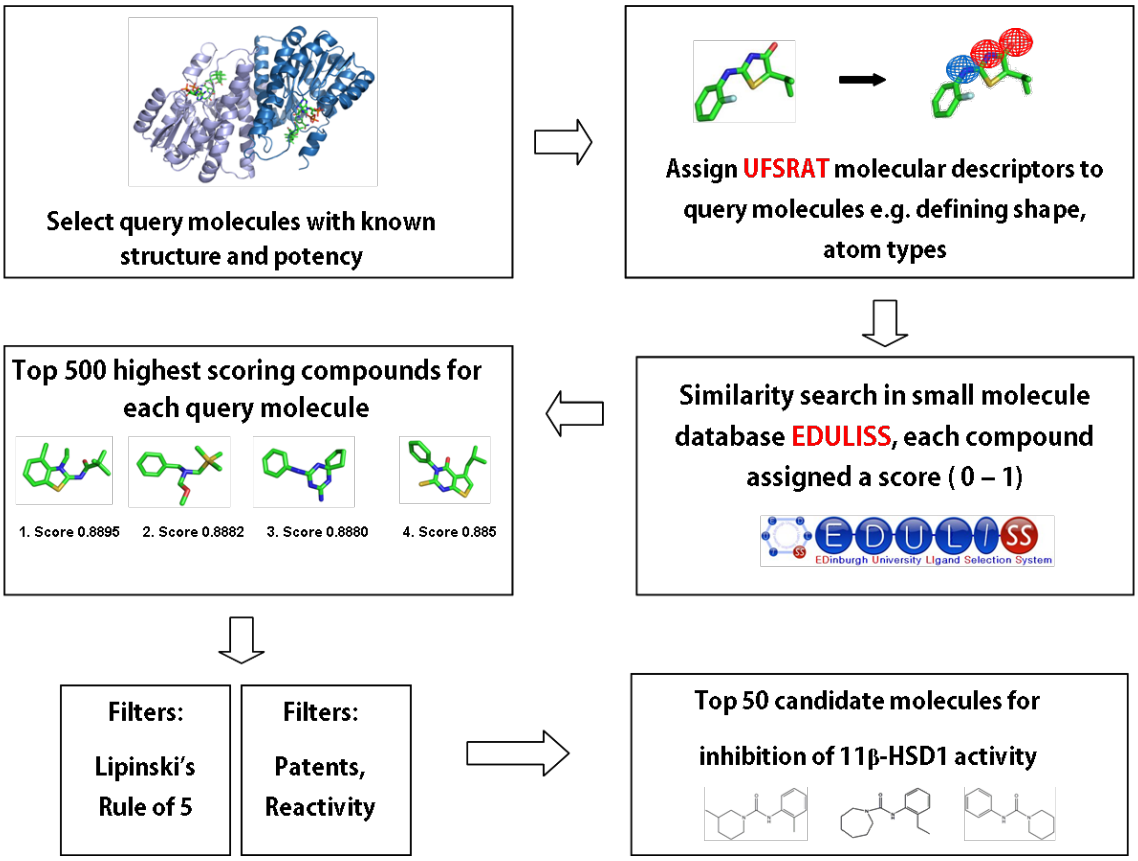

Figure 4.2: A flow chart of the overall methods used in searching for novel inhibitors of 11β-HSD1.

4.3 EDULISS

EDULISS is EDinburgh University LIgand Selection System; a small-molecule database of which the development and upkeep is currently overseen by Dr. Kun-Yi Hsin at the University of Edinburgh. This in-house, large database contains the 3-dimensional structure co-ordinates for each molecule in addition to thousands of molecular, physicochemical, and geometric (to name a few) descriptors for each of the 5.5 million compounds, 4 M of which are unique. These features are user-defined, a process facilitated by a user-friendly web interface. It sources these compounds from 29 commercial databases, ensuring that each chemical is currently available for purchase. The 29 different commercial databases and the number of compounds that each contributes are shown in figure 4.3.

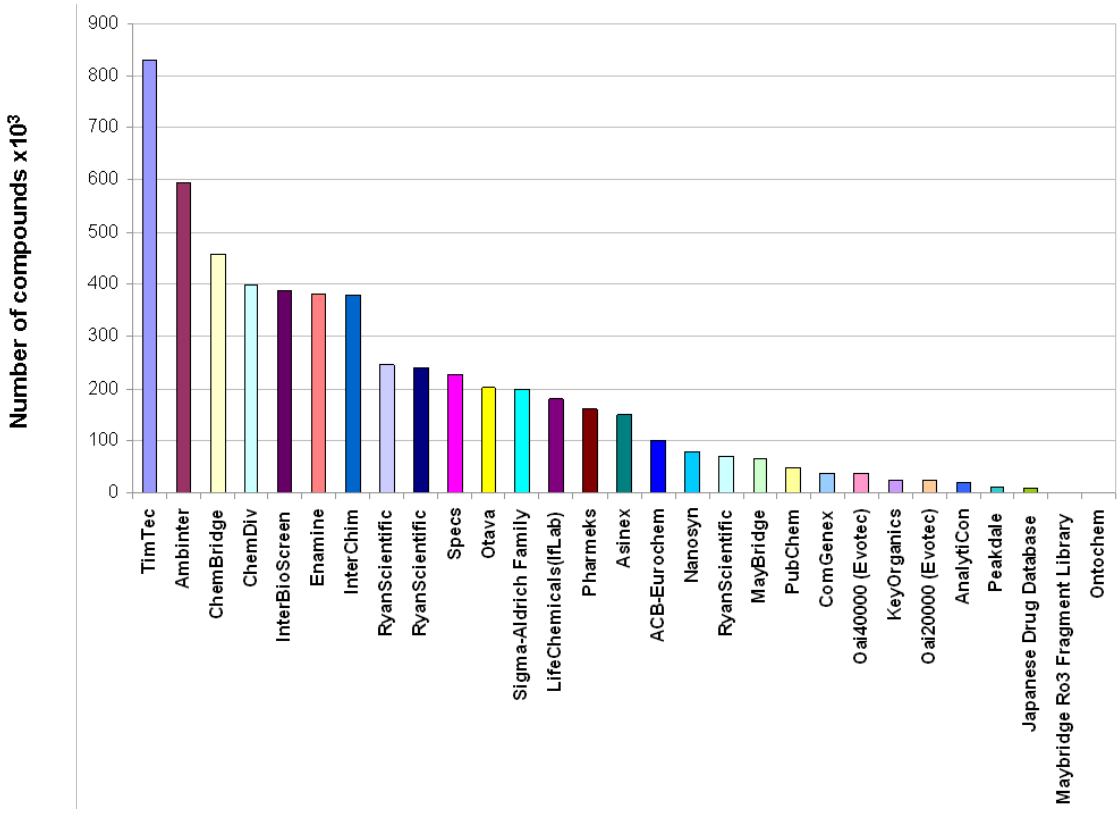

Figure 4.3: Histogram showing the 29 commercial databases and the number of compounds each contributes to EDULISS. Adapted with permission from Dr. Hsin.

The EDULISS database was originally developed by Dr. A Hinton (Hinton 2005) and has since been expanded to include more suppliers, more physicochemical information about each compound and is continuously updated. For example, each compound has over 1500 descriptors defining it, allowing users to search for very specific subsets of compounds. The 2-D atomic co-ordinates for compounds in EDULISS are collected from supplier catalogues. Generating a single, low-energy, 3-D co-ordinate map for each molecule from this 2-D data is then carried out using the program CONCORD™ (Hendrickson et al. 1993). It is this 3-D representation of each molecule that is stored and displayed in EDULISS.

In the present research, EDULISS was used as a source of compounds for the virtual screening (VS). Descriptors were defined by applying the UFSRAT algorithm to all molecules – query and candidate - and detecting similar compounds.

4.4 UFSRAT

Potential inhibitors were selected through the use of a novel virtual screening algorithm; Ultra Fast Shape Recognition with Atom Types (UFSRAT). The UFSRAT algorithm assesses the similarity between two compounds; in this case a query compound and the candidate compounds i.e. those contained in EDULISS. The query molecules used for the searches of novel 11β-HSD1 inhibitors are pictured below in figure 4.3. These are current inhibitors (A, carbenoxolone), pre-clinical inhibitors (B and D: adamantine series, and 2-anilinothiazolone) and the endogenous substrate (C, cortisol).

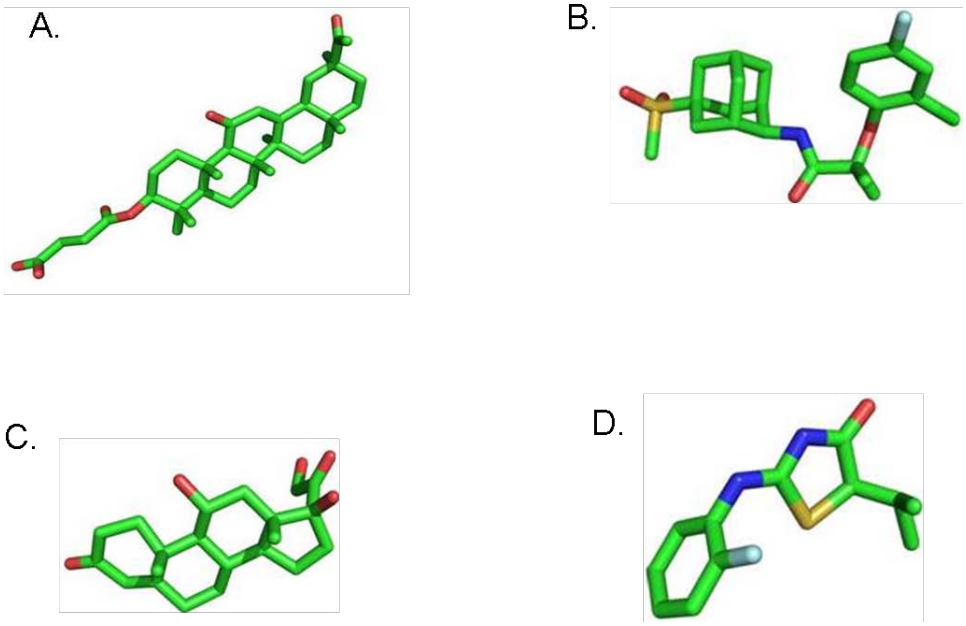

Figure 4.3: The 4 query molecules used as a template by UFSRAT and Eduliss.
A. Carbenoxolone, B. Adamantane, C. Cortisol, D. 2-anilinothiazolone.

These four structurally-varied compounds were selected as query molecules to encompass a broader molecular range as guidelines for potential inhibitors. For example, carbenoxolone (A) and cortisol (C) have a typically steroidal 4-ring structure, whereas adamantane (B) and 2-anilinothiazolone (D) represent non-steroidal inhibitors with varying substituents. In addition, co-crystal structures of human 11β-HSD1 and compounds B and D were available along with kinetic data, allowing for comparison of any subsequent candidates from virtual screening.

The importance of similarity in the overall shape of the novel 11β-HSD1 inhibitors is fundamental; it is evidently a prerequisite for being able to physically enter the active site pocket, and also for the ligand to approach catalytic residues within 3 - 5 Å to enable polar and hydrophobic contacts and to avoid empty space within the pocket (Ballester, Richards 2007;Kortagere et al. 2009). The atom type and atom location is also an important consideration; the pharmacophore features of an existing ligand govern its binding ability and its relative affinity to the target, thus compounds with similar pharmacophoric parameters should bind with similar interactions. The pharmacophore features of these query compounds are shown simplistically in figure 4.4.

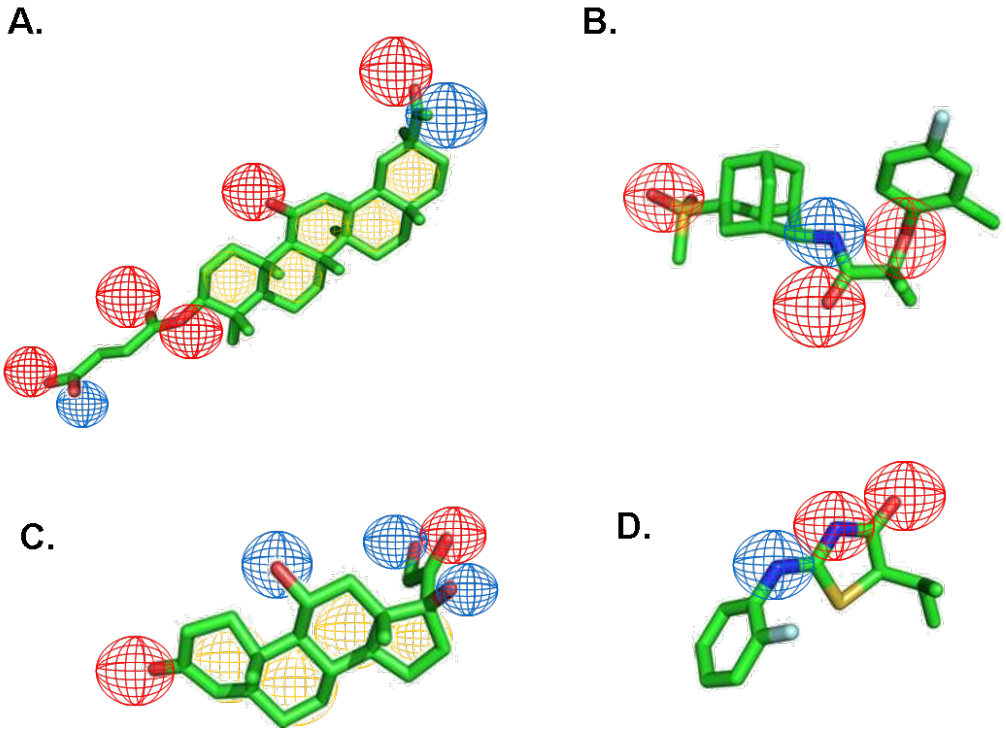

Figure 4.4: The four query compounds (from A-D; carbenoxolone, adamantane, cortisol and 2-anilinothiazolone). Hydrogen bond acceptors (HBA) are shown with red spheres, hydrogen bond donors (HBD) are shown with blue spheres, hydrophobic components are shown in yellow.

Figure 4.4 shows that each of the four query compounds contains at least two hydrogen bond acceptors (HBA) and one hydrogen bond donor (HBD) group. Application of the UFSRAT conditions in a virtual screening process leads to the subset of molecules being similar not only in overall shape but also in atom type and

molecular location of these atom types. The original method, coined UFSR (Ultra-Fast Shape Recognition) was developed by Ballester and Richards (Ballester, Richards 2007) and did not take into account the atom types. Thus the original UFSR algorithm is successful only in identifying similarly shaped molecules, irrespective of atom type (i.e. hydrogen acceptors, hydrogen donors and hydrophobic entities).

Recently, UFSR has been extended greatly to include discrimination between atom types. This research has been carried out by members of the Computational Biology Group at the University of Edinburgh, principally by Dr. Steven Shave (unpublished data). Simplistically, this method involves the assignation of descriptors to a query molecule (those shown in figure 4.3) and all candidate molecules (i.e. all molecules in EDULISS). This is followed by a comparison of the query and candidate molecule using the descriptor sets and applying a scoring function. The compounds are then ranked according to similarity to the query compound, with the highest scoring compounds as the most similar. In this research, the top scoring 500 compounds were selected for inspection.

Assigning descriptors to ligands using UFSRAT initially involves the calculations of 12 molecular shape descriptors. These are the calculations of the atomic distances of all atoms in the molecule to four main points: the molecular centroid (called point 1, or P1), the closest atom to the centroid (called P2), the furthest atom from the centroid (called P3) and the furthest atom from point 3 (called P4). This is shown in figure 4.5 overleaf.

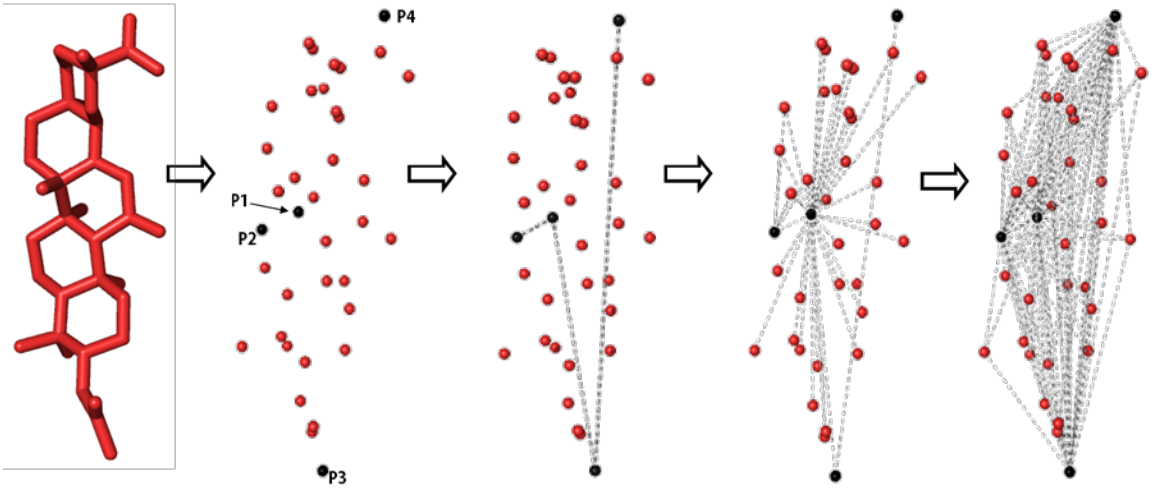

Figure 4.5: Illustration demonstrating the method of converting the molecular volume of carbenoxolone into distances between all atoms in the molecule to P1, P2, P3 and P4.

This provides 4 sets of distances which are regarded as statistical distributions. The first three moments of these distributions are taken: the mean, the variance and the skew. This gives a total number of 12 descriptors for the molecule (i.e. 4 subsets with 3 values each). These 12 descriptors are unique to each molecule and define its overall size, compactness and symmetry.

In addition to the 12 descriptors detailed above, UFSRAT also takes into account three atom types; whether they are hydrogen bond donors (HBD), hydrogen bond acceptors (HBA) or hydrophobic. The three possible atom types each generate a distribution, which contributes 12 descriptors (per distribution), giving an additional 36 descriptors to the existing 12. Figure 4.6 shows the four UFSRAT descriptions simplistically.

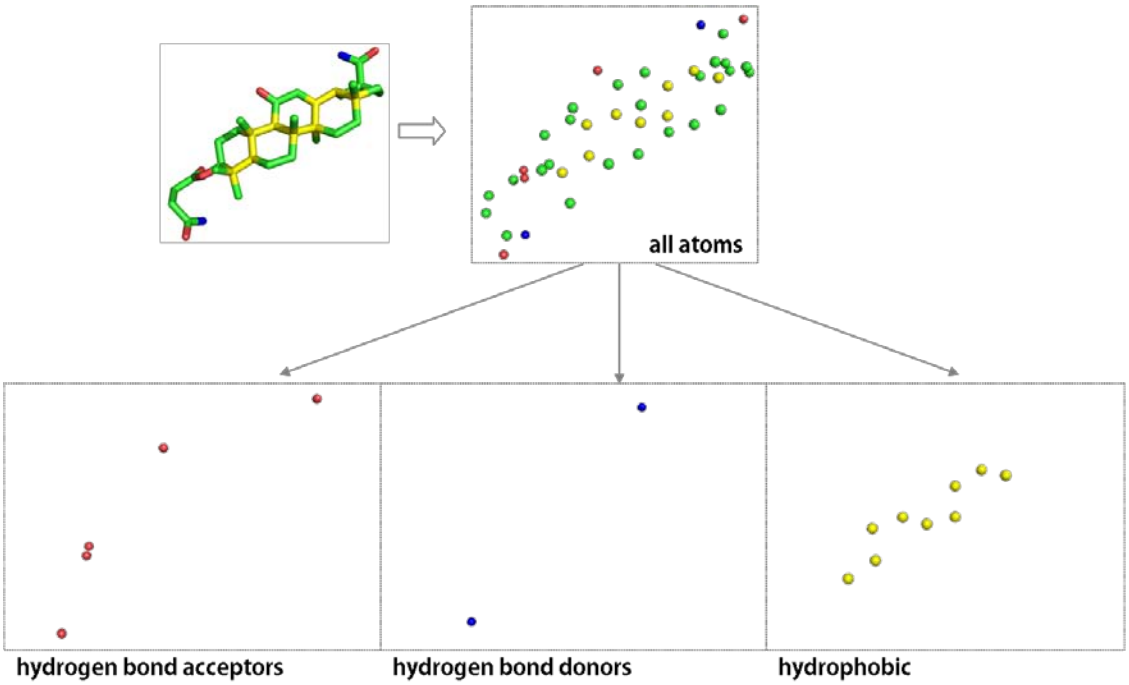

Figure 4.6: The algorithm UFSRAT describes four atom types; all atoms (as described in detail in figure 4.2), hydrogen bond acceptors, hydrogen bond donors, and hydrophobic atoms, as shown for the clinical 11β-HSD1 inhibitor carbenoxolone. Adapted with permission from Dr. Steven Shave.

In total, UFSRAT uses 48 descriptors to describe a molecule both topologically and biochemically. These descriptors were assigned to each query molecule. A search through the EDULISS database for each query compound was carried out to identify similar compounds to each one. The candidate compounds from the EDULISS database are scored based on their individual similarity to the query molecule. A normalised scoring function is used; a molecule with a score of 1 would be identical to the query molecule, a score closer to zero suggests less similarity. Some examples of these compounds and their scores are shown in figure 4.7.

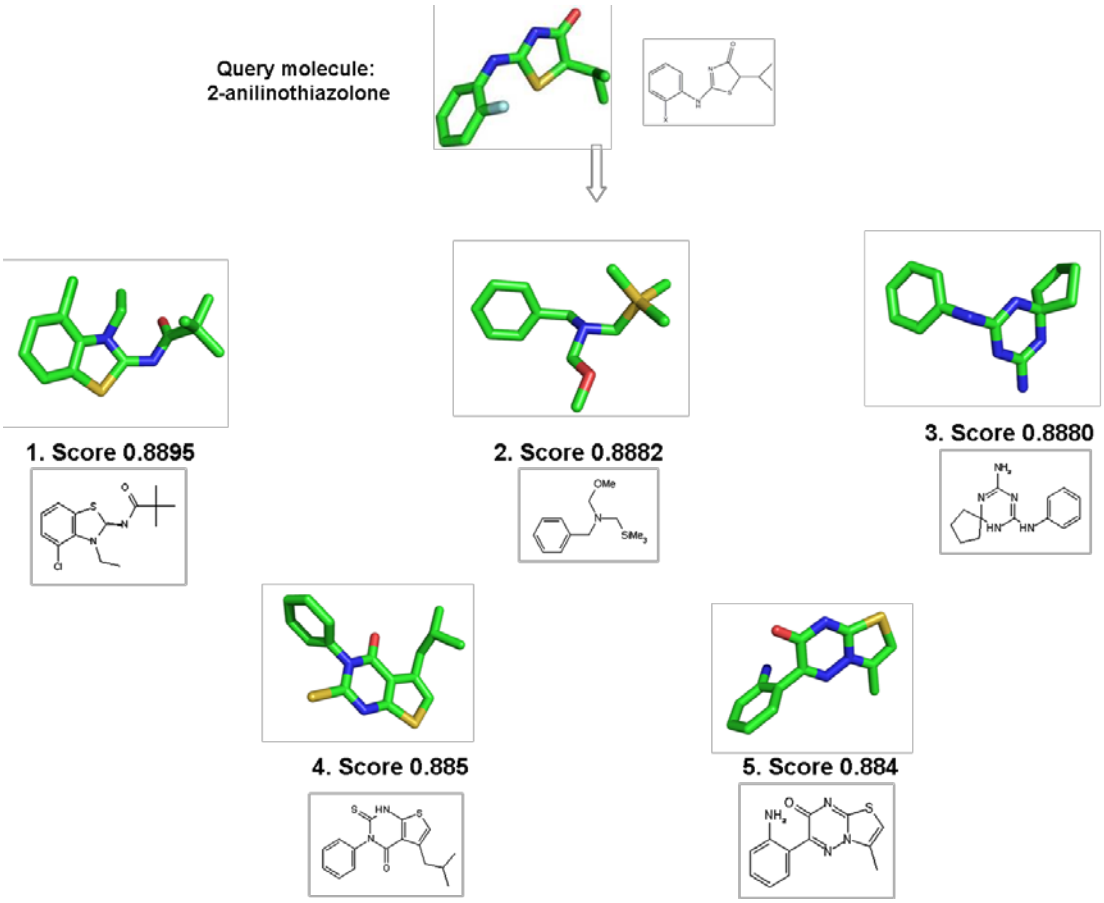

Figure 4.7: The query molecule 2-anilinothiazolone from the co-crystal structure 2RBE is shown here as the query molecule. The top 5 scoring candidates are shown (compounds which scored highly with regards to similarity to the query compound).

As can be seen from figure 4.7, the top five scoring compounds are similar in size, shape and the types of atoms present. Four out of the five top scoring hits contain a sulfur atom; three of these are incorporated into a 5-membered ring with, or in close proximity to a nitrogen, akin to the query molecule. In all cases a central hydrogen acceptor group is found either in the form of a carbonyl or a nitrogen.

4.5 Filtering Potential Inhibitor Compounds: Selecting 'Drug-likeness'

The top 500 hits selected with UFSRAT were taken (500 per query molecule, giving a total of 2000 compounds) and filtering was carried out. This followed several criteria based on established quantitative structure-activity relationship (QSAR) guidelines. These criteria were the commonly accepted Lipinski's rule of 5 (Ro5) (Lipinski et al. 2001).

The Lipinski criteria are listed (the 'Rule of Five' nomenclature refers to the persistent appearance of the number 5 in the rules, rather than five rules);

1. A molecular weight of < 500 Daltons
2. Less than 10 hydrogen bond acceptor (HBA) groups
3. Less than 5 hydrogen bond donor (HBD) groups
4. An MLogP < 5

Adherence to these rules results in a 'drug-like' compound which has better predictions for solubility, bio-availability, toxicology and metabolism. Simply defined; the compound will have 'functional groups, and/ or have physical parameters consistent with the majority of known drugs' (Walters, Murcko 2002). This provides a base for the pharmacokinetic and pharmacological predictions to be made. However difficulties may arise when defining physical drug-like characteristics and several studies have attempted to identify these (Muegge 2003;Sheridan 2002). The 'Lipinski Ro5' is one of several accepted sets of criteria used to filter compounds for drug-likeness. Similar concepts have been developed by Oprea (Hann, Oprea 2004) and Astex (Congreve et al. 2003).

The LogP is the water/ octanol partition coefficient, a measure of the hydrophobicity of a compound (Moriguchi et al. 1992;Delaney 2005). A higher LogP value (greater than 4 or 5) gives an indication of compounds which will have poor aqueous solubility. This implies that the compound will have a sub-optimal ADME profile as well as incurring difficulties at initial screening stages. A fine balance must be made between preserving potential bioavailability of the drug but also an adequate degree of lipophilicity to facilitate binding. It should be noted that several existing potent 11β-HSD1 inhibitors are exceptionally hydrophobic and thus do not meet the solubility criteria; indeed the 'LogP' is also the most difficult parameter to control combinatorially. In addition to this, many of the current pre-clinical inhibitors have a molecular weight greater than 500, the limit set by the Lipinski guidelines.

Application of these rules eliminated approximately 1600 candidate compounds, the majority of which were purged on the basis of an inappropriately high LogP value.

This is because other Lipinski drug-like parameters (i.e. number of HBD, number of HBA) were used as UFSRAT descriptors and so decreased the possible range of HBD and HBA in the candidate molecules. The range of LogP values and molecular weights in the top 500 highest scoring compounds are shown as an example in figure 4.8.

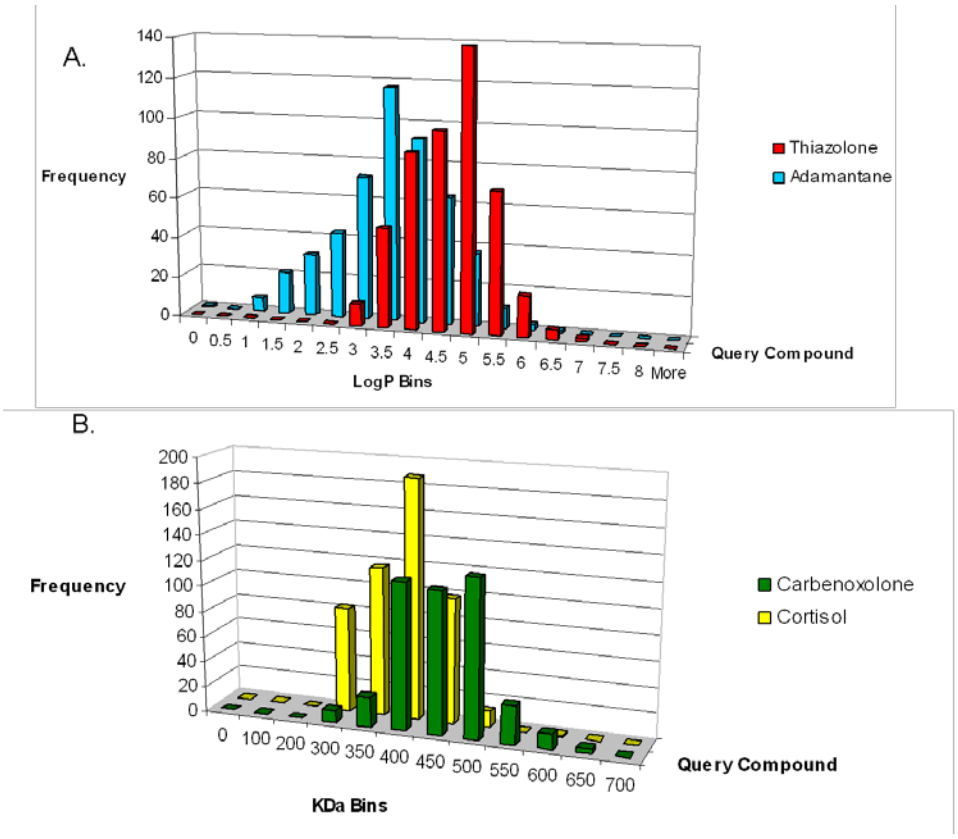

Figure 4.8: A: Range of LogP values obtained using either thiazolone (red) or adamantane (blue) as query molecules. B: Range of molecular weights of candidate compounds discovered using carbenoxolone (green) or cortisol (yellow) as query compounds. Compounds discovered using carbenoxolone have a higher mean MW than those compounds discovered with cortisol. This follows from the same trend in the query compounds.

Interestingly, it has been postulated that the average lipophilicity and molecular weight of compounds for clinical use currently being synthesized is slowly increasing (Gleeson et al. 2009) thought to be due to an over-emphasis on the *in vitro* potency of the compound rather than the safety / toxicity.

Following physicochemical filtering, further sorting to the subsequent final shortlist of compounds was carried out through a manual selection through the remaining compounds. This was to eliminate compounds which:

- May undergo further chemical alteration once in vivo or once in a reducing environment (e.g. Michael acceptors)
- May have already been patented
- May have already been evaluated in published literature with negative results
- Have a steroidal core structure

This enabled the short-list to be reduced to a total of 52 compounds, categorised into 6 structural classes. These compounds are shown in tables 4.2 – 4.7 below, in section 4.8.

4.6 Additional Compounds: Manual Selection

In addition to the 52 candidate compounds short-listed from UFSRAT, an additional 8 compounds were selected 'manually' from supplier catalogues on the basis of their similarity to several unavailable UFSRAT candidate compounds. These included compounds which had small variations in their side groups as compared to UFSRAT selected candidates. These 8 manually selected compounds fitted all physicochemical criteria for drug-like compounds.

4.7 Results: Short-listed Compounds

The short list of compounds was initially comprised of 52 compounds, out of which 27 were available for immediate dispatch from the suppliers; the remaining 25 were unavailable. A table with all 52 compounds may be found in the appendix; only the 27 analysed are shown here (tables 4.2 – 4.7). Out of these 52 candidate compounds, the majority were 'hits' from the query molecule carbenoxolone. This can be seen in figure 4.9.

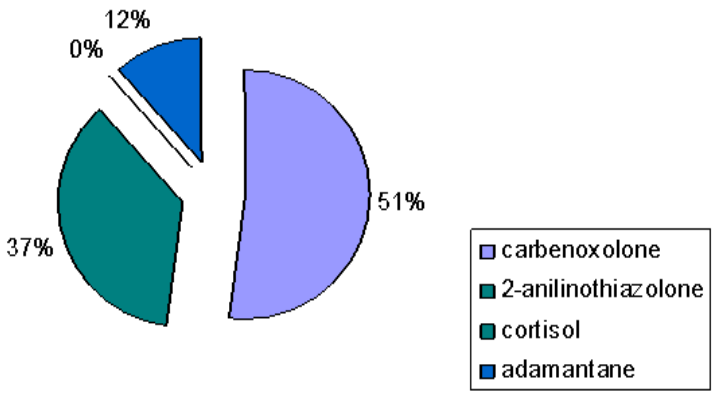

Figure 4.9: A summary of which query molecules provided the most feasible hits. Carbenoxolone generated the most number of feasible, drug-like compounds (51%), followed by 2-anilinothiazolone (37%), then adamantane (12%). The query molecule cortisol did not generate any feasible hits.

The query molecule adamantane generated hits which were bulky on one side, the majority of which central amino group resembling the parent molecule. The adamantane molecule has some interesting pharmacophore features, as shown previously, in figure 4.4. Cortisol generated compounds with a low score (predominantly scores lower than 0.6). Furthermore, no final hits were generated from this query molecule, as seen in figure 4.9 as the majority of consequent compounds were steroidal which would have been rejected by the filters applied.

In the following section (section 4.8) the short-listed compounds selected as candidates for inhibition of 11β-HSD1 using UFSRAT are tabulated. These are the compounds with reference numbers ranging from 1 – 52, in tables 4.2 – 4.7. Compounds with identification numbers ranging from 53 – 60 are those which were selected 'manually', that is, directly through supplier's catalogues based on their similarity to compounds from UFSRAT which were not in stock.

Of the 35 compounds analysed, 27 were from the application of UFSRAT and 8 were selected 'manually'.

4.8 Classification of compounds

The 35 compounds available were loosely clustered into 6 different groups according to the central structural features of the ligands. These were:

1. Ureas
2. Tetrazines and triazoles
3. Thioethers
4. Benzamides and amides
5. Cycloheptanones, cyclohexanones and keto-groups

This clustering is shown in tables 4.2, 4.3, 4.4, 4.5, 4.6, and 4.7 below.

1. Ureas

Current patents by Incyte cover many of the urea containing 11β-HSD1 inhibitor compounds, such as tetra-substituted ureas (patent number W02007130898). There were three main urea skeletons and variations thereof that were looked for; shown below in figure 4.10. These had varying degrees of substitution from one of the urea nitrogens.

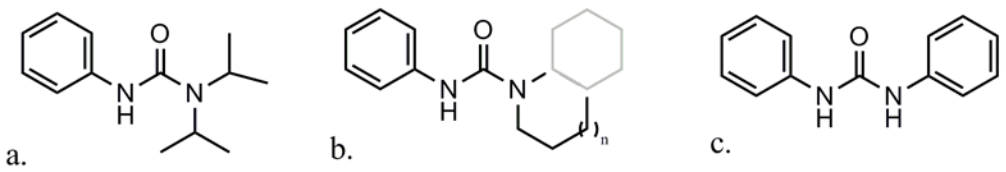

Figure 4.10: The three urea scaffolds searched for through the compounds generated with VS. Compound 'a' has two isopropyl substitutions off the right hand nitrogen of the urea (this part of the molecule, referred to as the right hand side, is thought to point toward the entrance of the binding pocket. The left hand side will be buried in the hydrophobic pocket in close proximity to NADP). Compound 'b' has the urea nitrogen forming one member of a 6 (or more)-membered cycle, putatively with another cyclic group substitution (shown in grey). Molecule 'c' is symmetric; each nitrogen has an aromatic ring substitution.

The scaffold of compound 'c' (figure 4.10c) appeared just once in the whole selection of compounds from UFSRAT, this is now known as compound 45 (table 4.2).

Table 4.2 (also continued on next page): Clustering of urea–type compounds (N-(C=O)-NH) from VS. The table describes the molecular weight, solubility in water (MLogP), Supplier and the query molecule it was generated from. The right-hand most column denotes whether the compound was selected manually ('R') or through the use of UFSRAT (where the query molecule used in the similarity search is quoted).

2D Structure	#	M.W (Da)	MLogP	Supplier	Query Molecule
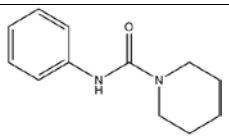	27	204.1	1.82	ChemBridge	2-anilinothiazolone
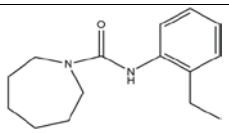	28	246.1	3	ChemBridge	2-anilinothiazolone
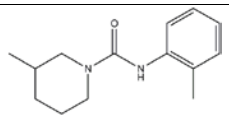	29	232.3	2.1	ChemBridge	2-anilinothiazolone
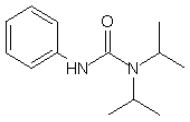	30	220.3	0.263	Sigma Aldrich	2-anilinothiazolone
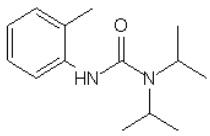	31	234.3	0.875	ChemBridge	2-anilinothiazolone
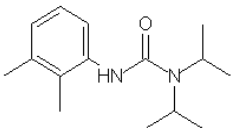	32	248.4	0.852	Sigma Aldrich	2-anilinothiazolone
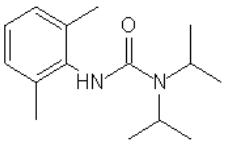	33	248.4	0.318	Sigma Aldrich	2-anilinothiazolone
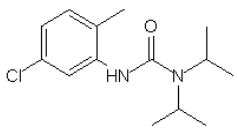	34	268.8	0.867	Sigma Aldrich	2-anilinothiazolone
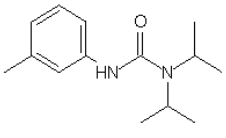	35	234.3	0.838	Sigma Aldrich	2-anilinothiazolone

2D Structure	#	M.W (Da)	MLogP	Supplier	Query Molecule
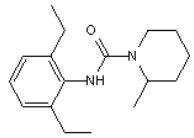	36	274.4	0.331	Sigma Aldrich	2-anilinothiazolone
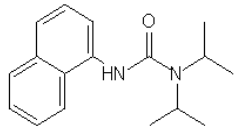	37	270.4	0.258	Sigma Aldrich	2-anilinothiazolone
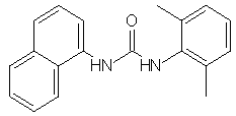	45	229.3	0.275	Sigma Aldrich	2-anilinothiazolone
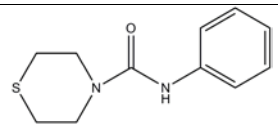	53	222.3	1.5	Specs	R
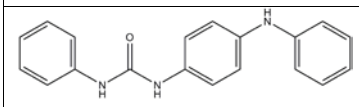	55	303.4	5.2	TimTec	R
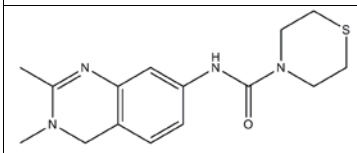	59	304.4	1.6	Specs	R
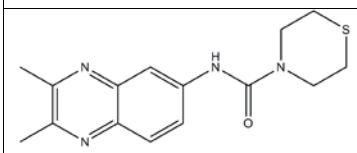	60	302.4	1.6	Specs	R

Table 4.2 continued from previous page.

2. Tetrazines and Triazoles

Many of these compounds also contain a thioether. Several of the tetrazine compounds generated from UFSRAT were found to be under patent (NovoNordisk, Denmark) or analogous to compounds discovered previously at the University of Edinburgh using a different approach to drug discovery. Several were predicted to be in the nanomolar range of IC_{50} values based on SAR with previous compounds. A number of the thiol-triazole compounds are also under patent by Novo Nordisk.

Table 4.3: Clustering of compounds with a tetrazine or triazole ring (with or without a thioether group) from UFSRAT. This table describes the molecular weight, solubility in water (MLogP), Supplier and the query molecule it was generated from. The right-hand most column denotes whether the compound was selected manually ('R') or through the use of UFSRAT (where the query molecule used in the similarity search is quoted).

2D Structure	#	M.W (Da)	MLogP	Supplier	Query Molecule
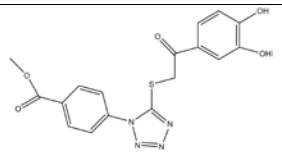	7	386.4	2.21	InterBioScreen	CBX
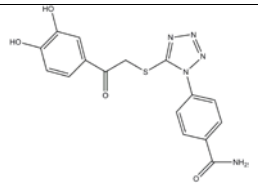	10	371.4	1.56	InterBioScreen	CBX
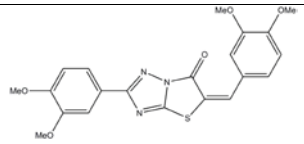	12	425.5	2.65	InterBioScreen	CBX
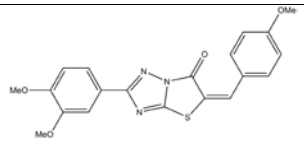	13	395.4	3.17	InterBioScreen	CBX
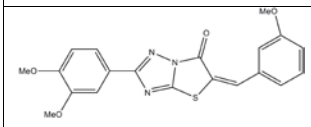	16	395.4	3.18	InterBioScreen	CBX
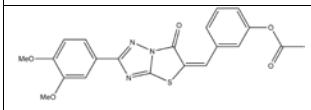	23	423.4	3.39	InterBioScreen	CBX

3. Thioethers

The basic skeleton in this class consists of an acetophenone with a thioether group, shown in figure 4.11.

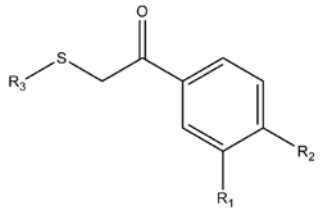

Figure 4.11: Acetophenone scaffold with a thioether.

The acetophenone group (figure 4.11) was predicted to be a good scaffold for novel inhibitors due to the central carbonyl acting as a hydrogen acceptor and the lipophilic group which would be buried inside the binding pocket. Various substitutions from this scaffold would affect the binding, making it an interesting scaffold for SAR analysis.

Table 4.4: Loose clustering of compounds containing a thioether (R-S-R') group (but no tetrazole or triazole) from VS. The table describes the molecular weight, solubility in water (MLogP), Supplier and the query molecule it was generated from. The right-hand most column denotes whether the compound was selected manually ('R') or through the use of UFSRAT (where the query molecule used in the similarity search is quoted).

2D Structure	#	M.W (Da)	MLogP	Supplier	Query Molecule
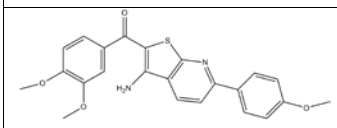	5	420.5	2.15	Specs	CBX
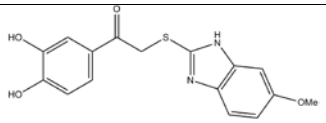	21	330.4	1.07	ChemBridge	CBX
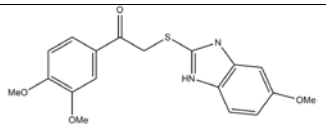	22	358.4	1.55	InterBioScreen	CBX

2D Structure	#	M.W (Da)	MLogP	Supplier	Query Molecule
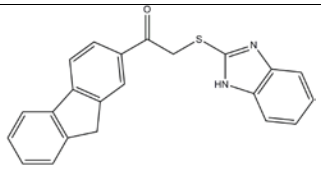	54	356.4	5.4	TimTec	R
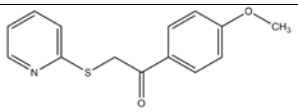	56	259.3	3	TimTec	R
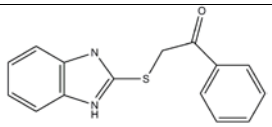	57	269.3	3.7	TimTec	R

Table 4.4 continued from previous page.

4. Benzamides and amides

A class of benzamide inhibitors has been previously screened in lysates for 11β-HSD1 inhibition, with a relatively low percentage inhibition (personal communication, Scott Webster). A SAR analysis from this study showed that there was an increase in 11β-HSD1 inhibition if an amide nitrogen formed part of a cyclic group, or if the group it is attached to is large and bulky, for example, an adamantane. For this reason, several benzamide derivative compounds were excluded if they did not comply with these guidelines.

Two of the compounds categorized in this class, 40 and 42 (table 8.8) were imidazole derivatives, analogous to drugs to treat diabetes currently on the market. Although the diabetes drugs do not target 11β-HSD1, Roche currently own a patent over imidazole containing compounds to inhibit 11β-HSD1 and so these compounds were excluded from the final short-list.

Table 4.5 (continued on next page): Loose cluster of amide- or benzamide containing compounds from VS. Description of molecular weight, solubility in water (MLogP), supplier and the query molecule are shown. The right-hand most column denotes whether the compound was selected manually ('R') or through the use of UFSRAT (where the query molecule used in the similarity search is quoted).

2D Structure	#	M.W (Da)	MLogP	Supplier	Query Molecule
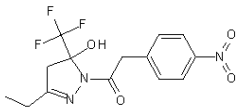	46	345.3	3.01	InterBioScreen	Adamantane
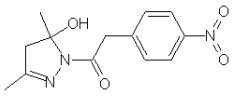	47	277.3	2.38	TimTec	Adamantane
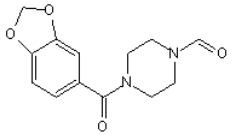	49	262.3	1.16	Sigma Aldrich	Adamantane
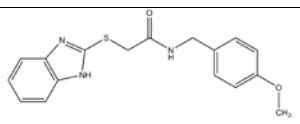	58	327.4	3.5	TimTec	R

6. Cycloheptanones, cyclohexanones and keto-groups

The reactivity of these compounds was a challenge as many are Michael acceptors. Decalins (2 fused cyclohexane rings, non-aromatic) were avoided due to existing patents.

Table 4.6: Clustering of cycloheptanone / cyclohexanone / central ketone containing compounds from VS. The table describes the molecular weight, solubility in water (MLogP), Supplier and the query molecule it was generated from. The right-hand most column denotes whether the compound was selected manually ('R') or through the use of UFSRAT (where the query molecule used in the similarity search is quoted).

2D Structure	#	M.W (g/mol)	MLogP	Supplier	Query Molecule
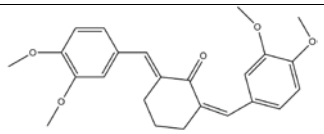	2	394.5	2.84	Sigma Aldrich	CBX
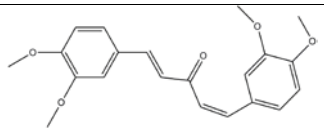	3	354.4	2.59	ChemBridge	CBX
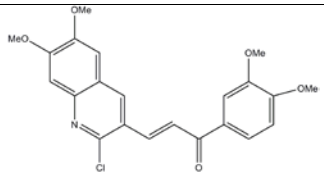	18	413.8	1.75	Specs	CBX

4.9 Pharmacology of candidate ligands

ADMET

Several important properties to consider are the absorption, distribution, metabolism, excretion, and toxicity (known as ADMET) of the candidate drug. Early screening of ADMET parameters can reduce the possibility of drug attrition later on during preclinical, or even clinical trials (Tsaioun et al. 2009). There are currently no straight forward predictive computational tests for ADMET, although studies exist where the potential impact of common substituents has been determined and tabulated (Gleeson et al. 2009).

Potential to cross the Blood-Brain Barrier

With the recent interest in 11β-HSD1 as a therapeutic target for improving cognitive decline (Sandeep et al. 2004) it is important that a potential drug candidate must be able to cross the blood-brain barrier (BBB). The BBB effectively separates the blood and brain through tight junctions between endothelial cells. Predictive combinatorial calculations for whether a compound will cross the BBB involve setting a limit to the solvent accessible polar surface area of the compound (e.g. < 90 $Å^2$), which also conveniently lays restrictions on other physicochemical properties of the compound. Experimental determination of whether or not the compound is a potential P-glycoprotein - an efflux pump - substrate is also an important factor in determining the CNS-penetrative prospects of the drug candidate. There are predictive computational systems for this (e.g. the program Almond v 3.2). In addition, the presence of the multi-drug-resistance protein (MRP) which actively removes exogenous molecules from within neural endothelial cells is another opposition in CNS targeting drugs. A recent development in the CNS-drug field is the novel co-culture of two types of cells: human brain capillary endothelial cells and human glial cells; currently the most accurate predictive test for passive and active transport of molecules into the CNS (Megard et al. 2002).

4.10 Conclusions

The virtual screening program UFSRAT provided a list of potential inhibitors of 11β-HSD1 which were selected on the basis of chemical and geometrical similarity to a set of four query molecules. This was achieved through the application of 48 descriptors which defined molecular and structural constraints in candidate molecules. The resulting candidate compounds looked feasible and contained a wide range of viable functional groups and substituents.

There is no general solution for virtual screening; the output is as good as the input data. Therefore, every prospective application requires tuning to user-defined parameters. All available information possible should be used to generate and validate the models, such as an X-ray crystal structure to define the binding site, or, as in this case existing potent ligands which provide a framework for candidate compounds. Clearly, virtual screening works best as a case by case process (Oprea, Matter 2004).

Also, subsequent filters should be as stringent as possible according to the particular future function of the candidate ligand. In this research, this was reflected in a slight leniency with regards to the MLogP value of the compounds, due to the hydrophobic environment of the binding pocket. The use of filters can significantly reduce the number of candidates for screening as it eliminates compounds with undesired chemotypes and thus undesired physicochemical properties. The second round of filtering in this research eliminated many compounds reducing the number by approximately 90%.

Also, UFSRAT is fast: the process of target preparation, pre-docking filters, docking, post-docking analysis and ranking of compounds takes a matter of hours per query molecule.

Future challenges for this field include the incorporation of adjustable parameters pertaining to pharmacodynamic (PD) and pharmacokinetic (PK) determinants, which may prevent the attrition rate of weak drugs in the early drug development stages (Tsaioun et al. 2009). Additional challenges lie with regards to the flexibility of the ligand and the protein target – e.g. conformational changes that may occur during binding, but also in dielectric constants and partial charges of ligands.

CHAPTER 5

ANALYSIS OF

11β – HYDROXYSTEROID DEHYDROGENASE TYPE I

INHIBITION BY NOVEL LIGANDS

5.1. Introduction

The enzyme 11β-hydroxysteroid dehydrogenase 1 regulates the tissue availability of cortisol through the interconversion of cortisone and cortisol. Dependent on the surrounding milieu, it will act as either a reductase or a dehydrogenase. An excess of 11β-HSD1 can lead to insulin resistance and metabolic syndrome as shown by transgenic models, thus it is a viable drug target for inhibition in the treatment of type 2 diabetes and related diseases (chapter 1). Novel inhibitors were selected through virtual screening to inhibit 11β-HSD1 (chapter 4), the potency of these 35 novel inhibitors belonging to 6 distinct structural classes are studied here.

The flow chart in figure 5.1 shows the sequence of events in testing the inhibitors. Initial screens were carried out which tested the efficiency of the compounds to inhibit 11β-HSD1 in the dehydrogenase and reductase directions. Each compound was tested at a concentration of 100 μM, and the percentage of inhibition determined. This was carried out in triplicate with appropriate controls. Following on from this, the most promising compounds were taken for further analysis to allow for calculation of a K_i. These compounds were those which caused a greater than 40% inhibition of the human enzyme in the initial screen. These more comprehensive assays involved inhibition of 11β-HSD1 in mammalian cells in addition to assays with recombinant protein, which allowed a comparison to be made between the potency of the compound *in vivo* and *in vitro*. Furthermore, a comparison between human and mouse inhibitor binding was achieved.

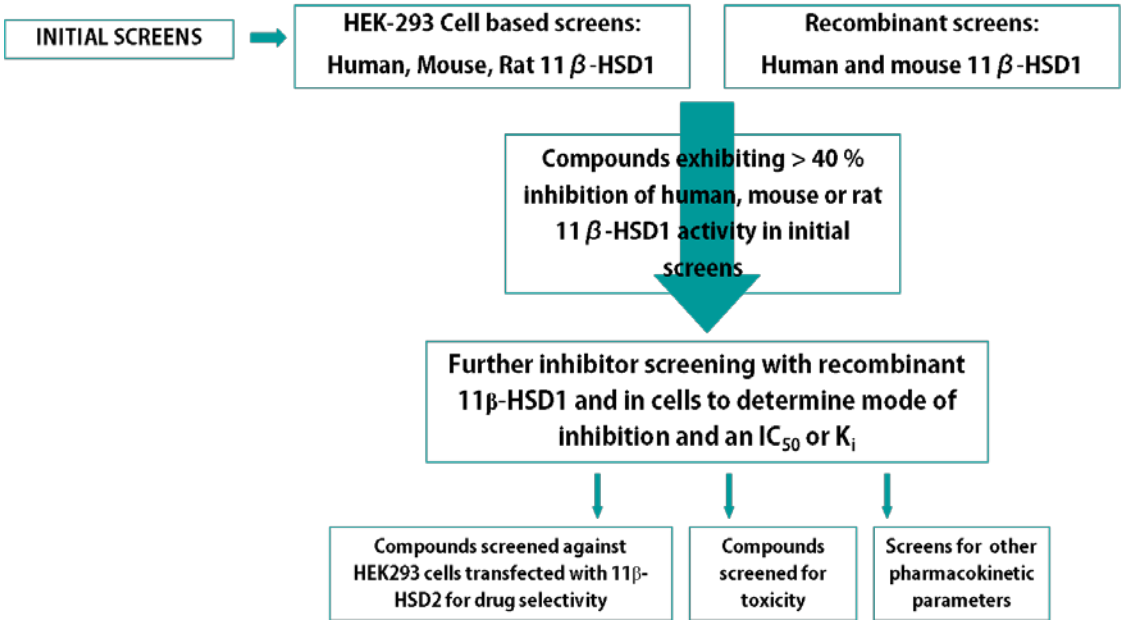

Figure 5.1: A flow chart showing the sequence of events in testing the novel inhibitors of 11β-HSD1. Initial screens are followed by full screening of compounds which inhibit greater than 25% of the recombinant enzyme activity or more than 40% activity in 11β-HSD1-transfected HEK-293 cells. Finally, the successful compounds are assayed for 11β-HSD1 selectivity with an 11β-HSD2 binding assay.

5.2 11β-HSD1 Inhibition Assays: Fluorescence and SPA

Inhibition assays were carried out using two methods: Scintillation Proximity Assay (SPA) and a fluorescence assay. The fluorescence assay has been discussed in chapter 3 and a brief description of SPA will be given here. Both are sensitive, high through-put assays which are able to monitor the reaction in both directions (reductase and dehydrogenase). The fluorescence assay was used to monitor the inhibition profiles of the compounds on the dehydrogenase reaction, shown in figure 5.2.

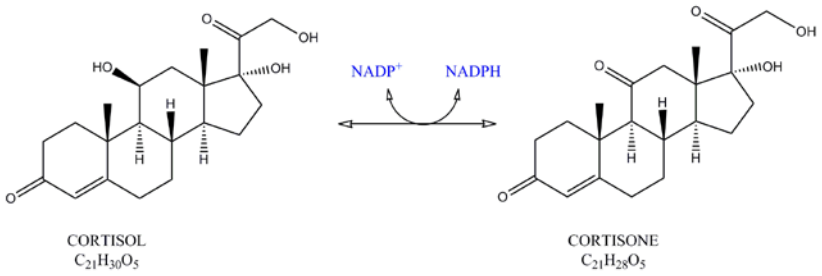

CORTISOL + $NADP^+$ → CORTISONE + NADPH

Figure 5.2: The reductase reaction of 11β-HSD1 monitored using a fluorescence assay.

SPA was used to monitor the reverse, reductase reaction, shown in figure 5.3.

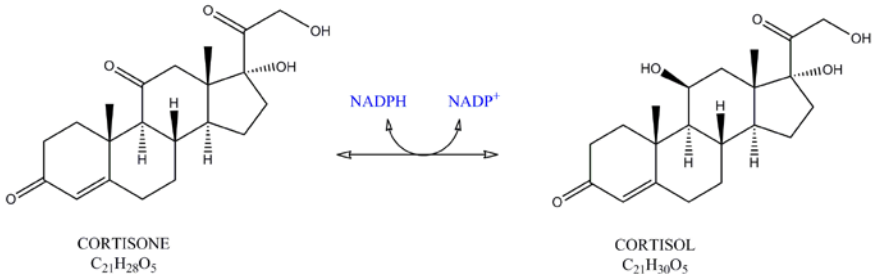

CORTISONE + NADPH → CORTISOL + NADP$^+$

Figure 5.3: The dehydrogenase reaction of 11β-HSD1 which was monitored using SPA.

5.3 Scintillation Proximity Assay

A Scintillation Proximity Assay (SPA) is a well established high throughput screening assay for ligand-11β-HSD1 binding (Mundt et al 2005; Solly et al 2005). SPA is founded on the principle of microscopic beads containing scintillant which are stimulated to emit light when radio-labelled cortisol binds to the surface of the bead via interaction with a previously coupled anti-cortisol antibody (figure 5.5). A mouse monoclonal antibody is coupled to protein A-coated beads with a greater than 100-fold affinity for cortisol than cortisone. The assays are carried out in buffers using radioisotopes which emit low energy radiation ([^{3}H] or [^{125}I]). For the purposes of this research, the assay is a method of measuring the conversion of:

[1,2(n)-^{3}H]Cortisone (^{3}H-$C_{21}H_{28}O_5$) → [1,2(n)-^{3}H]Cortisol (^{3}H-$C_{21}H_{30}O_5$) **Eqn 5.1**

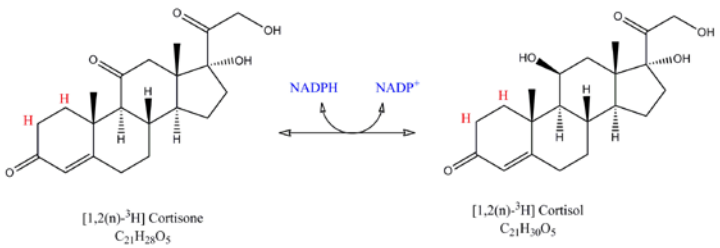

Figure 5.4: Chemical structures of [1,2(n)-^{3}H]Cortisone and [1,2(n)-^{3}H]Cortisol, showing the position of the tritium atoms. The forward reaction is the reductase reaction.

Equation 5.1 and figure 5.4 show the reductase reaction monitored with SPA. Once the radioactive substrate binds the bead-coupled anti-cortisol antibody, it is in close enough proximity for the emitted radiation to activate - through energy transfer - the scintillant

contained within the bead which then produces a light signal. The amount of light produced is proportional to the amount of labelled molecules bound to the beads. This is detected by a scintillation counter and converted into the concentration of cortisol present in the reaction. This is shown in figure 5.5.

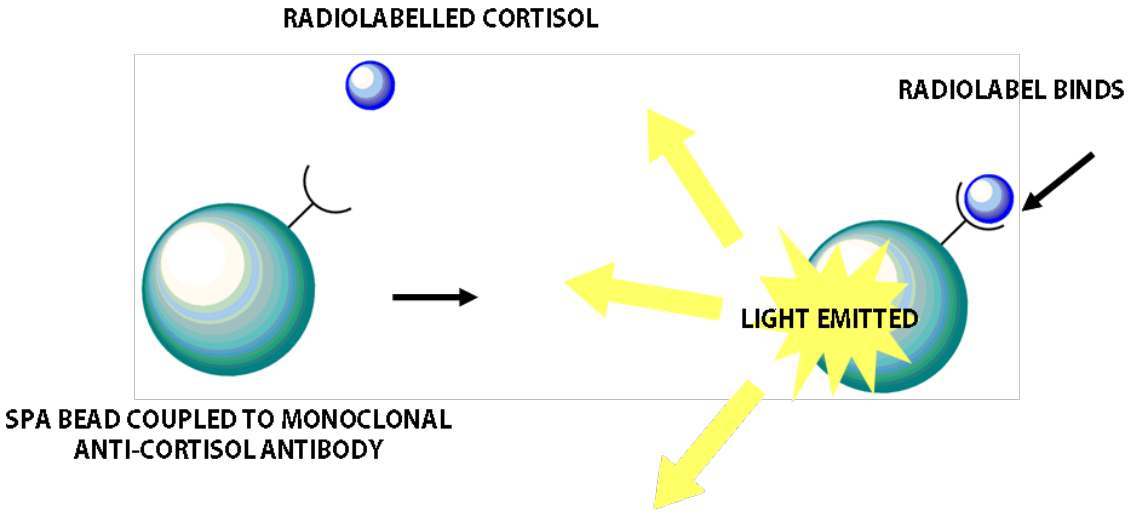

Figure 5.5: Diagram depicting the mechanism of SPA. On the left is a SPA bead (green sphere) coupled to an anti-cortisol antibody. Radio-labelled cortisol (blue sphere) is free in solution and will bind to this antibody (picture on right). At this point the proximity of the radioactivity excites the scintillant inside the SPA bead. This is detected and measured on a scintillation counter.

A high concentration of a potent inhibitor will result in less radioactive cortisol being produced and therefore a lower signal from SPA beads, as compared to controls with no inhibitor. The beads are typically composed of polyvinyltoluene (PVT) containing diphenylanthracine (DPA) and have an average diameter of 5 microns. SPA is a homogeneous binding assay (Janzen 2002) which is able to measure weak interactions without disturbing the equilibrium with a separation step, such as HPLC - as was previously employed to assay 11β-HSD1 activity and assess novel inhibitors (Maser et al 2003; Oppermann et al 2000).

Assays were carried out in a 96-well plate format, with each well carried out in duplicate or triplicate with appropriate controls. A detailed protocol for this and other assays is found in chapter 7 – Materials and Methods.

SPA was carried out with both recombinant mouse and human 11β-HSD1 and human embryonic kidney cells (HEK 293) (Graham et al 1977) overexpressing human, rat and mouse 11β-HSD1. SPA was used to follow the effects of inhibitors on the reductase reaction only; there are no anti-cortisone antibodies available that are as effective as the anti-cortisol antibodies used. The plates are set up with high and low controls of [^{3}H]-cortisone which is used as calibration for the assay, using the equation 5.2;

$$\%inhibition = \left[1 - \left(\frac{(compound - LC)}{(HC - LC)}\right)\right] \times 100 \qquad \textbf{Eqn 5.2}$$

Where 'compound' refers to the light emitted from the reaction with a particular inhibitor, LC is the low control and HC is the high control. The optimum conditions for SPA are well documented (Henriksson et al 2005, Zheng et al 2005, Mundt et al 2005). These assays were carried out at the QMRI at the Royal Infirmary, Edinburgh, with the help of Dr. Scott Webster, Ms. Kirsty McConnell, Dr. Karen Sooy and Ms. Margaret Binnie.

5.4 K_i Determination

Assays were carried out as described in chapter 7. The K_i values for carbenoxolone and the other inhibitors were calculated using nonlinear regression with a three parameter logistic model. The experimental data were fitted to equation 5.4 using Kaleidagraph software, assuming the following:

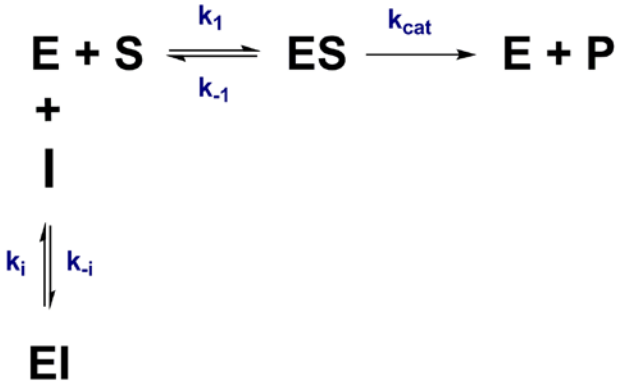

Figure 5.6: A Cleland notation (Cleland 1963) reaction of competitive inhibition, where E is enzyme (11β-HSD1), S is substrate (cortisol for dehydrogenase assays, cortisone for reductase assays) and I is inhibitor.

Figure 5.6 is representative of a competitive inhibition model of inhibition, where the inhibitor and substrate compete to bind exclusively at the same site. In this case:

$$K_i = \frac{k_{-i}}{k_i} \qquad \text{and} \qquad K_m = \frac{k_{-1}}{k_1} \qquad \textbf{Eqn 5.3}$$

In equation 5.4, $[E]_o$ and $[I]_o$ are the active enzyme and inhibitor concentration, respectively. K_i^{app} is the apparent inhibition binding constant, V_i and V_o are the rates of cortisone reduction in the absence or presence of inhibitor, respectively (Morrison 1969). This model has been used previously in 11β-HSD1 inhibitor assays (Castro et al 2007).

$$V_1 = V_o\left(1 - \frac{\left([E]_o + [I]_o + K_i^{app} - \sqrt{(([E]_0 + [I]_0 + K_i^{app})^2 - 4[E]_o[I]_o)}\right)}{2[E]_o}\right) \qquad \textbf{Eqn 5.4}$$

Two additional equations are required in this research, to take into account to effects of substrate and inhibitor both competing for the active site i.e. competitive inhibition.

To take into account the substrate when calculating K_i the following (equation 5.5) was used;

$$K_i^{app} = K_i + \frac{K_i}{K_m} \times [cortisol] \qquad \textbf{Eqn 5.5}$$

5.4.1 IC_{50} Determination

The Cheng-Prussoff equation (Cheng and Prussoff 1973) is shown as equation 5.6, and enables a calculation of a K_i from the IC_{50} as determined in cell-based assays for competitive inhibitors. As IC_{50} values may vary for the same ligand depending on experimental conditions, a more accurate and comparable quantity is required which does not depend upon the experimental set-up, i.e. a K_i. The IC_{50} is concentration of inhibitor which causes a 50 % inhibition of enzyme activity. It is experiment-dependent and is determined by three factors;

- The K_i of the compound,
- Concentration of cortisone (substrate): higher concentrations of cortisone will require higher concentrations of inhibitor to displace. Increasing the cortisone concentration will increase the IC_{50} (without altering K_i)
- The K_m of cortisone; it will require a higher concentration of inhibitor to displace a tightly bound substrate. A substrate with a lower K_m compared to cortisone (i.e. a tighter binding ligand) would increase the IC_{50}.

The K_i cannot be determined directly from the inhibition assay data as the enzyme concentration in the cultured cells is unknown. Therefore, a dose-response curve for each inhibitor is generated from which the IC_{50} is determined. Then equation 5.6 is applied:

$$K_i = \frac{IC_{50}}{1 + \frac{[cortisone]}{K_m}} \qquad \textbf{Eqn 5.6}$$

Conversion of IC_{50} values to K_i values is a much discussed problem in the literature (Brandt et al 1987; Cheng 2001; Cortes et al 2001; Lazareno and Birdsall 1993) and the most widely accepted conversion for competitive inhibitors is used here. The K_m for cortisol was taken as 21.9 μM.

5.5 The Short-Listed Compounds for Inhibition Analysis

The 35 inhibitors analysed are shown in figure 5.7 below.

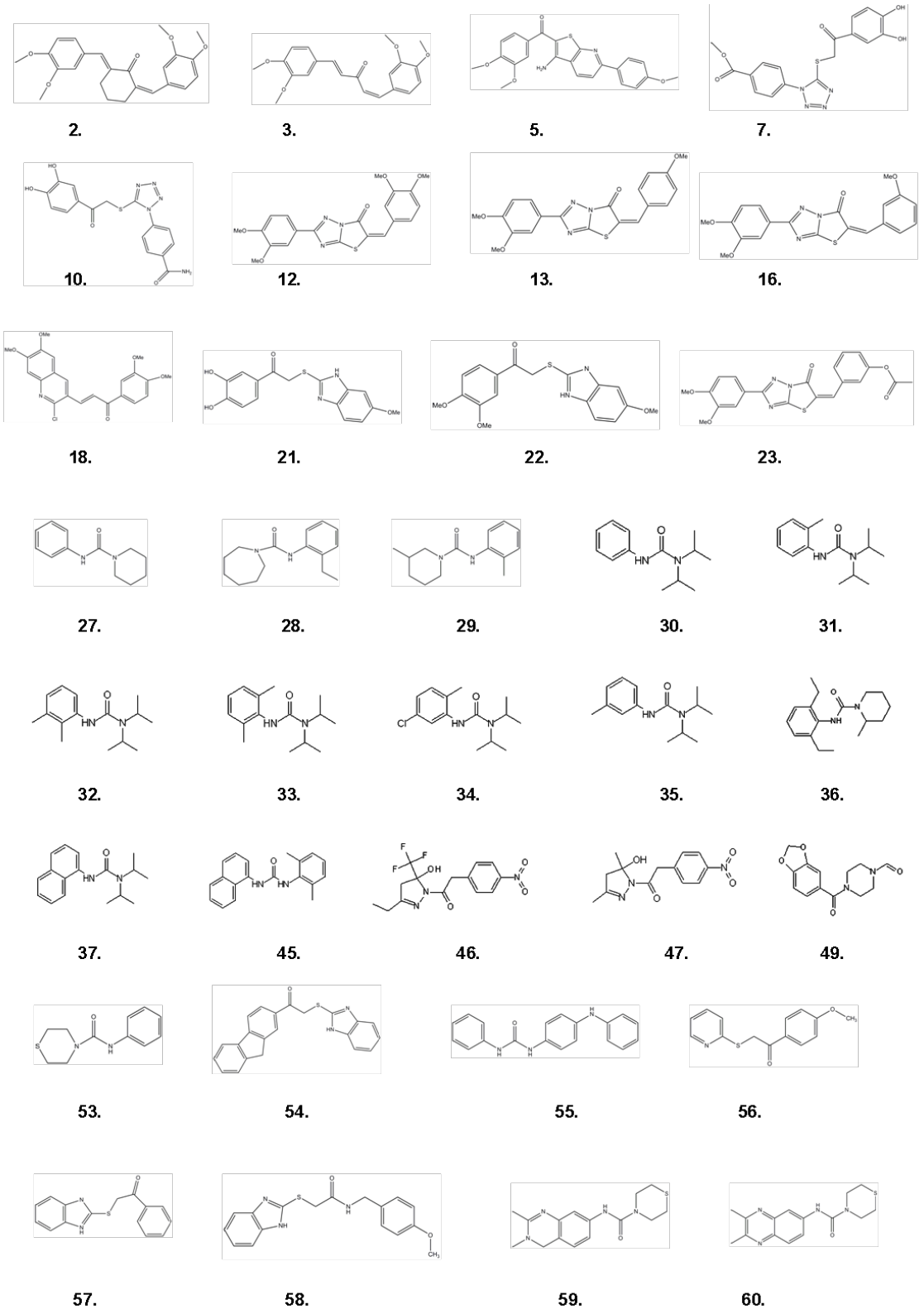

Figure 5.7: Each inhibitor analysed is depicted and numbered corresponding to chapter 4. Those numbered 53 to 60 are compounds selected manually, based on the top hits from virtual screening (VS). Compounds from VS are labelled 1 – 52.

5.6 Results of 11β-HSD1 Inhibitor Assays

Assays were carried out with recombinant protein and also with cultured HEK-293 cells transiently transfected with 11β-HSD1. The following sections are organised according to the assay material used i.e. recombinant enzyme or cultured cells. The assay technique used i.e. fluorescence assay or SPA, is also stated, and this was dependent on the reaction direction that was being monitored. For reductase reactions, SPA was employed; for dehydrogenase reactions, fluorescence was used. This is clarified in figure 5.8.

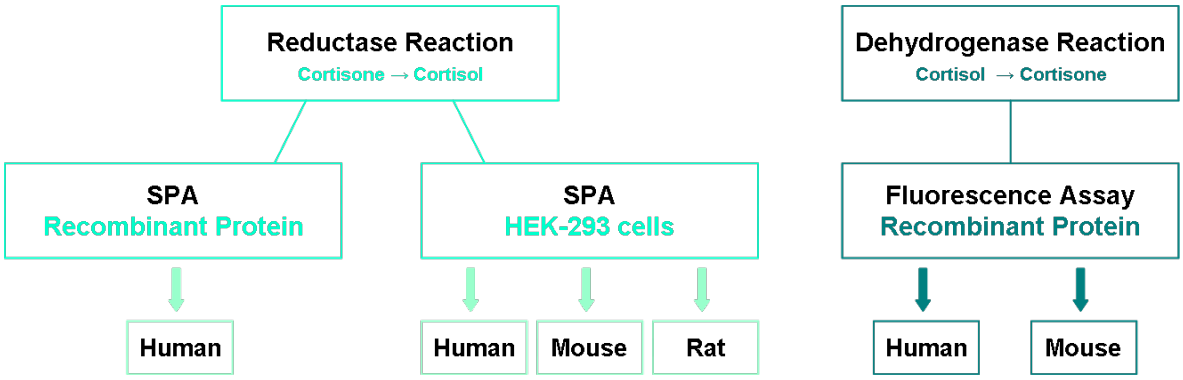

Figure 5.8: Summary of the analyses carried out on potential 11β-HSD1 inhibitors. Analyses carried out on the reductase reaction were: SPA with recombinant protein, and HEK-293 cells overexpressing 11β-HSD1 (the three species investigated are shown in sub-boxes). The fluorescence assay was carried out on the dehydrogenase reaction, with recombinant protein - the species examined shown in the sub-boxes.

5.6.1 Initial Screens of 11β-HSD1 Inhibitors with Recombinant Protein

Initial screens of the 35 compounds were carried out with mouse and human purified recombinant 11β-HSD1 to observe the efficiency of each compound at inhibiting the dehydrogenase reaction. As it was the dehydrogenase activity of 11β-HSD1 being observed, a fluorescence assay was used. Each compound was at a final concentration of 100 μM in 1% DMSO and the screen was carried out in triplicate, in a 96-well plate. Details of the protocol are found in chapter 7 (Materials and Methods). The results are shown in the histograms below (figure 5.9). The percentage inhibition was determined by using equation 5.2, where the high control was a sample well with no inhibitor present (labelled 'control' in figure 5.9) and the low control was a sample well with 100

μM carbenoxolone (labelled 'CBX') present. The mean value of the three wells was taken.

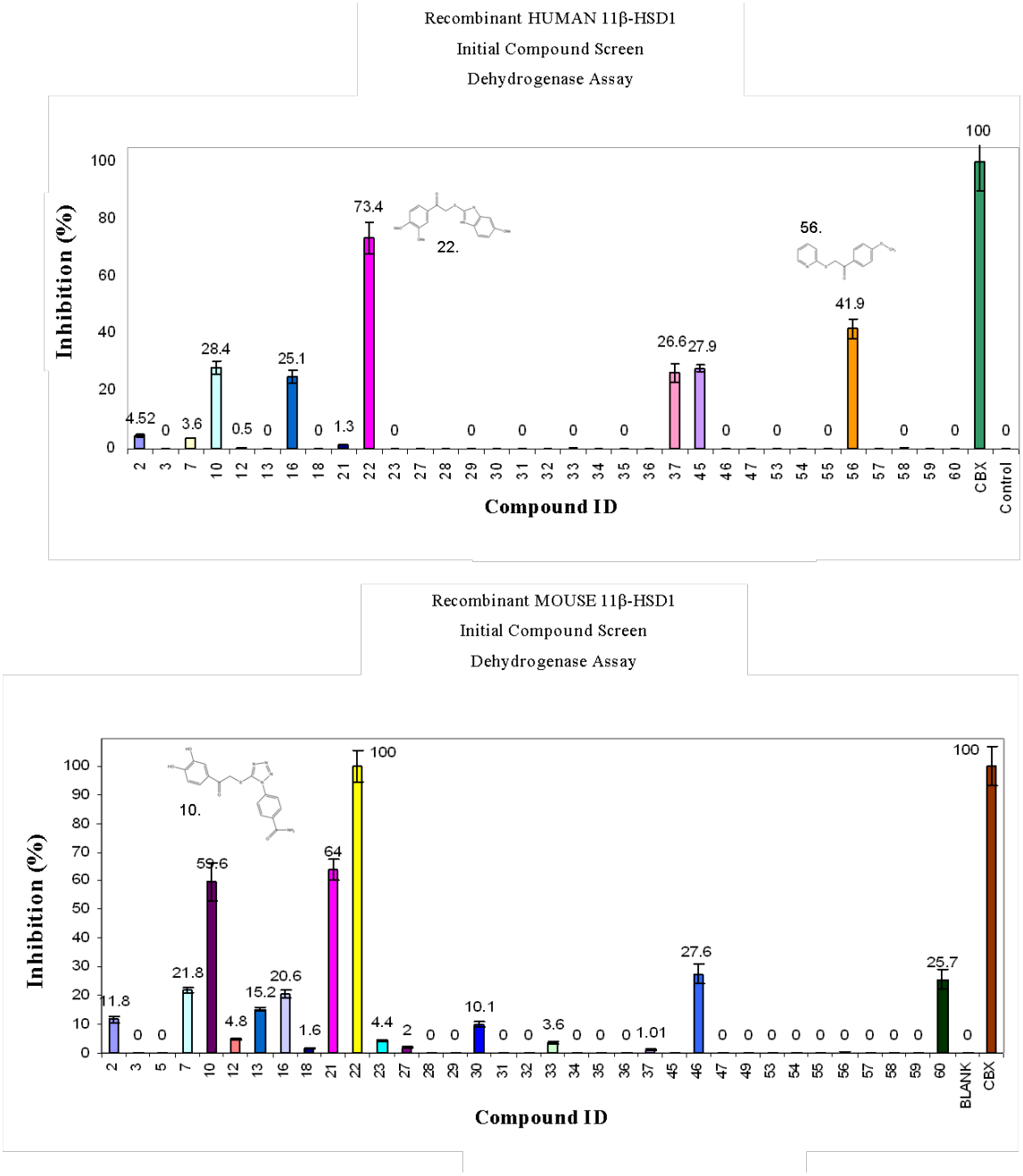

Figure 5.9: Histograms showing the degree of inhibition (%) of each compound tested at 100 μM with recombinant protein. A: Recombinant human 11β-HSD1, B: Recombinant mouse 11β-HSD1. Superimposed onto the charts are chemical structures of three ligands showing a significant inhibition of activity.

Overall, there were 6 compounds which caused a greater than 25 % inhibition in recombinant human 11β-HSD1 assays (10, 16, 22, 37, 45 and 56). With the consideration

of residual carbenoxolone from the protein expression protocol still present in the enzyme, this is a very high hit rate for a small set of selected compounds (14.3 %) with the expected hit rate estimated at 2 - 5%. The mouse enzyme assay also showed 5 compounds which inhibited greater than 25 % of 11β-HSD1 activity, with some overlap of the compounds seen to inhibit the human enzyme. In particular, compound 22 showed greater than 73 % inhibition in human and 100 % inhibition in mouse 11β-HSD1 assays. However, this compound, with a central thioether group and two aromatic structures either side showed a lower percentage inhibition in cell-based assays, as seen in figure 5.9. Promising compounds (those which showed a greater than 25 % inhibition with recombinant 11β-HSD1) in fluorescence assays were analysed further (section 5.6.4).

5.6.2 Initial Screens of 11β-HSD1 Inhibitors with Cell-Based Assays

Cell-based assays are an invaluable pre-determinant of *in vivo* drug properties; namely compound penetration of the cell membrane. Initial screens were also carried out in HEK-293 cells which had been transiently transfected with the mouse, human or rat enzyme. These were carried out as described in chapter 7. The results are shown in figure 5.11. As mentioned, compound 22 (shown in figure 5.10) exhibited a lower percentage inhibition in cells thought to be due to poor penetration of the cell plasma membrane.

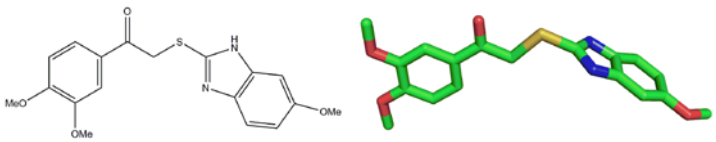

Figure 5.10: Chemical structure of compound 22 (left) in 3-D (right).

Despite its lipophilicity - a prime determinant of the rate of absorption - compound 22 is likely ionized at physiological pH which may be the cause of poor membrane permeability. The partitioning of a drug between water and octanol at a constant temperature; the partition co-efficient (logP) is a useful predictor of membrane transport, and generally the higher the logP then the more easily the compound will be transported across the membrane (Hansch and Clayton 1973). However, this simplistic view is

applicable only to those drugs which do not ionise. The degree of ionisation is also an important determinant for membrane permeability, and so an adjustment for the degree of ionisation of the drug can be made which gives a more accurate description of the drug behaviour. This is known as logD; the dissociation co-efficient (Evans 2004). The logP for compound 22 is 4.03, however by virtue of having polarisable groups (6 hydrogen bond acceptor groups and 1 hydrogen donor) it is potentially this that is preventing efficient membrane crossing.

For reductase assays in transfected HEK-293 cells, each compound was tested in duplicate. The wells containing no inhibitor (labelled 'control' in figure 5.11) were used as the high controls and wells containing 100 μM carbenoxolone ('CBX') were the low controls.

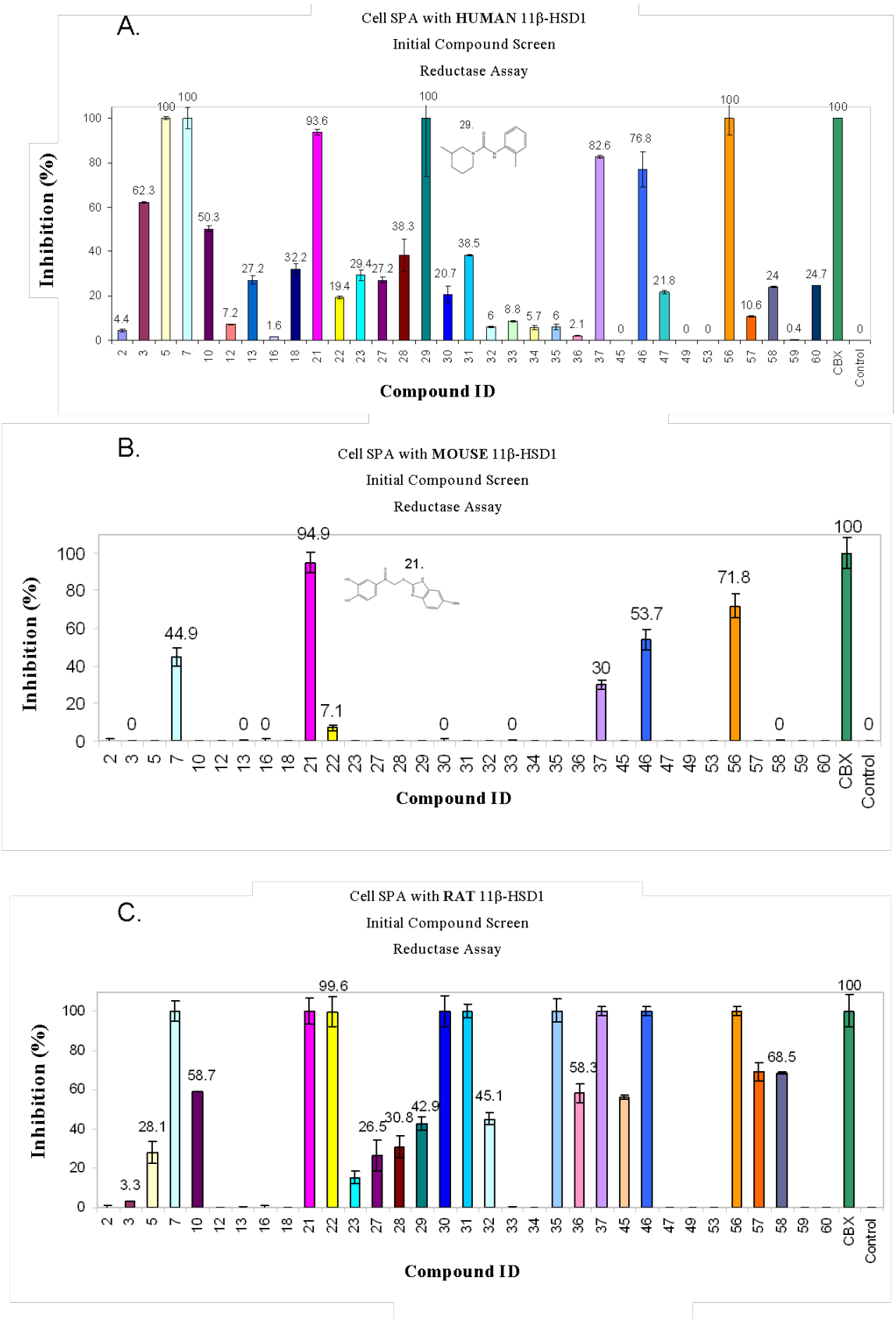

Figure 5.11: Bar charts showing the percentage inhibition effectuated by each compound at 100 μM in transfected HEK-293 cells in the reductase reaction. (A) Cells expressing with human 11β-HSD1 (B) Cells expressing with mouse 11β-HSD1 (C) Cells expressing rat 11β-HSD1.

As can be seen from figure 5.11, there are 5 compounds which cause greater than 30 % inhibition in all three species. These are compounds 7, 21, 37, 46 and 56, and were taken for further testing. Surprisingly, fewer compounds caused significant inhibition of the mouse enzyme in comparison to the rat and human assays, which is thought to be due to experimental difficulties with cell confluence.

Compounds exhibiting greater than 40 % enzyme inhibition in human 11β-HSD1 cell-based SPA underwent further analysis to quantify inhibition and determine IC_{50} and K_i values. These compounds are shown in table 5.1 (section 5.6.5).

Of particular interest are the compounds which showed inhibition and are structurally similar yet differ enough to allow an initial structure-activity analysis. For example: compounds 7 and 10, or compounds 28 and 29. Compounds 7 and 10 differ solely by the substituents off one of the benzene rings. These compounds are shown in figure 5.12.

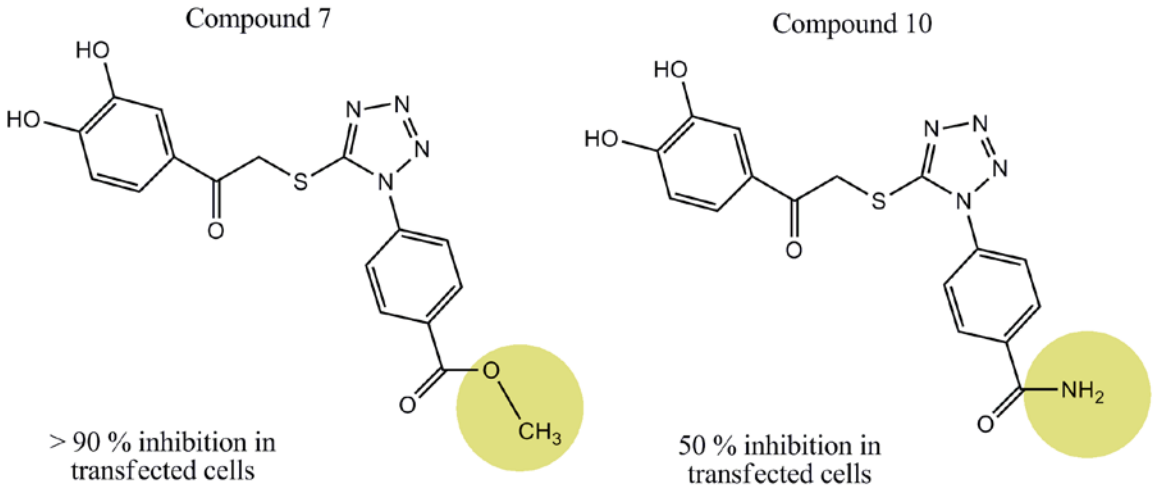

Figure 5.12: Chemical structure of compounds 7 and 10, with the varying substituents highlighted with a yellow circle. Image prepared with ChemDraw.

As can be seen in figure 5.12, compound 7 has a methoxy- substituent, 10 has a benzamide. This increases the hydrogen bond donors by a factor of 2 (from 2 to 4) and concurrently reduces the potency. This may suggest a preference for a lower number of HBD at this deeply buried end of the molecule (docking positions, figure 5.25) which would potentially interact with the co-factor. The non-aromatic substituents of the carboxamide compounds 28 and 29 differ as a piperidine and a 7-membered nitrogen-containing ring, also decreasing potency, shown in figure 5.13.

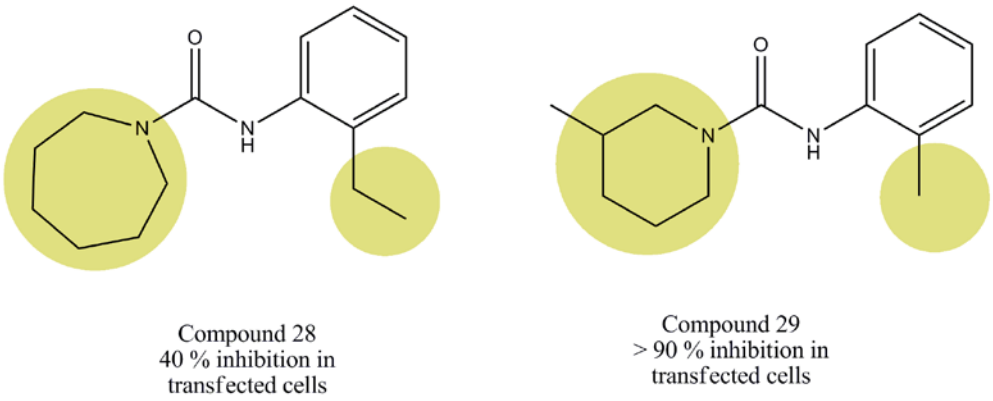

Figure 5.13: Chemical structure of compounds 28 and 29, the varying substituents are highlighted with a yellow circle. Images prepared with ChemDraw.

The presence of a 7-membered ring and an ethyl substituent from the benzene ring decreases the potency in transfected HEK-293 cells. Whether this is due to spatial restrictions or other factors is inconclusive.

5.6.3 A Comparison: Inhibitor Binding in Transfected Cells and Recombinant Protein

Overall the cell-based assays are a more accurate reflection of inhibitor binding, as they have not been in contact with the tight binding inhibitor carbenoxolone at any point prior to the assays, in contrast to the recombinant material. This may explain the occurrence of higher inhibition for the same compound in assays using recombinant protein compared to cell-based assays, for example, in mouse 11β-HSD1: compounds 7, 21 and 46 exhibit a higher percentage inhibition in cells than with recombinant material. With human 11β-HSD1, these are compounds 2, 7, 10, 37, and 56. In addition to effects related to carbenoxolone, the compounds may have a higher affinity for an enzyme-NADPH complex (an enzyme ready to reduce cortisone) as opposed to an enzyme-NADP+ complex (as an enzyme ready to oxidise cortisol), i.e. one reaction direction over another (Sahni-Arya et al 2007) or alternatively there may be non-specific binding events occurring accounted for by the differing complexities of each system.

5.6.4 Dose-Response Curves: Further Analysis of Inhibitor Binding

Dose-response plots have the form of a Langmuir isotherm and are frequently used to follow the effects of an inhibitor on the initial velocity of an enzymatic reaction at fixed substrate concentration. These were employed to analyse experimental data of compounds demonstrating sufficient inhibition in the initial screens and to determine an IC_{50}. Overall, the initial screens with human 11β-HSD1 produced 5 compounds which inhibited greater than 25 % of recombinant protein activity monitored by a fluorescence assay, and 10 compounds which showed greater than 40 % inhibition enzyme activity as determined by SPA. A lower criterion of percentage inhibition is set for recombinant protein in view of the presence of carbenoxolone. There is overlap between the compounds identified by the two screening methods. They are discussed and compared later in this text.

The following results section is divided into: assays carried out using SPA (section 5.6.5) which monitored the reductase reaction (figure 5.2), or fluorescence assays (section 5.6.6) which monitored the dehydrogenase reaction (figure 5.3).

5.6.5 Further Analysis: Inhibition Assays with SPA

The ten compounds exhibiting greater than 40 % inhibition are shown in table 5.1.

Table 5.1 (following page): Compounds which showed greater than 40 % inhibition in reductase assays with human 11β-HSD1 and similar inhibition in recombinant human 11β-HSD1 assays. The fluorescence assays are less sensitive to inhibition due to the partial presence of carbenoxolone in the enzyme binding site, reflected in lower inhibition by the same compounds in this assay. It is also due to differences in the assays and reaction directions.

Structure	Compound ID	**SPA** % inhibition (reductase reaction)	**Fluorescence** % inhibition (dehydrogenase reaction)
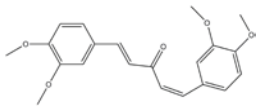	3	62.3 %	1 - 2 %
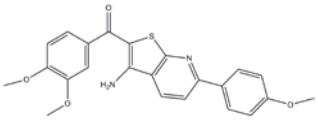	5	> 90 %	0
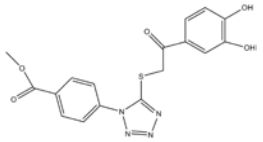	7	> 90 %	3.6 %
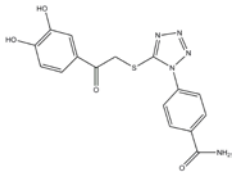	10	50.3 %	28.4 %
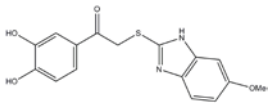	21	93.6 %	1 - 2 %
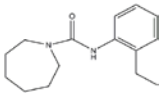	28	40 %	1 - 2 %
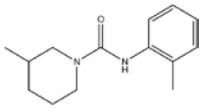	29	>90 %	1 - 2 %
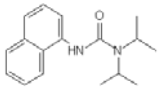	37	82.6 %	26.6 %
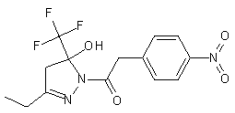	46	76.8 %	1 - 2 %
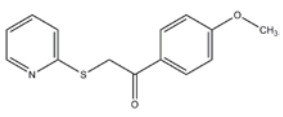	56	> 90 %	41.9 %

Further analysis carried out on these ten compounds employed SPA. Wells were set up in triplicate with 8 inhibitor concentration points per compound, spanning 3.5 orders of magnitude. Further details are found in Chapter 7 – Materials and Methods.

A high control (no inhibitor, 100% activity) and low control (no enzyme, 0% activity) were present on each 96-well plate, which gave values for the top and bottom asymptotes, respectively, in the log dose-response plot. The Log dose-response plot was the sigmoidal plot of enzyme activity (in counts per minute) versus log[I] (nM). Without the 0% and 100% controls, the data obtained is useless therefore appropriate controls were always used. From these plots, an IC_{50} is obtained and application of the Cheng-Prussoff equation (equation 5.6) gives values for the K_i. As the K_i cannot be directly calculated from SPA, a dose-response curve is plotted to calculate the IC_{50}, with subsequent calculation of the K_i.

Figure 5.14 shows the results of human 11β-HSD1 cell-based SPA inhibition assays, with calculated K_i values in table 5.2. In addition to transfected cells, recombinant human protein was used with SPA, with the results shown in figure 5.15, to complement the data from cells overexpressing 11β-HSD1 of the same species.

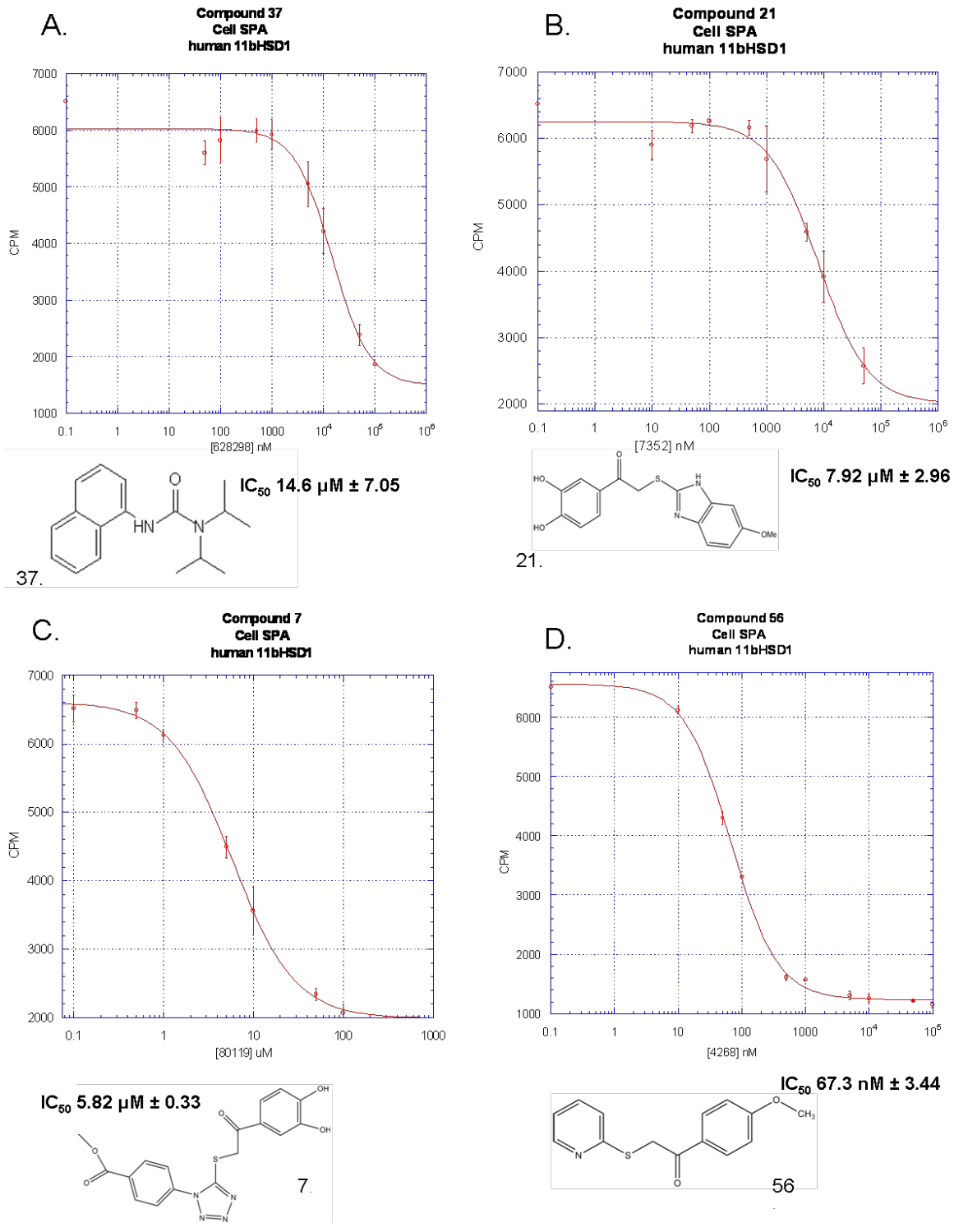

Figure 5.14: continued overleaf.

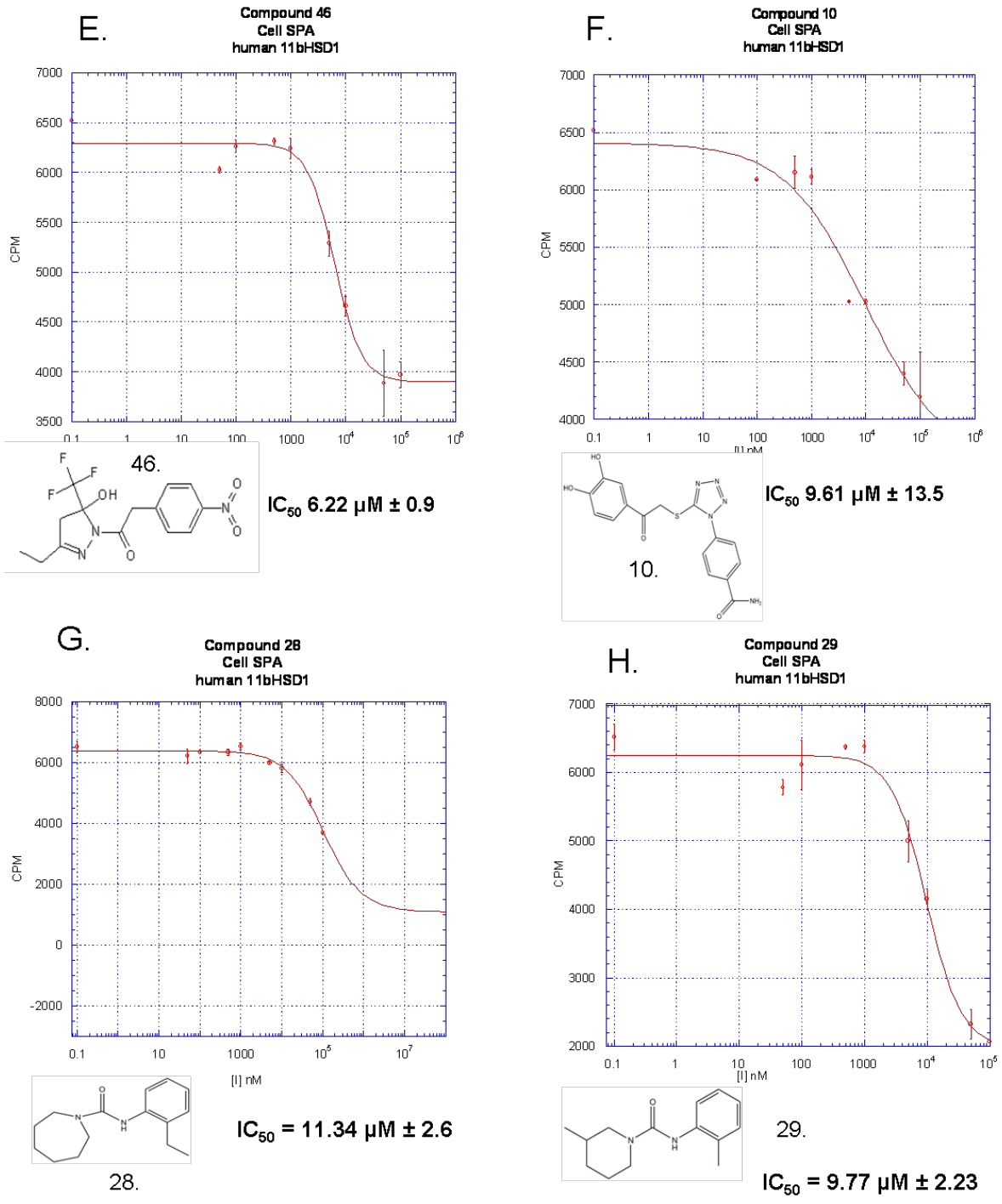

Figure 5.14: continued overleaf.

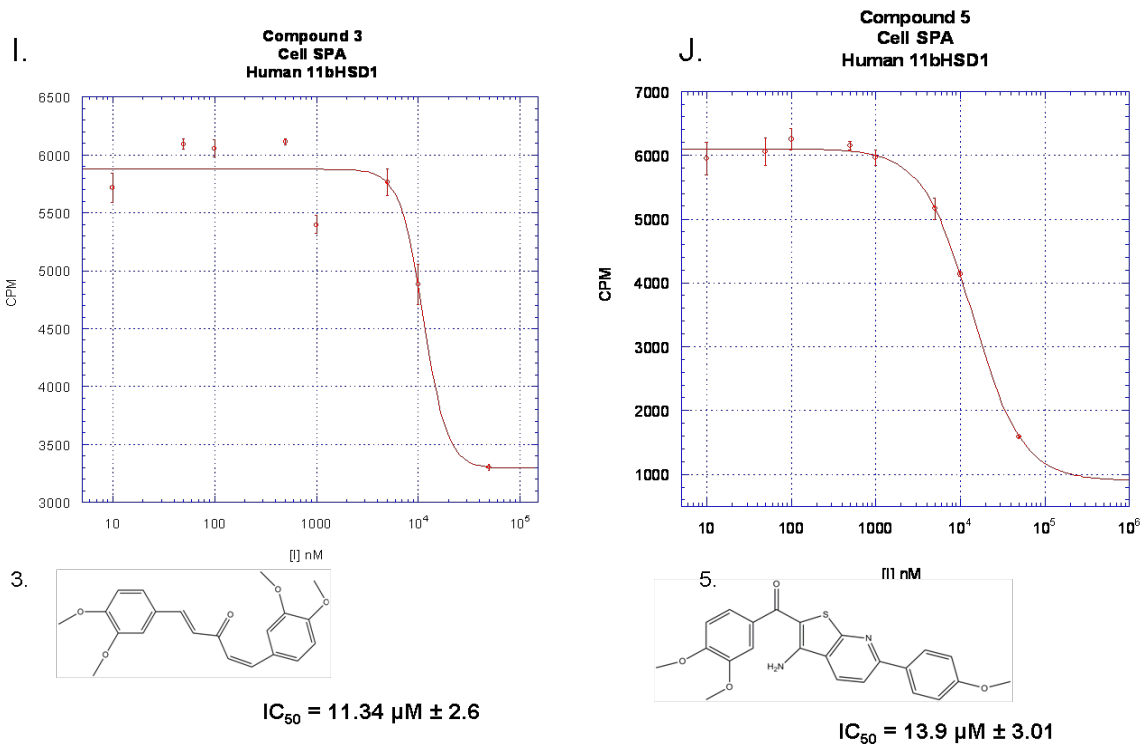

Figure 5.14: Plots of cpm versus Log(inhibitor concentration) or Log[I] (nM) for human 11β-HSD1 transfected cells. The ordinate has units of cpm (counts per minute) which is the signal detected from the scintillation counter. For each compound, a dose-response plot, the chemical structure and the IC_{50} is shown. These are; (A) compound 37, (B) compound 31, (C) compound 7, (D) compound 56, (E) compound 46, (F) compound 10, (G) compound 28, (H) compound 29, (I) compound 3, (J) compound 5. Standard deviation shown calculated using the 'n-1' method where n=2. Graphs prepared using Kaleidagraph version 4 software from Synergy Software.

As may be observed in figure 5.14, the top plateau corresponds to the value of radioactive substrate binding in the absence of competing drug (total binding). The bottom plateau is more difficult to obtain experimentally due to solubility restrictions of the compounds analysed – high concentrations of inhibitors were not always possible in addition to a minimum 1 % DMSO final volume restriction. This is why a 'no-enzyme' control is used as the low control.

It may be seen that for all ten compounds tested in cell SPA, the majority have low micromolar IC_{50} values and K_i values, with the exception of compound 28 (IC_{50} 102.7 µM) and compound 56 (IC_{50} 67.1 nM). These were converted to K_i values (table 5.2) and

compared to the K_i values determined for the same compounds with recombinant protein with SPA (table 5.2).

In several cases the data were difficult to fit to a sigmoidal dose-response curve due to high error (e.g. compound 10 in cell based assays) and many showed no inhibition with the recombinant protein; these included compounds 3, 21, 28, 29, 37 and 46. As an example of this, compound 5 has been shown in figure 5.9D. The data fit to a dose-response curve however the error on the IC_{50} is almost the same as the IC_{50} itself (table 5.2). This is due to the presence of remaining carbenoxolone in the protein preparation, which acts to disguise any low-level inhibition exhibited by the new compounds. Those that were not affected were plotted, and are shown in figure 5.15A, B and C.

Table 5.2: A summary of results from cell SPA of the ten compounds seen in table 5.1. Equation 5.6 is applied to the IC_{50} values above, taking [cortisol] = 100 nM and K_m= 340 nM (Frick et al 2004).

Compound ID	IC_{50} cell SPA (figure 5.6)	Calculated K_i cell SPA	Calculated K_i recombinant SPA (figure 5.7)
3	11.34 ± 2.6 µM	8.7 µM	N/A
5	13.9 ± 3.01 µM	10.7 µM	109.5 nM ± 95.6
7	5.82 ± 0.33 µM	4.5 µM	68.9 µM ± 25
10	9.61 ± 13.5 µM	7.4 µM	174.9 µM ± 29.9
21	7.92 ± 2.96 µM	6.1 µM	N/A
28	102.7 ± 11.7 µM	79.3 µM	N/A
29	9.77 ± 2.23 µM	7.5 µM	N/A
37	14.6 ± 7.05 µM	11.3 µM	N/A
46	6.22 ± 0.93 µM	4.8 µM	N/A
56	67.1 ± 3.35 nM	51.8 nM	853.4 nM ± 53.5

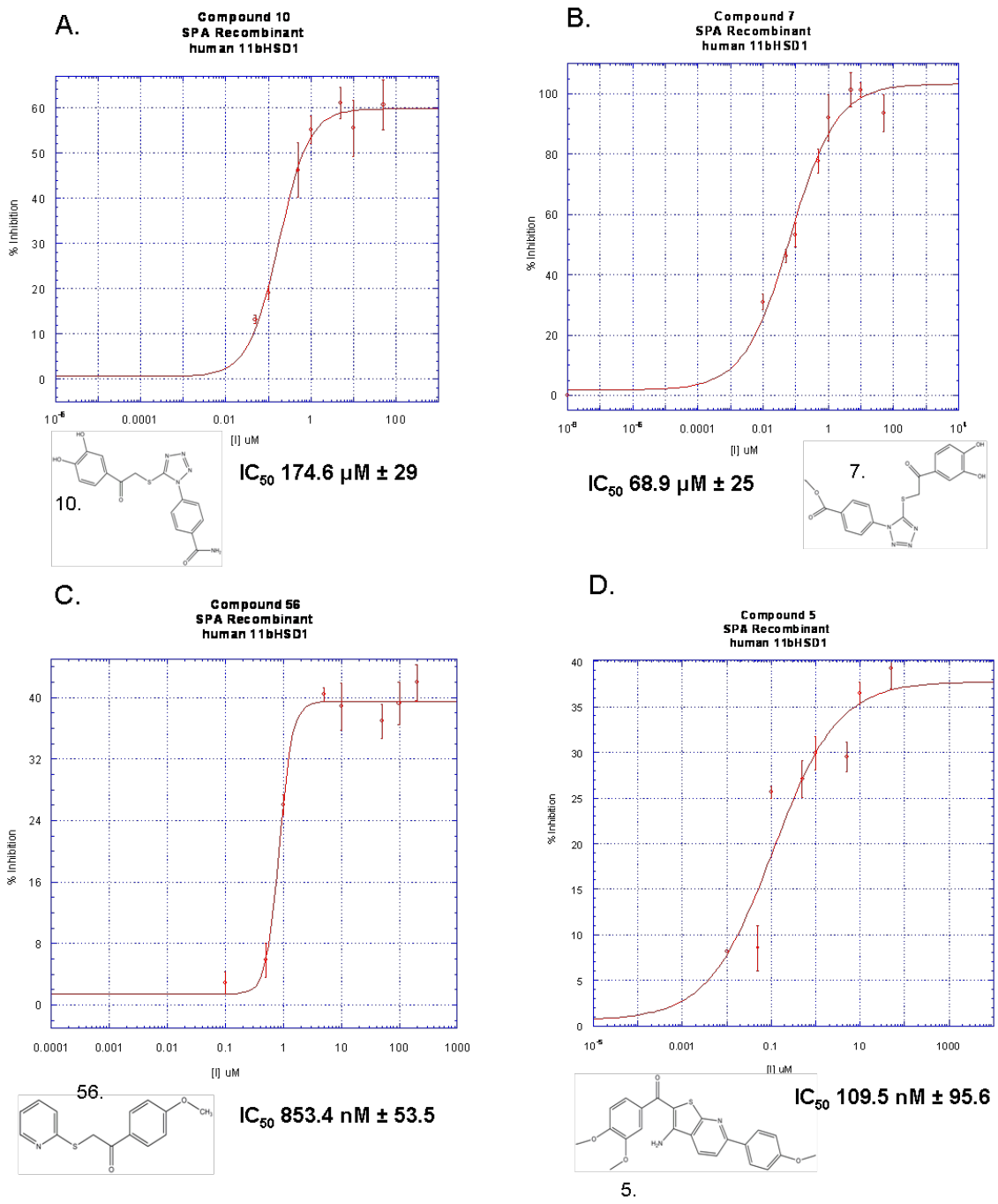

Figure 5.15: Recombinant human 11β-HSD1 dose-response curves for four compounds from the top ten of the initial human screen analysed with SPA. Six of the compounds showed data with high error which did not fit to a sigmoidal dose-response. (A) compound 10, (B) compound 7, (C) compound 56, (D) compound 5 – an example of a 'bad' fit.

5.6.6 Further Analysis: Fluorescence Inhibition Assays with Recombinant 11β-HSD1

In addition to SPA analysis of inhibitor potency on the reductase direction, fluorescence assays were carried out observing inhibitor effects on the dehydrogenase reaction with recombinant protein. The compounds analysed were those exhibiting greater than 25 % inhibition in initial screens with recombinant enzyme. These are shown in table 5.3. In addition, ligands exhibiting more than 40 % inhibition of enzyme activity in cell-based assays were analysed with fluorescence. These were compounds 3, 5, 7, 21, 28, 29 and 46 (shown in table 5.1).

Table 5.3: The six compounds which showed greater than 25 % inhibition in dehydrogenase assays with recombinant human 11β-HSD1, and the corresponding inhibition in cell-based human 11β-HSD1 assays. Variations observed between the two right-most columns (between the two assays) are due to differences in method, protein quality and reaction direction.

Structure	Compound ID	Fluorescence % inhibition (dehydrogenase reaction)	SPA % inhibition (reductase reaction)
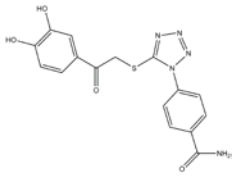	10	50.3 %	28.4 %
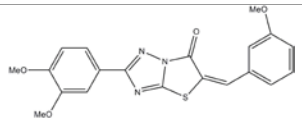	16	25.1 %	1.6 %
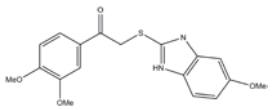	22	73.4 %	19.4 %
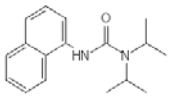	37	82.6 %	26.6 %
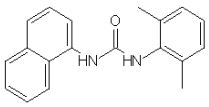	45	27.9 %	-
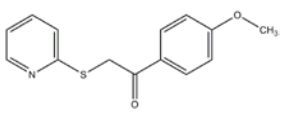	56	> 90 %	41.9 %

Three of the compounds shown in table 5.3 overlap with the group of compounds found to effectively inhibit activity in cell-based assays with 11β-HSD1. These are compounds 10, 37 and 56. Methods are detailed in chapter 7. The data were analysed as described in section 5.4, the results are shown in figure 5.16.

Despite a promising level of inhibition in the initial screen, compound 45 - which did not inhibit 11β-HSD1 in cell-based assays at all - was found to show little inhibition in further fluorescence screens and is not shown here. Similar performances were observed for compounds 5, 7, 28, 29 and 46; gaving K_i values of 10.7 μM, 4.5 μM, 79.3 μM, 7.5 μM and 4.8 μM respectively, in the cell-based assay. Compound 22 displayed a noisy spectrum, and data were not analysable. Results are summarised in table 5.4, plots in figure 5.16.

Table 5.4: A summary of results from fluorescence assays with recombinant protein, assaying inhibition of 11β-HSD1 in the dehydrogenase direction. The six potent compounds are shown here with the calculated K_i^{app} values.

Compound ID	K_i^{app} (**Fluorescence Assay**, recombinant 11β-HSD1)	Calculated K_i (**Fluorescence Assay**, recombinant 11β-HSD1)	Calculated K_i (cell **SPA)**
3	141.53 ± 66.1 μM	2.36 μM	8.7 μM
10	46.8 ± 12.7 μM	0.78 μM	7.4 μM
16	27.35 ± 2.5 μM	0.45 μM	-
21	247.7 ± 72.5 μM	4.14 μM	6.1 μM
37	234.2 ± 27.6 μM	3.91 μM	11.3 μM
56	26.1 ± 6.5 μM	0.43 μM	51.8 nM

Of the twelve compounds which were assessed for 11β-HSD1 inhibition with this assay; 6 were impotent and 6 were potent. Out of the 6 potent inhibitors, 5 were also effective at inhibiting 11β-HSD1 activity in HEK-293 cells.

A potential challenge faced during fluorescence assays is the possible interfering effects of the compounds on the assay. The majority of the compounds analysed contain at least one aromatic component, which means that they may interfere with the fluorescence assay by excitation and emission at the same wavelengths. Alternatively the compound may exert an inner filter effect on light emitted by NADPH, absorbing the light before it can be detected by the fluorometer. In addition, quenching of fluorescence at 340 nm by the compounds is a possibility (Albinsson et al 1994). To detect possible effects of each compound, background controls were consistently carried out. For example, compound 22 showed high background fluorescence in the presence of NADP. In the absence of co-factor and enzyme, a much reduced signal is detected. A full visible light emission spectrum for the compound (excited at 340 nm) carried out in assay buffer only showed emission at 680 nm, outside the detection range of the assay. Thus, there is potentially an interaction between NADP and compound 22 which results in a high level of emitted light at 458 nm.

A.

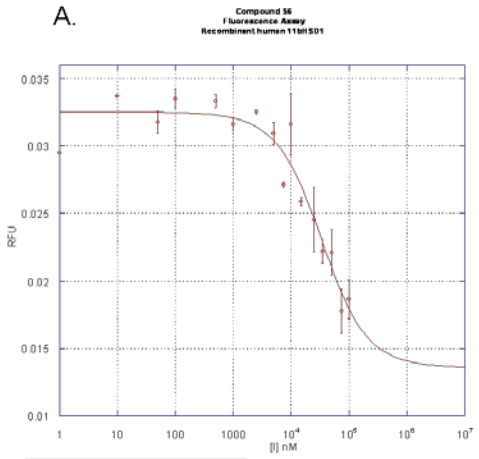

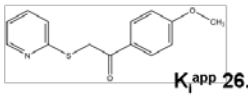

56.

K_i^{app} 26.1 µM ± 6.5

B.

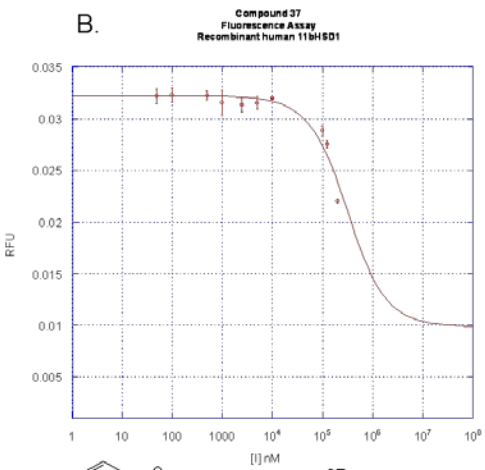

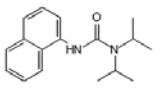

37.

K_i^{app} 234.2 µM ± 27.6

C.

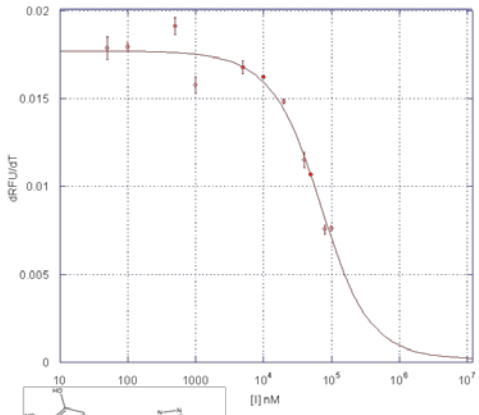

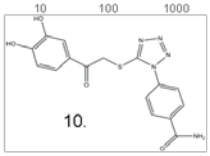

10.

K_i^{app} 46.8 µM ± 12.7

D.

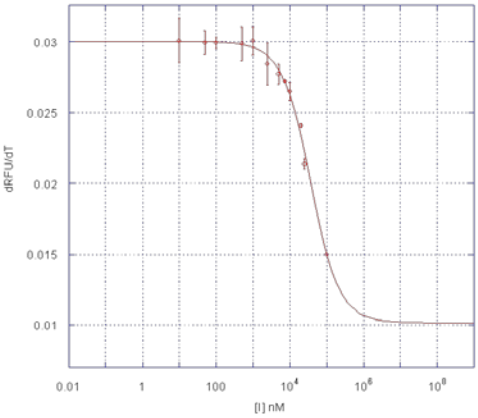

K_i^{app} 27.35 µM ± 2.5

16.

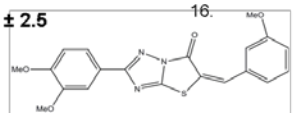

E.

Compound 3
Fluorescence Assay
Recombinant human 11bHSD1

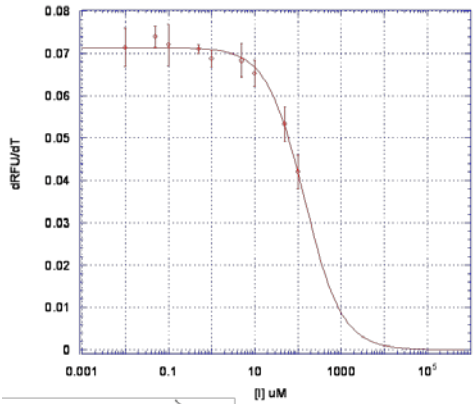

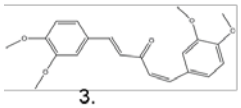

3.

K_i^{app} 141.53 µM ± 66.1

F.

Compound 21
Fluorescence Assay
Recombinant human 11bHSD1

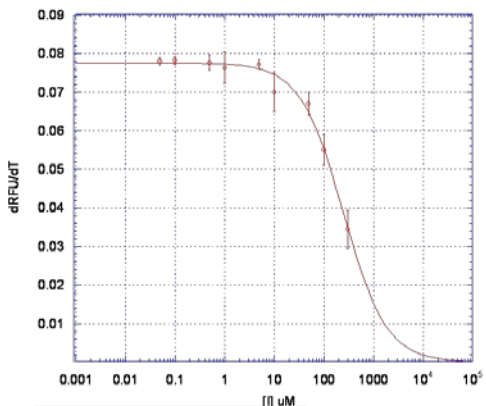

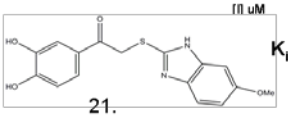

21.

K_i^{app} 247.4 µM ± 72.5

Figure 5.16: Recombinant human dose response plots for the top ten compounds assayed with fluorescence, monitoring inhibition of the dehydrogenase reaction. The most potent compound, 56, is shown in A. This compound also potently inhibited 11β-HSD1 in cell-based assays (K_i 51.8 nM). B: compound 37; C: compound 10; D: compound 16; E: compound 3; F: compound 21.

Differences in the K_i values calculated between the two screening methods are due to the presence of carbenoxolone in the recombinant protein, and potentially the affinity of the compound for a particular conformation of the enzyme. In this respect, the recombinant enzyme can only be used to calculate approximate values in inhibition assays and will almost always give an apparently higher K_i value than the true value.

The most potent compound in both assays is compound 56. This compound has a simple thioether scaffold, with a piperidine ring on one side and benzene with a methoxy substituent opposite. Compound 16 inhibits recombinant 11β-HSD1 with a very low micromolar K_i, however, it does not appear to inhibit 11β-HSD1 in cell-based assays, indicating membrane permeability difficulties. For this reason, the compound was not included in the top 5 compounds for inhibiting 11β-HSD1 in this research.

The five compounds: 3, 10, 21, 37 and 56 are the most potent inhibitors of human 11β-HSD1 from the pool of 35 ligands assayed. All have K_i values in the low micromolar range, with compound 56 having a nanomolar K_i. These are shown in figure 5.29.

The most potent compounds were subsequently docked into the enzyme active site using LIDAEUS to predict ligand-enzyme interactions (section 5.8). Simultaneously, crystallisation trials were carried out in an effort to co-crystallise a ligand-enzyme complex (chapter 6).

5.6.7 Structure – Activity Relationships in the Inhibition of Human 11β-HSD1

It is apparent from this research that a broad structural range of compounds can inhibit 11β-HSD1 activity. An initial structure–activity analysis of the compounds tested in this research reveals some of the structural features which facilitate inhibitor binding and potency. As a general rule of thumb, 11β-HSD1 inhibitors have a central HBA group (typically containing oxygen) flanked on either side by lipophilic groups which interact hydrophobically in the enzyme active site (Webster and Pallin 2007). To a great extent, this molecular arrangement is observed with the hit compounds in this research. A SAR analysis of compounds 2 and 3 suggest that although a central HBA is essential, what it is attached to is also a point of importance – the presence of a central phenol as opposed to an aliphatic carbon chain ketone disrupts potency completely (figure 5.7). In addition, certain HBD groups at one or both ends of the molecule can enhance potency, as exemplified well by compounds 21 and 22 (figure 5.17, the dark blue region shows the shared region of similarity).

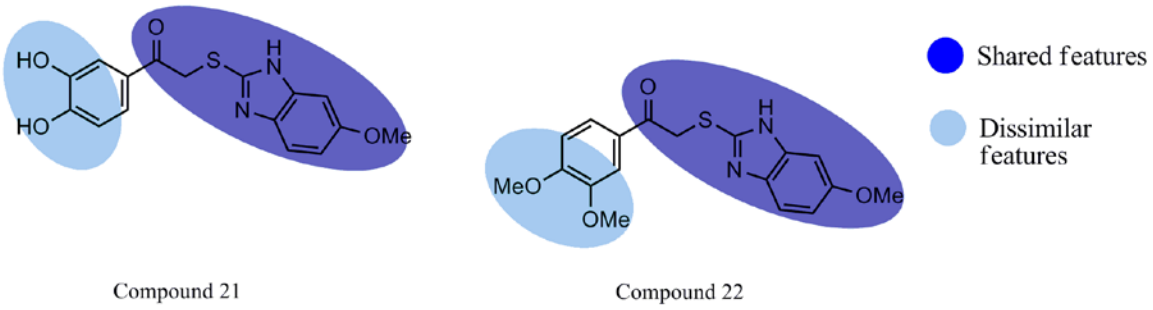

Figure 5.17: Structure of compounds 21 (K_i 6.1 µM) and 22 (no inhibition). Dark blue regions show the similar structural features, pale blue show the dissimilar regions.

The only structural difference between these two compounds is the presence of 2 HBA groups in compound 22, which are replaced with 2 HBD groups in compound 21. Compound 22 does not inhibit 11β-HSD1; however compound 21 has a K_i of 6.1 µM (data from transfected HEK-293 cells). Complete removal of all HBA and HBD substituents at either end of the molecule ablates potency, as observed with compounds 21 and 57 (figure 5.18, the yellow regions depict similarity, pink depict differences).

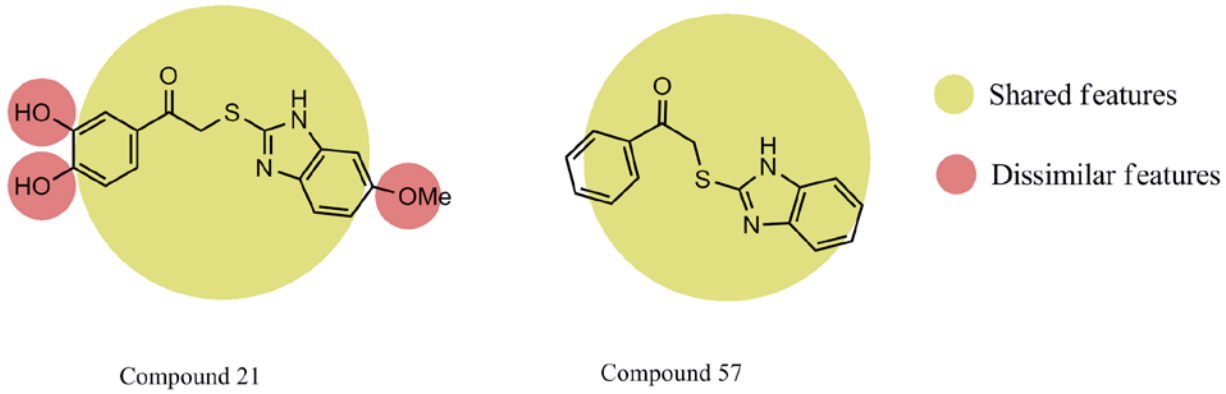

Compound 21 Compound 57

Figure 5.18: Structure of compounds 21 (K_i 6.1 µM) and 57 (10% inhibition of activity in initial screens). Yellow regions are the similar structural features; pink regions are where the compounds differ.

Replacement of substituents capable of forming hydrogen bond interactions (i.e. groups highlighted in pink in figure 5.18) with aromatic ring structures does not improve potency (e.g. compound 54, figure 5.7). Of additional interest is the effect of added methyl substituents on compounds; these substituents simply add volume to a ligand but do not form interactions within the active site therefore it is surprising that they create such a significant increase in potency. This is shown with compounds 27 and 29 (figure 5.19). Compound 27 shows a small amount of inhibition in initial screens; compound 29 has a K_i of 7.5 µM.

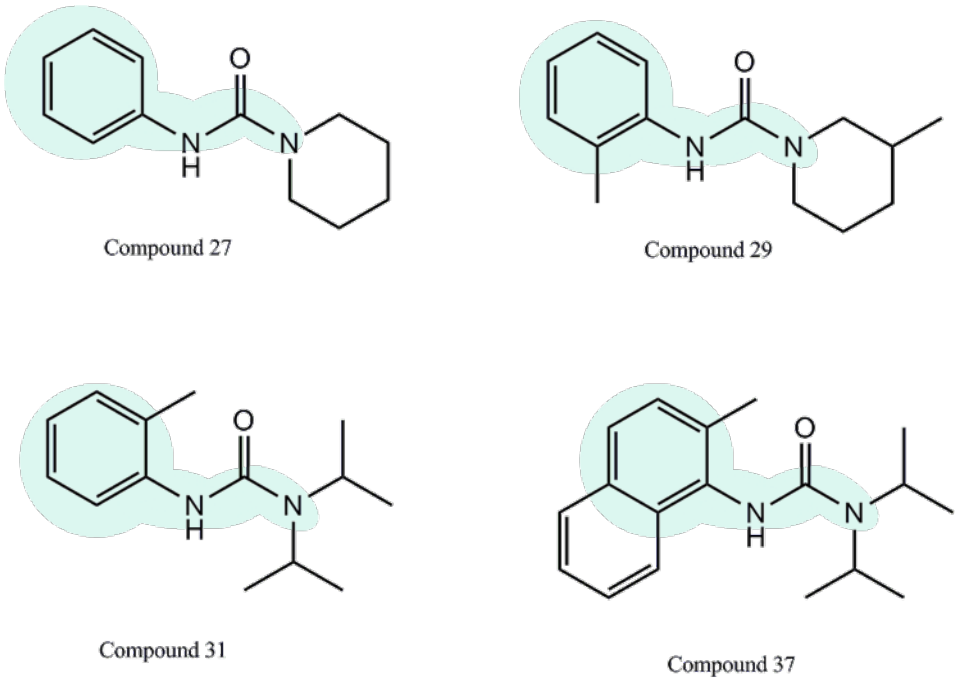

Figure 5.19: Structure of compounds 27 (little inhibition) and 29 (K_i 7.5 µM). The presence of two methyl groups significantly affects the potency.

Interestingly, removal of the non-aromatic ring from compound 29 disrupts inhibitory activity even with the addition of varying substituents from the aromatic ring (as seen in compounds 31 (pictured, figure 5.19), 32, 33, 34, 35 and 37 (pictured figure 5.19) none of which displayed inhibition of 11β-HSD1).

5.7 Species Differences between Mouse and Human 11β-HSD1 Inhibitor Binding

An excellent example in previously published research of the distinct effects of one compound on 11β-HSD1 from many species is from Arampatzis et al. A selected compound: T0504 (Figure 5.20, Enamine Ltd) which was previously described by Merck (patent WO 03/065983) displayed approximately 100-fold selectivity for the inhibition of human 11β-HSD1 (K_i 15 nM) compared with human 11β-HSD type 2 (K_i 2 μM).

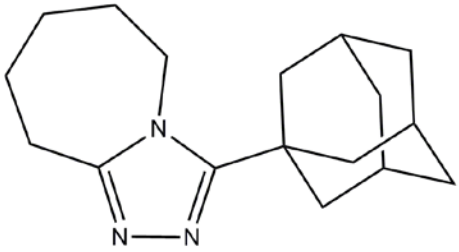

Figure 5.20: Chemical structure of T0504 (Enamine) which was found to be 67 times more potent in human 11β-HSD1 enzyme than mouse enzyme (expressed in HEK-293 cells).

In addition, T0504 effectively inhibited all species enzymes analysed; however there appeared to be significant differences between potency: a 67-fold difference between human and mouse (Arampatzis et al 2005). This provided the first evidence that subtle differences in the molecular structures of both active site and inhibitor may have a big impact on ligand affinity and potency, respectively.

Initial screens with mouse recombinant and *in vivo* 11β-HSD1 (in HEK-293 cells) showed that there were eight compounds which displayed greater than 25 % inhibition. These were compounds 7, 10, 21, 22, 37, 46, 56 and 60. Four of these compounds are in the top five from human screens (10, 21, 37, and 56). Further analysis was carried out with the top 8 hits from the mouse screens, which were assayed using the fluorescence technique with recombinant mouse enzyme. As carbenoxolone is added to the mouse expression cultures, the values determined from these assays are again approximate figures.

Compounds 21, 22 and 60 were the only compounds which displayed sufficient inhibition of mouse 11β-HSD1 to allow dose-response plots and the subsequent calculation of a K_i^{app}. These are shown in figure 5.21. Interestingly, none of these compounds showed great affinity for the human enzyme. Furthermore, compound 56 - the most potent human 11β-HSD1 inhibitor - showed mild inhibition of mouse 11β-

HSD1, with a predicted K_i^{app} of approximately 500 μM which is a 10,000 fold decrease in potency, compared to ~50 nM in cells with human 11β-HSD1.

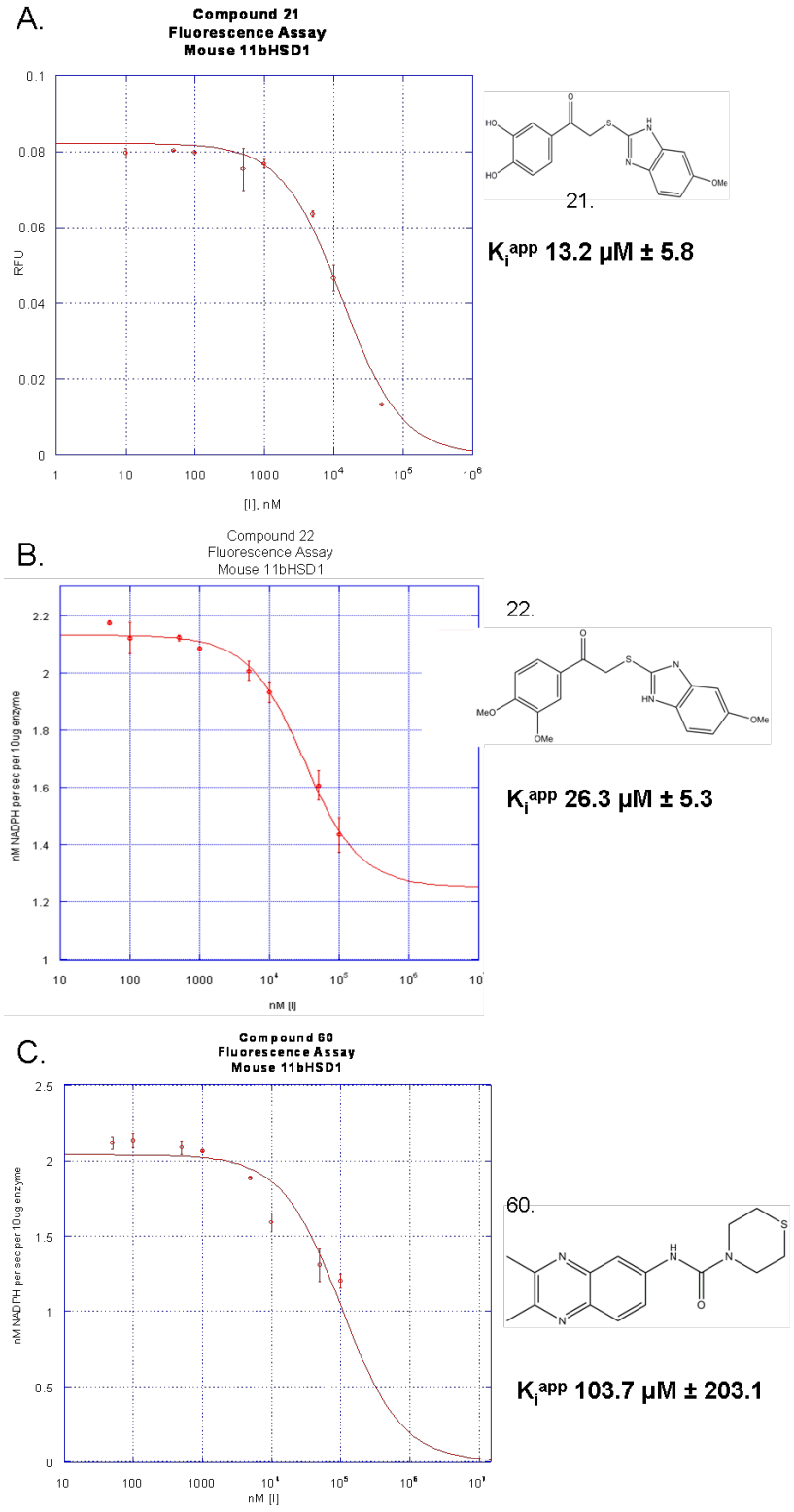

Figure 5.21: Dose-response plots of mouse 11β-HSD1 inhibition assays. A: compound 21, B: compound 22, C: compound 60.

5.7.1 Structure – Activity Relationships in the Inhibition of Mouse 11β-HSD1

As can be seen from figure 5.22, compounds 21 and 22 inhibit mouse 11β-HSD1 with a low micromolar range K_i. The compounds differ by the dihydroxyphenyl (21) / dimethoxyphenyl ring (22) and the substituent positions on this ring, as shown in figure 5.14 and highlighted in yellow.

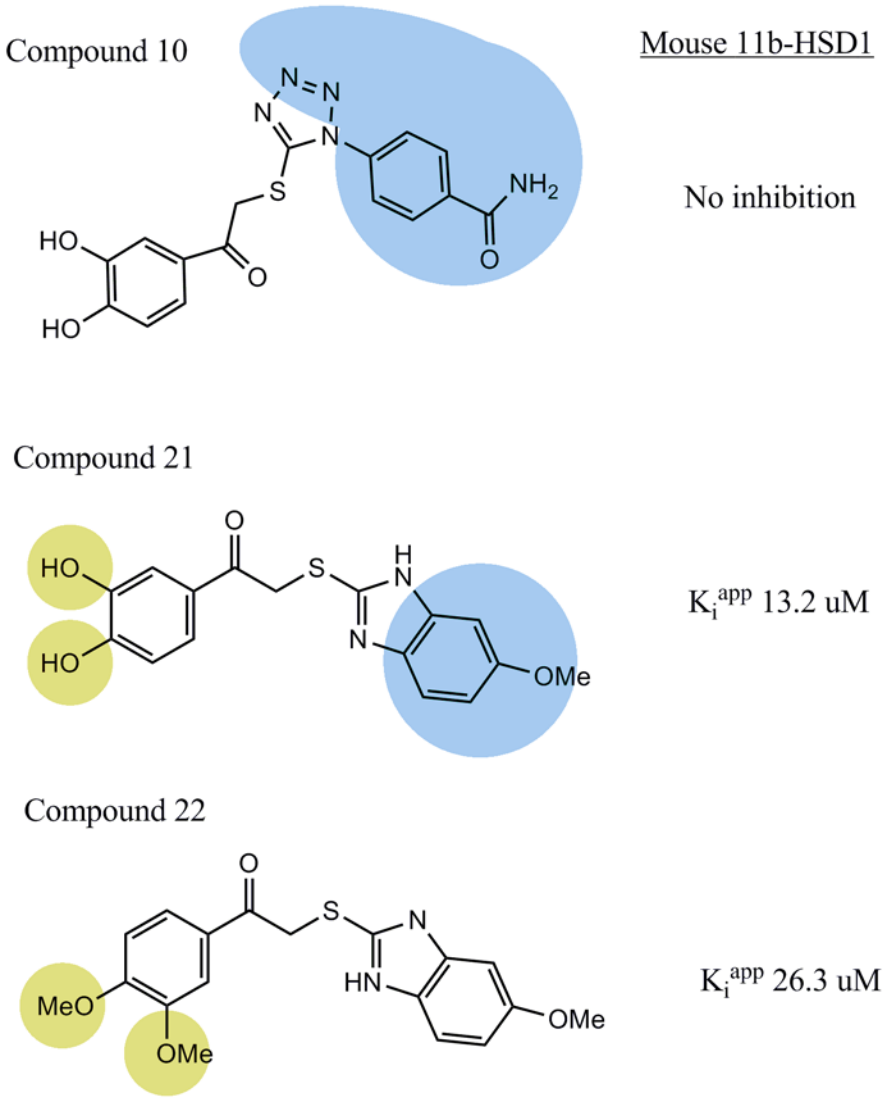

Figure 5.22: Chemical structures of compounds 10, 21 and 22. The latter two inhibit mouse 11β-HSD1. Differences in structures are highlighted with a yellow or blue circle.

With regards to compounds 21 and 22, an exchange of two hydroxyl substituents for two methoxy substituents (yellow circles, figure 5.22) results in a 2-fold drop in mouse enzyme potency due to the loss of two hydrogen donor groups. Docking studies (figure 5.25) show that these substituents would most likely be at the mouth of the active site potentially forming hydrogen bonds with Gln 177 (which is Tyr 177 in humans), Leu 171

or the backbone of Ala 172. The benzimidazole moiety would be buried deep within the pocket. Compound 10 differs from compound 21 (shown with blue circles, figure 5.22) and is a V-shape (due to the tetrazole ring substitutions) rather than linear. This results in a complete loss of inhibition of mouse 11β-HSD1. As can be seen in figure 5.25 and 5.26 (docking figures), the V-shape of compound 10 means that it sits differently in the active site as compared to compound 21, with important HBD groups buried deeper within the pocket, as opposed to being nearer the mouth of the pocket as seen in compound 21. This has a knock-on effect with regards to potency. As seen with human 11β-HSD1, the presence of HBD groups near the entrance of the active site improves potency.

5.8 Docking of New 11β-HSD1 Inhibitors

As the search for novel 11β-HSD1 inhibitors ensues, there is ever-more published research into the potential docking of these compounds in the absence of a co-crystal structure (Lee et al 2008; Miguet et al 2006; Schuster et al 2006; Vicker et al 2007; Yang et al 2009; Yang et al 2008).

The program LIDAEUS (LIgand Discovery at Edinburgh University) was used for docking studies of the inhibitors investigated in this research. The X-ray crystal structures 2BEL (Hale et al 2008) and 2RBE (Yuan et al 2007) of human 11β-HSD1 were used for docking studies. These two particular structures were used as they were the best available data at the time of research, with resolutions at 2.11 Å and 1.9 Å respectively. Furthermore, each structure was in complex with carbenoxolone and a 2-anilinothiazolone inhibitor respectively, allowing definition of the binding site and comparisons.

5.8.1 LIDAEUS

LIDAEUS (Taylor et al 2008; Wu et al 2003) is an in-house virtual screening program which screens 3-D structures by docking the inhibitor atoms onto pre-determined site points in the active cavity. The pre-determined site points (or grid-points) define the preferred protein interaction e.g. HBA, HBD or hydrophobic. As the inhibitors are docked and matched to the site points, each pose is given a score which is based on

several factors including the van der Waals and hydrogen donor and acceptor bonding energies. Various orientations of the ligand are attempted to achieve a chemical and shape complementarity between the ligand and the binding site. The site points generated using LIDAEUS for the crystal structure 2BEL (Wang et al 2008) are shown in figure 5.23.

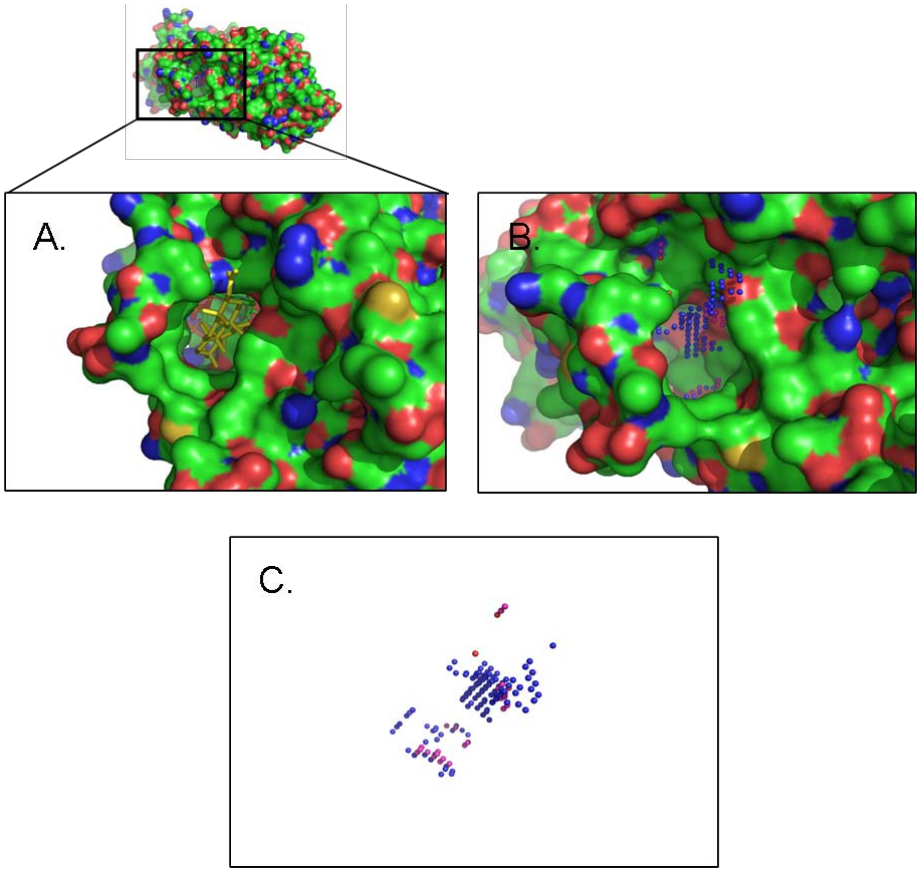

Figure 5.23: Illustration prepared with Pymol showing: (A) the active site in 2BEL with ligand (carbenoxolone) in yellow stick format. The enzyme has been given a surface, coloured according to atom type. (B) the active site with grid points generated by LIDAEUS, Blue spheres are HBD, red spheres are HBA and grey spheres are hydrophobic. (C) the grid points alone (colours as described).

The end product is a list of ligand poses for each inhibitor, ranked according to their score. This score function represents how well the ligands fit into the binding site. It is a sum of the energy factors mentioned, but it is not representative of the free energy as it is not complete (e.g. it does not take into account the movement of water molecules) and is used as a guide. The scores in this study ranged from -36 to -11 kcal mol^{-1}, with a good fit having a negative score. The energy scores of each of the docking positions are shown in

table 5.5, as determined by LIDAEUS. The energies calculated by LIDAEUS are all in the acceptable range.

Compound ID:	**3**	**5**	**7**	**10**	**21**	**37**	**46**	**56**
Score (kcal mol^{-1}):	-35.47	-11.89	-18.86	-18.87	-16.17	-11.92	-16.72	-19.75

Table 5.5: The scores generated by LIDAEUS to demonstrate the 'goodness' of a docking pose. All the docking positions shown here are in the top 4 positions identified by LIDAEUS.

5.8.2 Docking Hits into 11β-HSD1

Eight compounds (3, 5, 7, 10, 21, 37, 46 and 56) were docked into the ligand binding pocket. Five of these were predicted to form interactions with the catalytically active residues Tyr 183 and /or Ser 170 in the docking poses shown here (figure 5.24). The poses shown in figure 5.24 were always one of the top four positions identified by LIDAEUS. The relative energy scores of the 8 compounds docked are shown in table 5.5. The three dimensional structures are shown in figure 5.24 of each compound docked, beside an overview of the compound in the binding site.

Compounds 10 and 21 enter deeply into the binding site (figure 5.24, 4b and 5b respectively) due to different spatial characteristics of the two compounds; the V-shape of 10, and the small volume of 21. In contrast, the planarity of compound 3 means that it protrudes from the binding site entrance. The remaining five compounds fill a fairly similar space in the binding site, as seen in figure 5.24.

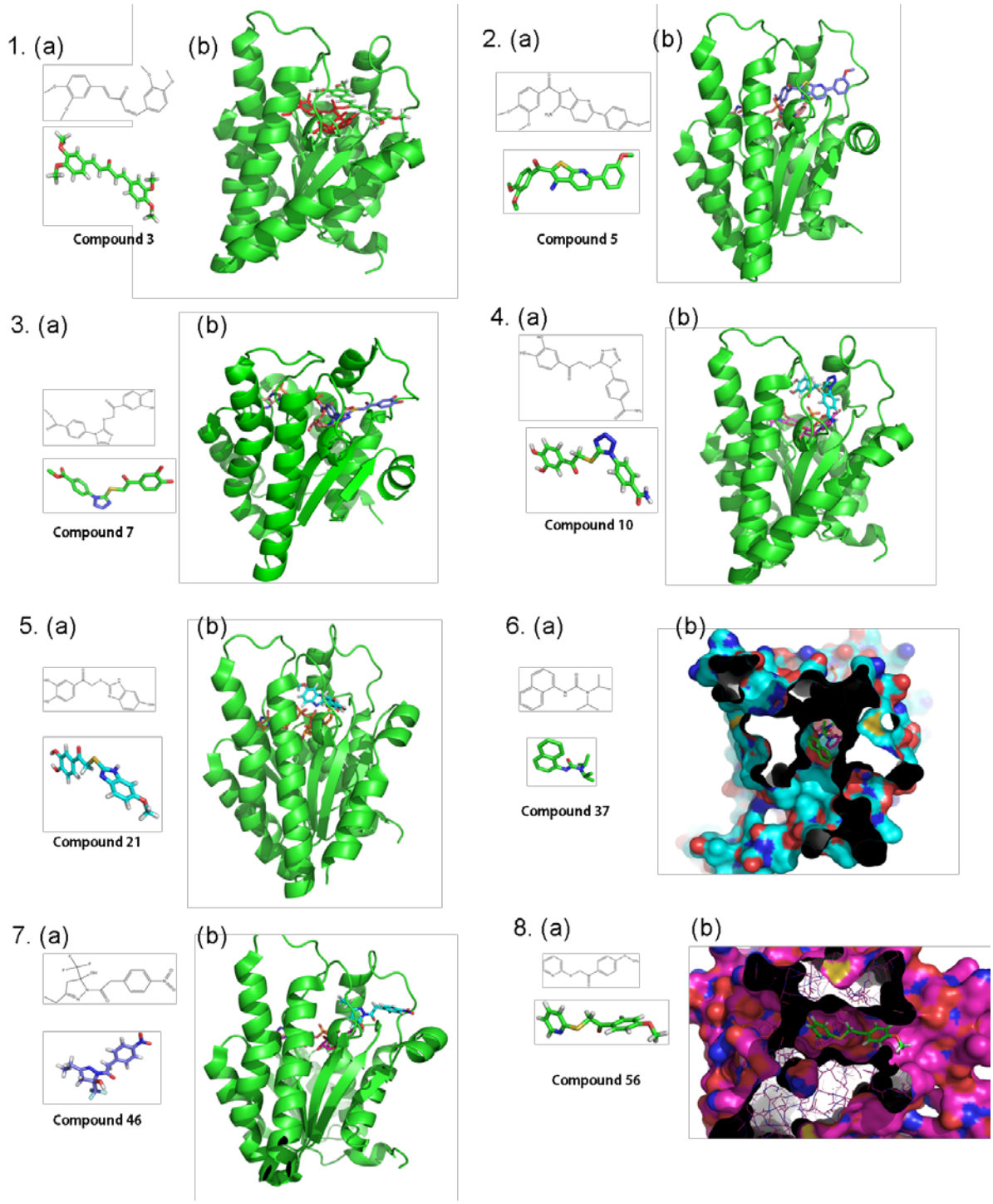

Figure 5.24: (a) Depiction of each compound docked, 2-D and 3-D representation, (b) overview of the compound in the active site. 11β-HSD1 is shown in green, in cartoon form, as this facilitates viewing. The co-factor may be seen behind the compound, in magenta/red. This applies to (A) compound 3, (B) compound 5, (C) compound 7, (D) compound 10, (E) compound 21, (F) compound 37, (G) compound 46, and (H) compound 56. Compounds 37 and 56 are shown in the binding site with 11β-HSD1 depicted with a surface. This allows a better spatial perspective of binding however was only possible for these compounds.

5.8.3 Compounds with Catalytic Triad Interaction

There were five compounds which showed interactions with one or more of the catalytic triad of residues in the active site (Ser 170, Tyr 183 and Lys 187). The polar interactions shown between each compound and residues in the binding pocket are shown in figure 5.25 for compounds 5 (fig 5.25A), 7 (fig 5.25B), 21(fig 5.25C), 46 (fig 5.25D) and 56 (fig 5.25E).

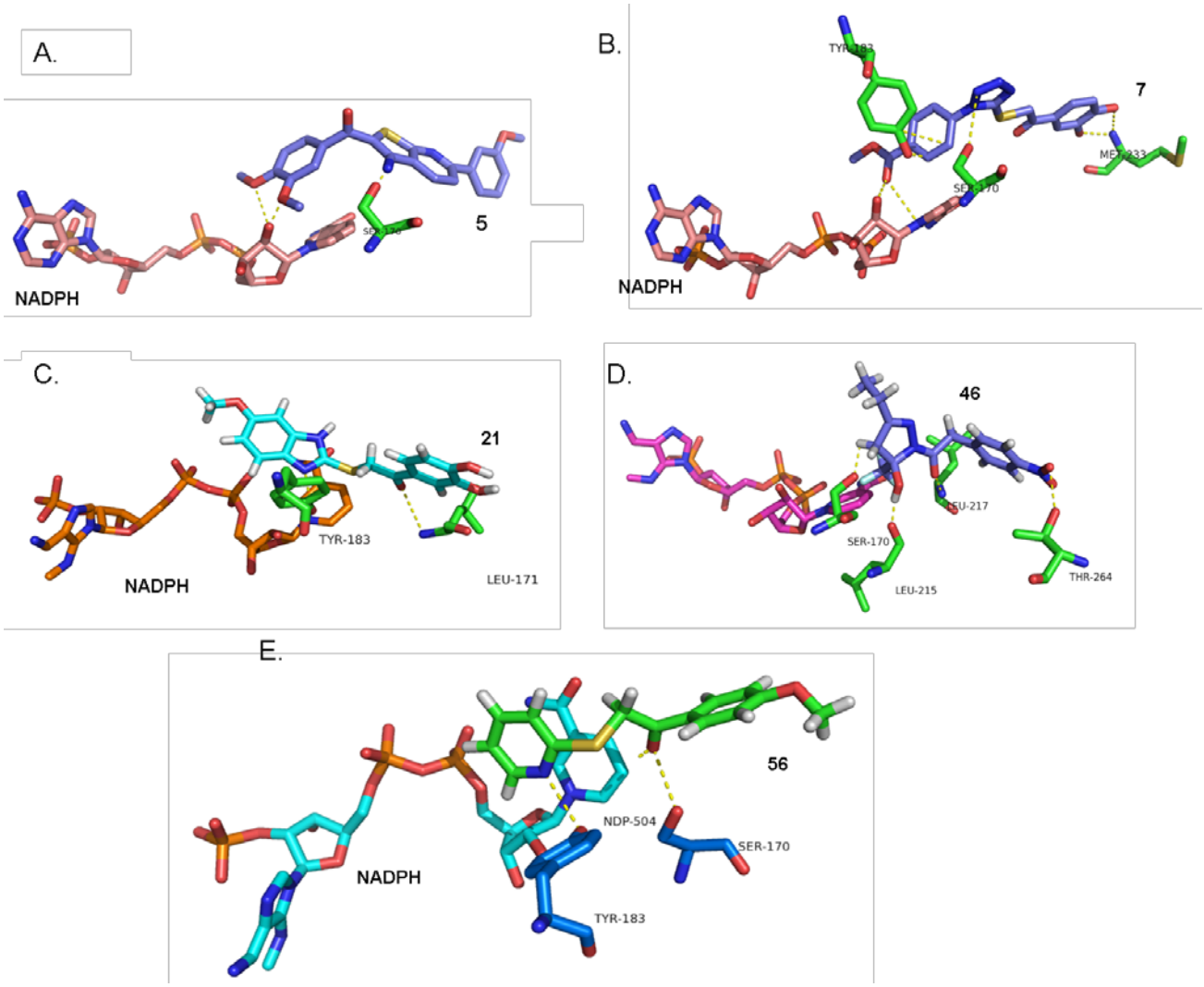

Figure 5.25: Close up view of inhibitor binding in the active site of 11β-HSD1, as determined by LIDAEUS. Shown are the highest scoring positions of each compound. (A) compound 5, (B) compound 7, (C) compound 21, (D) compound 46 and (E) compound 56. The co-factor is shown on the left-hand side in each case, with inhibitor on the right. Interacting residues are shown in stick format and labelled accordingly.

Docking of compound 7 into 2BEL (figure 5.25B) highlights six polar interactions which may occur, far more than any other compound examined. This is due to a higher number of HBAs (9) and HBDs (2) on compound 7 as compared to the other inhibitors. The diphenyl ring points toward the solvent, but also acts as a HBA to the methionine (Met 233) amino nitrogen backbone. Several high scoring docking poses positioned the molecule very deep within the binding pocket so it appeared to be exiting the enzyme through the co-factor entrance, at the opposite end of the substrate entrance.

Docking of compound 46 into 2RBE (figure 5.25D) showed entry of the electronegative fluoro-pyrazole moiety first into the binding pocket and four polar interactions between the compound and 11β-HSD1. The fluoro- moiety of compound 46 is in close proximity to the nicotinamide ring of NADPH (approximately 2.5 Å) putatively allowing the fluorine p-orbital electrons to delocalize into the Π-bonding network of the nicotinamide pyridine ring of NADPH (Loh et al 2003). Indeed, removal of this tri-fluoro group ablates potency, as seen when compared to compound 47 (figure 5.26).

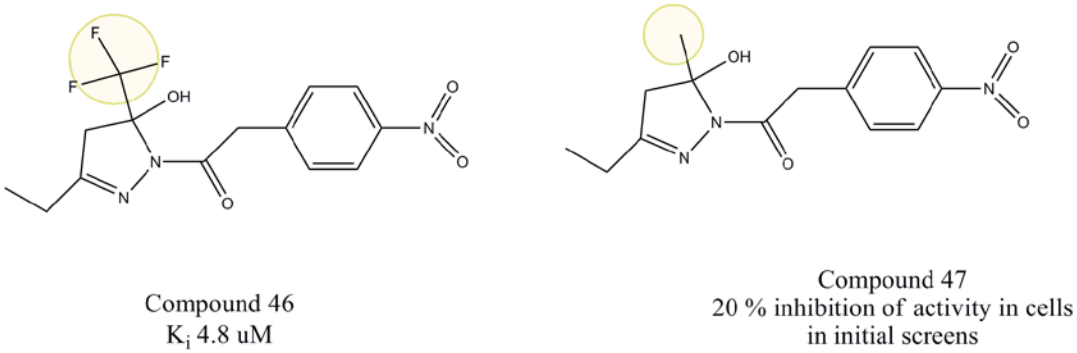

Compound 46
K_i 4.8 uM

Compound 47
20 % inhibition of activity in cells
in initial screens

Figures 5.26: Structure of compounds 46 and 47 showing the differences (shown in yellow) and effects.

Several previously developed inhibitors have included a halogen moiety at or around this position; it has been observed that a halogen positioned here may mimic a halogen at the 9-α position of a steroid skeleton (see chapter 1 for steroid numbering) reported in 1968 to inhibit the dehydrogenase reaction but to enhance the reductase reaction direction; as demonstrated with the use of 9α-fluorocortisone and 9α-fluorocortisol (Bush et al 1968). Analysis of compound 46 has been carried out previously in many instances with several diverse primary screens carried out and the results reported (PubChem BioActivity Services), for example; compound 46 has been tested for

inhibition of *T. Cruzi* replication, inhibition of human galactokinase (GALK), antagonism of the G-protein coupled receptor 7 (GPR7) and inhibition of the Plasmodium Falciparum M18 aspartyl aminopeptidase (PFM18AAP). Of 109 initial screens in which it exhibited activity (excluding the current research) 87 had a particular protein target, none of which were 11β-HSD1.

Docking of compound 5 with LIDAEUS (figure 5.25A) into 2BEL displays few polar interactions; the catalytic residue serine 170 is the only residue creating polar contacts with the inhibitor. Compound 21 displays two polar interactions, one with the catalytic residue Tyr 183, and another with the backbone nitrogen of Leu 171 (figure 5.25C).

Docking of compound 56 into 2RBE (figure 5.25E) shows the nitrogen of the pyridine moiety interacting with the catalytically active tyrosine 183 hydroxyl group. In addition the central carbonyl of compound 56 acts as a hydrogen acceptor with serine 170. The proximity of the nicotinamide ring allows for Π-stacking between inhibitor and the pyridine ring. This is a classic 11β-HSD1 inhibitor binding scenario, and is commonly seen with other inhibitors (chapter 1), that is; Tyr 183, Ser 170, the co-factor nicotinamide ring and several hydrophobic interactions.

5.8.4 Compounds with no Catalytic Triad Interaction

The three remaining compounds; 3, 10 and 37 do not interact with any of the catalytic residues, indeed 37 does not appear to make any polar contacts with the enzyme and relies predominantly on hydrophobic interactions for binding. Compounds 3 and 10 form hydrogen bonds with residues out-with the catalytic triad which surround the active site; Thr 124, Ala 172 (backbone), Leu 215 (backbone), as shown in figure 5.27.

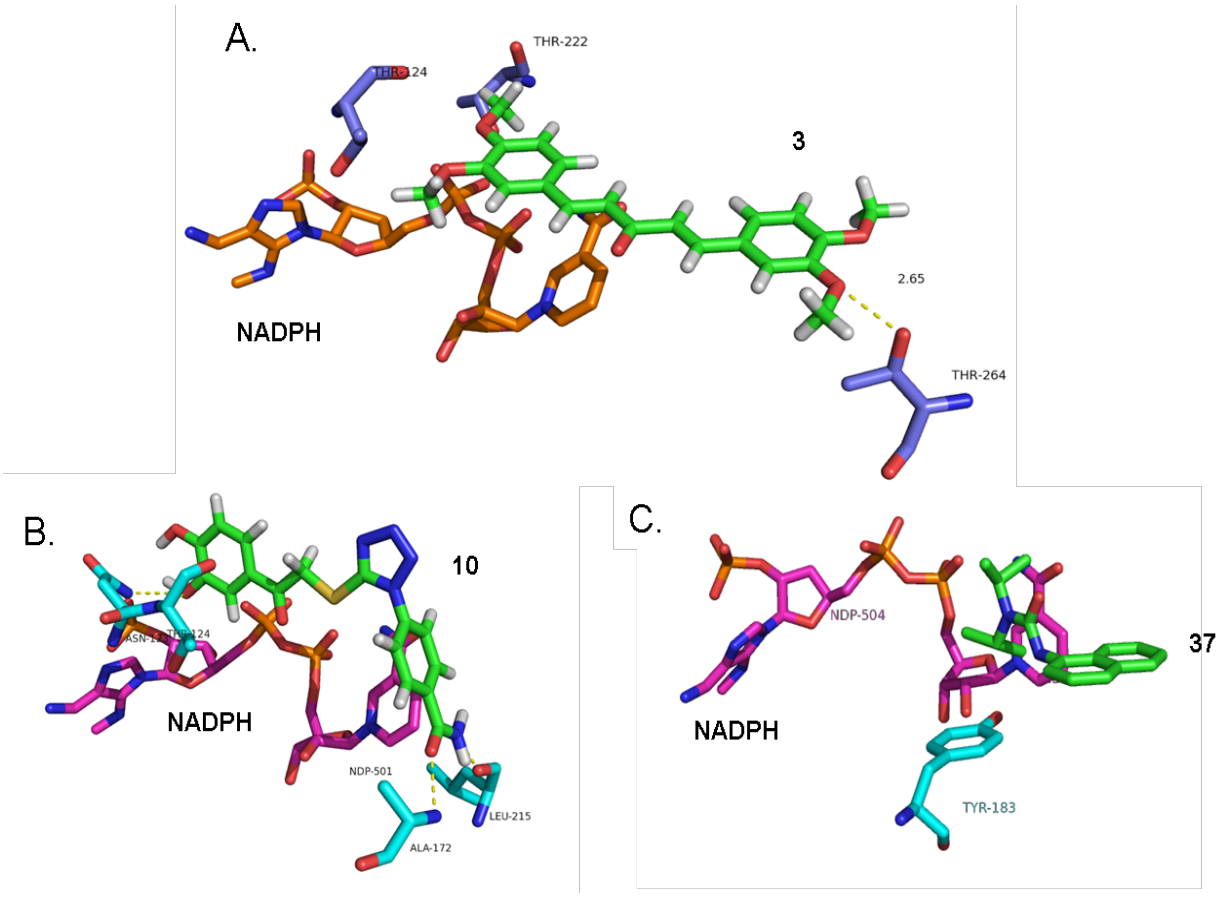

Figure 5.27 The four docked compounds which did not display polar interactions with the catalytic triad in the binding pocket; a close up view of binding in the active site of 11β-HSD1 and (A) compound 3, (B) compound 10, (C) compound 37. The inhibitor compound is shown on the right hand side in all cases, and co-factor NADPH on the right (as labelled). Residues playing a role in binding are depicted in stick form and are labelled accordingly. Diagram prepared with Pymol.

Compound 10 (figure 5.27B) showed slightly different binding, partially due to its awkward V-shape, allowing the compound to bury deeply into the pocket in close proximity to NADP(H). Despite this, there does not appear to be any co-factor interactions. There are four polar interactions which dominate binding; the backbone nitrogen of Thr 124 with the hydroxy oxygen from the benzene ring of compound 10; Asn 123 and the hydroxy hydrogen of compound 10; the backbone of Ala 172 and the amide oxygen on the other end of the molecule; Leu 215 and the amide nitrogen at the same end of the molecule (shown in figure 5.27B).

The docking model for compound 37 (figure 5.27C) showed that binding is dominated by hydrophobic interactions. The compound sits deeply buried within the pocket with

the naphthalene ring group planar to tyrosine 183, but at a distance of 6 Å prevents π-stacking. However, perpendicular π-stacking is possible between Tyr 177 and the naphthalene rings (~ 2 – 3 Å distance).

Compound 3 differs from the other inhibitors in that it is planar (figure 5.27A). The 11β-HSD1 binding pocket tilts downward slightly from the mouth toward the co-factor. A planar molecule will thus not complement this shape completely (a V-shaped molecule may have a better 'fit', refer to figure 1.32). Due to its planarity, compound 3 does not arch toward the co-factor so they cannot interact: they are a distance of 5 Å apart at their closest point. This inhibitor is held in place predominantly by hydrophobic features, in addition to one polar interaction with threonine 264, which shares its hydrogen with the methoxyphenyl oxygen at the mouth of the binding site. The compounds sits fairly high up in the binding tunnel and is flanked by three threonine residues at each corner, as shown in figure 5.28A. The residues Thr 222 and Thr 224 are just out of range for forming polar interactions with the methoxy oxygens on compound 3 (a distance greater than 3 Å). An interaction with threonine residues in the active site has been seen previously with other 11β-HSD1 inhibitors (chapter 1).

5.9 Discussion

Of the 35 compounds tested, 12 were based on carbenoxolone, 11 are based on 2-anilinothiazolone, 4 were based on adamantane (chapter 4) as UFSRAT query molecules and a further 8 were selected from supplier's catalogues to complement the 27 existing compounds. Those which displayed inhibition of 11β-HSD1 ranged in molecular weight (from approximately 200 – 400 Da), LogP and structural class.

Several compounds were found to inhibit in cell-based assays but not with recombinant protein, and vice versa. For example, compound 16 inhibited recombinant protein, but not 11β-HSD1 in HEK-293 cells. This is summarised in figure 5.28.

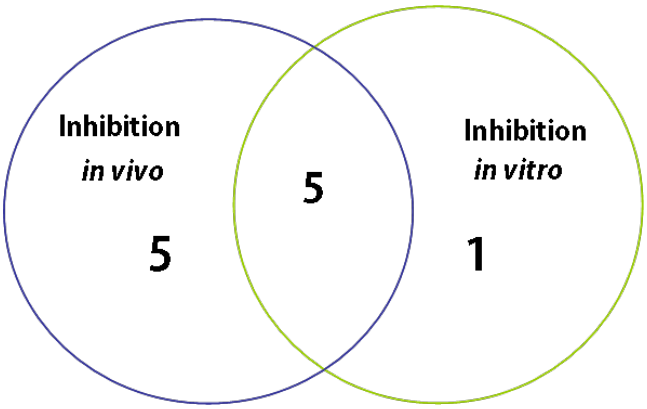

Figure 5.28: Chart showing the overlap of compounds which inhibited both in cells and in recombinant protein assays. Out of 35 compounds, 5 inhibited both in cell and recombinant human 11β-HSD1 inhibition assays (overlap between green and blue circles). One of these five also inhibited mouse 11β-HSD1 (two other compounds inhibited mouse 11β-HSD1 but not human). One compound inhibited recombinant 11β-HSD1 (in vitro) but not HEK293 expressed 11β-HSD1 (in vivo) shown in the green circle. Five compounds inhibited in cell based assays but not recombinant 11β-HSD1 (blue circle).

Five compounds inhibited 11β-HSD1 in HEK-293 cells but not recombinant protein; these compounds (5, 7, 28, 29, and 46) had low micromolar range K_i values in cell-SPA. The lack of inhibition of recombinant enzyme is due to the presence of carbenoxolone in the recombinant protein preventing the ligands binding, and possibly a preference for the NADPH-bound form of the enzyme over the NADP+ bound form. In a study carried out by Sahni-Arya et al, (Sahni-Arya et al 2007) the binding of a competitive pyridyl amide inhibitor showed that the presence of NADPH (as opposed to $NADP^+$) increased the affinity of the compound 5-fold (from a K_i 279 nM to 53.2 nM). In similar experiments, a sulfonamide compound was determined to preferentially bind to an $NADP^+$ bound form of 11β-HSD1, evidenced through a small negative effect on the affinity of the compound in the presence of NADPH.

The five compounds which exhibited inhibition of 11β-HSD1 in both cellular and recombinant enzyme assays were selected as the top five inhibitors. These are shown in figure 5.29 and summarised in table 5.6. In this table, the UFSRAT query molecule is denoted; this is the compound with which a similarity search was carried out according to its various physicochemical parameters. As can be seen from table 5.6, the majority of compounds used carbenoxolone as a query molecule.

Table 5.6: Summary of the top five compounds inhibiting 11β-HSD1, and the query molecules used to mine for similar compounds (chapter 4). The K_i values are taken from the cell SPA experiments where possible.

Compound ID	Query Molecule	Calculated K_i
3	Carbenoxolone	8.7 μM
10	Carbenoxolone	7.4 μM
21	Carbenoxolone	6.1 μM
37	2-anilinothiazolone	11.3 μM
56	Manually selected	51.8 nM

The five compounds which exhibited bidirectional inhibition of 11β-HSD1 were docked into the active site and showed a variety of interactions with the enzyme, with two of the compounds docked interacting with Ser 170 and Tyr 183 (compounds 21 and 56).

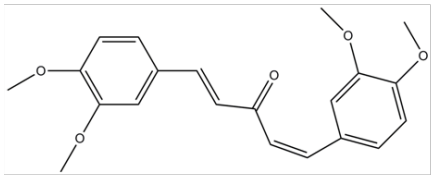

K_i 8.7 μM

3. (1E,4E)-1,5-bis(3,4-dimethoxyphenyl)penta-1,4-dien-3-one

MW	354,4 Da
LogP	4.53
HBA	5
HBD	0

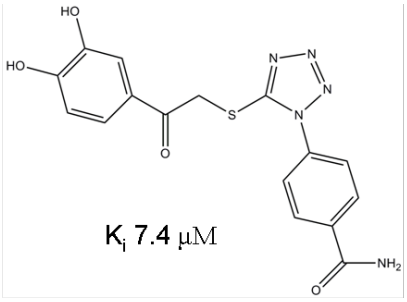

K_i 7.4 μM

10. 4-[5-[2-(3,4-dihydroxyphenyl)-2-oxo-ethyl]sulfanyltetrazol-1-yl]benzamide

MW	371.3 Da
LogP	2.05
HBA	9
HBD	4

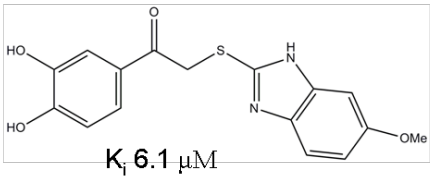

K_i 6.1 μM

21. 1-(3,4-dihydroxyphenyl)-2-[(6-methoxy-1H-benzimidazol-2-yl)sulfanyl]ethanone

MW	330.3 Da
LogP	3.49
HBA	6
HBD	3

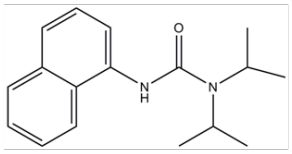

K_i 11.3 μM

37. 3-(1,4-dihydronaphthalen-1-yl)-1,1-dipropan-2-ylurea

MW	272.3 Da
LogP	4.13
HBA	2
HBD	1

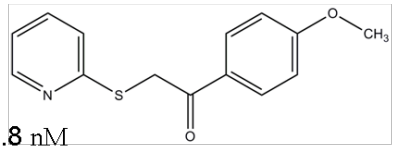

K_i 51.8 nM

56. 1-(4-methoxyphenyl)-2-(2-pyridylsulfanyl)ethanone

MW	259.3 Da
LogP	2.87
HBA	3
HBD	0

Figure 5.29: Summary of the structure and chemical parameters of the top five compounds found to inhibit both recombinant 11β-HSD1 and in cells transfected with human 11β-HSD1.

5.10 Conclusions and Future Work

Overall, five of the 35 compounds analysed showed low micromolar bidirectional inhibition of human 11β-HSD1; an estimated 14% hit rate.

Further work would determine the mode of inhibition by construction of a Dixon plot. This is a reciprocal graphical representation of the inhibitor data obtained by varying the inhibitor concentration over a fixed substrate concentration. This is carried out with, for example, four fixed substrate concentrations which would give four sets of data to be plotted on the 1/V vs [I] graph. The four resulting lines will intersect in a manner characteristic of the type of inhibition assayed. For example, for competitive inhibitors the lines will intersect beyond the ordinate, at a point $-K_i$. For non-competitive inhibitors the lines will intersect on the abscissa, below zero, defining the $-K_i$. Alternatively, a Lineweaver-Burk plot can be used to determine inhibition type but due to its double reciprocal nature it cannot be used to derive reliable kinetic data.

The selectivity of these inhibitors must also be assessed for cross-inhibition of 11β-HSD2. Inhibition of this isoform in the kidney would result in activation of the mineralocorticoid receptor (through inhibition of inactivation of the active steroid) and cause hypertension and hypokalemia (Frey et al 2004). In addition, due to a higher sequence identity (36%), 17β-HSD2 cross-inhibition screening may be useful, although recent research shows that it is the spatial structure similarities rather than the amino acid sequence identity which determines whether a ligand will bind (Koch et al 2004).

Further preclinical assays will include PXR selectivity, and additional tests to investigate the metabolic stability and safety of the ligands. These include P450 assays, a clearance assay in liver microsomes, a membrane permeability assay in intestinal cells, and cytotoxicity assays alongside further structural and enzymatic characterization.

CHAPTER 6

CRYSTALLISATION AND STRUCTURE OF

11β – HYDROXYSTEROID DEHYDROGENASE TYPE I

6.1 Introduction

There are a total of 17 crystal structures deposited in the online protein data bank (PDB) to-date (table 6.1). To a great extent, the crystal structures of human 11β-HSD1 - which constitute 14 out of the 17 deposited structures - are a very recent emergence, powered by the surge of interest by the pharmaceutical industry at around the same time in 11β-HSD1 as a novel drug target. This flurry of interest drove forward important developments in 11β-HSD1 expression and purification which was previously the principal obstruction in 11β-HSD1 crystallographic research: attaining sufficient quantities of recombinant human enzyme.

At the start of this present research, there were two mouse structures, three human structures (one of which still remains to be published) and one guinea-pig structure in the PDB, all produced through academic efforts. From the start of 2007 until November 2008, a further 11 crystal structures were deposited in the PDB of the coveted human enzyme. All of these structures came from pharmaceutical industry laboratories, with Amgen Inc. being the major player with 8 of these published structures, all in complex with novel inhibitors (table 6.1). Figure 6.1 shows one of the X-ray crystallography derived structures from Amgen; a tetramer of 11β-HSD1 deposited in 2008 (3BYZ) in complex with a thiazolone compound.

With similar goals, attempts at human and mouse 11β-HSD1 crystallisation were carried out in this research in an endeavour to produce single, diffracting co-crystals of 11β-HSD1 with a novel inhibitor (from chapter 5).

#	PDB Code & co-crystallised ligand	Title of deposited crystal structure	Title & Date of publication (PubMed ID)	Authors	Parameters	Crystal Conditions
1	**1Y5R** Corticosterone	The Crystal Structure of Murine 11B-HSD1 complexed with corticosterone	(PubMed ID: 15865440) May 2005	(Zhang et al., 2005)	Resolution [Å]: 3 R-value: 21 % R-free: 24.7 % Space Group: $P4_122$	Vapour Diffusion 1.8M Li_2SO_4, 0.1M HEPES pH 7.5, 293K
2	**1Y5M**	The Crystal structure of Murine 11B-HSD1: an important therapeutic target for diabetes	(PubMed ID: 15865440) May 2005	(Zhang et al., 2005)	Resolution [Å]: 2.3 R-value: 21.9 % R-free: 25 % Space Group: $P4_122$	Vapour Diffusion 1.8M Li_2SO_4, 0.1M HEPES pH 7.5, 293K
3	**1XU9**	Crystal Structure of the Interface Closed Conformation of 11B-HSD1 isozyme 1	(PubMed ID: 15513927) November 2004	(Hosfield et al., 2005)	Resolution [Å]: 1.5 R-value: 15.8 % R-free: 18.1 % Space Group: $P12_11$	Vapour Diffusion PEG, MES pH 7.0, 298K
4	**2BEL** Carbenoxolone	Structure Of Human 11B-HSD1 In Complex With NADP And Carbenoxolone	(PubMed ID:) December 2004	(Hale, 2008)	Resolution [Å]: 2.11 R-value: 19 % R-free: 24.6 % Space Group: $P2_12_12$	0.1 M $MgCl_2$ 15 % PEG 3350 pH 5.5
5	**1XU7**	Crystal Structure of the Interface Open Conformation of Tetrameric 11b-HSD1	(PubMed ID: 15513927) November 2004	(Hosfield et al., 2005)	Resolution [Å]: 1.8 R-value: 19.8 % R-free: 21.7 % Space Group: $P12_11$	Vapour Diffusion PEG, MES pH 7.0, 298K

#	PDB Code & co-crystallised ligand	Title of deposited crystal structure	Title & Date of publication (PubMed ID)	Authors	Parameters	Crystal Conditions
6	**1XSE**	The Crystal Structure of Guinea Pig 11β-HSD Type 1 Provides a Model for Enzyme-Lipid Bilayer Interactions	(PubMed ID: 15542590) November 2004	(Ogg et al., 2005)	Resolution [A]: 2.5 R-value: 19. 6% (obs) R-free: 26.7 % Space Group: I 4 2 2	Vapour Diffusion 38-40 % PEG 550 MME, 0.1 M BisTris pH 6.5, 291K
7	**2RBE** 2-anilino thiazolone	The discovery of 2-anilinothiazolones as 11B-HSD1 inhibitors	(PubMed ID: 17919905) AMGEN January 2008	(Yuan et al., 2007)	Resolution [A]: 1.9 R-value: 21.9 % (work) R-free: 26.4 % Space group: $P2_12_12_1$	No details supplied.
8	**2ILT** 2-adamantyl sulfone	Human 11B-HSD1 with NADP and Adamantane Sulfone Inhibitor	Adamantane sulfone and sulfonamide 11-beta-HSD1 Inhibitors (PubMed ID: 17070044) ABBOTT, April 2007	(Sorensen et al., 2007)	Resolution [A]: 2.3 R-value: 21.2 % (obs) R-free: 27.5 % Space group: I 2 3	No details supplied.
9	**2IRW** Adamantyl ether	Human 11-beta-Hydroxysteroid Dehydrogenase (HSD1) with NADP and Adamantane Ether Inhibitor	Discovery of adamantane ethers as inhibitors of 11beta-HSD-1: Synthesis and biological evaluation (PubMed ID: 17110106) ABBOTT, January 2007	(Patel et al., 2007)	Resolution [Ä]: 3.1 R-value: 23.9 % (obs) R-free: 27.8 % Space group: H 3 2	No details Supplied.

#	PDB Code & co-crystallised ligand	Title of deposited crystal structure	Title & Date of publication (PubMed ID)	Authors	Parameters	Crystal Conditions
10	**3BYZ** 2-Amino-1,3-thiazol-4(5H)-one	2-Amino-1,3-thiazol-4(5H)-ones as Potent and Selective 11-Hydroxysteroid Dehydrogenase Type 1 Inhibitors	2-amino-1,3-thiazol-4(5H)-ones as potent and selective 11beta-hydroxysteroid dehydrogenase type 1 inhibitors: enzyme-ligand co-crystal structure and demonstration of pharmacodynamic effects in C57Bl/6 mice (PubMed ID: 18419108) AMGEN, February 2008	(Johansson et al., 2008)	Resolution [Å]: 2.69 R-value: 22.2 % (obs) R-free: 29.3 % Space Group: $P2_12_12_1$	Vapour Diffusion 25% PEG 3350, 0.1M Na Citrate pH 5.6, 0.2M Am Ac, 298K
11	**3BZU**	Crystal structure of human 11-beta-hydroxysteroid dehydrogenase(HSD1) in complex with NADP and thiazolone inhibitor	Structural characterization and pharmacodynamic effects of an orally active 11beta-hydroxysteroid dehydrogenase type 1 inhibitor (PubMed ID: 18069989) AMGEN, June 2008	(Hale et al., 2008)	Resolution [Å]: 2.25 R-Value: 20.4 % (obs) R-Free: 26.3 % Space Group: $P\ 2_1$ (P1 2_1 1)	Vapour Diffusion, sitting drop, 16-18% PEG 3350, 0.1M MES pH 6.2 298K
12	**3CH6** (3,3-dimethylpiperidin-1-yl)(6-(3-fluoro-4-methylphenyl)pyridin-2-yl)methanone	Crystal Structure of 11beta-HSD1 Double Mutant (L262R, F278E) Complexed with (3,3-dimethylpiperidin-1-yl)(6-(3-fluoro-4-methylphenyl)pyridin-2-yl)methanone	Pyridine amides as potent and selective inhibitors of 11beta-hydroxysteroid dehydrogenase type 1 (PubMed ID: 18485702) BRISTOL-MYERRS SQUIBB June 2008	(Wang et al., 2008)	Resolution [Å]: 2.35 R-Value: 18.8% (obs) R-Free: 23% Space Group: $P\ 2_1\ 2_1\ 2_1$	Vapour Diffusion, hanging drop 22% (w/v) PEG 3350, 200 mM potassium formate pH 7.3, 1.5mM Zwittergent 3-12, 277K

#	PDB Code & co-crystallised ligand	Title of deposited crystal structure	Title & Date of publication (PubMed ID)	Authors	Parameters	Crystal Conditions
13	**3CZR** Arylsulfonylpiperazine	Crystal Structure of Human 11-beta-Hydroxysteroid Dehydrogenase (HSD1) in Complex with Arylsulfonylpiperazine Inhibitor	Discovery and initial SAR of arylsulfonylpiperazine inhibitors of 11beta-hydroxysteroid dehydrogenase type 1 (PubMed ID: 18511278) AMGEN June 2008	(Sun et al., 2008)	Resolution [Å] : 2.35 R-Value: 22.1% (obs) R-Free: 24.7% Space Group: P 3_1 2 1	Vapour Diffusion, sitting drop 16% PEG 3350, 0.1M MES pH 6.4, 289K
14	**3D3E** Benzamide (truncated at 284. Also –missing 232H and 233M)	Crystal Structure of Human 11-beta-Hydroxysteroid Dehydrogenase (HSD1) in Complex with Benzamide Inhibitor	Discovery of novel, potent benzamide inhibitors of 11beta-hydroxysteroid dehydrogenase type 1 (11beta-HSD1) exhibiting oral activity in an enzyme inhibition ex vivo model (PubMed: 18553955) AMGEN July 2008	(Julian *et al.*, 2008a)	Resolution [Å]: 2.6 R-Value: 23 % (obs) R-Free: 28.3% Space Group: P 2_1 (P 1 2_1 1)	Vapour Diffusion, sitting drop 19% PEG 3350, 0.1M MES pH 6.4, 289K
15	**3EY4** 2-amino-1,3-thiazol-4(5H)-one	Further studies with the 2-amino-1,3-thiazol-4(5H)-one class of 11-HSD1 inhibitors: Reducing pregnane X receptor (PXR) activity and exploring activity in a monkey pharmacodynamic model	Not published. AMGEN November 2008	(Fotsch et al., 2008)	Resolution [Å]: 3.00 R-Value: 21.9% (work) R-Free: 31.9% Space Group: P $2_12_12_1$	Vapour Diffusion, hanging drop 25% PEG 3350, 0.1M Na Citrate pH 5.6, 0.2M ammonium acetate, 298K

#	PDB Code & co-crystallised ligand	Title of deposited crystal structure	Title & Date of publication (PubMed ID)	Authors	Parameters	Crystal Conditions
16	**3D4N** Sulfonamide	Crystal Structure of Human 11-beta-Hydroxysteroid Dehydrogenase (HSD1) in Complex with Sulfonamide Inhibitor	Discovery of Novel, Potent Benzamide Inhibitors of 11beta-HSD1 Exhibiting Oral Activity in an Enzyme Inhibition ex Vivo Model (PubMed ID: 18553955) AMGEN, July 2008	(Julian *et al.*, 2008b)	Resolution [Å]: 2.50 R-Value: 22.8% (obs.) R-Free: 25.9% Space Group: P 2_1	Vapour Diffusion, 19% PEG 3350, 0.1M MES pH 6.4, 289K
17	**3D5Q** Triazole Inhibitor	Crystal Structure of 11b-HSD1 in Complex with Triazole Inhibitor	Distinctive molecular inhibition mechanisms for selective inhibitors of human 11beta-hydroxysteroid dehydrogenase type 1. (PubMed ID: 18789704) AMGEN, October 2008	(Tu et al., 2008)	Resolution [Å]: 2.55 R-Value: 23.2% (obs.) R-Free: 26.5% Space Group: P 2_1	Vapour diffusion 19% PEG 3350, MES pH 6.4, 289K
18	**3FRJ** Benzamide inhibitor	Crystal Structure of 11b-HSD-1 (11b-HSD1) in Complex with Piperidyl Benzamide Inhibitor.	Discovery and optimization of piperidyl benzamide derivatives as a novel class of 11beta-HSD1 inhibitors (PubMed ID: 19217779) AMGEN, June 2009	(Rew et al., 2009)	Resolution [Å]: 2.30 R-Value: 19.4% (obs.) R-Free: 23.1% Space Group: P $3_1$2 1	Vapour Diffusion 36% P400, 0.1M Hepes pH 6.4, 289K
19	**3FCO**	Crystal Structure of 11beta-Hydroxysteroid Dehydrogenase 1 (11b-HSD1) in Complex with Benzamide Inhibitor	November 2008	Wang, Z., Sudom, A., Walker, N.P.	Structure Factors Deposited, to be Released on 2009-11-21	No data

#	PDB Code & co-crystallised ligand	Title of deposited crystal structure	Title & Date of publication (PubMed ID)	Authors	Parameters	Crystal Conditions
20	**Present Research**	Crystal Structure of murine 11β-HSD1 in complex with Carbenoxolone Inhibitor	July 2009	Iain McNae	Resolution [Å]: 2.30 R-Value: 20.1% (obs.) R-Free: 25.8% Space Group: C 2 2 2_1	Vapour Diffusion, Hanging Drop 22 % PEG 8000, 10 % propanol, 0.1 M Hepes pH 7.5 277.15 K

Table 6.1: A summary of available crystal structures of 11β-HSD1 in the protein data bank (PDB), as of 10th November 2009.

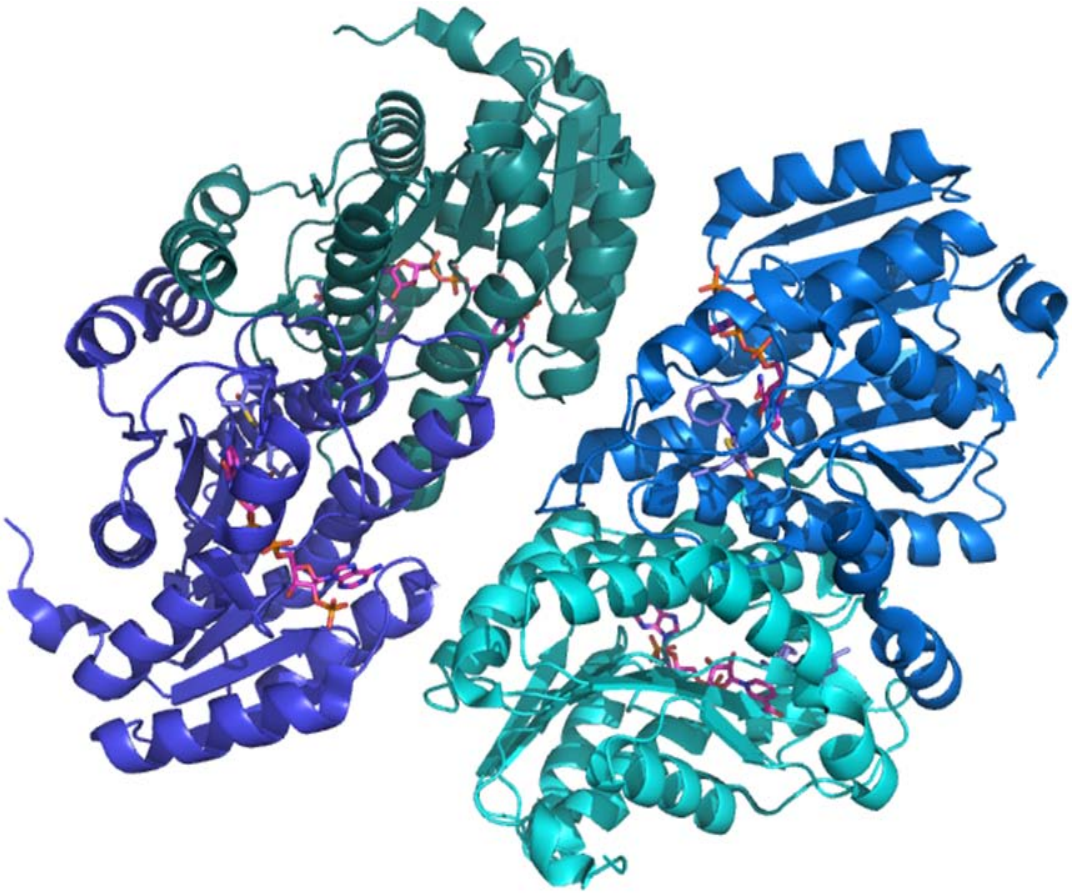

Figure 6.1: The crystal structure 3BYZ of 11β-HSD1 from the PDB (Johansson et al 2008c). Each monomer is coloured differently in this representation which was prepared with Pymol. The co-factor NADPH is shown in pink, the thiazolone inhibitor is shown in pale blue.

The majority of the 11β-HSD1 constructs used for crystallization are N-terminal truncated forms (Δ1 - 23) which occasionally lack parts of the C-terminus (as shown in table 6.2, column 3). The majority of recently deposited structures also have a Cys 272 to Ser mutation (table 6.2, column 2). These truncations and mutations serve to facilitate the production and yield of soluble protein but also aid in crystallography by reducing the net hydrophobicity of the protein.

In this research, two forms of human 11β-HSD1 were used in crystallography trials, in addition to the mouse enzyme. These were both expressed and purified under identical conditions and were found to have similar activities. These were; a 'wild type' 11β-HSD1 which had an N-terminal truncation (residues 1 – 23) as described in chapters 1, 2 and 7; and a C272S mutant which also had an N-terminal truncation (1 – 23).

The majority of structures deposited into the PDB in the last 12 – 18 months have had the C272S mutation, and it is thought to facilitate crystallization of the enzyme.

PDB code:	Mutations:	Truncations:	Chemical co-complexes:
3FRJ	C272S	21 - 292	Piperidine Benzamide inhibitor
3CZR	C272S	24 - 292	Arylsulfonylpiperazine inhibitor
3D3E	C272S	24 - 292	Benzamide inhibitor
3D4N	C272S	24 - 292	Sulfonamide inhibitor
3EY4	C272S	25 - 292	Thiazolone inhibitor
3CZR	C272S	24 - 292	Sulfonyl Piperizine inhibitor
3CH6	L262R, F278E	24 - 292	Pyridine Amide inhibitor
3BZU	C272S	24 - 292	Thiazolone inhibitor
3BYZ	C272S	25 – 292	Thiazolone inhibitor
2IRW	NONE	25 - 288	Adamantane inhibitor
2ILT	NONE	23 - 284	Adamantane inhibitor
2RBE	C272S	24 - 292	Thiazolone inhibitor
2BEL	NONE	26 - 284	Carbenoxolone
1XU9	C272S	21 - 292	No chemical complex
1XU7	C272S	21 - 292	No chemical complex
3FCO	-	-	As yet unreleased

Table 6.2: Sequence details of all current structures of human 11β-HSD1 in the PDB. The full-length sequence is 292 amino acids in length.

Human 11β-HSD1 contains four cysteines, three of which are conserved across species. The residue cysteine 272 is located in the C-terminal and is unique to primates. Mutation of this cysteine to a serine residue produced a mutant with similar activity and kinetics (Walker et al 2001) as observed in this research. Despite initial experiments with non-reducing gels indicating the inability of the C272S mutant to dimerise (Walker et al 2001, Maser et al 2002), more clear-cut experiments using static light scattering with the C272S mutant demonstrated its retained ability to form dimers and tetramers in solution, similar to the wild-type control (Hosfield et al 2005). This has since been supported by crystal structures of the C272S mutant. Truncation of the C-terminus from residue 264 onwards abolished the tendency to

tetramerise (supporting the role of the C-terminal helices in tetramer formation) but did not prevent dimerisation (Hosfield et al 2005). It has since been postulated that Cys 272 is not directly involved in dimer formation but can form disulphide bridges between two dimer partners under favourable conditions.

6.2 Detergents and Additives in 11β-HSD1 Crystallography

Detergents play a number of roles in the present research. It solubilises 11β-HSD1 prior to purification and confers stability during purification procedures. It is removed for kinetic and inhibitor assays, and replaced in the crystal buffers to facilitate protein crystallisation.

To enable successful crystallization of the guinea-pig enzyme, Ogg et al. determined through screening various combinations that the presence of 0.05 % triton X-100 and 0.5 M of the denaturant guanidinium hydrochloride (GuHCl) were necessary additives in the drops. It was suggested that these sub-denaturing conditions allowed the protein to maintain the monodispersity required for crystallization. It was noted that the enzyme also retained full activity after a 16 hour incubation in these conditions (Ogg et al 2005). Triton X-100 is a non-ionic surfactant which has a high molecular weight and a low critical micelle concentration (CMC) which means that it is often difficult to remove if used during a protein purification protocol.

It is also reported that certain detergents (including triton X-100) and a variety of phospholipids (dilauryl phosphatidylserine, dioleeoyl phosphatidylcholine, dilauryl phosphotidylcholine, sphingomyelin and dioleoyl L-α-phosphotidylethanolamine) may have a positive effect on the activity of 11β-HSD1 (Castro et al 2007) as supported in chapter 3. Previous unpublished crystal structures have been obtained with the addition of triton X-100, for which electron density can be seen close to the hydrophobic substrate pocket opening.

Similar published data is available with the detergent CHAPS (3-[(3-Cholamidopropyl) dimethylammonio]-1-propanesulfonate)(Hosfield et al 2005) depicted in figure 6.2B.

In these structures (PDB accession 1XU9 and 1XU7) the CHAPS molecule is observed in the steroid binding pocket, with the A-ring of the steroidal core of CHAPS at the

catalytic end of the pocket toward to NADP+ nicotinamide, and the zwitterionic tail of the detergent extending toward the solvent. The molecule CHAPS was found to bind in an opposite manner to substrate, which projects the A-ring carbonyl toward the entrance of the pocket. This is shown in figure 6.2.

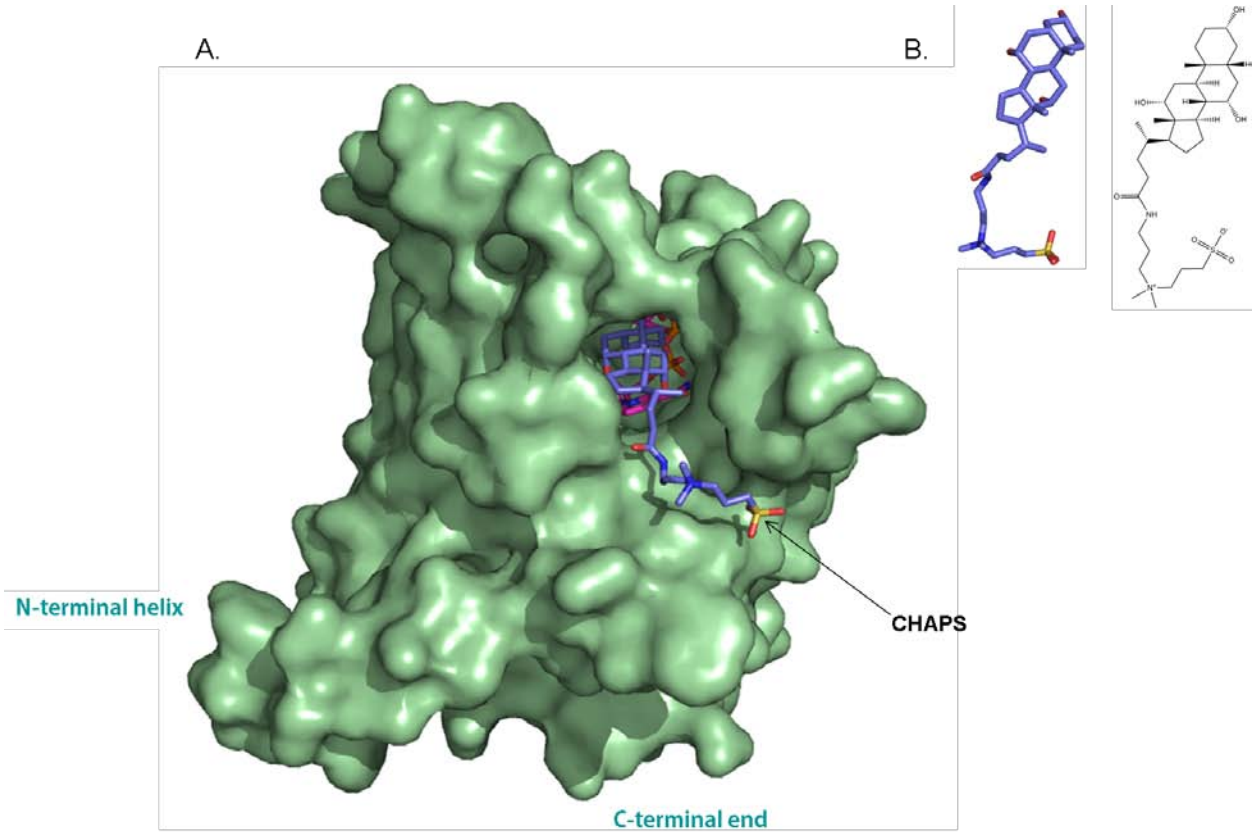

Figure 6.2: (A) Monomer from the crystal structure 1XU7 showing the molecule CHAPS entering the active site. The co-factor NADPH is behind CHAPS (pink). (B) Steroidal structure of CHAPS.

Several hydrophilic contacts with the cofactor NADPH and also Tyr 183 from the catalytic triad of residues can be seen with the detergent, with the majority of the interactions being hydrophobic.

Thesit is another non-ionic detergent which is used in this research in the enzyme purification procedure as it has a lower CMC as compared to triton X-100 and CHAPS and was found to be easier to remove through dialysis and chromatography procedures. In contrast, detergent may also hinder the process of protein

crystallisation due to interference with the crystal lattice formation – preventing the close approach of the particles for intermolecular polar contacts to occur (Fethiere 2007). Buffer additives (i.e. PEG, dextran, glycerol, sugars), pH, temperature and ionic strength may have significant effects on the CMC or cloud point of detergents, inducing an unexpected phase separation in the crystallography drop. For example; a high salt concentration can decrease the CMC of a detergent (the CMC of SDS is decreased 16 fold when NaCl concentration is increased from 0 to 500 mM) (Arnold and Linke 2008). This phenomenon is taken into account when preparing for protein crystallography, as above the CMC the drop solution will separate into a detergent rich and a detergent poor phase, with crystals often being found close to the phase separation. Figure 6.3 shows a detergent phase diagram for a general detergent where crystals may form above the CMC at lower precipitant concentrations, or below the CMC at higher precipitant concentrations. At high detergent and salt concentrations, the protein will aggregate or precipitate out of the drop, at low concentrations the drops will remain clear and crystals will not form.

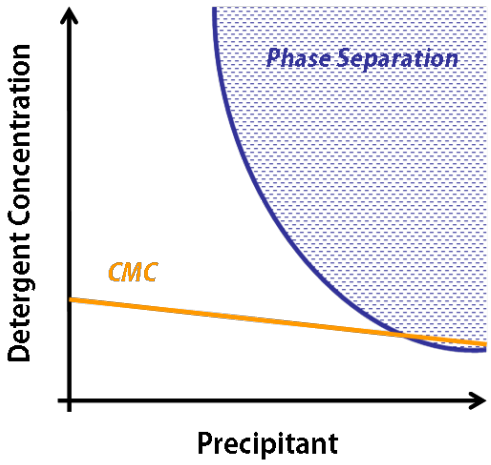

Figure 6.3: A Detergent phase diagram for protein crystallography. The yellow line indicating CMC decreases with increasing precipitant concentration. Protein crystals are often found at the phase boundaries.

6.3 Crystallography of Murine 11β-HSD1: Initial Trials

Active murine 11β-Hydroxysteroid Dehydrogenase 1 was prepared for crystallography at 16 mg/ml in a crystal buffer (20 mM Tris pH 7.8, 20 mM NaCl, 1 mM EDTA, 1 % glycerol). The hanging drop method was used to crystallise the enzyme (details in chapter 7 – Materials and Methods). The initial strategy to determine crystallisation conditions for mouse 11β-HSD1 was a simple ammonium sulphate screen to determine the phase change in the protein drops. This was due to published protocols for obtaining crystalline 11β-HSD1 often being ambiguous and irreproducible in the laboratory.

A solubility curve of 11β-HSD1 with increasing ammonium sulphate concentration is shown in figure 6.4. The plates were set up with varying $(NH_4)_2SO_4$ concentrations (taken as a percentage of a 3.5 M solution per well) and varying pH of Hepes buffer. It was observed that there was a slight phase change at between 42 – 48 % $(NH_4)_2SO_4$. These conditions from the initial screen were set up again, varying additives and the temperature of crystallisation (290 K and 277 K) to improve crystal form and size. These additives were different detergents and the tightest binding ligand from the set of compounds chosen as 11β-HSD1 inhibitors (compound 21). As can be seen in figure 6.4, the detergents triton X-100 and CHAPS had a mild effect on the enzyme solubility by shifting the solubility curve to the left. This is expected; the presence of detergent increases the total amount of precipitants present in the drop. Compound 21 had the opposite effect, increasing the solubility of the mouse enzyme, while thesit had no significant effects.

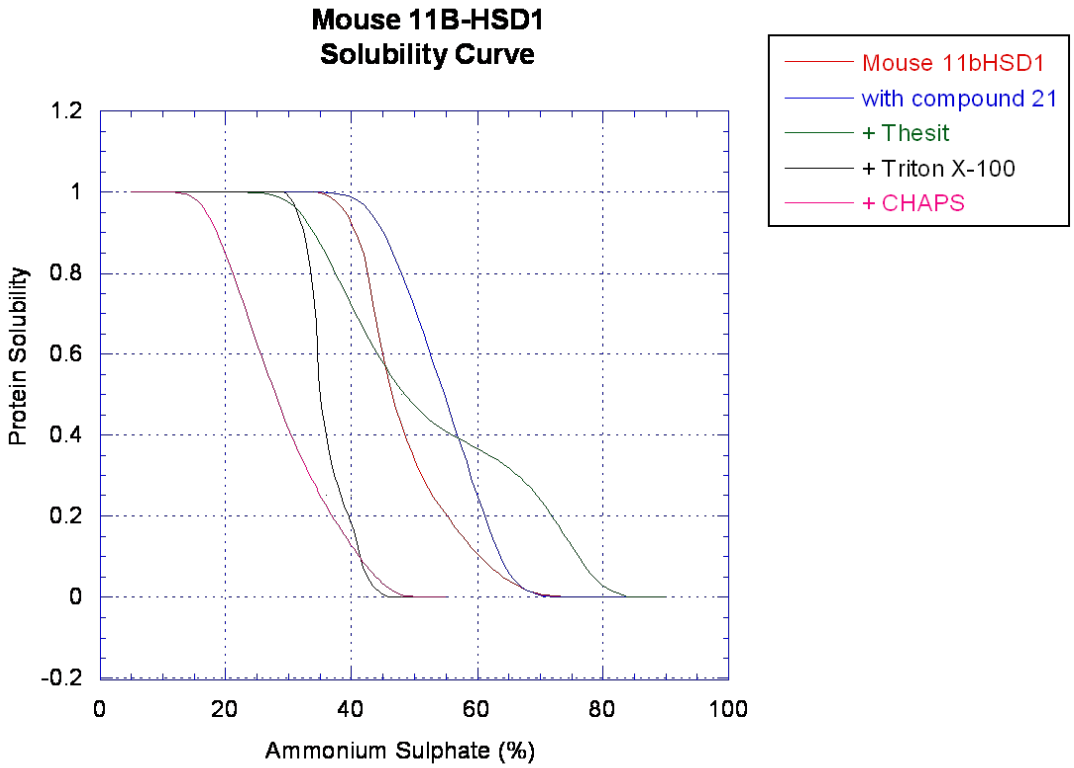

Figure 6.4: Solubility of mouse 11β-HSD1 with increasing $(NH_4)_2SO_4$ concentration, as a v/v percentage of a 3.5 M solution. Solubility has been normalised, with clear drops assigned a value of 1 and fully precipitated drops assigned a value of 0. Values of 0.4 – 0.6 are phase changes, and were wells in which micro-crystals were observed.

As a detergent screen was not available, three detergents were selected as additives on the basis of their previous use, either in protein preparations or published crystal structures. These were CHAPS, Triton X-100 and Thesit. Each reservoir contained the following components in addition to the detergents; $(NH_4)_2SO_4$ ranging from 42 – 48 % and 0.2 M Hepes pH range 6.8 – 8.0. Drops containing thesit formed micro-crystals over a period of 48 – 72 hours at 290.15 K (17°C) which are shown in figure 6.5C. Micro-crystals can often be difficult to distinguish from precipitate however they have a shiny appearance and may polarise light. Optimisation of microcrystal conditions can lead to larger crystals, preferred for X-ray crystallography. The micro-crystals were generally clustered, however there were single rods present (figure 6.5B). As X-ray crystallographic data is collected at low temperatures (generally 100 K) protein crystals must be treated with a cryoprotectant prior to freezing to prevent cracking. Low temperatures are necessary to minimise degradation of the crystal by

free radicals generated by the X-ray beam. There are many different types of cryoprotectant that can be used (the JAXA cryoprotectant database lists all those used in structures deposited in the PDB); the most common are glycerol, ethylene glycol, sucrose or glucose. Attempts were made at cryoprotecting the crystals of mouse 11β-HSD1, with a solution of the mother liquor and increasing amounts of glycerol (v/v) ranging from 5 – 40 %. This method damaged the already fragile crystals and so they were simply frozen in liquid N_2 without cryoprotectant. The crystals were screened at the Grenoble Synchrotron, and showed diffraction at a resolution of 11 Å which is too low a resolution to obtain any good quality data. A high resolution (a lower number signifies higher resolution) will give more qualitative experimental data; this results in a more reliable and accurate model.

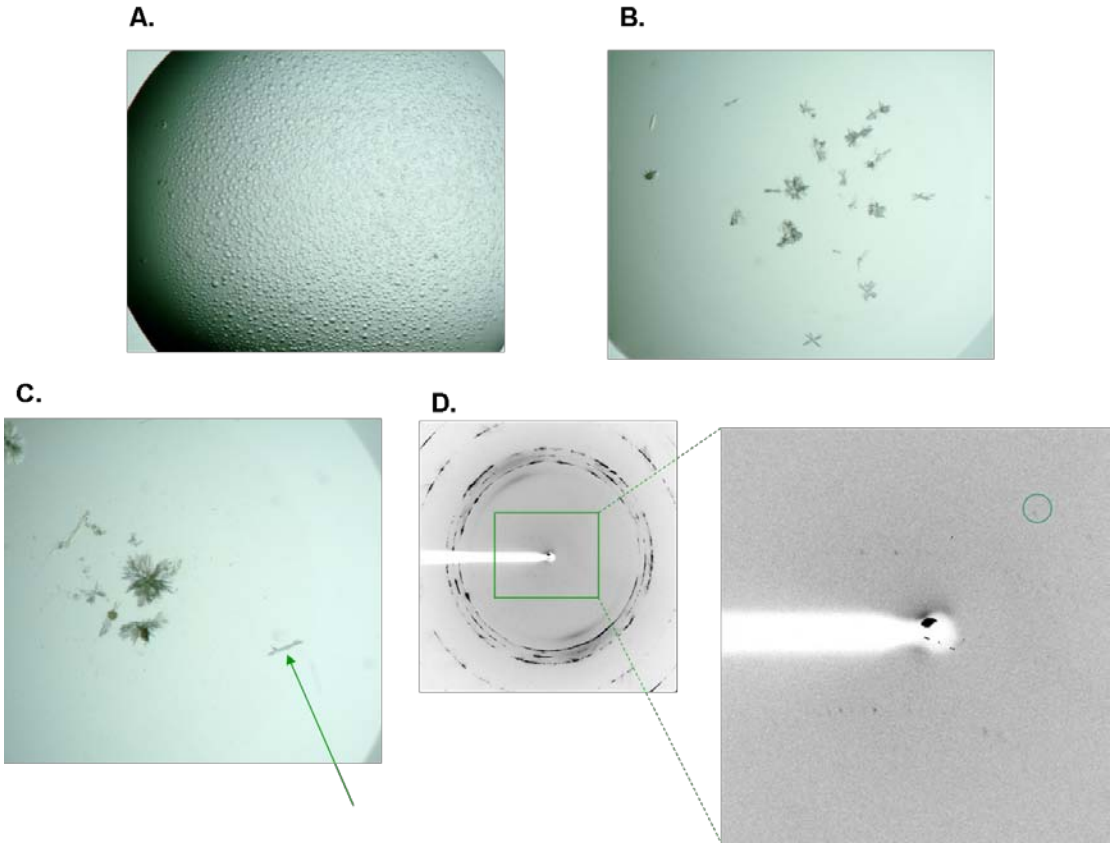

Figure 6.5: A –C are photographs of drops taken with a Nikon DXM1200 camera attached to a Nikon SMZ100 microscope. (A) A drop with 0.4 mM Triton X-100, the drop is oily in appearance, as many of the drops with triton X-100. (B) Drop with 0.01 mM thesit, showing the micro-crystals obtained, grown over a period of 48 – 72 hours. These were mostly clustered; there were also some single thin rods, which were taken for screening at the Grenoble Synchrotron. (C) A close-up of the same drop in B, the green arrow shows a single rod which was approximately 0.075 mm in length. (D) The diffraction pattern from the crystals shown in B and C at the Grenoble Synchrotron, October 2008. The dark rings around the centre are ice rings, a result of no cryoprotectant used. A close-up of the centre of the diffraction pattern shows the reflections at 11 Å (circled in green).

The micro-crystals were subsequently used to seed into wells with identical conditions but for the addition of inhibitors from virtual screening. In particular, compound 21 (from Chembridge) shown in figure 6.6B, produced crystals that were single, thin rods after several days incubation at 20^{o}C. The crystals are shown in figure 6.6A. Seeding is a technique used in protein crystallography which promotes nucleation and single crystal growth by ensuring the presence of already established nuclei - the seeds (Stura and Wilson 1990). The seeds are micro-crystals which are

crushed gently producing a large number of microscopic crystals. This solution is then diluted and added to a fresh, supersaturated crystallisation drop. There are three seeding methods; streak seeding – where the crystals seeds are streaked across the fresh crystallisation drop; microseeding – where the seeds are crushed and diluted prior to use; and macroseeding – where intact seeds are used.

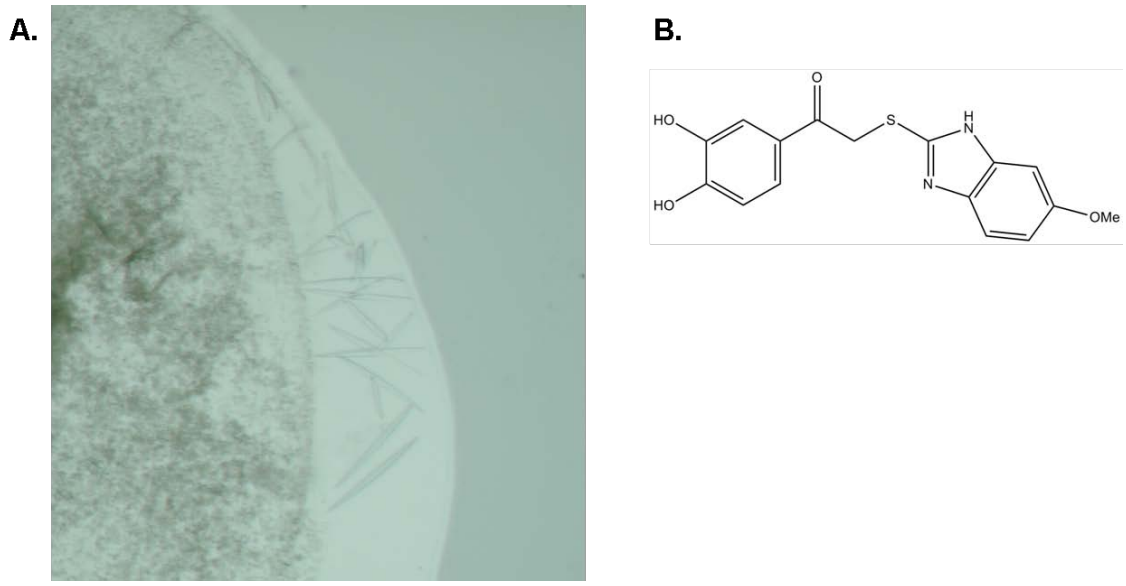

Figure 6.6: A: Photograph taken with a Nikon DXM1200 camera attached to a Nikon SMZ100 microscope; a drop containing mouse enzyme, thesit and compound 21, grown over a period of 72 hours at 290.15 K. The needles are approximately smaller than 0.1 mm in length. B: Structure of compound 21.

However, these delicate crystals did not grow beyond a size of 0.1 mm, and were unable to be screened. In addition, the published conditions for mouse 11β-HSD1 were set-up (Zhang et al., 2005). These were 1.8 M Li_2SO_4, Hepes pH 7.5, and conditions which ranged around this, although did not yield any form of crystal.

6.4 Crystallography of Murine 11β-HSD1: Further Trials

Subsequent work to this research, carried out by Dr. Iain McNae, gave rise to rod shaped mouse 11β-HSD1 crystals, as shown in figure 6.7. To obtain these fast growing crystals (48 hours), an unintentionally different purification protocol was employed to the one developed in this research. This protocol differed as the chaperonin proteins were not co-expressed with the mouse or human 11β-HSD1

enzyme; in addition, Rosetta cells were employed in the place of BL21(DE3) *E. coli* cells (chapter 2 for expression and purification details). Following an IMAC purification procedure, the protein was used for crystallography in a buffer containing 50 mM Tris pH 8.0, 250 mM NaCl, 750 mM imidazole, and the crystallisation conditions were: 22 % PEG 8000, 10 % propanol, 0.1 M Hepes pH 7.5 carried out at 277.15 Kelvin (figure 6.7).

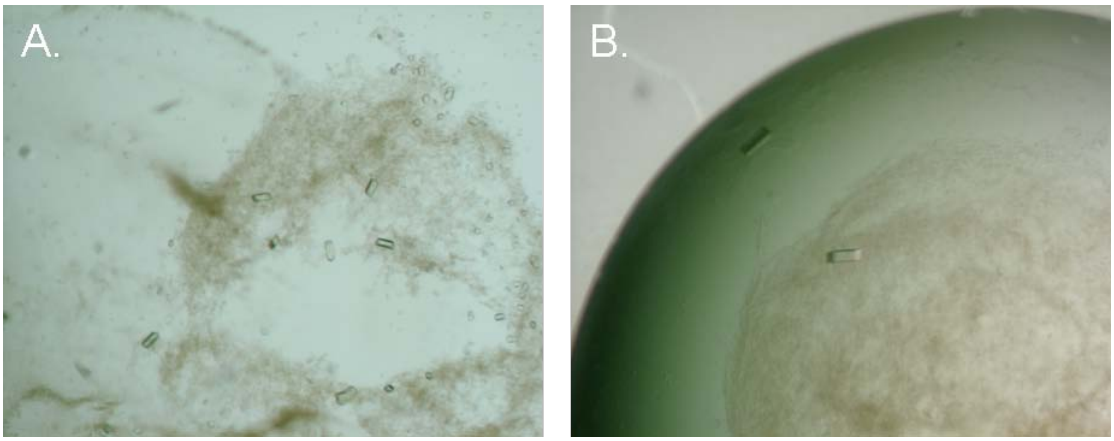

Figure 6.7: (A) and (B) Photograph taken with a Nikon DXM1200 camera attached to a Nikon SMZ100 microscope; a drop containing 10 mg/ml mouse 11β-HSD1, 22 % PEG 8000, 10 % propanol, 0.1 M Hepes pH 7.5, grown over 48 hours at 277.15 K. (B) is a close-up of the rod-shaped mouse 11β-HSD1 crystals. The crystals are approximately 0.1 mm in length.

These crystals were found to diffract up to a resolution of 2.7 Å. Upon refinement of the mouse 11β-HSD1 crystal data, an electron density fitting carbenoxolone is seen to occupy the active site of the enzyme. This is expected; this inhibitor is added to the culture media prior to expression to stabilise the nascent protein, and binds tightly with a K_i of 20 nM. More surprisingly is the presence of NADP(H); it is derived from bacterial cells, post-expression - it was not added to buffers at any stage of the expression, purification or preparation for crystallography. Similar to carbenoxolone, which was also not replenished at any preparative stage, it has remained bound to the enzyme through out.

Several of these crystals were soaked into a solution containing one of the novel inhibitors from this research. The inhibitors used in the soaking experiments are shown in table 6.3. These particular compounds were chosen as they exhibited

inhibition in both mouse and human enzyme assays, or a strong inhibition in either one of the species.

Table 6.3: Table listing the ten compounds discovered using virtual screening which were soaked into the crystals shown in figure 6.6. Assay results are shown in the middle column; in vivo refers to the human 11β-HSD1 expressed in HEK-293 cells. Approximately a ten-fold higher concentration than the experimental K_i was used in soaking experiments.

ID:	Inhibition Assay Results:	Structure:
3	Excellent inhibition of human 11β-HSD1 in HEK-293 cells (42% at 100 μM)	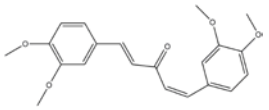
5	Inhibition in human 11β-HSD1 in HEK-293 cells (K_i 10 μM) and rat 11β-HSD1	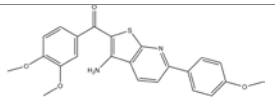
7	Good inhibition of recombinant human and *in vivo* 11β-HSD1 (K_i 4.5 μM). Mouse and rat 11β-HSD1 also show excellent inhibition.	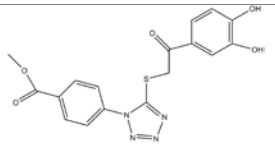
10	Good inhibition in recombinant (K_i 25 μM) and *in vivo* human 11β-HSD1 (K_i ~ 4 μM). Also with rat 11β-HSD1.	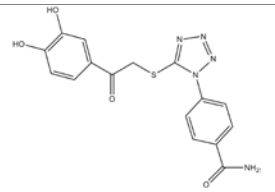
21	Human 11β-HSD1 *in vivo* (IC_{50}=7.6 μM). Significant inhibition in mouse (95 %) and rat (95%) 11β-HSD1 in cells at 500 μM.	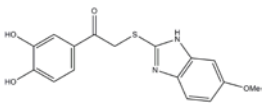
28	Good inhibition in human 11β-HSD1 *in vivo* (26 % at 1 mM) and rat (30 % at 1 mM).	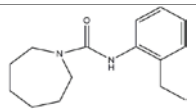
29	Human *in vivo* (IC_{50}=10 μM) and rat 11β-HSD1 (43 % at 100 μM) showed inhibition.	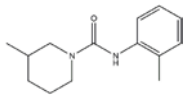
37	Recombinant (K_i ~ 200 μM) and *in vivo* human 11β-HSD1 (K_i 10 μM) 30 % mouse 11β-HSD1 at 10 μM Rat 11β-HSD1 100 % at 10 μM.	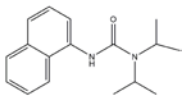
46	Inhibition in recombinant (K_i ~ 100 μM) and *in vivo* (K_i 4.5 μM) human 11β-HSD1. Also in mouse (54%) and rat 11β-HSD1 (100% at 100 μM).	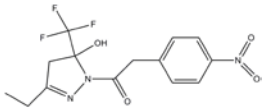
56	Inhibition in recombinant (K_i 23 μM) and *in vivo* (82% at 100 μM) human 11β-HSD1. Also in mouse (72%) and rat (100%) 11β-HSD1 at 100 μM.	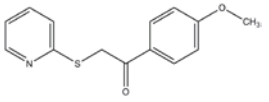

In particular, one compound was found to decrease the occupancy of carbenoxolone in the active site: compound 28. This ligand was added to a final concentration of 500 μM to mother liquor, into which the crystal was soaked. The occupancy of carbenoxolone decreased from ~ 90 % to ~ 75 % in crystals soaked with compound 28. Unfortunately there is no visible electron density for compound 28, and further refinements of the crystal / soaking conditions are required. This protein crystal diffracted to 2.71 Å at the Diamond Light Source Synchrotron (Oxfordshire, U.K) and may be seen in figure 6.8 as 4 11β-HSD1 monomers in the crystal unit forming a tetramer. Carbenoxolone may be seen interacting with Tyr 183, Ser 170 and Asp 259 in the active site, in addition to hydrogen bonding interactions with the co-factor pentose hydroxyls.

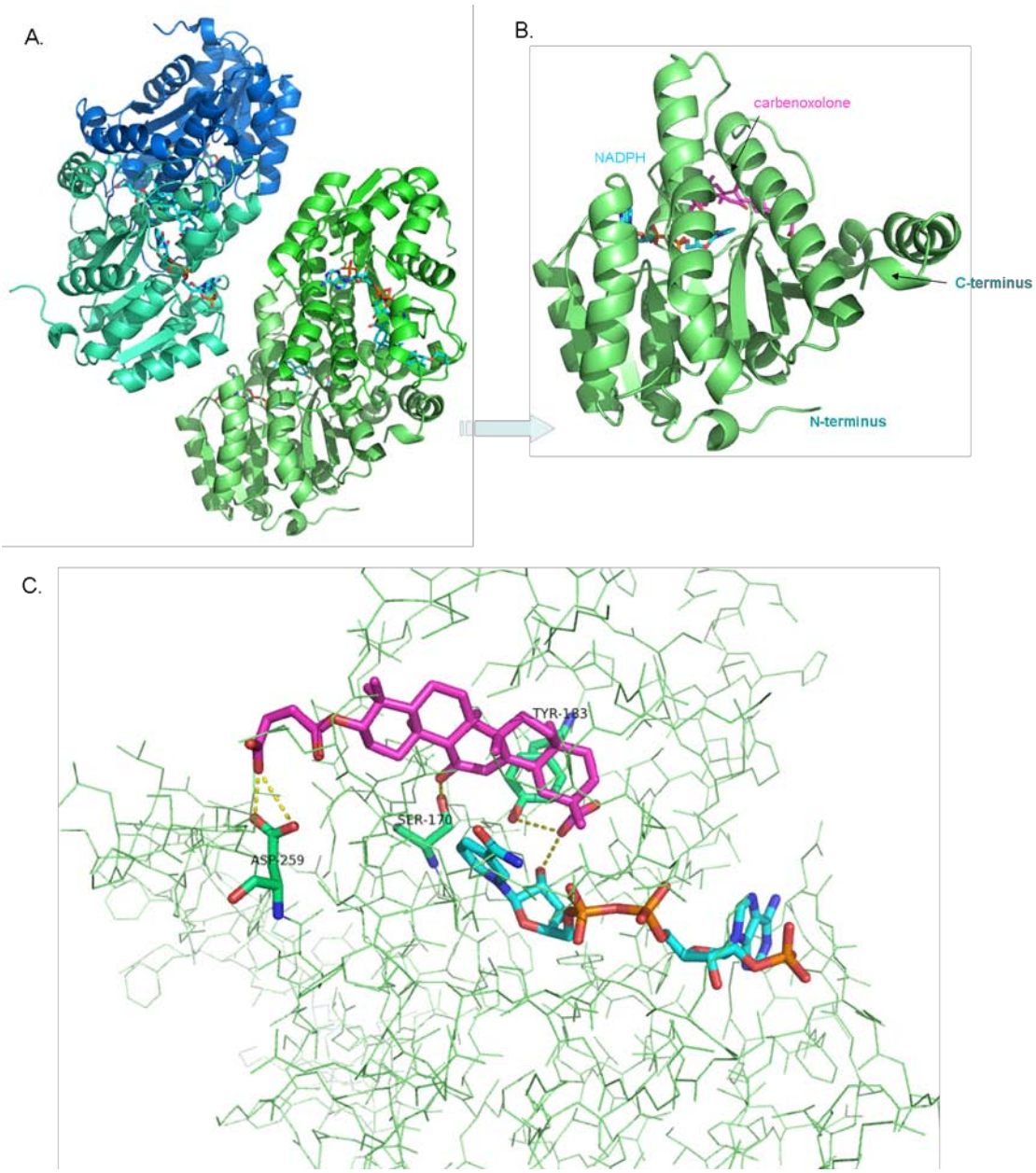

Figure 6.8: (A) 3-D representation of murine 11β-HSD1 tetramer in complex with carbenoxolone to a resolution of 2.71 Å, each subunit is a different colour. (B) One monomer, with N- and C-termini labelled, (C) aerial view of active site, showing CBX and NADPH and the interactions with the active site. Polar interactions are shown in yellow dashed lines. Image prepared with Pymol.

Similar to the human–carbenoxolone co-crystal structure (2BEL, figure 1.19), there are polar interactions between the enzyme and Tyr 183 and Ser 170; two members of the catalytic triad. In mouse 11β-HSD1, there is an additional interaction with Asp 259, which is not observed in 2BEL, the human structure. In both cases, Leu 217 is

positioned parallel to the plane of carbenoxolone's steroidal rings at a distance of 3.5 Å, potentially allowing for interaction although this is not observed in the mouse structure. The aspartic acid at position 259 in the mouse structure is perpendicular to the steroidal ring plane and is able to form hydrogen bonds with the carbenoxolone tail, as depicted in figure 6.8. In the human structure, this residue lies ~ 6 Å away from the ligand preventing interaction.

The crystal data was refined by Dr. McNae using the program Phenix (Adams et al 2002) to obtain an R-value of 20.97 % and an R-free of 25.78 %. The R-value is a reflection of how well the X-ray crystallographic data and the proposed crystallographic model agree. As a general rule, this value ranges from 0 to 0.35 in refined structures - a smaller value of R suggesting a closer agreement between the calculated and the observed data and so is an important indicator in model quality (Rhodes 1992). The crystal belongs to a C 2 2 2_1 space group (C centred orthorhombic).

The mouse variant of 11β-HSD1 is easier to crystallise compared to the human form; this is the third mouse crystal structure obtained by the Walkinshaw research group, two structures in complex with carbenoxolone (including this research) and one with another tight binding inhibitor (not from this series).

6.5 Crystallography of Human 11β-HSD1

Human 11β-HSD1 protein was prepared for crystallography with an initial purification of IMAC, followed by a gel filtration step to yield a homogeneous, pure sample as shown with SDS-PAGE. Protein samples should be as pure and as homogeneous as possible for commencing crystallisation screens; the 11β-HSD1 sample was checked for sufficient activity with a fluorescence assay and densitometric analysis employed to determine the relative purity. Human 11β-HSD1 was concentrated to 24 mg/ml in a buffer of 500 μM NADPH, 0.01 % Thesit, 1 mM EDTA, 50 mM Tris pH 7.7, 50 mM NaCl and 2 % glycerol.

A recently deposited crystal structure from Amgen Inc. (Johansson et al 2008b) under the PDB code 3BYZ has published crystallisation conditions for the co-crystallisation of human 11β-HSD1 in complex with a novel inhibitor currently in development;

(5S)-2-(cyclooctylamino)-5-methyl-5-propyl- 1,3-thiazol-4(5H)-one – a ligand from the thiazolone class of inhibitors produced by Amgen / Biovitrum. These crystals, which were obtained with vapour diffusion and diffracted to a resolution of 2.69 Å, were derived in the following conditions; 25 % polyethylene glycol (PEG) 3350, 0.1 M Sodium Citrate pH 5.6, 0.2 M ammonium acetate, at a temperature of 298 K (24.85 ^{o}C). These conditions and others are shown in table 6.1. Using these conditions as guidance, crystal plates were set up in this research with varying PEG 3350 (15 % - 35 %), varying ammonium acetate (0.2 M, 0.4 M, 0.6 M) and varying pH of 0.2 M sodium citrate. The hanging drop method is detailed in chapter 7 - Materials and Methods. Two of these conditions provided micro-crystals; conditions are shown in table 6.4 below. As can be seen, the published conditions and those determined in this research are extremely similar with the exception of a higher concentration of precipitant required in this research. This is potentially due to a lower concentration of salt in the protein buffer, which is not disclosed by Amgen (Johansson et al 2008a) in this instance.

3BYZ	**Condition 1:**	**Condition 2:**
25 % PEG 3350 0.1 M Na Citrate pH 5.6 0.2 M ammonium acetate 298 K	21 % PEG 3350 0.2 M Na Citrate pH 5.2 0.6 M ammonium acetate 290.15 K	23 % PEG 3350 0.2 M Na Citrate pH 5.2 0.6 M ammonium acetate 290.15 K

Table 6.4: Table showing the conditions used for 3BYZ and the two conditions which produced micro-crystals in this research. All conditions formed crystals under hanging drop conditions.

A photograph of the micro-crystals obtained in one of these conditions is shown in figure 6.9. Regrettably, these crystals were too small and too fragile to allow for fishing, mounting and screening of the crystals.

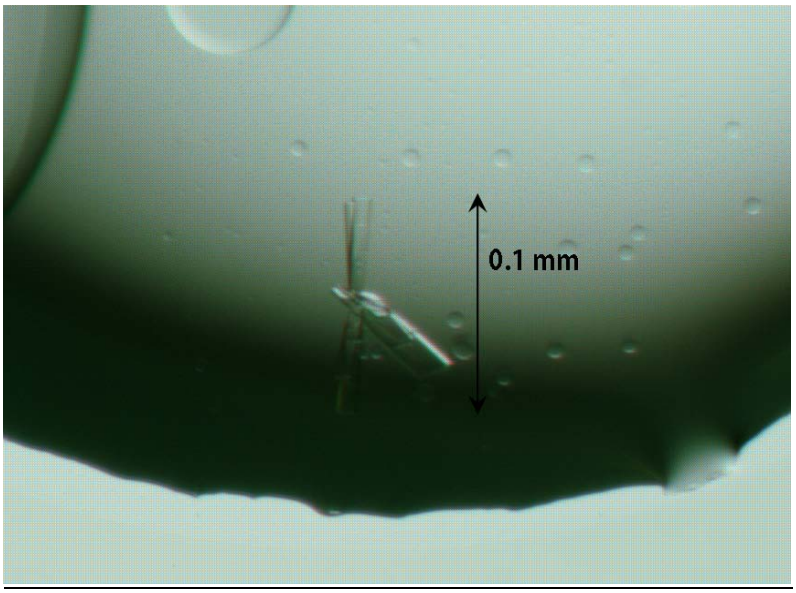

Figure 6.9: Photograph taken with a Nikon DXM1200 camera attached to a Nikon SMZ100 microscope; A: a drop containing 24 mg/ml human 11β-HSD1, 21 % PEG 3350, 0.2 M sodium citrate pH 5.2, 0.6 M Ammonium Acetate, grown over 48 hours at 290.15 K.

Similar conditions were set up with the addition of one or more varying inhibitors, discovered using the UFSRAT algorithm and EDULISS (chapter 4). These were inhibitors found to have a high affinity for the human enzyme.

In addition to reproducing the published conditions for 3BYZ, alternative initial screens for crystallisation were performed; these consisted of screening a range of pH from 5 – 7 (using sodium cacodylate, MES and piperazine), a range of PEG 3350 (10 – 50 % v/v) and / or varied $(NH_4)_2SO_4$ (10 – 45 % v/v). An ammonium sulphate solubility screen is shown in figure 6.10. As expected, PEG shifts the solubility to the left, as it is a precipitant. Thesit has a mild effect, also decreasing the solubility, in contrast to very little effect on the mouse enzyme (*c.f.* figure 6.3).

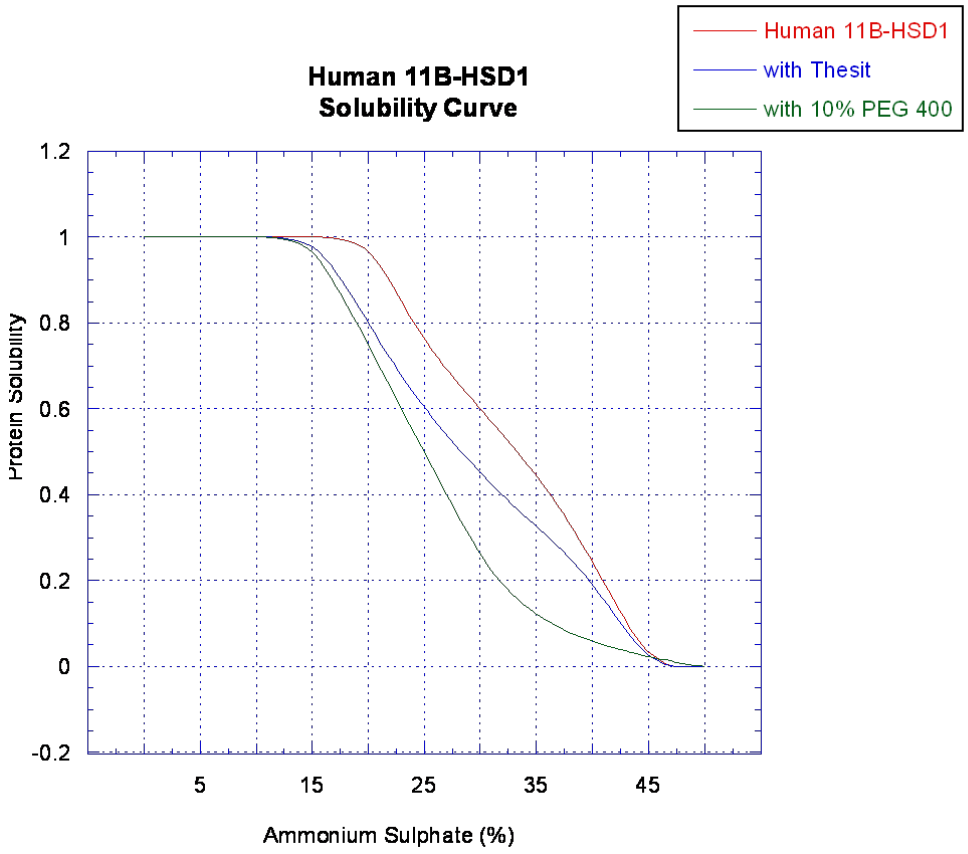

Figure 6.10: Solubility of human 11β-HSD1 with increasing $(NH_4)_2SO_4$ concentration, as a v/v percentage of a 3.5 M solution. Solubility has been normalised, with clear drops assigned a value of 1 and fully precipitated drops assigned a value of 0. Values of 0.4 – 0.6 are phase changes, and were wells in which micro-crystals were observed.

Interestingly, the 'wild-type' enzyme precipitated immediately in the presence of sodium cacodylate pH 5.0 whereas the mutant variant did not (not shown). Several wells under the relatively wide ranging conditions of sodium cacodylate (pH 5 -6) and $(NH_4)_2SO_4$ (10 – 25 % v/v of 3.5 M solution) produced micro-crystals. These resembled a small crystalline cluster in the centre of the drops, and were tested for protein content with the addition of IZIT (Hampton Research). IZIT is a blue protein dye which may distinguish between salt and protein crystals. The micro-crystals rapidly absorbed the dye; however despite further optimisation did not grow beyond ~ 0.1 mm and were fixed to the siliconised cover slip. This optimisation involved additives such as ligands (chapter 4) and DTT, and variation in the ratio of protein to reservoir solution, from 1:1, to 1:2 and 1:3.

Several commercial screens were also tested for protein crystallisation conditions. These were sparse matrix screens (Hampton Research) with widely varying pH, salt and precipitants, and a membrane-protein screen which contains varying additives suitable for the crystallisation of relatively hydrophobic proteins.

6.6 Conclusions

Crystallisation of 11β-HSD1 is a difficult and intricate process. It was possible to obtain crystals of mouse and human 11β-HSD1 (Δ1 - 23) which appeared as needle clusters or micro-crystals, often unsuitable for X-ray studies, and were used in seeding experiments. Seeding into fresh wells produced single, thin rod shaped crystals. In addition, varying the crystallisation conditions for mouse 11β-HSD1 produced several small rod-like crystals which diffracted to 2.71 Å and enabled a good quality crystallographic model to be constructed and refined. This will enable future soaking experiments with the novel inhibiting compounds from chapter 5 to be carried out with the anticipation of a co-complex structure.

Ammonium sulphate screens for both mouse and human 11β-HSD1 were carried out, and it was observed that mouse 11β-HSD1 will begin to nucleate at a slightly higher concentration of $(NH_4)_2SO_4$ than human enzyme. The mutation at residue 272 in the human 11β-HSD1 (C272S) did not facilitate crystallisation in this research, and did not affect the solubility curve of the enzyme; however did stabilise the protein at lower pH. Crystallisation trials with this variant of human 11β-HSD1 are ongoing to produce larger single crystals.

Future work would involve further screening; potentially not dissimilar to published conditions, addition of the novel inhibitors to stabilise the overall structure from an earlier stage (potentially prior to or during purification) or would involve the mutagenesis of one or more residues (following the example from Bristol-Myerrs Squibb, PDB accession code 3CH6, Wang et al 2008) such as leucine 262 to arginine, and phenylalanine 278 to glutamic acid.

CHAPTER 7

MATERIALS AND METHODS

7.1 Cloning and Expression Methods

The methods employed with all three species of 11β-HSD1 are identical, except where noted in the text.

Murine and Human 11β-HSD1: Expression Vectors

The base pairs 70 – 876 (amino acids 23 – 292) of human 11β-HSD1 DNA and base pairs 70 – 876 (amino acids 23 – 292) of murine 11β-HSD1 were cloned into the pET-28b expression vector (Novagen). These expression plasmids in addition to the bacterial expression plasmid pGro7 encoding GroEL and GroES (Takara, Japan) were a generous gift from Dr. Scott Webster at the Endocrinology Unit at the QMRI, University of Edinburgh. The plasmid maps of both expression vectors are shown in figure 7.1.

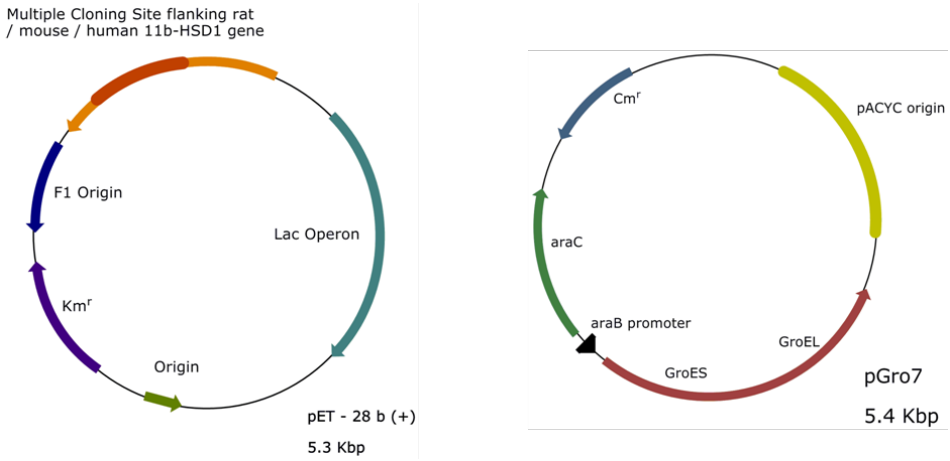

Figure 7.1: Simplified plasmid map for (a) the bacterial expression vector pET28-b and the placement of the human, mouse or rat 11β-HSD1 gene in the multiple cloning site (dark orange), the kanamycin resistance gene (Km^r), the origin of replication and the lac operon, and (b) pGro7 plasmid showing the location of the polycistronic chaperone protein genes GroEL and GroES, the araB promoter and the chloramphenicol resistance gene (Cm^r). Illustrations prepared using ChemDraw 11.0.

The full DNA sequences of human and mouse 11β-HSD1 are shown in figures 7.2 and 7.3. The segment of the 5′ end in red corresponds to amino acids 1 to 23 (in human and mouse, base pairs 1 - 69) which were truncated to facilitate expression. In black is the DNA sequence used in this research.

```
  1  ATGGCTTTTA TGAAAAAATA TCTCCTCCCC ATTCTGGGGC TCTTCATGGC
 51  CTACTACTAC TATTCTGCAA ACGAGGAATT CAGACCAGAG ATGCTCCAAG
101  GAAAGAAAGT GATTGTCACA GGGGCCAGCA AAGGGATCGG AAGAGAGATG
151  GCTTATCATC TGGCGAAGAT GGGAGCCCAT GTGGTGGTGA CAGCGAGGTC
201  AAAAGAAACT CTACAGAAGG TGGTATCCCA CTGCCTGGAG CTTGGAGCAG
251  CCTCAGCACA CTACATTGCT GGCACCATGG AAGACATGAC CTTCGCAGAG
301  CAATTTGTTG CCCAAGCAGG AAAGCTCATG GGAGGACTAG ACATGCTCAT
351  TCTCAACCAC ATCACCAACA CTTCTTTGAA TCTTTTTCAT GATGATATTC
401  ACCATGTGCG CAAAAGCATG GAAGTCAACT TCCTCAGTTA CGTGGTCCTG
451  ACTGTAGCTG CCTTGCCCAT GCTGAAGCAG AGCAATGGAA GCATTGTTGT
501  CGTCTCCTCT CTGGCTGGGA AAGTGGCTTA TCCAATGGTT GCTGCCTATT
551  CTGCAAGCAA GTTTGCTTTG GATGGGTTCT TCTCCTCCAT CAGAAAGGAA
601  TATTCAGTGT CCAGGGTCAA TGTATCAATC ACTCTCTGTG TTCTTGGCCT
651  CATAGACACA GAAACAGCCA TGAAGGCAGT TTCTGGGATA GTCCATATGC
701  AAGCAGCTCC AAAGGAGGAA TGTGCCCTGG AGATCATCAA AGGGGGAGCT
751  CTGCGCCAAG AAGAAGTGTA TTATGACAGC TCACTCTGGA CCACTCTTCT
801  GATCAGAAAT CCATGCAGGA AGATCCTGGA ATTTCTCTAC TCAACGAGCT
851  ATAATATGGA CAGATTCATA AACAAGTAGG
```

Figure 7.2: The DNA sequence of human 11β-HSD1, 876 base pairs in length (translates to 292 amino acids full length). Truncated base pairs are coloured red.

```
  1  ATGGCAGTTA TGAAAAATTA CCTCCTCCCG ATCCTGGTGC TCTTCCTGGC
 51  CTACTACTAC TATTCTACAA ATGAAGAGTT CAGACCAGAA ATGCTCCAGG
101  GAAAGAAAGT GATTGTCACT GGGGCCAGCA AAGGGATTGG AAGAGAAATG
151  GCATATCATC TGTCAAAAAT GGGAGCCCAT GTGGTATTGA CTGCCAGGTC
201  GGAGGAAGGT CTCCAGAAGG TAGTGTCTCG CTGCCTTGAA CTCGGAGCAG
251  CCTCTGCTCA CTACATTGCT GGCACTATGG AAGACATGAC ATTTGCGGAG
301  CAATTTATTG TCAAGGCGGG AAAGCTCATG GGCGGACTGG ACATGCTTAT
351  TCTAAACCAC ATCACTCAGA CCTCGCTGTC TCTCTTCCAT GACGACATCC
401  ACTCTGTGCG AAGAGTCATG GAGGTCAACT TCCTCAGCTA CGTGGTCATG
451  AGCACAGCCG CCTTGCCCAT GCTGAAGCAG AGCAATGGCA GCATTGCCGT
501  CATCTCCTCC TTGGCTGGGA AAATGACCCA GCCTATGATT GCTCCCTACT
551  CTGCAAGCAA GTTTGCTCTG GATGGGTTCT TTTCCACCAT TAGAACAGAA
601  CTCTACATAA CCAAGGTCAA CGTGTCCATC ACTCTCTGTG TCCTTGGCCT
651  CATAGACACA GAAACAGCTA TGAAGGAAAT CTCTGGGATA ATTAACGCCC
701  AAGCTTCTCC CAAGGAGGAG TGCGCCCTGG AGATCATCAA AGGCACAGCT
751  CTACGCAAAA GCGAGGTGTA CTATGACAAA TCGCCTTTGA CTCCAATCCT
801  GCTTGGGAAC CCAGGAAGGA AGATCATGGA ATTTTTTTCA TTACGATATT
851  ATAATAAGGA CATGTTTGTA AGTAAC
```

Figure 7.3: The DNA sequence of mouse 11β-HSD1 which is 876 base pairs in length (translates to 292 amino acids full-length), truncated base pairs are red.

Transformation

The expression vectors pET-28b-mHSD1 for murine (or pET-28b-hHSD1 for human) and pGro7 were co-transformed into chemically competent BL21(DE3) *Escherichia coli*

cells (Calbiochem) by the following method. The cells were always sourced commercially. Cells were thawed on ice for 10 minutes, after which 1 μl of pET-28b-mHSD1 and 1 μl of pGro7 were added to the cells. The cell mixture was left on ice for a further 10 minutes, and then heat-shocked at 42°C for 45 seconds in a heat block. The cell mixture was then returned to ice for a further 5 minutes. LB media (1 ml) was added to the cells followed by incubation at with shaking 37°C for a 45 minute recovery period. The transformed cells are then spun down gently (3000 rpm, 5 minutes) and plated on room temperature LB agar plates containing both 50 μg/ml kanamycin and 50 μg/ml chloramphenicol (both Sigma-Aldrich Inc., U.K). The plates were then incubated overnight at 37°C.

Starter Culture

One colony was picked from the inoculated LB-agar plate and grown in 25 ml LB media with 50 μg/ml kanamycin and 50 μg/ml chloramphenicol. The cultures were incubated at 37°C, shaking at 250 rpm until reaching an OD_{600} of 0.6, then stored at 4°C until further use. This culture was then used to inoculate a larger scale culture at a 1 % v/v ratio.

Expression Trials

Expression trials were carried out in either a 50 ml falcon tube containing a volume of 5 ml culture media, or alternatively in 250 ml glass expression flasks, containing 50 ml of culture media to ensure adequate aeration of the cultures, which were shaken at 250 rpm (i.e. the flasks were filled 10 – 20 % of the total volume capacity with LB media). The final culture was centrifuged to pellet the cells, which were then lysed and the soluble and insoluble fractions separated through centrifugation. These samples and a whole cell fraction were then run on 12 % SDS-PAGE.

Large Scale Grow-ups

Larger scale *E.coli* cultures of 4 – 8 L were carried out as follows. In a 2 L glass conical flask, 500 ml of LB (with 50 μg/ml kanamycin and 50 μg/ml chloramphenicol) were inoculated with 5 ml of starter culture. The culture was incubated at 37°C, shaking at

250 rpm until the bacterial culture reached an OD_{600} of 0.6. At this point, the incubation temperature was reduced to 20°C and 0.1 % v/v L-arabinose, 1 % glucose, and 1 % sucrose was added to the culture to induce the expression of the molecular chaperones. After 1 hour incubation, a final concentration of 100 μM carbenoxolone (Sigma, prepared in 100% ethanol) and 1 mM IPTG (Melford Laboratories) were added to the culture. They were then left for 16 hours at 20°C to over-express 11β-HSD1. The cultures were then harvested the following day by collection of the cells via gentle centrifugation (Beckman Coulter Avanti j-26 XPI centrifuge, JLA 8.1000 rotor) at 15,000 rpm at 4°C for 45 minutes. The cell pellet was either snap-frozen in liquid nitrogen and stored at -20°C for later use, or resuspended in lysis buffer (50 mM Tris pH 8.0, 150 mM NaCl, 20 mM imidazole, 0.01 % v/v thesit) and the cell lysis procedure carried out.

Cell Lysis and Clarification

Cell pellets were resuspended in lysis buffer (50mM Tris pH 8.0, 150mM NaCl, 20mM imidazole, 0.01% v/v thesit) by vortexing and inversion, with one EDTA-free mini-protease inhibitor tablet (Roche Diagnositics, U.K) per 500ml culture added. Once completely resuspended and smooth, the cell suspension was filtered crudely prior to using a cell disruptor (Constant Systems Ltd, U.K) at a pressure of 20 – 25 KPsi. This disrupts the cell membranes and liberates cytoplasmic proteins. The cell lysate was then clarified through centrifugation at 50,000 rpm, 4°C for 30 minutes (Beckman Coulter Avanti J-26 XPI centrifuge, JA25.50 rotor). The clarified lysate was filtered through a 0.22 μm filter unit (Millipore, Co. Cork, Ireland) and applied to a chromatography column for purification.

Rat 11β-HSD1: Cloning and Expression

Source and Expression Vectors

The rat 11β-HSD1 DNA was purchased from Codon Devices (Codon Devices Inc, Cambridge, MA), a company which synthesises specified genes. The gene sequence was provided (from GenBank NM_017080.2) for Codon Devices where it was codon optimised for *E. coli* and synthesised. The sequence is shown in figure 7.4.

```
  1  ATGAAAAAAT ACCTCCTCCC CGTCCTGGTG CTCTGCCTGG GTTACTACTA
 51  TTCTACAAAT GAAGAGTTCA GACCAGAAAT GCTCCAGGGG AAGAAAGTGA
101  TTGTCACTGG GGCCAGCAAA GGGATCGGAA GAGAAATGGC ATATCATCTG
151  TCAAAAATGG GAGCCCATGT GGTATTGACT GCAAGGTCGG AGGAAGGGCT
201  CCAGAAGGTG GTGTCTCGCT GCCTTGAACT CGGAGCAGCC TCTGCTCACT
251  ATATTGCCGG CACTATGGAA GACATGGCTT TTGCAGAGCG ATTTGTTGTT
301  GAGGCAGGAA AGCTCTTGGG TGGACTGGAC ATGCTCATTC TCAATCACAT
351  CACACAGACC ACTATGTCTC TCTTCCACGA TGATATCCAC TCTGTGCGAA
401  GAAGCATGGA GGTCAACTTC CTCAGCTATG TGGTCCTGAG CACAGCAGCC
451  TTGCCCATGC TGAAACAGAG CAATGGCAGC ATTGCCATCA TCTCCTCCAT
501  GGCTGGGAAA ATGACCCAAC CTCTGATTGC TTCCTACTCT GCAAGCAAGT
551  TTGCTCTGGA TGGGTTCTTT TCCACCATTA GAAAAGAACA CTTGATGACC
601  AAGGTCAACG TGTCCATCAC TCTCTGTGTC CTCGGCTTCA TAGACACAGA
651  AACAGCTTTG AAAGAAACCT CTGGGATAAT CTTGAGTCAA GCTGCTCCCA
701  AGGAGGAATG CGCCCTGGAG ATCATCAAAG GCACAGTTCT GCGCAAAGAT
751  GAGGTATACT ATGACAAATC ATCTTGGACT CCACTTCTGC TTGGGAATCC
801  AGGAAGGAGG ATCATGGAAT TTCTTTCATT ACGGTCATAT AACAGGGACC
851  TATTTGTAAG CAACTAG
```

Figure 7.4: The rat DNA sequence, taken from GenBank, 867 base pairs, which translates to 289 amino acids. Shown in red are the base pairs which are not present in the cDNA used in this research (base pairs 1 to 57, corresponding to amino acids 1 - 19).

The sequence was designed to contain the consensus sequences for the restriction enzymes NdeI at the 5′ end and XhoI at the 3′ end to facilitate cloning, as shown in figure 7.5. In addition, the sequence had been codon-optimised by Codon Devices, to facilitate expression in *E. coli*. Cloning was required to exchange expression vectors from the pUC19 vector in which it was supplied, into the pET28b vector desired. Cloning was carried out using enzymes and recommended reagents from New England Biolabs Inc. The first 19 membrane-anchoring residues of the rat enzyme were truncated (similar to the human and mouse sequences) to improve the solubility profile of the enzyme.

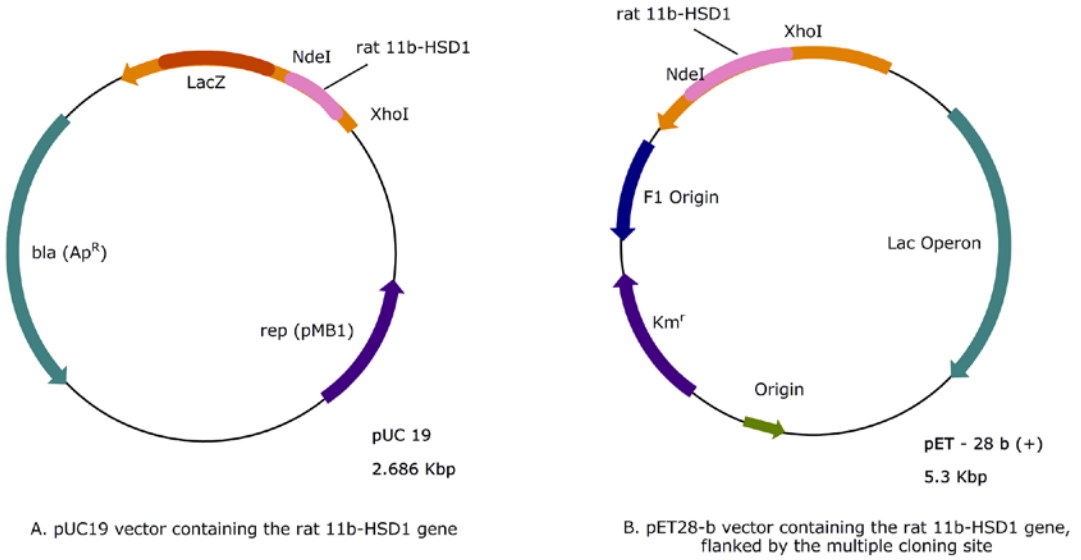

A. pUC19 vector containing the rat 11b-HSD1 gene

B. pET28-b vector containing the rat 11b-HSD1 gene, flanked by the multiple cloning site

Figure 7.5: Expression plasmid pUC-19 (Fermentas, left) and the location of the rat 11β-HSD1 gene. Expression plasmid pET28-b (Novagen) is shown on the right, with the location of the rat 11β-HSD1 gene shown. Picture prepared with ChemDraw 11.0.

Cloning: Preparation of the receiving vector pET28-b

An aliquot of DH5α chemically competent cells (Invitrogen) was transformed with the pET28-b vector (approximately 10 ng) and plated out on 50 μg / ml kanamycin LB-agar plates. A 10 ml overnight culture from one colony was prepared for DNA extraction using a mini-prep kit, following manufacturer's instructions (QIAprep spin miniprep kit, Qiagen Ltd, U.K). The DNA extracted from the transformed bacterial cells was sent for sequencing at the Edinburgh University Sequencing Service. Once verified, this expression plasmid was run on a 1 % agarose gel containing ethidium bromide and visualised with an ultraviolet light box. The amount of DNA was quantified from the gel. A double digestion was set-up for the remaining pET28-b vector. This consisted of: Xho1 (1.4 μl: equivalent to 28 enzyme units), Nde1 (1.4 μl: equivalent to 28 enzyme units) and buffer 4 (10 mM Tris-HCl, 50 mM KCl, 1 mM DTT, 0.1 mM EDTA, 200 μg / ml BSA, 50 % glycerol) provided by NEB (total volume: 14 μl reaction, 2 hours at 37°C). After 60 minutes, the DNA was dephosphorylated with CIP (calf intestinal phosphatase, 0.5 units per 1 μg DNA, NEB Inc.) which removes the 5′ phosphate groups from the newly cleaved expression vector, and was incubated for a further 60 minutes at 37°C. The final reaction mixture was run on a 1 % agarose gel to purify the products and the

corresponding band (at 5.3 Kbp) was excised from the gel and extracted (Gel Extraction Kit, Qiagen Ltd, U.K). The cleaved vector was stored at -20°C until use.

Preparation of the Synthesised DNA Insert (*Rattus Norvegicus* 11β-HSD 1)

The online tool 'Webcutter' (http://rna.lundberg.gu.se/cutter2/) was used to ensure the codon optimised sequence would not be digested by restriction enzymes except at the two specified regions. Chemically competent DH5α cells (Invitrogen) were transformed with pUC19-rattus-11bHSD1 (approximately 50 ng). The lyophilised gene supplied from Codon Devices was resuspended in sterile ddH_2O giving a final concentration of 5 μg / 50 μl (100 ng/ μl). The transformed cells were plated out on 100 μg / ml ampicillin LB-agar plates. One colony was picked and inoculated in an overnight culture for DNA extraction with a MiniPrep kit (Qiagen Ltd, U.K). The extracted DNA was doubly digested with Xho1 (1.4 μl) and Nde1 (1.4 μl), buffer '2' (10 μl) (total volume: 14 μl reaction, 2 hours at 37°C). The products were gel-purified as before and extracted from the gel as described previously.

Ligation of the Expression Vector and DNA Insert

Ligation reactions were attempted with the Rapid Ligation Kit (Roche) and with T4 DNA Ligase (NEB), varying the insert to plasmid ratio and varying the incubation times and temperatures according to each manufacturer's recommendations until a ligated product was detected. The successful reaction consisted of 1 μl of T4 DNA Ligase (NEB) in a total reaction volume of 20 μl, overnight at 18°C. The insert (100 ng / μl) to plasmid (also 100 ng / μl) ratio was 10:1. The ligation products were run on a 1 % agarose gel to separate the reaction components and the corresponding gel band (the pET28-b + rat 11bHSD1 gene) at 5.4 Kbp) was extracted as described previously. This DNA was transformed into chemically competent DH5α cells and plated out overnight on 50 μg / ml kanamycin LB-agar plates. Several colonies were picked and used to inoculate separate overnight cultures (5 ml LB media) for DNA extraction. The extracted DNA from the transformed DH5α cells was then doubly digested, as described previously. Running the reaction products on an agarose gel (1%, with ethidium bromide, as before) ensures that both components are present. A band for

the digested vector is clearly seen in addition to a smaller band for the digested gene insert. The DNA was also sent for sequencing.

Expression Trials

The pET28-b-rat-11bHSD1 plasmid was transformed into chemically competent BL21(DE3) cells in addition to the pGro7 plasmid (for GroEL/ES expression). Initial expression trials with the rat variant determined that it was present in the insoluble fraction, thus it was decided to attempt re-solubilisation of the protein.

Extracting Insoluble Rat 11β-HSD1 through Denaturation

For this experiment, BL21(DE3) cells containing expressed rat 11β-HSD1 were harvested and spun for 45 minutes at 8000 rpm in a centrifuge (Beckman Coulter Avanti J-26 XPI centrifuge). To the resultant cell pellet (equivalent to 1 L of bacterial cell culture) 50 ml of the denaturation solution (8 M Urea, 100 mM Tris pH 8.0, 300 mM NaCl) was added and the cells resuspended, then filtered under vacuum (Whatman No.1 filter paper). Ideally, the supernatant will contain a host of denatured and previously insoluble proteins. Due to the presence of the hexa-His tag on the N-terminus of the rat enzyme, the protein should still bind to an IMAC column, as it does not require an intact structural integrity unlike tags such as GST (glutathione-S-transferase). The filtrate was spun again at 8000 rpm (Beckman Coulter Avanti J-26 XPI centrifuge) and the supernatant was then loaded onto an equilibrated IMAC column (both 1 ml HiTrap Chelating Column, (GE Healthcare) and a 3 ml Superflow Ni-NTA gravity column (Qiagen)) charged with Ni^{2+} ions. Elution from the IMAC column was achieved through step-wise variation of the buffer pH; decreasing the pH will cause protonation of the histidine weakening the binding of this residue to the chelated metal until it detaches, as shown in figure 7.6.

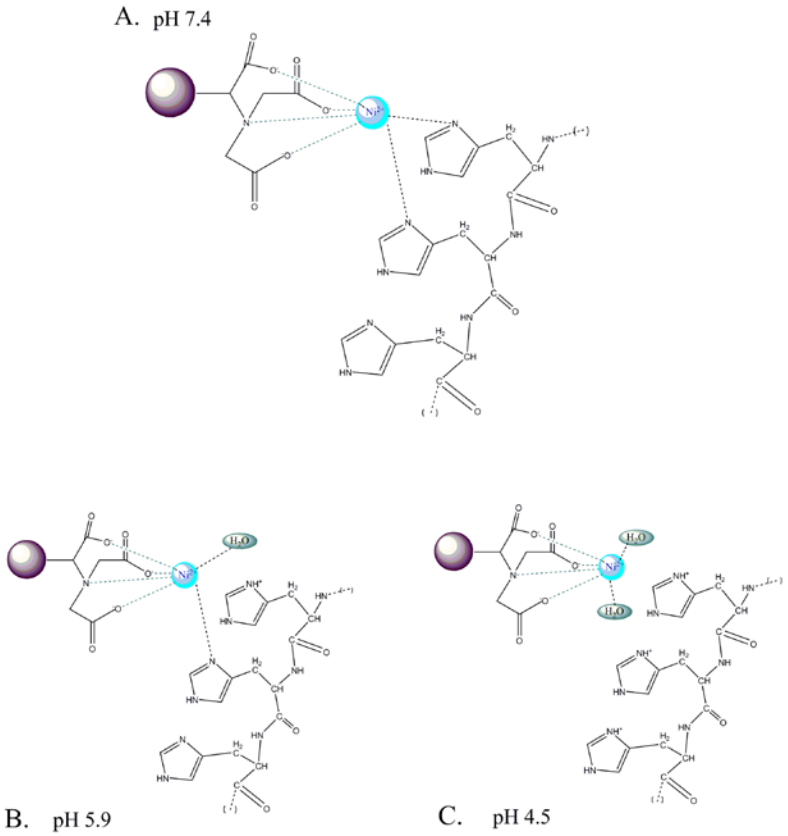

Figure 7.6: Diagram illustrating the binding mechanisms of 2 residues of a 6 x histidine tag to the IMAC Ni^{2+} chelated NTA molecule, with varying pH. The pH is selected to allow protonation of the pyrrole NH in order to weaken the interaction between the histidine tag and the Ni-NTA. (A) shows binding when the pH is 7.4 : above the pKa of the pyrrole NH (pKa 6.04). Lowering the pH (below 6.04) results in protonation of the histidine residues, the lower the pH – the more residues will be protonated, as observed in B and C.

Free, unbound histidine has three pKa values which correspond to the carboxylic acid (pKa_1 1.82), the pyrrole NH (pKa_2 6.04), and the ammonium NH (pKa_3 9.17). As it is the pyrrole nitrogen which binds the divalent metal atom, it is pKa_2 that the pH is varied around. At a pH 7.4, almost all of the histidine residues will be uncharged and able to interact with the divalent nickel atom (figure 7.6A). Reducing the pH to 5.9 results in approximately half of the residues having a positive charge, which weakens the interaction between the tag and the nickel atom considerably, but is enough to remain attached while non-specific binding artefacts will detach from the solid matrix and rejoin the mobile phase (figure 7.6B). At pH 4.5 effectively all of the histidine residues will be positively charged, and the histidine tag no longer interacts

with the IMAC matrix (figure 7.6C). The buffers were freshly prepared prior to use due to the large pH drift that may occur with 8 M urea.

With this method, the column is equilibrated with buffer pH 7.4, a wash step with buffer pH 5.9, and an elution step at pH 4.5. The resultant fractions were run on 12% SDS-PAGE. However, attempts to purify the denatured enzyme with this technique were not successful as the rat 11β-HSD1 was found to elute at pH 5.9 alongside other contaminating proteins or in the flow-through fractions. It was concluded that Ni^{2+}-NTA chromatography was not a suitable technique for the purification of denatured rat 11β-HSD1, however it was used for the other species' purification.

7.2 Purification

First Step Purification for Mouse and Human 11β-HSD1: Immobilised Metal Affinity Chromatography (IMAC)

All chromatography procedures were carried out using Äkta™ explorer and FPLC™ machinery (GE Healthcare Life Sciences). Murine, human and rat 11β-HSD1 all contain an N-terminal hexa-histidine tag, by virtue of the pET28-b expression vector encoding a His-tag upstream of the multiple cloning site. Exploiting the affinity of the amino acid histidine for divalent metal cations is a classic, efficient and simple first step procedure in purification. Several different metal cations are employed in IMAC, notably Ni^{2+}, Zn^{2+} and Co^{2+}.

Uncharged columns composed of fast-flow (FF) sepharose beads (GE Healthcare) were washed with 10 column volumes (C.V) of H_2O and charged using 100 mM $NiSO_4$ for 3 C.V. The average column volume for the first step procedure (for an initial *E. coli* culture volume of 2 L) was a 1 ml column. Buffers used in this purification step were binding buffer (50 mM Tris pH 8.0, 150 mM NaCl, 20 mM imidazole, 0.01 % v/v thesit) and elution buffer (50 mM Tris pH 8.0, 150 mM NaCl, 500 mM imidazole, 0.01 % v/v thesit). Once the column is charged with divalent cations, it was washed with 5 C.V of binding buffer and then a 'ghost run' performed, where the concentration of elution buffer is gradually increased from 0 – 100 % over a short time period. The column was again washed with binding buffer until a steady UV baseline was achieved. The clarified, filtered lysate - filtered under

vacuum with 0.22 μm filter paper (Whatman, GE Lifesciences) - was automatically applied to the column slowly (0.5 ml / min), followed by a protracted wash step of 25 C.V. Applying the lysate too quickly results in a lower yield eluted from the column. Although recommended flow rates for the FF IMAC 1 ml column can be up to 1 ml / min, for the purposes of purification of 11β-HSD1, slower application flow rates were found to be optimal. In addition, a lengthy wash step after application of the clarified lysate ensured less chaperone proteins were present in the final eluate. To elute 11β-HSD1 from the Ni^{2+} IMAC, the concentration of elution buffer was increased step-wise and through a steady gradient. This will elute as many of the non-specific binding material to the column as possible, without disturbing the hexa-histidine – Ni^{2+} interaction and therefore eluting the protein of interest. At approximately 20 – 30 % elution buffer (which corresponds to 100 – 150 mM imidazole) 11β-HSD1 was eluted from the column; imidazole replaces the histidines bound to the sepharose bead.

The relevant fractions were pooled (determined by visualisation on 10 – 12 % SDS-PAGE) and dialysed overnight into dialysis buffer (50 mM Tris, 50 mM NaCl, 0.01 % v/v Thesit) using a dialysis membrane (SpectraPor Dialysis Tubing, Spectrum Labs) with a dilution factor of 1000:1. Alternatively, it was applied to a rapid desalt column.

Rapid Desalt

A rapid desalt 26/10 column (GE Healthcare) was employed to quickly and simply remove ions and other contaminating chemicals from the protein suspension. A volume of 10 ml sample is applied at one time, with one full run taking approximately 20 minutes. Dialysis buffer (50 mM Tris, 50 mM NaCl, 0.01 % v/v Thesit) was used to equilibrate and elute from the column. A lower salt concentration than 50 mM NaCl caused protein precipitation. The relevant fractions were pooled and concentrated to a final volume of 500 – 1000 μl (approximately 25 - 30 mg / ml typical concentration).

Anion Exchange Chromatography

This purification step was used only if the fractions from IMAC required further purification. Cation exchange (using a 1 ml SP-sepharose chromatography column (GE Healthcare)) was attempted and deemed unsuitable for reasons described in chapter 2. Anion exchange was selected as the enzyme was stable at higher pH values. An anion exchange binding buffer (100 mM Tris pH 9.0, 0.01 % Thesit v/v, 10 mM NaCl) was used to equilibrate a 1 ml Q-sepharose column (GE Healthcare). Samples from IMAC were desalted prior to loading onto the Q-sepharose column to eradicate imidazole and other salts which prevent the enzyme binding to Q-sepharose. Loading was followed by a wash step with low salt (20 mM NaCl). A salt gradient of 0 – 500 mM NaCl was used to elute the protein from the column, at approximately 75 mM (murine 11β-HSD1) or 100 mM (human 11β-HSD1). Fractions were run on 12% SDS-PAGE gels to ascertain which fractions contain 11β-HSD1. These fractions were then tested for enzyme activity.

Concentration and Storage of Protein

Once purified, the protein must be concentrated for crystallization trials. The buffer solution is exchanged through dialysis for one with a low Hepes / Tris concentration (20 mM), minimal salt (20 mM) and a low volume of detergent. The crystallization buffer is 20 mM Tris pH 7.8, 20 mM NaCl, 1 mM EDTA, 1 % glycerol. Alternatively, the protein was buffer exchanged into assay buffer (20 mM Tris pH 8.0, 50 mM NaCl). Protein samples were concentrated using either one of two methods.

1. A Vivaspin (Sartorius Stedim Biotech, Germany) concentrator with a 10,000 MWCO (molecular weight cut-off) which is an ultra-filtration technique. Problems arise with protein sticking to the filtration membrane, with subsequent loss of yield. To prevent this, the Vivaspin is left on ice after concentration in a centrifuge to allow the gentle resuspension of the sample before using a needle and syringe to remove the protein sample.

2. Polyethylene Glycol flakes with a molecular weight of 20,000 daltons (PEG 20K, Sigma-Aldrich) were applied to the external side of a dialysis tubing membrane

(SpectraPor Dialysis Tubing, Spectrum Labs) which contained the enzyme preparation and soaked up liquid which passed through the membrane.

Gel Filtration Chromatography

Gel Filtration is a technique used to separate proteins on the basis of size and 3-dimensional shape. Unlike other methods of chromatography, the proteins being separated do not bind to the solid phase, but instead are 'retained' in the column for varying amounts of time dependent on the protein size and the type of matrix used in the gel filtration column. For this purpose, a Superdex 200 10/300 column (GE Healthcare) was used to separate out the various oligomeric species of human or mouse 11β-HSD 1, as the column has a molecular weight separation range of 10 KDa to 600,000 KDa and will therefore separate the expected monomeric (31 KDa), dimeric (62 KDa) and tetrameric (124 KDa) forms of human 11β-HSD 1. Superdex is a composite of dextran and cross-linked agarose with a bead size of approximately 13 μm. The buffer used was (50 mM Tris pH 8.0, 50 mM NaCl, 0.01 % v/v thesit). Runs were carried out with 200 μl of concentrated 11β-HSD1 sample at one time (typically 37 mg/ml). Calibration was carried out using the Amersham Biosciences Calibration Kit for gel filtration.

MALDI-TOF

Mass spectrometry was carried out either on full-length protein samples or on gel bands excised from SDS-PAGE gels followed by a trypsin digest procedure. For full-length samples, 1 μl (typically 10 mg /ml protein) was spotted on a gold or stainless steel mass spectrometry plate on top of which 1 μl of 20 mg / ml sinapinic acid (3,5-dimethoxy-4-hydroxycinnamic acid) was applied as a matrix. The protocol for a trypsin digest was supplied by Dr. Andy Cronshaw at the University of Edinburgh. For peptides the matrix used was 5 mg / ml CHCA (α-cyano-4-hydroxycinnamic acid). A Voyager DE-STR MALDI-TOF (Applied Biosystems) instrument was used, with analyses carried out on Voyager software.

Dynamic Light Scattering

Assays were carried out in a total volume of 100 µl. For assays with detergent, 1.6 µM enzyme and assay buffer (20 mM Tris pH 8.0, 20 mM NaCl) was used.

7.3 Assay methods

Fluorescence

Fluorescence assays were carried out on a Molecular Devices SpectraMax M5 Multimode plate reader instrument using SoftMax Pro v 5.2, Excel and Kaleidagraph to analyse the data. The excitation and emission wavelengths were 340 and 458 nm, respectively. Conditions were initially optimised and chosen with no more than 20 % of substrate conversion. Measurements were carried out in the linear range of product formation versus reaction time and enzyme concentration. Where applicable, background controls were run alongside reactions each time. For the dehydrogenase reactions, the relationship between the increase of fluorescence and the rate of $NADP^+$ reduction was initially established by generating a calibration curve using freshly prepared solutions of NADPH (Sigma-Aldrich). Samples of NADPH were prepared in assay buffer (50 mM Tris pH 7.7, 50 mM NaCl) and sterile filtered. The concentrations ranged from 0 to 500 µM although only the lower concentration points were necessary. Each concentration point was carried out in sextuplicate. The graph is shown in figure 7.7 overleaf. The calibration plot enabled the conversion of RFU obtained in activity and inhibitor assays to a concentration of NADPH produced in the reaction.

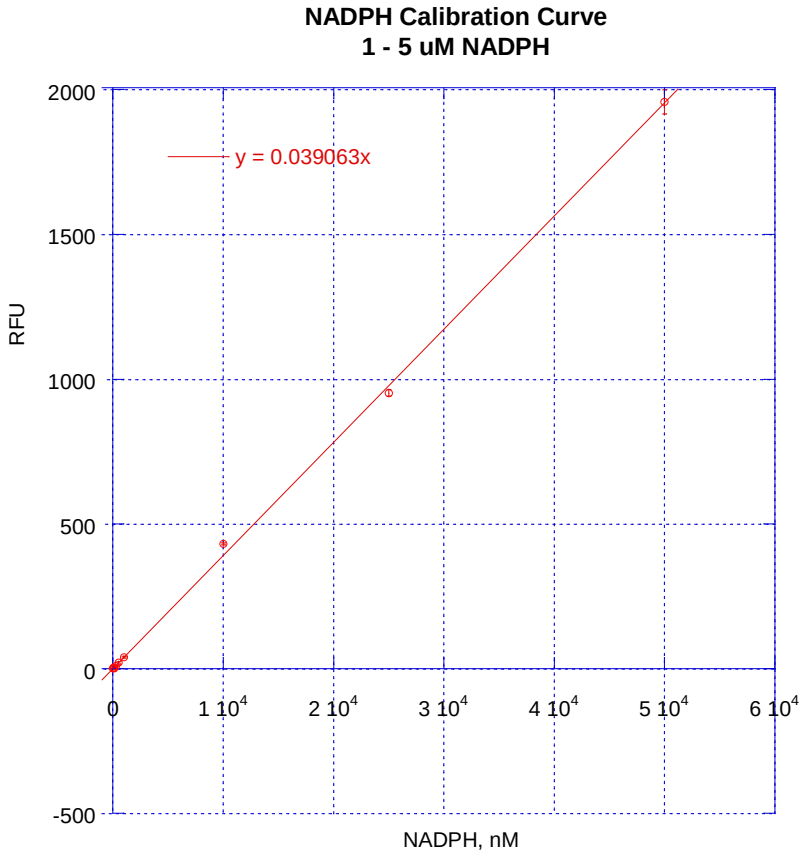

Figure 7.7: A plot of the Raw Fluorescence Units (RFU) versus the concentration of NADPH (nM) in each well, at a wavelength of 458 nm.

Activity Assays

Dehydrogenase activity assays were carried out immediately following purification and identification of fractions containing 11β-HSD1 by SDS-PAGE. A typical assay was set-up in a black 96-well microplate (Thermo-Fischer Scientific (Nunc GmbH), Germany), where each well contained a total volume of 300 µl. This consisted of 500 µM NADP, 1 µM 11β-HSD1, 2 µM cortisol (or a set volume of 30 µl with varying cortisol concentrations) and topped up with assay buffer (50 mM Tris pH 7.7, 50 mM NaCl, sterile filtered). All components except the cortisol were incubated for 15 – 20 minutes on ice. Prior to aliquoting the reaction mixture into the 96-well plate, cortisol was added. This is achieved quickly and efficiently by using a multi-channel pipette and troughs for the sample. The 96-well plate was then inserted into the fluorometer and read.

Active Site Titration

The specific activity of the dehydrogenase reaction was measured with fixed enzyme (10 μg, 3.13 μM), cortisol (50 μM) and NADP (500 μM) concentrations in a 96-well black plate with a total reaction volume of 100 μl. This was in the presence of increasing concentrations of carbenoxolone (Sigma Aldrich, U.K) at concentrations between 1 nM and 200 nM. Data were then fitted by non-linear regression to equation 9.2.

Initial Inhibitor Screens with Recombinant Enzyme (Chapter 5)

Each inhibitor compound was diluted to 10 mM in DMSO allowing for final concentrations of 100 μM and below to be achieved with a final concentration of 1 % DMSO per reaction. The initial screens were carried out in a 96-well plate with each well containing a different inhibitor at 100 μM; wells were in triplicate. A mastermix of the enzyme (10 μg), NADP (final 500 μM) and assay buffer (50 mM Tris pH 8.0, 50 mM NaCl) was pre-incubated for 20 minutes at room temperature. Substrate was added to the mastermix immediately prior to transferring into each well. Controls with carbenoxolone (100 μM) and blanks were also run adjacent to inhibitor wells. Blanks contained all components excluding enzyme. Reactions were run for a time period of 20 minutes at 25^{o}C.

Inhibitor Assays: Dose-Response Curves (Chapter 5)

Assays were carried out at room temperature (i.e. ~22^{o}C, set temperature) in an assay buffer (50 mM Tris pH 8.0, 50 mM NaCl). A typical reaction was as follows: In each well of a black 96-well plate (Nunc) a reaction was set-up with a total volume of 300 μl. This was composed of: 30 μl of inhibitor (of varying concentrations, in 10 % DMSO, which gave a final 1 % DMSO v/v concentration), 30 μl of 5 mM NADP (final concentration 500 μM), 30 μl of 2 mM cortisol (final concentration 200 μM) and 20 μg of enzyme (60 μl of 160 μg/ml). The enzyme, assay buffer and NADP were incubated together at room temperature for 20 minutes prior to adding the substrate, at which point the mixture was then immediately transferred into each well. Each well contained a different inhibitor or concentration of inhibitor. Each reaction was

carried out in triplicate. The reaction was initiated by addition of the mastermix to each well, at which point the 96-well plate was placed in the fluorometer immediately for detection to begin. Each compound had a blank run carried out, with no enzyme. This was to ensure that the compound itself did not fluoresce at the particular wavelengths used. The pH of each reaction well was also checked with pH paper to ensure the pH remained between pH 7 – 8.

K_i determination

The inhibition of 11β-HSD1 is analysed by fitting the data to equation 7.1 using Kaleidagraph:

$$V_1 = V_o\left(1 - \frac{\left([E]_o + [I]_o + K_i^{app} - \sqrt{([E]_o + [I]_o + K_i^{app})^2 - 4[E]_o[I]_o}\right)}{2[E]_o}\right) \qquad \textbf{Eqn 7.1}$$

Where $[E]_o$ and $[I]_o$ are the active enzyme and inhibitor concentration, respectively. K_i^{app} is the apparent inhibition binding constant, V_i and V_o are the rates of cortisone reduction in the absence or presence of inhibitor, respectively (Morrison, 1969).

SPA

SPA was carried out with pure recombinant protein (mouse or human) and also with mammalian cells; HEK293 cells which were transiently transfected with either human 11β-HSD1, mouse 11β-HSD1 or rat 11β-HSD1. Confluent cells were prepared by Dr. Karen Sooy or Ms. Margaret Binnie at the Queens Medical Research Institute (QMRI) at Edinburgh University.

Assays were run in a total volume of 100 µl, including 0.5 µg purified enzyme, 10 µl diluted compound (with a final 1% DMSO concentration), 10 µl [^{3}H]-cortisone (40 nM final), 10 µl NADPH (1 mM final) and 25 µl assay buffer (50 mM Tris pH 8.0, 50 mM NaCl) and 25 µl SPA buffer. The assay was initiated by the addition of the enzyme (final concentration 20 nM) which had been incubated with cortisone at 37^{o}C prior for 10 minutes, followed by 20 minute incubation with NADPH. Assay plates (96-well) were incubated on an orbital shaker for 1 hour at room temperature. At this time, 0.5 µl of 1:50 diluted anti-cortisol antibody (HyTest, Finland) and 5 ml of 15

mg/ml SPA beads in 5 ml SPA buffer were prepared. 25 µl of this preparation was added to 25 µl of each well solution. Plates were incubated for a further 2 hours at room temperature, then a radiometric quantification was carried out using a Perkin Elmer TopCount instrument.

Initial Inhibitor Screens: Cell-based Assays

Cell-based screens were carried out as described for recombinant protein except HEK-293 cells transiently transfected with 11β-HSD1 were added to the wells in place of recombinant protein.

7.4 Crystallography Methods

Murine 11β-Hydroxysteroid Dehydrogenase 1 was prepared for crystallography at 16 mg/ml in a crystal buffer (20 mM Tris pH 7.8, 20 mM NaCl, 1 mM EDTA, 1 % glycerol) and taken as 95 % pure from SDS-PAGE densitometric analysis. Human 11β-HSD1 was concentrated to 24 mg/ml - as determined by a Bradford Protein Assay - using a 1 ml or 20 ml Vivaspin concentrator (Sartorius) with a molecular weight cut off of 10,000 Daltons. The enzyme was concentrated in a buffer of 500 µM NADPH, 0.01 % Thesit, 1 mM EDTA, 50 mM Tris pH 7.7, 50 mM NaCl and 2 % glycerol. Both enzymes were assayed prior to crystallisation trials for dehydrogenase activity to show that the enzyme was active. In addition, the protein samples were centrifuged at 13000 x g, for 5 – 10 minutes at 4°C to remove any dust or precipitated protein.

Hanging Drop Method

For the hanging drop method; a 24 well plate was greased using a 50:50 preparation of paraffin wax and petroleum jelly. Into each well, 0.5 – 1.0 ml of the reservoir solution was pipetted. A volume of 0.5 – 1 µl of protein sample was pipetted into the centre of 22 mm siliconised circular cover slips, and immediately 0.5 – 1.0 µl of reservoir solution pipetted into the protein drop. A ratio of 1:1 resevoir to protein was used unless otherwise stated. The drop was not mixed and the coverslip was

immediately inverted over the well containing the corresponding reservoir solution and twisted 45° to ensure a good seal. The crystal trays were then incubated at 17°C.

Crystal Freezing

Crystals of mouse 11β-HSD1 were frozen in liquid N_2 with a solution of the mother liquor and increasing amounts of glycerol (v/v) ranging from 5 – 40 %, prior to being mounted and screened.

Crystal Seeding

Micro-crystals were crushed gently before being removed from the original drop and diluted significantly. This prevented too many crystal seeds from being added to a fresh drop. To a fresh protein-crystallisation trial, 1 µl of the diluted seeding sample was added.

11β-HSD1 Crystallography Screens using a Crystallography Robot

A multi-channel pipette was used to transfer the crystal screen (Emerald Biosystems) from the 96-well plate into the 96-well microplate for robotic crystallography trials. The crystal screens used were diluted 1:1 with ddH_2O. Once complete, these were inserted into the crystal robot (Oryx-8, Douglas Instruments) set-up, and the manufacturer's instructions followed. Drops were 0.1 µl protein, 0.1 µl reservoir. The plates were then sealed with crystal tape (Crystal Clear, Manco Inc., Ohio).

CHAPTER 8

APPENDIX

8.1 Additional Information

Alternative names:	HDL; 11-DH; HSD11; HSD11B; HSD11L; SDR26C1; MGC13539; 11-beta-HSD1; HSD11B1
EC number:	1.1.1.146

Table 8.1: Additional information for 11β-HSD1

	Human type 1	Human type 2*	Mouse	Rat
RefSeq RNA	NM_005525	NM_000196	NM_008288	NM_017080
RefSeq Protein	NP_005516	NP_000187	NP_032314	NP_058776

Table 8.2: Sequence information for human, mouse and rat 11β-HSD1 and human 11β-HSD2.

8.2 Gel Filtration: Calibration Charts (Chapter 2)

The Superdex 200 10/30 column (GE Healthcare) was calibrated prior to use using a set of proteins with a known molecular weight, oligomeric state and a regular spherical 3-D structure. From the elution volumes of this known set of proteins, the size of the test protein may be estimated. The kits for calibration are supplied by GE Healthcare Life sciences. The calibration proteins are shown in table 8.3.

Protein:	Size (KDa) :
Blue Dextran	Void Volume
Ferritin	440
Catalase	232
Aldolase	158
Ovalbumin	43
Albumin	67
Chymotrypsinogen	25
Ribonuclease I	13.7

Table 8.3: Molecular weights of calibration proteins for gel filtration chromatography.

These calibration proteins were run over the Superdex 200 according to the manufacturer's instructions (figure 8.1). The K_{AV} (the diffusion co-efficient) was calculated for each protein, according to equation 8.1.

$$K_{AV} = \frac{(V_e - V_o)}{V_t - V_o} \qquad \textbf{Eqn 8.1}$$

Where K_{AV} is the diffusion coefficient, V_e is the elution volume of the peak of interest, V_o is the void volume and V_t is the total column volume. The K_{AV} values were then plotted against the Log molecular weight to produce the calibration plot in figure 8.2. This allows an accurate estimation of protein molecular weight from a gel filtration column.

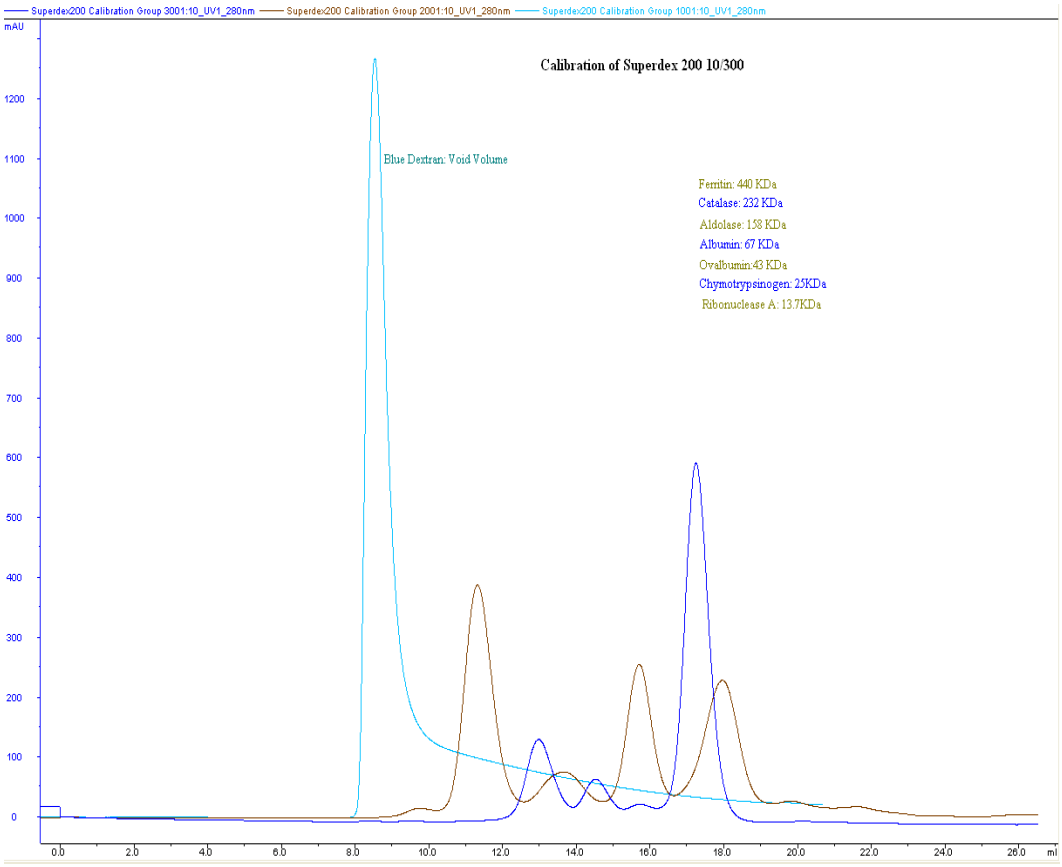

Figure 8.1: A Superdex 200 10/300 UV trace for the calibration proteins as described in table 8.3.

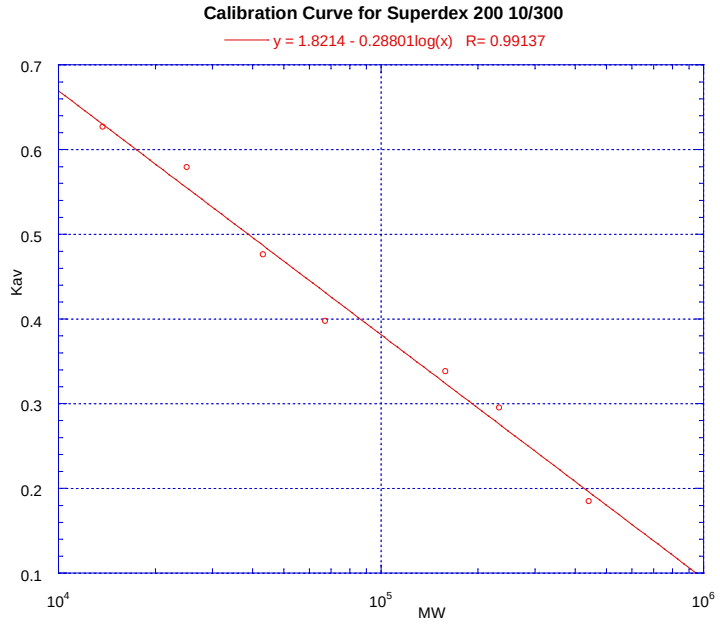

Figure 8.2: A plot of K_{AV} versus Log molecular weight (MW) for proteins eluted from the Superdex 200 10/300, prepared in Kaleidagraph.

From this calibration curve, it was possible to determine the approximate sizes of the eluted 11β-HSD1.

8.3 Trypsin Digest MALDI-TOF Results

A tryptic digest on mouse, rat and human 11β-HSD1 was carried out following the protocol provided by Dr. Andy Cronshaw. The results of the mouse digest are shown here in figure 8.3. Each peak represents a particular peptide mass from digested 11β-HSD1. This technique was carried out to validate the identity of the protein. The combination of peptides obtained, known as a protein fingerprint, will be unique for each protein, allowing an accurate identification to be made. The results from the mass spectrometer were then fed into the search engine MS-Fit, which searched through the unique fingerprints of several million proteins and quickly finds a match in the SwissProt database (expasy.ch/sprot/). The top matches are shown overleaf.

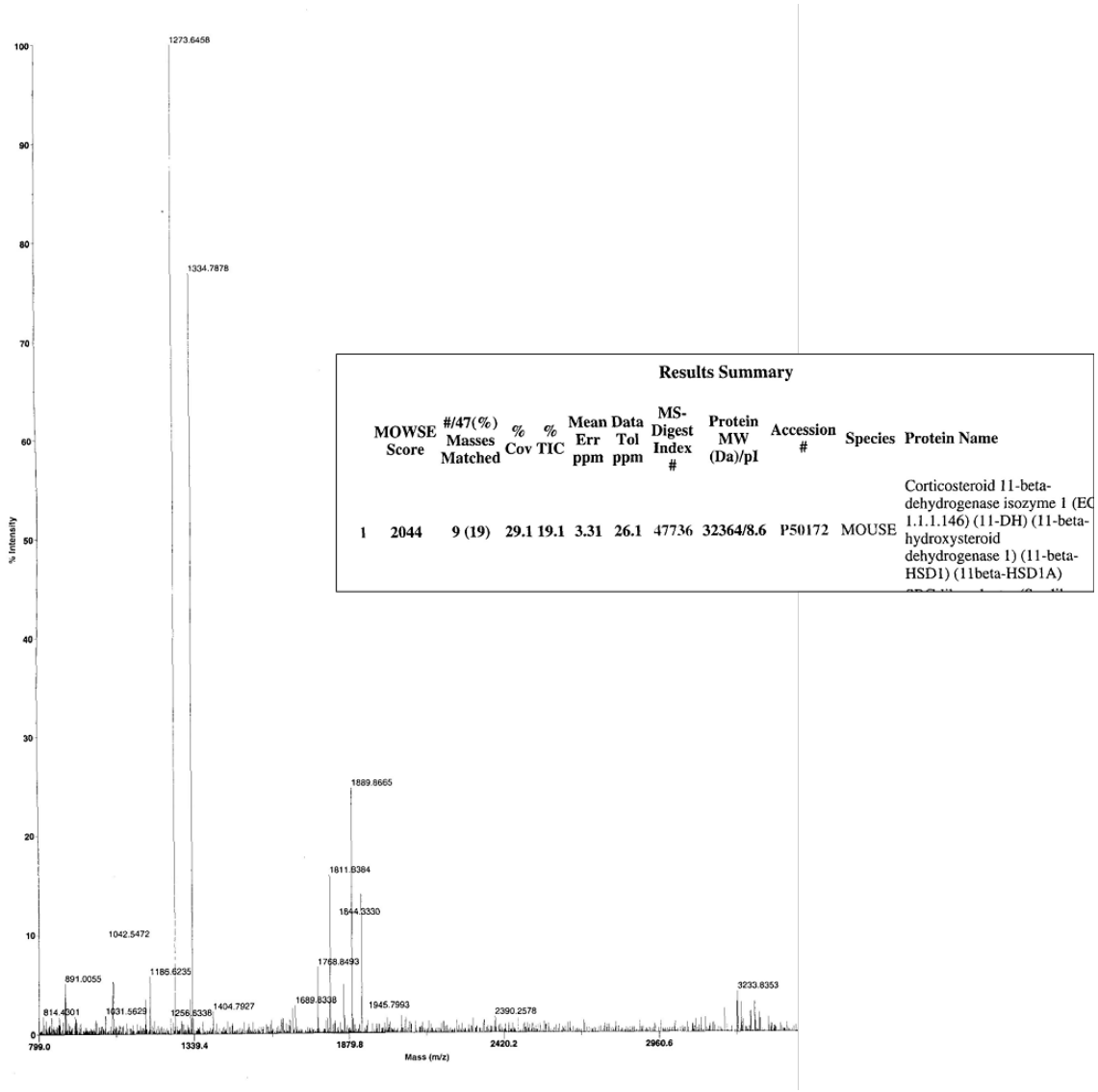

Figure 8.3: Trypsin digest fingerprint of murine 11β-HSD1. The results from the database search of the fingerprint are inset. This shows that the top hit was mouse 11β-HSD1, SwissProt accession P50172.

8.4 Candidate Ligands for the Inhibition of 11β-HSD1

The following tables show all 60 compounds which were initially selected as candidate inhibitors of 11β-HSD1. Eight of these candidate compounds were selected manually, and are labeled as such in the tables. The remaining 52 compounds were discovered through the use of virtual screening with UFSRAT. The compounds are binned into 6 structural classes;

1. Ureas (table 8.5)
2. Tetrazines and Triazoles (table 8.6)
3. Thiols (table 8.7)
4. Benzamides and amides (table 8.8)
5. Cycloheptanones, cyclohexanones and keto-groups (table 8.9 and 8.10)

8.4.1 Ureas

Table 8.5 (on next page): Clustering of urea–type compounds (N-(C=O)-NH) from VS. The table describes the molecular weight, solubility in water (MLogP), Supplier and the query molecule it was generated from. An asterisk denotes the compound was selected and available for further analysis.

2D Structure	#	M.W (g/mol)	MLogP	Supplier	Query Molecule
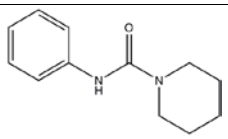	27*	204.1	1.82	ChemBridge	2-anilinothiazolone
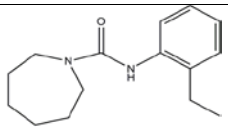	28*	246.1	3	ChemBridge	2-anilinothiazolone
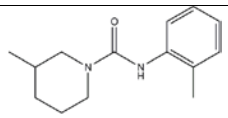	29*	232.3	2.1	ChemBridge	2-anilinothiazolone
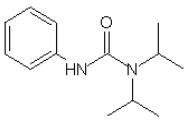	30*	220.3	0.263	Sigma Aldrich	2-anilinothiazolone
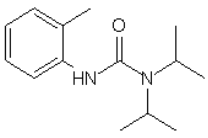	31*	234.3	0.875	ChemBridge	2-anilinothiazolone
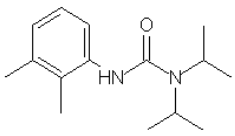	32*	248.4	0.852	Sigma Aldrich	2-anilinothiazolone
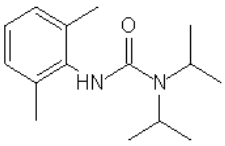	33*	248.4	0.318	Sigma Aldrich	2-anilinothiazolone
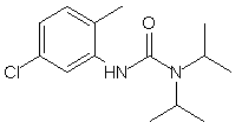	34*	268.8	0.867	Sigma Aldrich	2-anilinothiazolone
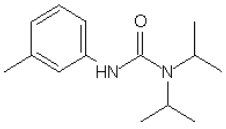	35*	234.3	0.838	Sigma Aldrich	2-anilinothiazolone

2D Structure	#	M.W (g/mol)	MLogP	Supplier	Query Molecule
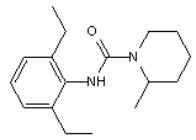	36*	274.4	0.331	Sigma Aldrich	2-anilinothiazolone
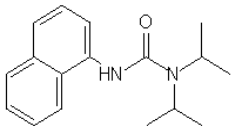	37*	270.4	0.258	Sigma Aldrich	2-anilinothiazolone
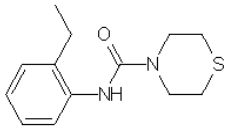	38	250.4	0.335	Maybridge	2-anilinothiazolone
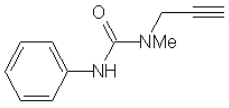	39	188.2	0.259	National Cancer Institute	2-anilinothiazolone
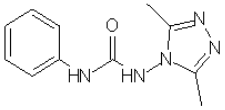	44	231.2	0.199	TimTec	2-anilinothiazolone
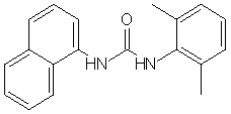	45*	229.3	0.275	Sigma Aldrich	2-anilinothiazolone
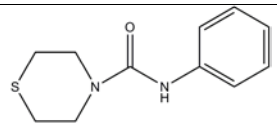	53*	222.3	1.5	Specs	Manually Selected
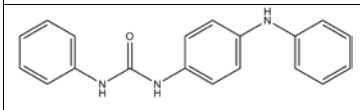	55*	303.4	5.2	TimTec	Manually Selected
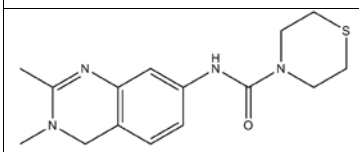	59*	304.4	1.6	Specs	Manually Selected
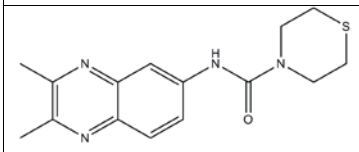	60*	302.4	1.6	Specs	Manually Selected

Table 8.5 continued from previous page.

8.4.2 Tetrazines and Triazoles

Table 8.6 (continued on next page): Clustering of compounds with a tetrazine or triazole ring (with or without a thiol group) from VS. Table describes the molecular weight, solubility in water (MLogP), Supplier and the query molecule it was generated from. An asterisk denotes the compound was selected and available for further analysis.

2D Structure	#	M.W (g/mol)	MLogP	Supplier	Query Molecule
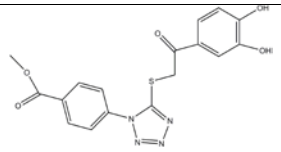	7*	386.4	2.21	InterBioScreen	CBX
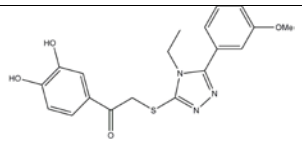	9	385.4	2.62	Ambinter	CBX
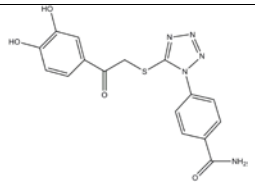	10*	371.4	1.56	InterBioScreen	CBX
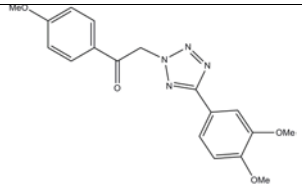	11	354.4	2.44	Asinex	CBX
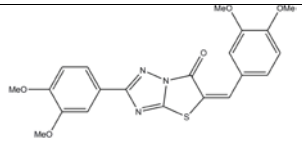	12*	425.5	2.65	InterBioScreen	CBX
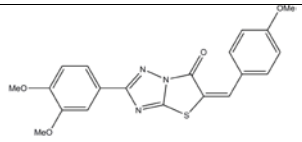	13*	395.4	3.17	InterBioScreen	CBX
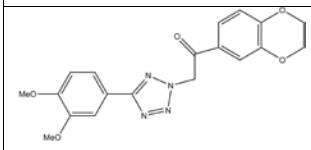	14	382.4	1.94	Asinex	CBX

2D Structure	#	M.W (g/mol)	MLogP	Supplier	Query Molecule
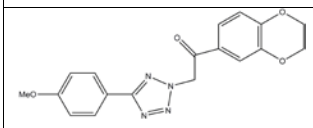	15	352.3	2.45	Asinex	CBX
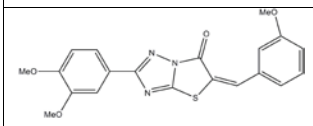	16*	395.4	3.18	InterBioScreen	CBX
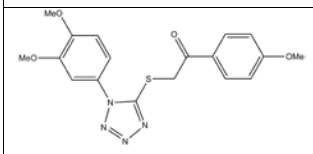	19	386.4	2.44	Asinex	CBX
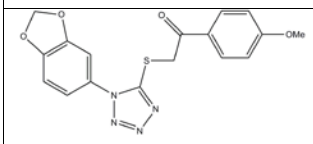	20	370.4	3.02	Asinex	CBX
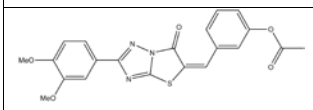	23*	423.4	3.39	InterBioScreen	CBX
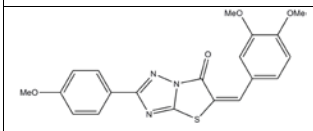	24	395.4	3.17	InterChim	CBX
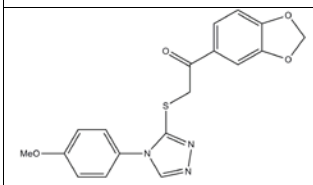	25	369.4	3.19	Enamine	CBX

Table 8.6 continued from previous page.

8.4.3 Thioethers

Table 8.7: Loose clustering of compounds containing a thioether (R-(C=O)-S) group (but no tetrazole or triazole) from VS. Table describes the molecular weight, solubility in water (MLogP), Supplier and the query molecule it was generated from. An asterisk denotes the compound was selected and available for further analysis.

2D Structure	#	M.W (g/mol)	MLogP	Supplier	Query Molecule
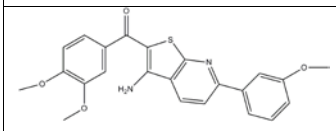	4	420.5	2.15	ChemBridge	CBX
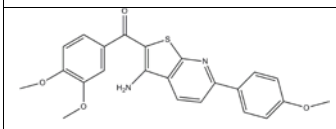	5*	420.5	2.15	Specs	CBX
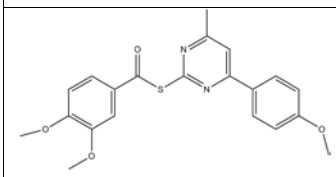	6	396.5	2.16	TimTec	CBX
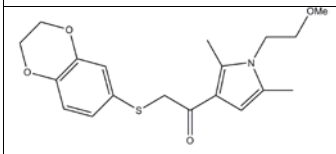	8	361.5	1.94	Enamine	CBX
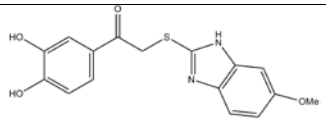	21*	330.4	1.07	ChemBridge	CBX
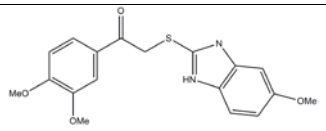	22*	358.4	1.55	InterBioScreen	CBX
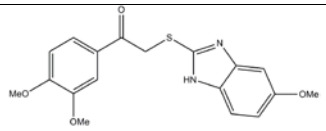	26	358.4	1.55	TimTec	CBX
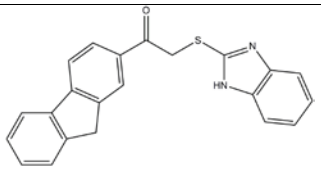	54*	356.4	5.4	TimTec	Manually Selected

2D Structure	#	M.W (g/mol)	MLogP	Supplier	Query Molecule
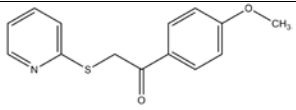	56*	259.3	3	TimTec	Manually Selected
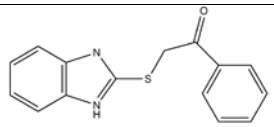	57*	269.3	3.7	TimTec	Manually Selected

Table 8.7 continued from previous page.

8.4.4 Benzamides and Amides

Table 8.8 (continued on next page): Loose cluster of amide- or benzamide containing compounds from VS. Description of molecular weight, solubility in water (MLogP), supplier and the query molecule are shown. An asterisk denotes the compound was selected and available for further analysis.

2D Structure	#	M.W (g/mol)	MLogP	Supplier	Query Molecule
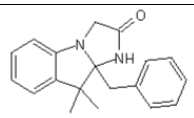	40	292.4	3.91	InterBioScreen	2-anilinothiazolone
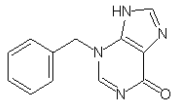	41	226.2	2.41	National Cancer Institute	2-anilinothiazolone
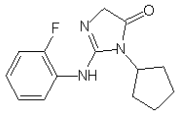	42	261.3	2.85	Asinex	2-anilinothiazolone
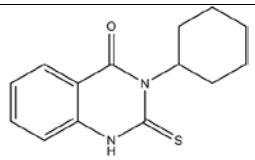	43	260.3	3.05	Sigma Aldrich	2-anilinothiazolone
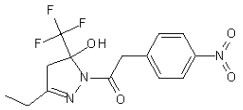	46*	345.3	3.01	InterBioScreen	Adamantane
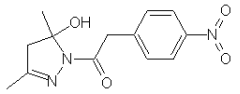	47*	277.3	2.38	TimTec	Adamantane
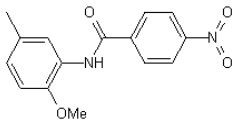	48	286.3	3.06	Enamine	Adamantane
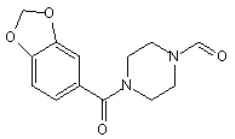	49*	262.3	1.16	Sigma Aldrich	Adamantane

2D Structure	#	M.W (g/mol)	MLogP	Supplier	Query Molecule
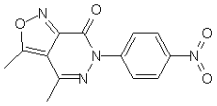	50	286.2	2.22	Sigma Aldrich	Adamantane
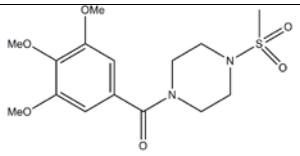	51	358.4	-0.042	TimTec	Adamantane
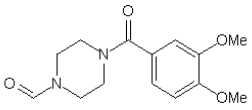	52	278.3	0.616	Chembridge	Adamantane
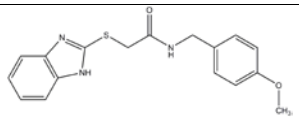	58*	327.4	3.5	TimTec	Manually Selected

Table 8.8 continued from previous page.

8.4.6 Cycloheptanones, cyclohexanones and keto groups

Table 8.9: Clustering of cycloheptanone / cyclohexanone / central ketone containing compounds from VS. Table describes the molecular weight, solubility in water (MLogP), Supplier and the query molecule it was generated from. An asterisk denotes the compound was selected and available for further analysis.

2D Structure	#	M.W (g/mol)	MLogP	Supplier	Query Molecule
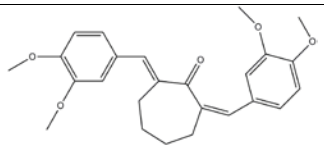	1	408.5	3.05	Sigma Aldrich	CBX
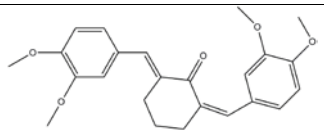	2*	394.5	2.84	Sigma Aldrich	CBX
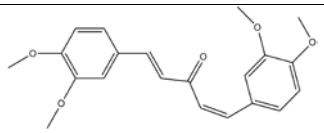	3*	354.4	2.59	ChemBridge	CBX
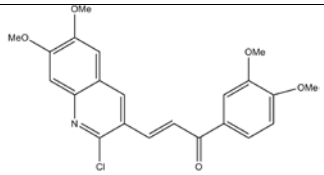	18*	413.8	1.75	Specs	CBX

And one sulfonyl compound:

2D Structure	#	M.W (g/mol)	MLogP	Supplier	Query Molecule
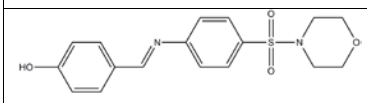	17	346.4	1.32	Ambinter	CBX

Table 8.10: One sulfonyl group was selected as a potential ligand for 11β-HSD1, shown here, with the molecular weight, solubility in water (MLogP), Supplier and the query molecule it was generated from. This compound was not selected for further analysis.

Adams,P.D., Grosse-Kunstleve,R.W., Hung,L.W., Ioerger,T.R., McCoy,A.J., Moriarty,N.W., Read,R.J., Sacchettini,J.C., Sauter,N.K., and Terwilliger,T.C. (2002). PHENIX: building new software for automated crystallographic structure determination. *Acta Crystallogr. D. Biol. Crystallogr.* **58**:1948-1954.

Agarwal,A.K., Monder,C., Eckstein,B., and White,P.C. (1989). Cloning and expression of rat cDNA encoding corticosteroid 11 beta-dehydrogenase. *J. Biol. Chem.* **264**:18939-18943.

Agarwal,A.K., Tusie-Luna,M.T., Monder,C., and White,P.C. (1990). Expression of 11 beta-hydroxysteroid dehydrogenase using recombinant vaccinia virus. *Mol. Endocrinol.* **4**:1827-1832.

Alberts,P., Nilsson,C., Selen,G., Engblom,L.O., Edling,N.H., Norling,S., Klingstrom,G., Larsson,C., Forsgren,M., Ashkzari,M., Nilsson,C.E., Fiedler,M., Bergqvist,E., Ohman,B., Bjorkstrand,E., and Abrahmsen,L.B. (2003). Selective inhibition of 11 beta-hydroxysteroid dehydrogenase type 1 improves hepatic insulin sensitivity in hyperglycemic mice strains. *Endocrinology* **144**:4755-4762.

Albinsson,B., Kubista,M., Eriksson,R., and Sjoback,R. (1994). Experimental Correction for the Inner-filter Effect in Fluorescence Spectra. *Analyst* **119**:417-419.

Albiston,A.L., Obeyesekere,V.R., Smith,R.E., and Krozowski,Z.S. (1994). Cloning and tissue distribution of the human 11 beta-hydroxysteroid dehydrogenase type 2 enzyme. *Mol. Cell Endocrinol.* **105**:R11-R17.

Aleixandre de Artinano,A. and Miguel,C.M. (2009). Experimental rat models to study the metabolic syndrome. *Br. J. Nutr.*1-8.

Andrew,R., Phillips,D.I., and Walker,B.R. (1998). Obesity and gender influence cortisol secretion and metabolism in man. *J. Clin. Endocrinol. Metab* **83**:1806-1809.

Andrews,R.C., Rooyackers,O., and Walker,B.R. (2003). Effects of the 11 beta-hydroxysteroid dehydrogenase inhibitor carbenoxolone on insulin sensitivity in men with type 2 diabetes. *J. Clin. Endocrinol. Metab* **88**:285-291.

Arampatzis,S., Kadereit,B., Schuster,D., Balazs,Z., Schweizer,R.A., Frey,F.J., Langer,T., and Odermatt,A. (2005). Comparative enzymology of 11beta-hydroxysteroid dehydrogenase type 1 from six species. *J. Mol. Endocrinol.* **35**:89-101.

Armanini,D., Nacamulli,D., Francini-Pesenti,F., Battagin,G., Ragazzi,E., and Fiore,C. (2005). Glycyrrhetinic acid, the active principle of licorice, can reduce the thickness of subcutaneous thigh fat through topical application. *Steroids* **70**:538-542.

Armstrong,D.Z.R. Wheel.pl v1.3. [1.3]. 21-10-2004.

Arnold,T. and Linke,D. (2008). The use of detergents to purify membrane proteins. *Curr. Protoc. Protein Sci.* **Chapter 4**:Unit-4.

Atanasov,A.G., Nashev,L.G., Schweizer,R.A., Frick,C., and Odermatt,A. (2004). Hexose-6-phosphate dehydrogenase determines the reaction direction of 11beta-hydroxysteroid dehydrogenase type 1 as an oxoreductase. *FEBS Lett.* **571**:129-133.

Atanasov,A.G. and Odermatt,A. (2007). Readjusting the glucocorticoid balance: an opportunity for modulators of 11beta-hydroxysteroid dehydrogenase type 1 activity? *Endocr Metab Immune. Disord. Drug Targets.* **7**:125-140.

Ballester,P.J., Finn,P.W., and Richards,W.G. (2009). Ultrafast shape recognition: Evaluating a new ligand-based virtual screening technology. *J. Mol. Graph. Model.*

Ballester,P.J. and Richards,W.G. (2007). Ultrafast shape recognition to search compound databases for similar molecular shapes. *J. Comput. Chem.* **28**:1711-1723.

Barf,T., Vallgarda,J., Emond,R., Haggstrom,C., Kurz,G., Nygren,A., Larwood,V., Mosialou,E., Axelsson,K., Olsson,R., Engblom,L., Edling,N., Ronquist-Nii,Y., Ohman,B., Alberts,P., and Abrahmsen,L. (2002). Arylsulfonamidothiazoles as a new class of potential antidiabetic drugs. Discovery of potent and selective inhibitors of the 11beta-hydroxysteroid dehydrogenase type 1. *J. Med. Chem.* **45**:3813-3815.

Barnes,P.J. (2005). Molecular mechanisms and cellular effects of glucocorticosteroids. *Immunol. Allergy Clin. North Am.* **25**:451-468.

Barroso,J.F., Elholm,M., and Flatmark,T. (2003). Tight binding of deoxyribonucleotide triphosphates to human thymidine kinase 2 expressed in Escherichia coli. Purification and partial characterization of its dimeric and tetrameric forms. *Biochemistry* **42**:15158-15169.

Benyajati,C., Place,A.R., Powers,D.A., and Sofer,W. (1981). Alcohol dehydrogenase gene of Drosophila melanogaster: relationship of intervening sequences to functional domains in the protein. *Proc. Natl. Acad. Sci. U. S. A* **78**:2717-2721.

Berrow,N.S., Bussow,K., Coutard,B., Diprose,J., Ekberg,M., Folkers,G.E., Levy,N., Lieu,V., Owens,R.J., Peleg,Y., Pinaglia,C., Quevillon-Cheruel,S., Salim,L., Scheich,C., Vincentelli,R., and Busso,D. (2006). Recombinant protein expression and solubility screening in Escherichia coli: a comparative study. *Acta Crystallogr. D. Biol. Crystallogr.* **62**:1218-1226.

Bjellqvist,B., Basse,B., Olsen,E., and Celis,J.E. (1994). Reference points for comparisons of two-dimensional maps of proteins from different human cell types defined in a pH scale where isoelectric points correlate with polypeptide compositions. *Electrophoresis* **15**:529-539.

Bjellqvist,B., Hughes,G.J., Pasquali,C., Paquet,N., Ravier,F., Sanchez,J.C., Frutiger,S., and Hochstrasser,D. (1993). The focusing positions of polypeptides in immobilized pH gradients can be predicted from their amino acid sequences. *Electrophoresis* **14**:1023-1031.

Blum,A., Martin,H.J., and Maser,E. (2000b). Human 11beta-hydroxysteroid dehydrogenase type 1 is enzymatically active in its nonglycosylated form. *Biochem. Biophys. Res. Commun.* **276**:428-434.

Blum,A., Martin,H.J., and Maser,E. (2000a). Human 11beta-hydroxysteroid dehydrogenase 1/carbonyl reductase: recombinant expression in the yeast Pichia pastoris and Escherichia coli. *Toxicology* **144**:113-120.

Braig,K., Otwinowski,Z., Hegde,R., Boisvert,D.C., Joachimiak,A., Horwich,A.L., and Sigler,P.B. (1994). The crystal structure of the bacterial chaperonin GroEL at 2.8 A. *Nature* **371**:578-586.

Brandt,R.B., Laux,J.E., and Yates,S.W. (1987). Calculation of inhibitor Ki and inhibitor type from the concentration of inhibitor for 50% inhibition for Michaelis-Menten enzymes. *Biochem. Med. Metab Biol.* **37**:344-349.

Buhler,H., Perschel,F.H., and Hierholzer,K. (1991). Inhibition of rat renal 11 beta-hydroxysteroid dehydrogenase by steroidal compounds and triterpenoids; structure/function relationship. *Biochim. Biophys. Acta* **1075**:206-212.

Bujalska,I.J., Kumar,S., and Stewart,P.M. (1997). Does central obesity reflect "Cushing's disease of the omentum"? *The Lancet* **349**:1210-1213.

Burgess-Brown,N.A., Sharma,S., Sobott,F., Loenarz,C., Oppermann,U., and Gileadi,O. (2008). Codon optimization can improve expression of human genes in Escherichia coli: A multi-gene study. *Protein Expr. Purif.* **59**:94-102.

Bush,I.E., Hunter,S.A., and Meigs,R.A. (1968). Metabolism of 11-oxygenated steroids. Metabolism in vitro by preparations of liver. *Biochem. J.* **107**:239-258.

Cannon,E.O., Nigsch,F., and Mitchell,J.B. (2008). A Novel Hybrid Ultrafast Shape Descriptor Method for use in Virtual Screening. *Chem. Cent. J.* **2**:3.

Castro,A., Zhu,J.X., Alton,G.R., Rejto,P., and Ermolieff,J. (2007). Assay optimization and kinetic profile of the human and the rabbit isoforms of 11beta-HSD1. *Biochem. Biophys. Res. Commun.* **357**:561-566.

Cheeseright,T., Mackey,M., Rose,S., and Vinter,A. (2006). Molecular field extrema as descriptors of biological activity: definition and validation. *J. Chem. Inf. Model.* **46**:665-676.

Cheng and Prussoff (1973). Relationship between the inhibition constant (K1) and the concentration of inhibitor which causes 50 per cent inhibition (I50) of an enzymatic reaction. *Biochemical Pharmacology* **22**:3099-3108.

Cheng,H.C. (2001). The power issue: determination of KB or Ki from IC50. A closer look at the Cheng-Prusoff equation, the Schild plot and related power equations. *J. Pharmacol. Toxicol. Methods* **46**:61-71.

Classen-Houben,D., Schuster,D., Da,C.T., Odermatt,A., Wolber,G., Jordis,U., and Kueenburg,B. (2009). Selective inhibition of 11beta-hydroxysteroid dehydrogenase 1 by 18alpha-glycyrrhetinic acid but not 18beta-glycyrrhetinic acid. *J. Steroid Biochem. Mol. Biol.* **113**:248-252.

Cleland,W. (1963). The kinetics of enzyme-catalyzed reactions with two or more substrates or products. II. Inhibition: nomenclature and theory. *Biochim. Biophys. Acta* **67**:173-187.

Congreve,M., Carr,R., Murray,C., and Jhoti,H. (2003). A 'rule of three' for fragment-based lead discovery? *Drug Discov. Today* **8**:876-877.

Cortes,A., Cascante,M., Cardenas,M.L., and Cornish-Bowden,A. (2001). Relationships between inhibition constants, inhibitor concentrations for 50% inhibition and types of inhibition: new ways of analysing data. *Biochem. J.* **357**:263-268.

Davies,G.J., Rhodes,J., and Calcraft,B.J. (1974). Complications of carbenoxolone therapy. *Br. Med. J.* **3**:400-402.

de Quervain,D.J., Poirier,R., Wollmer,M.A., Grimaldi,L.M., Tsolaki,M., Streffer,J.R., Hock,C., Nitsch,R.M., Mohajeri,M.H., and Papassotiropoulos,A. (2004). Glucocorticoid-related genetic susceptibility for Alzheimer's disease. *Hum. Mol. Genet.* **13**:47-52.

Deary,I.J., Hayward,C., Permana,P.A., Nair,S., Whalley,L.J., Starr,J.M., Chapman,K.E., Walker,B.R., and Seckl,J.R. (2006). Polymorphisms in the gene encoding 11B-hydroxysteroid dehydrogenase type 1 (HSD11B1) and lifetime cognitive change. *Neurosci. Lett.* **393**:74-77.

Delaney,J.S. (2005). Predicting aqueous solubility from structure. *Drug Discov. Today* **10**:289-295.

Dzyakanchuk,A.A., Balazs,Z., Nashev,L.G., Amrein,K.E., and Odermatt,A. (2009). 11beta-Hydroxysteroid dehydrogenase 1 reductase activity is dependent on a high ratio of NADPH/NADP(+) and is stimulated by extracellular glucose. *Mol. Cell Endocrinol.* **301**:137-141.

Eckel,R.H., Grundy,S.M., and Zimmet,P.Z. (2005). The metabolic syndrome. *Lancet* **365**:1415-1428.

Ekins,S., Mestres,J., and Testa,B. (2007a). In silico pharmacology for drug discovery: applications to targets and beyond. *Br. J. Pharmacol.* **152**:21-37.

Ekins,S., Mestres,J., and Testa,B. (2007b). In silico pharmacology for drug discovery: methods for virtual ligand screening and profiling. *Br. J. Pharmacol.* **152**:9-20.

Elleby,B., Svensson,S., Wu,X., Stefansson,K., Nilsson,J., Hallen,D., Oppermann,U., and Abrahmsen,L. (2004). High-level production and optimization of monodispersity of 11beta-hydroxysteroid dehydrogenase type 1. *Biochim. Biophys. Acta* **1700**:199-207.

Evans,G. 2004. *A handbook of bioanalysis and drug metabolism*, 1 ed. CRC Press.

Fethiere,J. 2007. Three-Dimensional Crystallisation of Membrane Proteins. In *"Preparation and Crystallisation of Macromolecules"*, 1 ed. (ed. Sylvie Doublie), pp 191-210. Humana Press.

Filling,C., Berndt,K.D., Benach,J., Knapp,S., Prozorovski,T., Nordling,E., Ladenstein,R., Jornvall,H., and Oppermann,U. (2002). Critical residues for structure and catalysis in short-chain dehydrogenases/reductases. *J. Biol. Chem.* **277**:25677-25684.

Frey,F.J., Odermatt,A., and Frey,B.M. (2004). Glucocorticoid-mediated mineralocorticoid receptor activation and hypertension. *Curr. Opin. Nephrol. Hypertens.* **13**:451-458.

Frick,C., Atanasov,A.G., Arnold,P., Ozols,J., and Odermatt,A. (2004). Appropriate function of 11beta-hydroxysteroid dehydrogenase type 1 in the endoplasmic reticulum lumen is dependent on its N-terminal region sharing similar topological determinants with 50-kDa esterase. *J. Biol. Chem.* **279**:31131-31138.

Gleeson,P., Bravi,G., Modi,S., and Lowe,D. (2009). ADMET rules of thumb II: A comparison of the effects of common substituents on a range of ADMET parameters. *Bioorg. Med. Chem.* **17**:5906-5919.

Graham,F.L., Smiley,J., Russell,W.C., and Nairn,R. (1977). Characteristics of a human cell line transformed by DNA from human adenovirus type 5. *J. Gen. Virol.* **36**:59-74.

Grossman,T.H., Kawasaki,E.S., Punreddy,S.R., and Osburne,M.S. (1998). Spontaneous cAMP-dependent derepression of gene expression in stationary phase plays a role in recombinant expression instability. *Gene* **209**:95-103.

Hale,C., Veniant,M., Wang,Z., Chen,M., McCormick,J., Cupples,R., Hickman,D., Min,X., Sudom,A., Xu,H., Matsumoto,G., Fotsch,C., St,J.D., Jr., and Wang,M. (2008). Structural characterization and pharmacodynamic effects of an orally active 11beta-hydroxysteroid dehydrogenase type 1 inhibitor. *Chem. Biol. Drug Des* **71**:36-44.

Hall,S.W. and VandenBerg,S.R. (1989). Solid phase extraction of the zwitterionic detergent chaps. *Prep. Biochem.* **19**:1-11.

Hann,M.M. and Oprea,T.I. (2004). Pursuing the leadlikeness concept in pharmaceutical research. *Curr. Opin. Chem. Biol.* **8**:255-263.

Hansch,C. and Clayton,J.M. (1973). Lipophilic character and biological activity of drugs. II. The parabolic case. *J. Pharm. Sci.* **62**:1-21.

Hawkins M, Hunter D., Kishore P., Schwartz S., Hompesch M., Hollis G., Levy R., Williams B., and Huber R. INCB013739, a selective inhibitor of 11ß-hydroxysteroid dehydrogenase type 1 (11ßHSD1), improves insulin sensitivity and lowers plasma cholesterol over 28 days in patients with type 2 diabetes mellitus. 1-6-2008.

Hendrickson,M.A., Nicklaus,M.C., Milne,G.W.A., and Zaharevitz,D. (1993). Concord and Cambridge - Comparison of Computer-Generated Chemical Structures with X-Ray Crystallographic Data. *Journal of Chemical Information and Computer Sciences* **33**:155-163.

Henriksson,M., Liu,Q., Bartberger,M.D., Moniz,G.A., Frizzle,M.J., Homan,E., Johansson,L., Vallgarda,J., Williams,M., and Bercot,E. Inhibitors of 11-beta HydroxySteroid Dehydrogenase Type 1. PCT/US2005/018081[**(WO/2005/116002)**]. 8-12-2005. 24-5-2005.

Hewitt,K.N., Walker,E.A., and Stewart,P.M. (2005). Minireview: hexose-6-phosphate dehydrogenase and redox control of 11{beta}-hydroxysteroid dehydrogenase type 1 activity. *Endocrinology* **146**:2539-2543.

Hinton,A.C. Database Mining: EDULISS a Descriptor Based Approach. 2005. Institute of Structural and Molecular Biology, University of Edinburgh.

Hosfield,D.J., Wu,Y., Skene,R.J., Hilgers,M., Jennings,A., Snell,G.P., and Aertgeerts,K. (2005). Conformational flexibility in crystal structures of human 11beta-hydroxysteroid

dehydrogenase type I provide insights into glucocorticoid interconversion and enzyme regulation. *J. Biol. Chem.* **280**:4639-4648.

Hozjan,V., Guo,K., Wu,X., and Oppermann,U. (2008). Ligand supplementation as a method to increase soluble heterologous protein production. *Expert. Rev Proteomics.* **5**:137-143.

Hult,M., Jornvall,H., and Oppermann,U.C. (1998). Selective inhibition of human type 1 11beta-hydroxysteroid dehydrogenase by synthetic steroids and xenobiotics. *FEBS Lett.* **441**:25-28.

Hult,M., Nobel,C.S., Abrahmsen,L., Nicoll-Griffith,D.A., Jornvall,H., and Oppermann,U.C. (2001). Novel enzymological profiles of human 11beta-hydroxysteroid dehydrogenase type 1. *Chem. Biol. Interact.* **130-132**:805-814.

Hult,M., Shafqat,N., Elleby,B., Mitschke,D., Svensson,S., Forsgren,M., Barf,T., Vallgarda,J., Abrahmsen,L., and Oppermann,U. (2006). Active site variability of type 1 11beta-hydroxysteroid dehydrogenase revealed by selective inhibitors and cross-species comparisons. *Mol. Cell Endocrinol.* **248**:26-33.

Janzen,W.P. 2002. *High Throughput Screening*, 1 ed. Humana Press.

Johansson,L., Fotsch,C., Bartberger,M.D., Castro,V.M., Chen,M., Emery,M., Gustafsson,S., Hale,C., Hickman,D., Homan,E., Jordan,S.R., Komorowski,R., Li,A., McRae,K., Moniz,G., Matsumoto,G., Orihuela,C., Palm,G., Veniant,M., Wang,M., Williams,M., and Zhang,J. (2008). 2-amino-1,3-thiazol-4(5H)-ones as potent and selective 11beta-hydroxysteroid dehydrogenase type 1 inhibitors: enzyme-ligand co-crystal structure and demonstration of pharmacodynamic effects in C57Bl/6 mice. *J. Med. Chem.* **51**:2933-2943.

Julian,L.D., Wang,Z., Bostick,T., Caille,S., Choi,R., DeGraffenreid,M., Di,Y., He,X., Hungate,R.W., Jaen,J.C., Liu,J., Monshouwer,M., McMinn,D., Rew,Y., Sudom,A., Sun,D., Tu,H., Ursu,S., Walker,N., Yan,X., Ye,Q., and Powers,J.P. (2008). Discovery of novel, potent benzamide inhibitors of 11beta-hydroxysteroid dehydrogenase type 1 (11beta-HSD1) exhibiting oral activity in an enzyme inhibition ex vivo model. *J. Med. Chem.* **51**:3953-3960.

Kim,K.W., Wang,Z., Busby,J., Tsuruda,T., Chen,M., Hale,C., Castro,V.M., Svensson,S., Nybo,R., Xiong,F., and Wang,M. (2006). The role of tyrosine 177 in human 11beta-hydroxysteroid dehydrogenase type 1 in substrate and inhibitor binding: an unlikely hydrogen bond donor for the substrate. *Biochim. Biophys. Acta* **1764**:824-830.

Kim,K.W., Wang,Z., Busby,J., Tsuruda,T., Chen,M., Hale,C., Castro,V.M., Svensson,S., Nybo,R., Xiong,F., and Wang,M. (2007). The selectivity of tyrosine 280 of human 11beta-hydroxysteroid dehydrogenase type 1 in inhibitor binding. *FEBS Lett.* **581**:995-999.

Kim,R., Yokota,H., and Kim,S.H. (2000). Electrophoresis of proteins and protein-protein complexes in a native agarose gel. *Anal. Biochem.* **282**:147-149.

Koch,M.A., Wittenberg,L.O., Basu,S., Jeyaraj,D.A., Gourzoulidou,E., Reinecke,K., Odermatt,A., and Waldmann,H. (2004). Compound library development guided by

protein structure similarity clustering and natural product structure. *Proc. Natl. Acad. Sci. U. S. A* **101**:16721-16726.

Kortagere,S., Krasowski,M.D., and Ekins,S. (2009). The importance of discerning shape in molecular pharmacology. *Trends Pharmacol. Sci.*

Kotelevtsev,Y., Holmes,M.C., Burchell,A., Houston,P.M., Schmoll,D., Jamieson,P., Best,R., Brown,R., Edwards,C.R., Seckl,J.R., and Mullins,J.J. (1997). 11beta-hydroxysteroid dehydrogenase type 1 knockout mice show attenuated glucocorticoid-inducible responses and resist hyperglycemia on obesity or stress. *Proc. Natl. Acad. Sci. U. S. A* **94**:14924-14929.

Lakshmi,V. and Monder,C. (1988). Purification and characterization of the corticosteroid 11 beta-dehydrogenase component of the rat liver 11 beta-hydroxysteroid dehydrogenase complex. *Endocrinology* **123**:2390-2398.

Lamark,T., Ingebrigtsen,M., Bjornstad,C., Melkko,T., Mollnes,T.E., and Nielsen,E.W. (2001). Expression of active human C1 inhibitor serpin domain in Escherichia coli. *Protein Expr. Purif.* **22**:349-358.

Latif,S.A., Pardo,H.A., Hardy,M.P., and Morris,D.J. (2005). Endogenous selective inhibitors of 11beta-hydroxysteroid dehydrogenase isoforms 1 and 2 of adrenal origin. *Mol. Cell Endocrinol.* **243**:43-50.

Lazareno,S. and Birdsall,N.J. (1993). Estimation of antagonist Kb from inhibition curves in functional experiments: alternatives to the Cheng-Prusoff equation. *Trends Pharmacol. Sci.* **14**:237-239.

Lee,J.H., Kang,N.S., and Yoo,S.E. (2008). Docking-based 3D-QSAR study for 11beta-HSD1 inhibitors. *Bioorg. Med. Chem. Lett.* **18**:2479-2490.

Lee,K.H., Kim,H.S., Jeong,H.S., and Lee,Y.S. (2002). Chaperonin GroESL mediates the protein folding of human liver mitochondrial aldehyde dehydrogenase in Escherichia coli. *Biochem. Biophys. Res Commun.* **298**:216-224.

Lin,Z. and Rye,H.S. (2006). GroEL-mediated protein folding: making the impossible, possible. *Crit Rev Biochem. Mol. Biol.* **41**:211-239.

Lipinski,C.A., Lombardo,F., Dominy,B.W., and Feeney,P.J. (2001). Experimental and computational approaches to estimate solubility and permeability in drug discovery and development settings. *Adv. Drug Deliv. Rev* **46**:3-26.

Liu,Y., Sun,Y., Zhu,T., Xie,Y., Yu,J., Sun,W.L., Ding,G.X., and Hu,G. (2007). 11 beta-hydroxysteroid dehydrogenase type 1 promotes differentiation of 3T3-L1 preadipocyte. *Acta Pharmacol. Sin.* **28**:1198-1204.

Livingstone,D.E., Jones,G.C., Smith,K., Jamieson,P.M., Andrew,R., Kenyon,C.J., and Walker,B.R. (2000). Understanding the role of glucocorticoids in obesity: tissue-specific alterations of corticosterone metabolism in obese Zucker rats. *Endocrinology* **141**:560-563.

Livingstone,D.E. and Walker,B.R. (2003). Is 11beta-hydroxysteroid dehydrogenase type 1 a therapeutic target? Effects of carbenoxolone in lean and obese Zucker rats. *J. Pharmacol. Exp. Ther.* **305**:167-172.

Loh,K.P., Yang,S.W., Soon,J.M., Zhang,H., and Wu,P. (2003). Ab initio studies of borazine and benzene cyclacenes and their fluoro-substituted derivatives. *Journal of Physical Chemistry A* **107**:5555-5560.

Lupien,S.J., de,L.M., de,S.S., Convit,A., Tarshish,C., Nair,N.P., Thakur,M., McEwen,B.S., Hauger,R.L., and Meaney,M.J. (1998). Cortisol levels during human aging predict hippocampal atrophy and memory deficits. *Nat. Neurosci.* **1**:69-73.

Marin,P., Darin,N., Amemiya,T., Andersson,B., Jern,S., and Bjorntorp,P. (1992). Cortisol secretion in relation to body fat distribution in obese premenopausal women. *Metabolism* **41**:882-886.

Maser,E. (1998). 11Beta-hydroxysteroid dehydrogenase responsible for carbonyl reduction of the tobacco-specific nitrosamine 4-(methylnitrosamino)-1-(3-pyridyl)-1-butanone in mouse lung microsomes. *Cancer Res* **58**:2996-3003.

Maser,E., Friebertshauser,J., and Volker,B. (2003). Purification, characterization and NNK carbonyl reductase activities of 11beta-hydroxysteroid dehydrogenase type 1 from human liver: enzyme cooperativity and significance in the detoxification of a tobacco-derived carcinogen. *Chem. Biol. Interact.* **143-144**:435-448.

Maser,E. and Oppermann,U.C. (1997). Role of type-1 11beta-hydroxysteroid dehydrogenase in detoxification processes. *Eur. J. Biochem.* **249**:365-369.

Maser,E., Volker,B., and Friebertshauser,J. (2002). 11 Beta-hydroxysteroid dehydrogenase type 1 from human liver: dimerization and enzyme cooperativity support its postulated role as glucocorticoid reductase. *Biochemistry* **41**:2459-2465.

Masuzaki,H., Paterson,J., Shinyama,H., Morton,N.M., Mullins,J.J., Seckl,J.R., and Flier,J.S. (2001). A transgenic model of visceral obesity and the metabolic syndrome. *Science* **294**:2166-2170.

McEwen,B.S., de Leon,M.J., Lupien,S.J., and Meaney,M.J. (1999). Corticosteroids, the Aging Brain and Cognition. *Trends Endocrinol. Metab* **10**:92-96.

Megard,I., Garrigues,A., Orlowski,S., Jorajuria,S., Clayette,P., Ezan,E., and Mabondzo,A. (2002). A co-culture-based model of human blood-brain barrier: application to active transport of indinavir and in vivo-in vitro correlation. *Brain Res* **927**:153-167.

Mericq,V., Medina,P., Bouwman,C., Johnson,M.C., Godoy,J., Lopez,T., and Iniguez,G. (2009). Expression and activity of 11beta-hydroxysteroid dehydrogenase type 1 enzyme in subcutaneous and visceral adipose tissue of prepubertal children. *Horm. Res* **71**:89-93.

Miguet,L., Zhang,Z., Barbier,M., and Grigorov,M.G. (2006). Comparison of a homology model and the crystallographic structure of human 11beta-hydroxysteroid dehydrogenase type 1 (11betaHSD1) in a structure-based identification of inhibitors. *J. Comput. Aided Mol. Des* **20**:67-81.

Monder,C., Lakshmi,V., and Miroff,Y. (1991). Kinetic studies on rat liver 11 beta-hydroxysteroid dehydrogenase. *Biochim. Biophys. Acta* **1115**:23-29.

Monder,C., Stewart,P.M., Lakshmi,V., Valentino,R., Burt,D., and Edwards,C.R. (1989). Licorice inhibits corticosteroid 11 beta-dehydrogenase of rat kidney and liver: in vivo and in vitro studies. *Endocrinology* **125**:1046-1053.

Moriguchi, Hirono, Liu, Nakagome, and Matsushita (1992). Simple Method of Calculating Octanol / Water Partition Coefficient. *Chemical & pharmaceutical Bulletin* **40**:127-130.

Morris,D.J., Latif,S.A., Hardy,M.P., and Brem,A.S. (2007). Endogenous inhibitors (GALFs) of 11beta-hydroxysteroid dehydrogenase isoforms 1 and 2: derivatives of adrenally produced corticosterone and cortisol. *J. Steroid Biochem. Mol. Biol.* **104**:161-168.

Morris,D.J., Semafuko,W.E., Latif,S.A., Vogel,B., Grimes,C.A., and Sheff,M.F. (1992). Detection of glycyrrhetinic acid-like factors (GALFs) in human urine. *Hypertension* **20**:356-360.

Morrison,J.F. (1969). Kinetics of the reversible inhibition of enzyme-catalysed reactions by tight-binding inhibitors. *Biochim. Biophys. Acta* **185**:269-286.

Muegge,I. (2003). Selection criteria for drug-like compounds. *Med. Res Rev* **23**:302-321.

Mundt,S., Solly,K., Thieringer,R., and Hermanowski-Vosatka,A. (2005). Development and application of a scintillation proximity assay (SPA) for identification of selective inhibitors of 11beta-hydroxysteroid dehydrogenase type 1. *Assay. Drug Dev. Technol.* **3**:367-375.

Nashev,L.G., Chandsawangbhuwana,C., Balazs,Z., Atanasov,A.G., Dick,B., Frey,F.J., Baker,M.E., and Odermatt,A. (2007). Hexose-6-phosphate dehydrogenase modulates 11beta-hydroxysteroid dehydrogenase type 1-dependent metabolism of 7-keto- and 7beta-hydroxy-neurosteroids. *PLoS. One.* **2**:e561.

Niu,P. and Yang,K. (2002). The 11 beta-hydroxysteroid dehydrogenase type 2 activity in human placental microsomes is inactivated by zinc and the sulfhydryl modifying reagent N-ethylmaleimide. *Biochim. Biophys. Acta* **1594**:364-371.

Nobel,C.S., Dunas,F., and Abrahmsen,L.B. (2002). Purification of full-length recombinant human and rat type 1 11beta-hydroxysteroid dehydrogenases with retained oxidoreductase activities. *Protein Expr. Purif.* **26**:349-356.

Norman,P. Metabolic and Inflammatory Disease R&D: An Assessment of 5 Highly Promising Therapeutic Classes. 1-170. 2-4-2007. 250 First Avenue, Suite 300 Needham MA 02494, Cambridge HealthTech Institute Reports. Insight Pharma Reports.

Nuotio-Antar,A.M., Hachey,D.L., and Hasty,A.H. (2007). Carbenoxolone treatment attenuates symptoms of metabolic syndrome and atherogenesis in obese, hyperlipidemic mice. *Am. J. Physiol Endocrinol. Metab* **293**:E1517-E1528.

Odermatt,A., Arnold,P., Stauffer,A., Frey,B.M., and Frey,F.J. (1999). The N-terminal anchor sequences of 11beta-hydroxysteroid dehydrogenases determine their orientation in the endoplasmic reticulum membrane. *J. Biol. Chem.* **274**:28762-28770.

Odermatt,A., Atanasov,A.G., Balazs,Z., Schweizer,R.A., Nashev,L.G., Schuster,D., and Langer,T. (2006). Why is 11beta-hydroxysteroid dehydrogenase type 1 facing the endoplasmic reticulum lumen? Physiological relevance of the membrane topology of 11beta-HSD1. *Mol. Cell Endocrinol.* **248**:15-23.

Ogg,D., Elleby,B., Norstrom,C., Stefansson,K., Abrahmsen,L., Oppermann,U., and Svensson,S. (2005). The crystal structure of guinea pig 11beta-hydroxysteroid dehydrogenase type 1 provides a model for enzyme-lipid bilayer interactions. *J. Biol. Chem.* **280**:3789-3794.

Oppermann,U.C., Maser,E., Mangoura,S.A., and Netter,K.J. (1991). Heterogeneity of carbonyl reduction in subcellular fractions and different organs in rodents. *Biochem. Pharmacol.* **42 Suppl**:S189-S195.

Oppermann,U.C., Netter,K.J., and Maser,E. (1995). Cloning and primary structure of murine 11 beta-hydroxysteroid dehydrogenase/microsomal carbonyl reductase. *Eur. J. Biochem.* **227**:202-208.

Oprea,T.I. and Matter,H. (2004). Integrating virtual screening in lead discovery. *Curr. Opin. Chem. Biol.* **8**:349-358.

Ozols,J. (1995). Lumenal orientation and post-translational modifications of the liver microsomal 11 beta-hydroxysteroid dehydrogenase. *J. Biol. Chem.* **270**:10360.

Patel,J.R., Shuai,Q., Dinges,J., Winn,M., Pliushchev,M., Fung,S., Monzon,K., Chiou,W., Wang,J., Pan,L., Wagaw,S., Engstrom,K., Kerdesky,F.A., Longenecker,K., Judge,R., Qin,W., Imade,H.M., Stolarik,D., Beno,D.W., Brune,M., Chovan,L.E., Sham,H.L., Jacobson,P., and Link,J.T. (2007). Discovery of adamantane ethers as inhibitors of 11beta-HSD-1: Synthesis and biological evaluation. *Bioorg. Med. Chem. Lett.* **17**:750-755.

Rajan,V., Chapman,K.E., Lyons,V., Jamieson,P., Mullins,J.J., Edwards,C.R., and Seckl,J.R. (1995). Cloning, sequencing and tissue-distribution of mouse 11 beta-hydroxysteroid dehydrogenase-1 cDNA. *J. Steroid Biochem. Mol. Biol.* **52**:141-147.

Rajan,V., Edwards,C.R., and Seckl,J.R. (1996). 11 beta-Hydroxysteroid dehydrogenase in cultured hippocampal cells reactivates inert 11-dehydrocorticosterone, potentiating neurotoxicity. *J. Neurosci.* **16**:65-70.

Rang,H.P., Dale,M.M., and Ritter,J.M. 2005. *Pharmacology*, 5th Edition ed. Churchill Livingstone.

Rao,S.T. and Rossmann,M.G. (1973). Comparison of super-secondary structures in proteins. *J. Mol. Biol.* **76**:241-256.

Rask,E., Walker,B.R., Soderberg,S., Livingstone,D.E., Eliasson,M., Johnson,O., Andrew,R., and Olsson,T. (2002). Tissue-specific changes in peripheral cortisol metabolism in obese women: increased adipose 11beta-hydroxysteroid dehydrogenase type 1 activity. *J. Clin. Endocrinol. Metab* **87**:3330-3336.

Rhodes,G. 1992. *Crystallography Made Crystal Clear*, 3rd Edition ed. Academic Press, Elsevier.

Robert Novy and Barbara Morris. Use of glucose to control basal expression in the pET System. inNovations 13, 8-10. 1-1-2001. Novagen Inc.

Roberto Todeschini and Viviana Consonni 2002. *Handbook of Molecular Descriptors*, 11 ed. Wiley-VCH.

Roche,D., Carniato,D., Leriche,C., Lepifre,F., Christmann-Franck,S., Graedler,U., Charon,C., Bozec,S., Doare,L., Schmidlin,F., Lecomte,M., and Valeur,E. (2009). Discovery and structure-activity relationships of pentanedioic acid diamides as potent inhibitors of 11beta-hydroxysteroid dehydrogenase type I. *Bioorg. Med. Chem. Lett.* **19**:2674-2678.

Rohde,J.J., Pliushchev,M.A., Sorensen,B.K., Wodka,D., Shuai,Q., Wang,J., Fung,S., Monzon,K.M., Chiou,W.J., Pan,L., Deng,X., Chovan,L.E., Ramaiya,A., Mullally,M., Henry,R.F., Stolarik,D.F., Imade,H.M., Marsh,K.C., Beno,D.W., Fey,T.A., Droz,B.A., Brune,M.E., Camp,H.S., Sham,H.L., Frevert,E.U., Jacobson,P.B., and Link,J.T. (2007). Discovery and metabolic stabilization of potent and selective 2-amino-N-(adamant-2-yl) acetamide 11beta-hydroxysteroid dehydrogenase type 1 inhibitors. *J. Med. Chem.* **50**:149-164.

Rusvai,E. and Naray-Fejes-Toth,A. (1993). A new isoform of 11 beta-hydroxysteroid dehydrogenase in aldosterone target cells. *J. Biol. Chem.* **268**:10717-10720.

Sahni-Arya,B., Flynn,M.J., Bergeron,L., Salyan,M.E., Pedicord,D.L., Golla,R., Ma,Z., Wang,H., Seethala,R., Wu,S.C., Li,J.J., Nayeem,A., Gates,C., Hamann,L.G., Gordon,D.A., and Blat,Y. (2007). Cofactor-specific modulation of 11beta-hydroxysteroid dehydrogenase 1 inhibitor potency. *Biochim. Biophys. Acta* **1774**:1184-1191.

Sandeep,T.C. and Walker,B.R. (2001). Pathophysiology of modulation of local glucocorticoid levels by 11beta-hydroxysteroid dehydrogenases. *Trends Endocrinol. Metab* **12**:446-453.

Sandeep,T.C., Yau,J.L., MacLullich,A.M., Noble,J., Deary,I.J., Walker,B.R., and Seckl,J.R. (2004). 11Beta-hydroxysteroid dehydrogenase inhibition improves cognitive function in healthy elderly men and type 2 diabetics. *Proc. Natl. Acad. Sci. U. S. A* **101**:6734-6739.

Saraste,M., Sibbald,P.R., and Wittinghofer,A. (1990). The P-loop--a common motif in ATP- and GTP-binding proteins. *Trends Biochem. Sci.* **15**:430-434.

Schiffer,M. and Edmundson,A.B. (1967). Use of helical wheels to represent the structures of proteins and to identify segments with helical potential. *Biophys. J.* **7**:121-135.

Schuster,D., Maurer,E.M., Laggner,C., Nashev,L.G., Wilckens,T., Langer,T., and Odermatt,A. (2006). The discovery of new 11beta-hydroxysteroid dehydrogenase type 1 inhibitors by common feature pharmacophore modeling and virtual screening. *J. Med. Chem.* **49**:3454-3466.

Seckl,J.R. and Walker,B.R. (2004). 11beta-hydroxysteroid dehydrogenase type 1 as a modulator of glucocorticoid action: from metabolism to memory. *Trends Endocrinol. Metab* **15**:418-424.

Seckl,J.R. and Walker,B.R. (2001). Minireview: 11beta-hydroxysteroid dehydrogenase type 1- a tissue-specific amplifier of glucocorticoid action. *Endocrinology* **142**:1371-1376.

Shafqat,N., Elleby,B., Svensson,S., Shafqat,J., Jornvall,H., Abrahmsen,L., and Oppermann,U. (2003). Comparative enzymology of 11 beta -hydroxysteroid dehydrogenase type 1 from glucocorticoid resistant (Guinea pig) versus sensitive (human) species. *J. Biol. Chem.* **278**:2030-2035.

Sheridan,R.P. (2002). The most common chemical replacements in drug-like compounds. *J. Chem. Inf. Comput. Sci.* **42**:103-108.

Solly,K., Mundt,S.S., Zokian,H.J., Ding,G.J., Hermanowski-Vosatka,A., Strulovici,B., and Zheng,W. (2005). High-throughput screening of 11beta-hydroxysteroid dehydrogenase type 1 in scintillation proximity assay format. *Assay. Drug Dev. Technol.* **3**:377-384.

Sorensen,B., Rohde,J., Wang,J., Fung,S., Monzon,K., Chiou,W., Pan,L., Deng,X., Stolarik,D., Frevert,E.U., Jacobson,P., and Link,J.T. (2006). Adamantane 11-beta-HSD-1 inhibitors: Application of an isocyanide multicomponent reaction. *Bioorg. Med. Chem. Lett.* **16**:5958-5962.

Sorensen,B., Winn,M., Rohde,J., Shuai,Q., Wang,J., Fung,S., Monzon,K., Chiou,W., Stolarik,D., Imade,H., Pan,L., Deng,X., Chovan,L., Longenecker,K., Judge,R., Qin,W., Brune,M., Camp,H., Frevert,E.U., Jacobson,P., and Link,J.T. (2007). Adamantane sulfone and sulfonamide 11-beta-HSD1 Inhibitors. *Bioorg. Med. Chem. Lett.* **17**:527-532.

Stewart,P.M. and Krozowski,Z.S. (1999). 11 beta-Hydroxysteroid dehydrogenase. *Vitam. Horm.* **57**:249-324.

Stura,E.A. and Wilson,I.A. (1990). Analytical and production seeding techniques. *Methods* **1**:38-49.

Su,X., Vicker,N., Lawrence,H., Smith,A., Purohit,A., Reed,M.J., and Potter,B.V. (2007). Inhibition of human and rat 11beta-hydroxysteroid dehydrogenase type 1 by 18beta-glycyrrhetinic acid derivatives. *J. Steroid Biochem. Mol. Biol.* **104**:312-320.

Sun,D., Wang,Z., Cardozo,M., Choi,R., DeGraffenreid,M., Di,Y., He,X., Jaen,J.C., Labelle,M., Liu,J., Ma,J., Miao,S., Sudom,A., Tang,L., Tu,H., Ursu,S., Walker,N., Yan,X., Ye,Q., and Powers,J.P. (2009). Synthesis and optimization of arylsulfonylpiperazines as a novel class of inhibitors of 11beta-hydroxysteroid dehydrogenase type 1 (11beta-HSD1). *Bioorg. Med. Chem. Lett.* **19**:1522-1527.

Sun,D., Wang,Z., Di,Y., Jaen,J.C., Labelle,M., Ma,J., Miao,S., Sudom,A., Tang,L., Tomooka,C.S., Tu,H., Ursu,S., Walker,N., Yan,X., Ye,Q., and Powers,J.P. (2008). Discovery and initial SAR of arylsulfonylpiperazine inhibitors of 11beta-hydroxysteroid dehydrogenase type 1 (11beta-HSD1). *Bioorg. Med. Chem. Lett.* **18**:3513-3516.

Taylor,A., Irwin,N., McKillop,A.M., Flatt,P.R., and Gault,V.A. (2008a). Sub-chronic administration of the 11beta-HSD1 inhibitor, carbenoxolone, improves glucose tolerance and insulin sensitivity in mice with diet-induced obesity. *Biol. Chem.* **389**:441-445.

Taylor,P., Blackburn,E., Sheng,Y.G., Harding,S., Hsin,K.Y., Kan,D., Shave,S., and Walkinshaw,M.D. (2008b). Ligand discovery and virtual screening using the program LIDAEUS. *Br. J. Pharmacol.* **153 Suppl 1**:S55-S67.

Thomas E.Creighton 1984. *Proteins; Structures and Molecular Properties*, 1 ed. W.H. Freeman and Company.

Tomlinson,J.W., Walker,E.A., Bujalska,I.J., Draper,N., Lavery,G.G., Cooper,M.S., Hewison,M., and Stewart,P.M. (2004). 11 beta-Hydroxysteroid Dehydrogenase Type 1: A Tissue-Specific Regulator of Glucocorticoid Response. *Endocr Rev* **25**:831-866.

Tsaioun,K., Bottlaender,M., and Mabondzo,A. (2009). ADDME - Avoiding Drug Development Mistakes Early: central nervous system drug discovery perspective. *BMC. Neurol.* **9 Suppl 1**:S1.

Tu,H., Powers,J.P., Liu,J., Ursu,S., Sudom,A., Yan,X., Xu,H., Meininger,D., DeGraffenreid,M., He,X., Jaen,J.C., Sun,D., Labelle,M., Yamamoto,H., Shan,B., Walker,N.P., and Wang,Z. (2008). Distinctive molecular inhibition mechanisms for selective inhibitors of human 11beta-hydroxysteroid dehydrogenase type 1. *Bioorg. Med. Chem.* **16**:8922-8931.

Vander Jagt,D.L., Deck,L.M., and Royer,R.E. (2000). Gossypol: prototype of inhibitors targeted to dinucleotide folds. *Curr. Med. Chem.* **7**:479-498.

Vicker,N., Su,X., Ganeshapillai,D., Smith,A., Purohit,A., Reed,M.J., and Potter,B.V. (2007). Novel non-steroidal inhibitors of human 11beta-hydroxysteroid dehydrogenase type 1. *J. Steroid Biochem. Mol. Biol.* **104**:123-129.

Wajchenberg,B.L. (2000). Subcutaneous and visceral adipose tissue: their relation to the metabolic syndrome. *Endocr Rev* **21**:697-738.

Wake,D.J., Rask,E., Livingstone,D.E., Soderberg,S., Olsson,T., and Walker,B.R. (2003). Local and systemic impact of transcriptional up-regulation of 11beta-hydroxysteroid dehydrogenase type 1 in adipose tissue in human obesity. *J. Clin. Endocrinol. Metab* **88**:3983-3988.

Walters,W.P. and Murcko,M.A. (2002). Prediction of 'drug-likeness'. *Adv. Drug Deliv. Rev* **54**:255-271.

Wang,H., Ruan,Z., Li,J.J., Simpkins,L.M., Smirk,R.A., Wu,S.C., Hutchins,R.D., Nirschl,D.S., Van,K.K., Cooper,C.B., Sutton,J.C., Ma,Z., Golla,R., Seethala,R., Salyan,M.E., Nayeem,A., Krystek,S.R., Jr., Sheriff,S., Camac,D.M., Morin,P.E., Carpenter,B., Robl,J.A., Zahler,R., Gordon,D.A., and Hamann,L.G. (2008). Pyridine amides as potent and selective inhibitors of 11beta-hydroxysteroid dehydrogenase type 1. *Bioorg. Med. Chem. Lett.* **18**:3168-3172.

Webster,S.P. and Pallin,T.D. (2007). 11ß-Hydroxysteroid dehydrogenase type 1 inhibitors as therapeutic agents. *Expert Opinion on Therapeutic Patents* **17**:1407-1422.

Webster,S.P., Ward,P., Binnie,M., Craigie,E., McConnell,K.M., Sooy,K., Vinter,A., Seckl,J.R., and Walker,B.R. (2007). Discovery and biological evaluation of adamantyl amide 11beta-HSD1 inhibitors. *Bioorg. Med. Chem. Lett.* **17**:2838-2843.

White,P.C., Mune,T., Rogerson,F.M., Kayes,K.M., and Agarwal,A.K. (1997). Molecular analysis of 11 beta-hydroxysteroid dehydrogenase and its role in the syndrome of apparent mineralocorticoid excess. *Steroids* **62**:83-88.

Wsol,V., Szotakova,B., Skalova,L., and Maser,E. (2004). The novel anticancer drug oracin: different stereospecificity and cooperativity for carbonyl reduction by purified human liver 11beta-hydroxysteroid dehydrogenase type 1. *Toxicology* **197**:253-261.

Wu,S.Y., McNae,I., Kontopidis,G., McClue,S.J., McInnes,C., Stewart,K.J., Wang,S., Zheleva,D.I., Marriage,H., Lane,D.P., Taylor,P., Fischer,P.M., and Walkinshaw,M.D. (2003). Discovery of a novel family of CDK inhibitors with the program LIDAEUS: structural basis for ligand-induced disordering of the activation loop. *Structure.* **11**:399-410.

Xiang,J., Ipek,M., Suri,V., Massefski,W., Pan,N., Ge,Y., Tam,M., Xing,Y., Tobin,J.F., Xu,X., and Tam,S. (2005). Synthesis and biological evaluation of sulfonamidooxazoles and beta-keto sulfones: selective inhibitors of 11beta-hydroxysteroid dehydrogenase type I. *Bioorg. Med. Chem. Lett.* **15**:2865-2869.

Xiang,J., Ipek,M., Suri,V., Tam,M., Xing,Y., Huang,N., Zhang,Y., Tobin,J., Mansour,T.S., and McKew,J. (2007). beta-Keto sulfones as inhibitors of 11beta-hydroxysteroid dehydrogenase type I and the mechanism of action. *Bioorg. Med. Chem.* **15**:4396-4405.

Yang,H., Dou,W., Lou,J., Leng,Y., and Shen,J. (2008). Discovery of novel inhibitors of 11beta-hydroxysteroid dehydrogenase type 1 by docking and pharmacophore modeling. *Bioorg. Med. Chem. Lett.* **18**:1340-1345.

Yang,H., Shen,Y., Chen,J., Jiang,Q., Leng,Y., and Shen,J. (2009). Structure-based virtual screening for identification of novel 11beta-HSD1 inhibitors. *Eur. J. Med. Chem.* **44**:1167-1171.

Yau,J.L., McNair,K.M., Noble,J., Brownstein,D., Hibberd,C., Morton,N., Mullins,J.J., Morris,R.G., Cobb,S., and Seckl,J.R. (2007). Enhanced hippocampal long-term potentiation and spatial learning in aged 11beta-hydroxysteroid dehydrogenase type 1 knock-out mice. *J. Neurosci.* **27**:10487-10496.

Yuan,C., St,J.D., Jr., Liu,Q., Cai,L., Li,A., Han,N., Moniz,G., Askew,B., Hungate,R.W., Johansson,L., Tedenborg,L., Pyring,D., Williams,M., Hale,C., Chen,M., Cupples,R., Zhang,J., Jordan,S., Bartberger,M.D., Sun,Y., Emery,M., Wang,M., and Fotsch,C. (2007). The discovery of 2-anilinothiazolones as 11beta-HSD1 inhibitors. *Bioorg. Med. Chem. Lett.* **17**:6056-6061.

Zhang,J., Osslund,T.D., Plant,M.H., Clogston,C.L., Nybo,R.E., Xiong,F., Delaney,J.M., and Jordan,S.R. (2005). Crystal structure of murine 11 beta-hydroxysteroid dehydrogenase 1: an important therapeutic target for diabetes. *Biochemistry* **44**:6948-6957.